Characterization and validation of the high accurate heat meter calibration facility of the Physikalisch-Technische Bundesanstalt PTB

vorgelegt von
MSc
Moritz Leopoldo Córdova Murillo
geb. in Oruro, Bolivien

von der Fakultät III Prozesswissenschaften
der Technischen Universität Berlin
zur Erlangung des akademischen Grades

Doktor der Ingenieurwissenschaften
- Dr.-Ing.-

genehmigte Dissertation

Promotionsausschuss:

Vorsitzender: Prof. Dr. Stephan Drusch
Gutachter: Prof. Dr.-Ing. Matthias Kraume
Gutachter: Prof. Dr. phil. Dr. techn. Franz Adunka
Gutachter: Dr. rer. nat. Thomas Lederer

Tag der wissenschaftlichen Aussprache: 4. Juli 2016

Berlin 2016

Danksagung

Bei der Realisierung dieser Arbeit haben mich sehr viele Menschen begleitet und durch Diskussionen, Anregungen und tatkräftige Hand- und Sacharbeit diesen Abschluss möglich gemacht.

Besonderer Dank gilt meinem Betreuer Dr. Thomas Lederer, Leiter des Fachbereichs Wärme und Vakuum, dem Doktorandenkreis und der Werkstatt der PTB-Berlin, die mich durch unzählige Beiträge weitergebracht haben.

Für die fachlichen und leidenschaftlichen Auseinandersetzungen bin ich auch Dr. Noriyuki Furuichi vom AIST-NMIJ, Dr. Peter Lau, ehem. SP, Dr. Rainer Engel, ehem. PTB und Dr. Jürgen Rose, PTB, sehr dankbar. Für die Begutachtung und Kritik an der Arbeit möchte ich Prof. Dr. Kraume, Prof. Dr. Dr. Adunka und nicht zuletzt den anonymen Reviewern danken.

Nicht unerwähnt dürfen meine Partnerin, meine Familie und meine lieben Freunde bleiben, die auch an Regentagen für mich da waren.

Abstract

Flow rate calibration facilities have the task to establish a flow rate under predefined conditions and to measure this flow rate within a declared uncertainty. To proof the correctness of the declared uncertainty requires in depth understanding of every hardware component. In cases where those components can not be directly isolated and modeled it is necessary to make assumptions and to make experimental validations.

After the heat meter calibration rig of the Physikalisch-Technische Bundesanstalt WZP (Wärmezähler Prüfstrecke) was overhauled, establishing an uncertainty budget for the flow rate range up to $1000\,\mathrm{m^3/h}$ and from 3 °C to 90 °C was necessary. All relevant components were modeled and characterized. Special attention was payed to the time measurement system, resulting in a novel characterization method that has been successfully applied.

The main objective of this research work is to validate the uncertainty declaration of the flow and heat meter calibration facility of the WZP and to establish for this purpose a methodology to improve the actual state-of-the-art on uncertainty validation methods for flow calibration facilities.

The developed methods are capable of detecting several types of unknown systematic influences on the measurement results. But in order to guarantee that no relevant systematic errors are still present a comparison to an external absolute reference was also necessary. This reference was the National Institute of Advanced Industrial Science and Technology in Japan (NMIJ). Reciprocally, the NMIJ considered the WZP as its external reference.

The challenge of this bilateral comparison trial was to find a transfer standard that was stable and robust enough to make it possible to relate discrepancies in the comparison results directly with the performance of the facilities and not with that of the flow meter itself. The flow rate and temperature ranges allowed only for ultrasonic flow meter to be considered. To define the required measurement conditions for an ultrasonic flow meter to meet the requirements of the interlaboratory comparison is one of the aims of the present work.

It was determined that the most relevant influence quantity besides the flow profile within the flow meter body is the influence of the transducer pockets into the flow and consequently into the flow meter signal. By taking advantage of a specially designed window chamber for performing local velocity measurements within the ultrasonic flow meter, it was possible to determine the magnitude of the errors introduced by the transducer pockets and to define, based on the findings, the best procedure to perform the comparison.

The comparison results proved directly the consistency of the measurements for 20 °C. That was not the case for higher temperatures, but considering additionally that the applied validation methods confirmed the internal consistency of the WZP across all temperatures, it can be confirmed that if the results for 20 °C are valid, the measurements at higher temperatures are necessarily also valid. Differences found in the measurement results of both laboratories could be attributed to the flow profile sensitivity of the used flow meter. The findings about ultrasonic flow metering can be used for further flow metering developments.

Zusammenfassung

Die Aufgabe einer Durchflusskalibrieranlage ist die Realisierung eines unter vordefinierten Bedingungen bestimmten Durchflusses innerhalb einer vorgegebenen Unsicherheit. Detailliertes Wissen über jede Komponente ist für die Nachweiserbringung dieser Unsicherheit unabdingbar. Wenn die Einflüsse sich nicht isolieren und modellieren lassen, ist es nötig, Vereinfachungen zu treffen und diese auf experimentelle Weise zu überprüfen.

Nach der Generalüberholung der Wärmezähler Prüfstrecke der Physikalisch- Technischen Bundesanstalt (WZP) ist eine erneute Evaluation der Unsicherheitsbilanz der Anlage im Durchflussbereich bis 1000 $\mathrm{m^3/h}$ und im gesamten Temperaturbereich zwischen 3 ℃ und 90 ℃ nötig geworden.

Das Hauptziel dieser Forschungsarbeit ist neue Verfahren und Methoden zu entwickeln, die für die Validierung der Unsicherheitsbestimmung von Durchflusskalibrieranlagen und konkret der WZP angewendet werden können.

Die entwickelten Methoden sind in der Lage, verschiedene unbekannte systematische Einflüsse der Messergebnisse zu erkennen, aber um garantieren zu können, dass keine weiteren relevanten sytematischen Fehler einen Einfluss auf die Messergebnisse haben, ist der Vergleich mit einer externen Referenz notwendig. Das National Institute of Advanced Industrial Science and Technology in Japan (NMIJ) diente als externe Referenz, reziprok diente für das NMIJ die WZP als externe Referenz.

Die größte Herausforderung für die bilateralen Vergleichsmessungen war ein geeignetes Durchflussmessgerät zu finden, welches stabil und robust genug war, eindeutig die Gründe für eine mögliche Diskrepanz der Performanz der Labore und nicht der eigenen Performanz zuordnen zu können. Die gegebenen Durchfluss- und Temperaturbereiche limitierten die Messprinzipauswahl auf Ultraschall Durchflussmessgeräte. Ziel dieser Arbeit war es auch, die erforderlichen Messbedingungen für die erfolgreiche Durchführung der Vergleichsmessungen zu definieren.

Als wichtigste Einflussgröße nach dem Durchflussprofil der Hauptströmung hat sich die Strömung innerhalb der Sensortaschen, die das Messsignal direkt beeinflussen können, herausgestellt. Durch den Einsatz einer speziell dafür entwickelten Fensterkammer war es möglich, das Geschwindigkeitsprofil im Ultraschallmessgerät zu messen und die Magnitude der Fehler zu bestimmen, die durch die Sensortaschen induziert wurden. Durch die gewonnenen Erkenntnisse wurde die beste Vorgehensweise für die Durchführung des Vergleichs definiert.

Die Ergebnisse des Vergleichs bei 20 ℃ können ohne weitere Betrachtungen die Konsistenz zwischen den teilnehmenden Laboren nachweisen. Das ist nicht der Fall für die Versuche bei höheren Temperaturen. Berücksichtigt man aber, dass sich die Messergebnisse innerhalb der Labore bei verschiedenen Temperaturen durch interne Validierungsmethoden als in sich konsistent bestätigt haben, kann man daraus folgern, dass die Messergebnisse für höhere Temperaturen auch valide sind. Die gemessenen Diskrepanzen konnten der Durchflussprofilempfindlichkeit der Durchflussmesstechnik zugeordnet werden. Die Erkenntnisse über die Ultraschalldurchflussmesstechnik können in Zukunft neuen Entwicklungen dienen.

Contents

List of Tables

List of Figures

List of Cumulative Publications

[Cor15b] L. Cordova and T. Lederer. A practical method to assess the performance of gravimetric flow test rigs by using the timing error. In *Flow Measurement and Instrumentation*, 44:61 – 70, 2015. doi:http://dx.doi.org/10.1016/j.flowmeasinst.2014.11.010. Flomeko 2013 Special Edition - Selected Extended Papers.

[Cor14b] L. Cordova and T. Lederer. Application of a novel method for validating the uncertainty estimation of a flow test facility. In *tm - Technisches Messen*, 81(9):431 – 441, 2014. doi:http://dx.doi.org/10.1515/teme-2014-1039

[Cor15a] L. Cordova, N. Furuichi and T. Lederer. Qualification of an ultrasonic flow meter as a transfer standard for measurements at Reynolds numbers up to $4x10^6$ between NMIJ and PTB. In *Flow Measurement and Instrumentation*, 45:28 – 42, 2015. doi:http://dx.doi.org/10.1016/j.flowmeasinst.2015.04.006.

List of Symbols

A empiric term for the determination of the discharge coefficient.

B empiric term for the determination of the discharge coefficient.

C_d discharge coefficient for the orifice plate.

C_{inf} asymptotic term for the orifice plate according to Reader-Harris.

C_{slope} slope term for the orifice plate according to Reader-Harris.

C_{taps} tap correction term for the orifice plate according to Reader-Harris.

D pipe diameter.

D pipe diameter 208 mm.

K flowmeter relative error.

K' biased relative flow meter error.

K_a the asymmetry factor for $r/R \leq \pm 0.65$.

K'_a the asymmetry factor for the horizontal path for $r/R \leq \pm 1$.

K_p the maximum profile factor for $r/R \leq \pm 0.65$.

K'_p the profile factor for the horizontal path for $r/R \leq \pm 1$.

$L(t)$ position of the blade at a given time during the diverter motion.

N sample size.

P_i measurement result of each ultrasonic path.

Q_k correction term for ultrasonic flow metering through weighted summation.

$Q_{0.65}$ Flow rate within $r/R \leq \pm 0.65$.

Q_{air} air flow rate flowing out of the weighing tank during a measurement.

Re pipe Reynolds number.

Re Reynolds number.

Re_d orifice Reynolds number.

Ro Roshko number.

S through regression estimated auxiliary parameter representing the slope.

St Strouhal number according to the CCM.FF-K2.

T Temperature.

Tu turbulence factor.

V_1 empty volume of the weighing tank.

V_2 remaining empty volume of the tank after the measurement.

V_{dw} volume of the dead weight including the empty weighing tank.

V_{jk} accumulated volume resulting from the integration of Qi between the instants j and k.

V_{mut} volume accumulated by the meter under test during the testing time.

V_{ref} volume indicated by the reference system expressed for the conditions at the meter under test.

W Indication of the weighing scale after tara.

ΔB_1 buoyancy force corrections originated by the dead weight including the empty weighing tank.

ΔB_2 buoyancy force corrections originated by the air inside the weighing tank.

ΔV volume increment due to air bubbles.

$\Delta \rho_w$ correction the the water density.

Δm mass corrections.

Δp pressure difference or pressure drop.

Δt_1 part of the timing error occurring at the first diverting action.

Δt_2 part of the timing error occurring at the second diverting action.

Δt_j filling time of only one filling period.

Δt_{iso} timing error determined by the method of the ISO-4185.

α ratio of increment on the absolute water content per cubic meter.

$\bar{Q}$ average flow rate.

β diameter ratio of the orifice plate.

χ^2 Chi-square.

$\dot{V}$ volumetric flowrate.

$\dot{V}_{mut}$ volumetric flow rate at the meter under test.

$\dot{V}_s$ reference flow rate generated by the flow test rig.

$\dot{m}$ mass flowrate.

$\dot{m}_c$ average mass flow rate measured by a flow meter during the continuous measurement.

$\dot{m}_i$ average mass flow rate measured by a flow meter during the filling intervals.

ϵ relative timing error.

λ auxiliary parameter for the determination of the variance of the diverter motion.

λus wavelength for the ultrasonic doppler method.

ϕ auxiliary parameter for the determination of the variance of the diverter motion.

ϕ_0 through regression estimated auxiliary parameter *phi* defined for the 0-crossing.

ϕ_{us} phase angle of the ultrasonic doppler method.

ρ_w water density.

ρ_{a1} air density at the beginning of the measurement.

ρ_{a2} air density at the end of the measurement.

ρ_{as} air density during weighing scale calibration.

ρ_a air density during the measurements.

ρ_f density of water during measurements.

ρ_{g1} air density inside the weighing tank at the beginning of the measurement.

ρ_{g2} air density inside the weighing tank at the end of the measurement.

ρ_{ws} density of the mass standards during the calibration of the weighing scale.

σ_S^2 variance of the auxiliary parameter S.

σ_δ^2 variance of the diverter motion.

σ_ϵ^2 variance of the timing error determination method.

$\sigma_{\dot{m}c}^2$ variance of the flow rate measurement during the continuos measurement.

$\sigma_{\dot{m}i}^2$ variance of the flow rate measurement during the n filling interval.

$\sigma_{\dot{m}}^2$ variance of the flow rate measurement.

$\sigma_{\phi 0}^2$ variance of the auxiliary parameter ϕ_0.

$\sigma_{\sigma\dot{m}}^2$ experimental determined variance of $\sigma_{\dot{m}}$.

$\sigma_{\sigma sv}^2$ variance of the sample variance.

σ_{cal}^2 variance of the calibration factor.

σ_{kf}^2 variance of the flow rate measurement ratios.

σ_{km}^2 variance of the mass determination ratios.

σ_{ref}^2 variance of the flow calibration rig.

a, b, c, d area representing missing or remaining water on the weighing tank during the diversion.

b_1 negligible term for buoyancy corrections of the dead weight.

b_2 negligible term for buoyancy corrections of the air inside the weighing tank.

c sound speed.

d orifice diameter.

d_a difference observed for laboratory a.

d_b difference observed for laboratory b.

d_p distance from the peak to the pipe axis.

d_v distance from the gravity center of the flow to the pipe axis.

e_i error of each ultrasonic path.

f_0 absolute water content per cubic meter air at the at the end.

f_i absolute water content per cubic meter air at the at the start.

f_m output frequency of the flow meter proportional to the flow rate.

f_t transducer frecuency.

f_{prf} pulse repetition frequency for the ultrasonic doppler method.

k correction factor for the weighted summation.

k_b factor correcting for buoyancy effects.

k_f ratio of the average mass flow rates measured by a flow meter.

k_i' apparent flow meter correction factor for n filling intervals.

k_m ratio of the accumulated masses during n and one continuous filling interval.

k_p' apparent flow meter correction factor for a continuous measurement.

k_r flow meter constant according to the CCM.FF-K1.

k_t ratio of the apparent filling times.

m_c mass accumulated during the continuous filling interval.

m_e evaporated amount of water.

m_i mass accumulated during all filling intervals.

m_{ew} worst case evaporated amount of water.

n amount of filling intervals used for the diverter test. Number of paths in an ultrasonic flow meter.

p absolut fluid pressure.

p_{max} maximum measurement depht for the ultrasonic doppler method.

q average volume flow rate measured by a flow meter during the continuous measurement.

q_i average volume flow rate measured by a flow meter during the filling intervals.

r correlation factor between two flow rate measurements.

s_+ observed standard deviation of the sum of two in series measured flow meters.

s_- observed standard deviation of the difference of two in series measured flow meters.

s_p standard deviation of the laboratory.

t_1 time when the measurement of the filling time is started.

t_2 time when the measurement of the filling time is stopped.

t'_c apparent measurement time of a continuous filling interval.

t'_i sum of the duration of all filling intervals.

t_j lower integration limit for the timing error.

t_k upper integration limit for the timing error.

t_{11} time when the flow rate begins to be accumulated in the weighing tank.

t_{12} time when the flow rate during the measurement is fully available at the weighing tank.

t_{21} time when the flow rate begins to be directed away from the weighing tank.

t_{22} time when flow rate into the weighing tank ceases after the measurement.

u_a uncertainty of laboratory a.

u_b uncertainty of laboratory b.

u_i relative uncertainty of the component i.

u_m relative mass uncertainty.

u_t relative uncertainty of the timing error.

u_{B1} uncertainty of the buoyancy correction due to dead weights.

u_{B2} Uncertainty of the buoyancy force corrections originated by the air inside the weighing tank.

u_{Ka} uncertainty of the relative error of the flow meter under test in absolute terms.

u_{K} uncertainty of the relative error of the flow meter under test in relative terms.

u_{Wa} uncertainty of the weighing scale indication.

$u_{\Delta ma}$ uncertainty of the mass corrections.

$u_{\Delta ta}$ uncertainty of the time measurement.

$u_{\Delta t}$ relative uncertainty of the time corrections.

$u_{\dot{V}muta}$ reproducibility of the flow meter under test in absolute terms.

$u_{\dot{V}sa}$ uncertainty of the flow rate generated by the flow test rig in absolute terms.

$u_{\dot{V}s}$ uncertainty of the reference flow rate generated by the flow test rig.

$u_{\rho 1}$ relative uncertainty of water density due to calibration.

$u_{\rho 2}$ relative uncertainty of water density due to compressibility.

$u_{\rho 3}$ relative uncertainty of water density due to temperature measurement.

$u_{\rho 4}$ relative uncertainty of water density due to dissolved air.

$u_{\rho\ a}$ uncertainty of the water density.

$u_{\rho a1}$ uncertainty of the air density at the beginning of the measurement.

$u_{\rho a2}$ uncertainty of the air density at the beginning of the measurement.

$u_{\rho g1}$ uncertainty of the air density inside the weighing tank at the beginning of the measurement.

$u_{\rho g2}$ uncertainty of the air density inside the weighing tank at the end of the measurement.

u_{ρ} relative uncertainty of water density.

u_{dm} relative uncertainty of the mass correction.

u_{kba} uncertainty of the buoyancy corrections.

u_{m1} reproducibility contribution of the mass measurement.

u_{m2} uncertainty contribution due to water movement.

u_{m3} uncertainty contribution due to temperature effects on the weighing system.

u_{m4} uncertainty contribution due to interpolation on the weighing system.

u_{m5} uncertainty contribution of systematic errors on the weighing system.

u_{m6} uncertainty contribution of the buoyancy corrections on the weighing system.

u_{mz} maximum axial fluid velocity.

u_{mz}/u_o maximum relative axial fluid velocity.

u_{p1a} uncertainty of the correction due to evaporation.

u_{p2a} uncertainty of the correction due to buoyancy effects due to the solid dead weight.

u_{p3a} uncertainty of the correction due to buoyancy effects of the air inside the weighing tank.

u_{p4a} uncertainty given by the accumulation of air in the diverter system.

u_{p5a} uncertainty contribution due to expansion of the pipe within the measurement.

u_{pa} uncertainty of the process related contributions.

u_p uncertainty of the process related contributions given in kg.

u_{t1a} uncertainty of the timing error due to flow stability.

u_{t2a} uncertainty of the timing error due to the inlet flow profile.

u_{t3a} uncertainty of the timing error given by repeatability.

u_{t4a} uncertainty of the timing error given by the determination method.

u_{t5a} uncertainty of the timing error given due to linearity deviations.

u_{ta} uncertainty of the timing error.

v_{max} maximum determinable speed for the ultrasonic doppler method.

w_i weight for the path i on ultrasonic time of flight flow measurement.

1. Introduction

Considering modern industrial processes where flow rates need to be monitored in real time, the uncertainty of the installed flow measurement systems has often a direct impact on the quality of the end product. Furthermore, when the environment, the safety, the efficiency of a process or the price paid in a commercial transaction are involved, the tolerable error on flow rate measurements are defined in advance either by a third party or through a previous mutual agreement or contract.

National Metrology Institutes (NMI) are created to provide from a technical point of view the frame to guarantee fair trade and commerce, not only at a local, but also at an international level. They are also entitled to provide support to the local industrial development through improvement of the quality of measurement tasks.

A very important step since the signature of the meter convention in 1875, was the signature of the Mutual Recognition Arrangement (MRA) in 1999. 38 NMI and two Independent Institutions committed to establish a mutual recognition of metrology services. This required the introduction of a methodology to control and to qualify the different metrology services offered by NMIs. The main objective was to *"provide governments and other parties with a secure technical foundation for wider agreements related to international trade, commerce and regulatory affairs"*[CIP99]. As a result of the MRA, in order to be recognized, NMIs have to proof their performance through the implementation of a quality system that ensures that their services correspond to the declared procedures, and through the participation in international interlaboratorial comparisons to ensure the results are correct. Interlaboratorial comparisons consist of the comparison of the measurement results of a predefined measurand materialized in an artifact, that have been obtained by the participating laboratories. The deviations to the conventional true value of the measurand defined for the comparison, should be consistent with every laboratories uncertainty declarations. The deviation is expected to be with a 95 % confidence within the declared uncertainty.

Comparisons of the International Bureau of Weights and Measures (BIPM) are performed typically at two levels. At a global level key-comparisons are performed between laboratories coming from several regional metrology organizations (RMO) like Euramet for Europe or APMP for the asian-pacific region. At regional or RMO-level the comparison is repeated with often considerably more laboratories including the regional participants using the same measurement equipment and applying the same conventional reference value as the corresponding key-comparison.

All calibration and measurement services that have been internationally recognized are stored on the public-access database of the MRA. Every entry describes an offered calibration service and its respective uncertainty. These entries are denominated Calibration and Measurement Capabilities (CMC). The concept of CMC of the MRA gained acceptance since its introduction on 1999. In 2002, only three years later there were about 11000 CMC entries on the database, in 2014 there were more than 24000 entries [Tho14].

The procedures defined for realizing international comparisons are best suitable for wide spread quantities as mass for example. These procedures require that the mag-

nitude in question can be materialized with sufficiently low uncertainty and stability, and that NMIs offering metrological services related to the magnitude are numerous and spread around the world.

In the case of some quantities there are only few NMIs in the world that have an adequate metrological structure to offer calibration services. Additionally, many magnitudes can not be materialized and transported between the laboratories, instead, a measurement device has to be transported between the NMI. Commercially available measurement devices are seldom suitable for such an exercise. In the case of flow rate, the measurand is the correction factor of a flow meter at predefined conditions.

The Physikalisch-Technische Bundestanstalt PTB holds the most accurate flow calibration facility for larger flowrates up to 1000 m^3/h and temperatures up to 90 °C in the world. This facility for flow and heat meter calibration is denominated WZP (for its german name Wärmezähler Prüfstrecke). Given to the mentioned reasons, the application of the concept of the MRA to flow measurement at higher temperatures is not practicable. As a consequence, it is necessary to find alternative ways to proof the laboratory proficiency. The aim of this research work is to proof the uncertainty declaration of the WZP at larger flow rates, and to establish a methodology to improve the actual state-of-the-art on uncertainty validation methods and on interlaboratory comparisons on flow calibration rigs.

One of the most important challenges to perform a successful comparison is to find an adequate artifact, also called transfer standard, to perform the measurements at different laboratories. The transfer standard has to be stable and robust enough in order to make it possible to relate unambiguities in the comparison results directly with the performance of the tested facilities and not with the performance of the used flow meter itself. Since interlaboratory comparisons are the most important criterion to validate the results of a flow calibration rig, to qualify a flow meter and to define the required measurement conditions in which it performs best are an essential part of the present work.

1.1. Metrological traceability of flow metering

According to the International Vocabulary for Metrology VIM [VIM08], metrological traceability is defined as: *"property of a measurement result whereby the result can be related to a reference through a documented unbroken chain of calibrations, each contributing to the measurement uncertainty"*. This formal definition of traceability states in the foreground the establishment of an uninterrupted chain of calibrations. Given the auditing nature of the MRA, it is necessary to apply such a pragmatic definition. But from a scientific point of view, it is the determination of uncertainty that determines the level of trust that we can give to measurement. The calibration is an important but still only one part of the overall uncertainty budget.

According to the philosophy of the MRA, every measurement should follow the scheme shown in Figure 1.1. Note that in this ideal representation the NMIs are the only "keepers" of the International System of units.

Not every measurement task can be reproduced at a laboratory, in-fact only very few real applications can be directly traced to NMIs. In such a scenario, extrapolation of actual calibration results to different conditions or even to higher or lower ranges is the only possibility left. In order to provide a solid extrapolation basis, small laboratory calibration uncertainties are required.

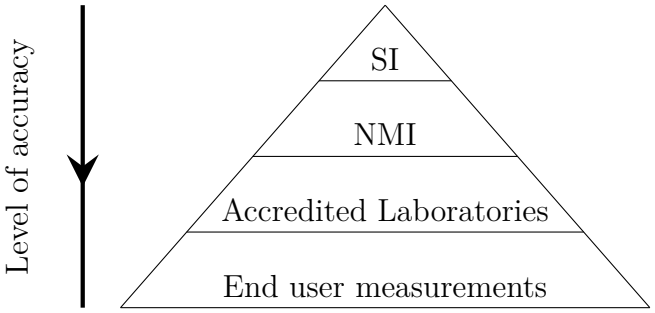

Figure 1.1.: General traceability Scheme

1.2. Flow calibration facility principles

Depending on the required conditions, the principal flow rate generation can be performed using different rotary or positive displacement pumps, or using pressure sources as constant head tanks or a pressurized chamber together with a control valve. The measurement of the flow rate can be performed gravimetrically through accumulation using a weighing scale; volumetrically using a known cylinder and a moving ball or piston; or as recently demonstrated in [Jul15] and [Jul14], by means of direct flow integration of the flow profile in a closed conduit by using Laser Doppler Velocimetry (LDV).

Influence quantities change the indication of the flow rate without affecting the real flow rate itself [1]. Given to the limitations to control every influence quantity it is necessary to make certain assumptions. Mass continuity is a basic assumption that implies that there are no leaking valves, or that the connecting fluid volume between the flow meter under test and the weighing tank is constant during the measurements. Flow calibration facilities are built in such a way, that the most relevant influence quantities can be controlled or at least bounded.

In the case of flow measurement using on-line flow meter, concerned manufacturers might provide with means of correcting the most important influences. But in general, when working outside of the conditions declared by the manufacturer accuracy limitations have to be accepted. In order to reduce the amount of influence factors that might affect the indication of the flow meter, a calibration laboratory has also to provide for optimal environmental and installation conditions.

1.3. Flow meter for hot water as a Transfer standard

Every flow meter available in the market is the result of a careful trade-off between requirements on cost, size, robustness, safety, easy of use and accuracy. The particular requirements on high accurate transfer standards are not aligned with the typical application; consequently, it is not possible to use an of the shelf system for its use as a transfer standard. Considering the flow meters available for the flow and temperature range covered by the WZP, only two measurement principles can be considered: Ultrasonic time of flight and orifice plate flow meter as explained below.

[1] The term influence quantity is defined in the International Vocabulary of Metrology [VIM08] and refers to quantities that might influence the measurement result, but without changing or influencing the value of the quantity being actually measured. For example the air temperature might affect the electronics, but without influencing the flow rate itself

1.3.1. Ultrasonic time of flight flow metering

When an ultrasonic signal travels through a moving fluid, the transmission speed between two fixed points varies depending on the velocity of the fluid moving between these two points. By knowing the speed of sound and the distance between the two points, it is possible to estimate the average speed of the moving fluid. These two fixed points are normally located at the walls of a pipe, and realized as sending and receiving ultrasonic transmitters. By measuring the traveling time in forward and also in backward direction makes the measurement independent of the speed of sound. A simplified sketch is presented in Figure 1.2.

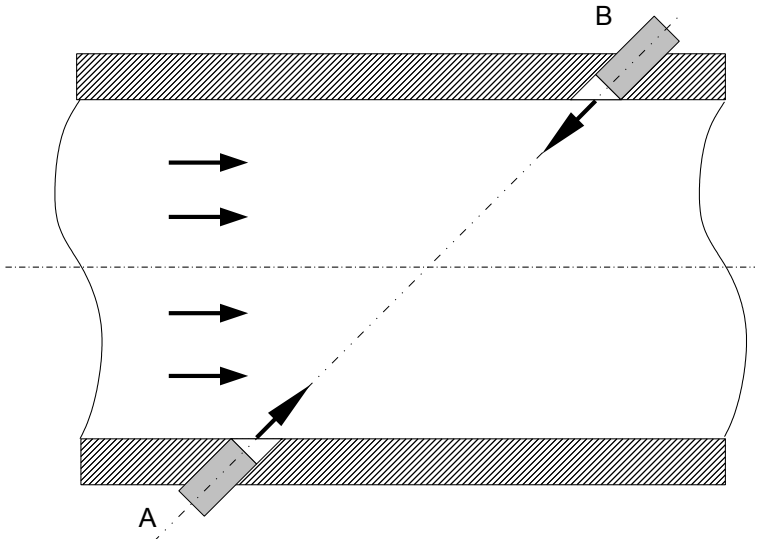

Figure 1.2.: Sketch of a single transducer time of flight ultrasonic flow meter. The ultrasonic signal is send from A to B and from B to A. The time of flight difference depends directly on the velocity of the fluid passing through

The distance between the transducers, the speed of sound in the fluid, the speed of the fluid itself and the required accuracy will determine the required resolution for the transit time measurements. For example for 1480 $^{m}/_{s}$, 0.2 m pipe diameter, 45 ° path angle and 1 $^{m}/_{s}$ fluid bulk speed there is a time of flight difference of 0.18 µs. Assuming a resolution of 0.1% the time measurement resolution should be 180 ps. This is about 1 / 5000 of the wavelength for 1 MHz. Considering that even smaller diameters at slower flow speeds are measured several times per second, at different temperatures and pressures, the requirements on signal processing and transducers are still focus of research.

Under ideal conditions where the flow profile is fully developed and if there are no influences of the secondary components within nor outside the pipe, the flow measurement results depend directly on the quality of the time of flight measurements. But in real applications, secondary components and non ideal flow profiles are unavoidable. Further fully developed flows require very long pipe installations and additional effects may arise from the fact that ultrasonic transducers change the geometry of pipe.

To rely on a flow meter as a transfer standard it is necessary to obtain repeatable and reproducible conditions. Absolute measurement results are not necessary, consequently it is not absolutely necessary to work under ideal conditions, provided the conditions are

allways the same. Hogendoorn[Hog11] and Drenthen et.al.[Dre09] made an uncertainty analysis of ultrasonic meters for a wide application-scope; their findings are mostly based on historical data collected from actual flow meters installed in the field; they address several uncertainty sources giving some details into their estimations. The estimated uncertainty resulted to be about 0.2 %.

Another uncertainty analysis has been performed by Cousins et al. [Cou04]. They published the uncertainty analysis of ultrasonic flow metering based on Caldon flow meters. Caldon has several ultrasonic flow meter installed in North-American power plants. Being power plant thermal recapture a field of application of their flow meters, an uncertainty analysis is unavoidable; however, these documentation is not publicly available. Cousins et al. base their analysis on practical experiences and remark relevant aspects of each influence factor; they determined the expanded uncertainty to be about 0.2 %, however, very few details on the estimation process are given. The Performance Test Codes PTC 18-2011 [PTC11] Hydraulic Turbines and Pump-Turbines for example estimate an overall uncertainty of ±1 % for ultrasonic flow meters.

Indisputable is the influence of the flow conditions, not only to accuracy, but also to repeatability and reproducibility of the measurements. For smaller flow meters, where the size of the transducer pockets is considerably large compared to the pipe diameter, the influences of the flow profile might become the limiting factor. Commercially available ultrasonic time of flight flow meter are calibrated before use at different Reynolds numbers. This allows for unknown systematic errors, even of several percent points, to become eliminated. Further analysis is given in section 3.3.

Furuichi [Nor09] proved the repeatability of time of flight ultrasonic flow meters when used as transfer standards on a fixed installation. These flow meters reached repeatability levels of 0.01 %. The flow profile effects given by different installation conditions are not included. These results suggest that if the flow profile influences can be controlled, a very high performance can be expected. Considering the high potential of ultrasonic flow meters for its application as transfer standards a DN200 flow meter will be focus of further analysis in section 3.3

1.3.2. The orifice plate flow meter

The working principle of an orifice plate with concentric square edges is the same as for any differential pressure flow meter. It is based on the pressure and momentum changes generated by a cross section area reduction in the pipe. By applying Bernoullis equation at the undisturbed flow upstream of the orifice plate and directly at the orifice a solution can be found. If diameter of the orifice is d, the diameter of the pipe is D and $\beta = d/D$ we can write:

$$\bar{Q} = \frac{1}{\sqrt{1-\beta^4}} \frac{\pi d^2}{4} \sqrt{2\Delta p \rho_1} \tag{1.1}$$

Following assumptions were made for equation 1.1 to be valid:

- The fluid density is constant across the pipe
- There are no energy losses due to friction
- The pressure was measured at an undisturbed condition upstream, and directly at the orifice
- The pressure measurements have no errors due to cavity effects
- The ratio of the mean velocities is equal to the cross section ratio at the pressure taps

- The flow is fully developed

In reality none of the assumptions can be held. To find an equation to compensate for all underlying phenomena is a difficult task. The most common type of correction is a semi empirical proportional factor ε to compensate for the density variation and the friction losses in gases and a proportional discharge coefficient C_d to compensate for all other phenomena. The DIN EN ISO 5167-2:2004 [ISOb] gives recommendations on design and construction of orifice plates in order to use the presented corrections.

Projects on the study of the discharge coefficients have a long tradition since 1933. A detailed description of the different improvements across the last decades, and a closer revision of the latest efforts can be found in the AGA Report N.3 Part 4 [AGA03]. Summarizing we can state that in the late 1970s the American Petroleum institute API, the Gas Processors Association and parallely the Commission of European Communities (CEC) started efforts to determine a description of the discharge coefficient based on physical principles. They reduced the degree of freedom of the orifice plate configuration and geometry, and of the measurement and installation conditions to a minimum and organized the collection of data sets. The variables were orifice and pipe diameter, the Reynolds number and the position and the type of the taps. A database with tens of thousand data-sets was generated. Datasets were only used if geometrical tolerances, as well as the upstream lengths to provide a fully developed flow profile were kept.

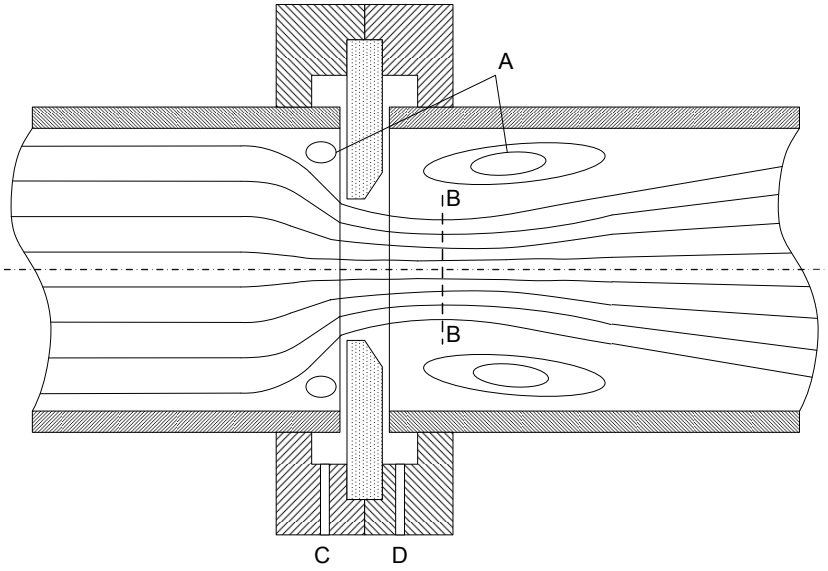

Figure 1.3.: Sketch of an concentric squared edge orifice plate. The flow separation areas are marked with A. The upstream pressure (C) and the downstream pressure (D) measure the pressure from the corner tab. The vena contracta is marked with B

The Reader-Harris Gallagher equation (RG-equation)

The actually most accepted equation for the discharge coefficient was developed by Michael Reader-Harris. His semi empirical model was presented officially at a meeting of a Fluid Flow International Committee in 1988. Reader-Harris based his work on the previous efforts of Stolz [Sto78]. It aimed to improve accuracy, to harmonize the measurements worldwide, and eliminate the discrepancy on the existing recommendations,

but keeping its applicability to different pressure taps, and all that without introducing too much complexity to allow an easy implementation.

The RG-equation is universally accepted and used in the majority of orifice plates installed. Not only in gas and hydrocarbon measurements as it was the initial intention, but in several other application fields including power plants. Thanks to this acceptance, orifice plates together with the RG-equation has been recognized as a primary method, i.e., a flow measurement technology that does not require a calibration, provided that all recommendations regarding installation and geometry have been followed.

The semi-empirical discharge coefficient developed by Reader-Harris has the form:

$$C_d = C_{taps} + C_\infty + C_{slope} \tag{1.2}$$

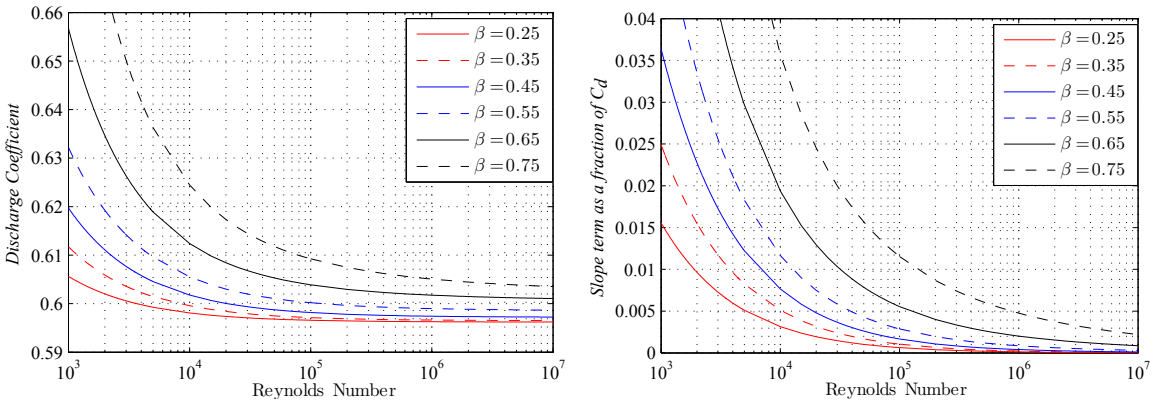

(a) Discharge coefficient

(b) Impact of the slope term

Figure 1.4.: Discharge coefficient and slope term according to the Reader-Harris Gallagher equation

The pressure tap correction term maps the differential pressure measured using regular pressure taps, into the pressure difference that would have been measured if corner taps would have been used. Since corner taps are being used, the tap correction term is not focus of our interest.

For any β, the discharge coefficient runs asymptotically to the value C_∞, following a similar characteristic as the friction factor in a moody diagram.

The slope term describes the characteristic curve of the discharge coefficient. It is the only term dependent on the Reynolds number. Depending on β it might assume different values. For small orifice diameters (small β) it is clear that the pipe Reynolds number should not be relevant, the orifice Reynolds number would become more important. For larger β values, the term should be more dependent on the friction factor λ and on the flow profile defined ideally by the pipe Reynolds number. For simplicity, Reader-Harris proposed to assume a fixed relative roughness and to replace the friction factor by a constant value included in C_∞ a small term that can be neglected, and an approximation of the form $\left(\frac{10^6}{Re_D}\right)^{0.3}$

Performance of orifice plates

According to the widely spread and accepted recommendation DIN EN ISO 5167-2:2004 [ISOb] following uncertainties can be reached when using orifice plates without calibration:

- $(0.7 - \beta)\,\%$ for $0.1 \leq \beta < 0.2$
- $0.5\,\%$ for $0.2 \leq \beta \leq 0.6$
- $(1.66\beta - 0.5)\,\%$ for $0.6 < \beta \leq 0.75$

These large uncertainty values cause an initial rejection of orifice plates as high accurate flow meters. For our application, however, the required reproducibility is at least ten times smaller than the declared uncertainties.

The DIN EN ISO 5167-2:2004 [ISOb] defines the installation conditions required for the fully developed assumption to be valid in the presence of bends, or other fittings. The initial requirements postulated have been massively changed, since several discrepancies have been found for example by [Zim99].

The performance of an orifice plate depends on the fact that the equilibrium between the static pressure, and the dynamic pressure is as close as possible to ideal conditions for a fully developed flow profile. If the flow profile changes, the dynamic pressure will also change introducing a bias in the measurements. For very small orifices, the flow profile at the pipe is expected to have a very low relevance in the determination of the discharge coefficient. For larger orifices it is also expected, that the influence of the flow profile, and consequently of flow profile disturbances increases. This can be recognized in the different slopes in Figure 1.4b.

Orifice plates react sensitive to flow profile peakedness even if axis-symmetry has been reached. Yeh et al. [Yeh94] determined the influence of peakedness on the discharge coefficient caused by a reducer. They found that the flow profile directly after this reducer was flat as expected. The maximum speed rised immediately above the maximum speed of a fully developed flow and reached its maximum at about 30D. The ideal flow profile is found at a distance of about 60D. The same effect is observed at the discharge coefficient for a β ratio of 0.75, the bias rised up to about $0.3\,\%$ at 30D to become zero at about 60D. Yeh et al. measured the discharge coefficients at several positions, for several Reynolds numbers. They found that the influence on the discharge coefficient increases slightly for Reynolds numbers lower than 55000, but for larger Reynolds values (measured up to 100000) the overall changes are smaller than $0.1\,\%$, and $0.03\,\%$ if averaged. Small β ratios are as expected less sensitive as higher β ratios.

The influence of geometry parameters of orifice plates, the influence of the flow conditions including swirling flows and turbulence, and the influence of pressure taps are still being subject of study. But for the present application, the question is not about establishing a more accurate orifice plate description, but to determine if a given geometry and pressure measurement system can deliver reproducible results at the ideal conditions present in a primary flow calibration laboratory.

Given that reproducibility measurements at this level have not been performed yet, it is one aim of the present work to determine experimentally if an orifice plate can be used to validate the uncertainty of a flow calibration facility.

1.4. Comments on uncertainty estimation

The uncertainty estimations declared by calibration and verification laboratories can be used for different purposes. They might be used for trade to reduce the risks taken by suppliers and cosumers, they might be also used for reducing the statistical variability of a process, or in some cases, they might be used as a weighing factor for applying further optimization methods to increase safety and production. This is the case in power plants, where uncertainty values might be used for further optimizations as described for example in the VDI-2048 [VDI00] and [VDI03]. In this particular application, the risk of underestimating uncertainty is as relevant as overestimating uncertainty as exposed in [Cor11b]. In the present analysis, uncertainties are rather overestimated, since uncertainty declaration in applications for power plants require typically a speciallized approach on calibration and uncertainty estimation.

Considering the uncertainty declared for flow comparisons, no comparison trial would deliver any useful results if the uncertainty estimation of the flow test rigs were not correct. But from the other side, if there were no interlaboratory comparisons, errors in the estimation of the uncertainty would not be detected.

For the estimation of the reference value of a comparison, the weighted average of the participants is calculated. The weight for this averaging is the inverse of the reported variance. Consequently, a wrong estimation on the uncertainty of a laboratory would have consequences on the final result of an interlaboratory comparison[2]. Neither under- nor overestimation are correct.

An interesting approach was introduced by the concept of the harmonized cubic meter [Ben15]. The high pressure gas flow laboratories of three European NMIs joined in an effort to realize periodical interlaboratory comparisons. The big difference is to the approach of the MRA: they use the result of the comparison not only to make qualitative judgments of consistency and equivalence, they use the encountered differences as an evidence of the presence of unknown systematic biases. Consequently, they applied the corrections d_i to their measurement results, which had also the effect to reduce their uncertainties down to the magnitude of the reference uncertainty.

This approach can not be unconditionally applied to every comparison, a requirement is that the estimation of the uncertainties are fully compatible, neither under- nor overestimated and that the correlation between laboratories is thoroughly known. Additionally, correcting for unknown systematic effects is risky, since its causes might also change in time; this could be solved by repeating measurements periodically[3].

The guide for the expression of the uncertainty in measurements ([GUM08]) provides enough tools to estimate uncertainty of a given model. It is the generation of the model, and all the simplifying assumptions that may lead to errors and discrepancies. One international recommendation dated from 1980, the DIN EN ISO 24185:1993 [ISOa], is still used as a basis for the estimation uncertainty of flow test rigs worldwide. It

[2] In this case, it is not possible to separate the uncertainty as an indicator of quality or confidence, and the measurement value as the real value to use. The uncertainty determination has a direct influence into the measurement value

[3] This principle is used also in the process and power plants, and is called data reconciliation. Data reconciliation compares basically redundantly generated measurement values, and determines the distance to the value that minimizes the root mean square. This correction is applied and consequently the variance is reduced. In on-site applications, where there are no uncertainty budgets for all relevant values, and where laboratory conditions can not be met, the use of such an approach is questionable

considers enough details to reach an expanded uncertainty of 0.1 % but for higher water temperatures, and uncertainties under this limit a more detailed analysis for each of the uncertainty contributions mentioned in the ISO recommendation is necessary.

In 2012, the working group of fluid flow of the Consultative Committee for Mass and Related Quantities (CCM), established guidelines for the submission of CMCs. The discussions held were about the way uncertainties are reported: It was finally stated that it is not only necessary to analyze the uncertainty of the flow test rig itself, but also of the calibrated flow meter. The repeatability of the calibrated flow meter alone, i.e., independently of the flow test rig, should be included into the uncertainty budget.

The repeatability of the flow meter alone is recommended to be determined by correlation methods. Poeschel [Poe99], based on the work of Hayward [Hay77], introduced a correlation based method, where two flow meters are calibrated simultaneously. By adding and subtracting the results, and calculating the observed standard deviations s_+ and s_-, the unknown systematic effects of the flow test rig responsible for the random-like variations would cancel out if subtracted, and doubled if added. This principle allows to extract these non-systematic effects that cause repeatability. The standard deviation of the laboratory alone is given by: $s_p = \sqrt{s_+^2 - s_-^2}$. Considering that in order for the variance of the sample variance to reach an accuracy of 20 % about 200 measurements are required, in order for this method to deliver adequate results highly repeatable conditions for these 200 measurements are necessary, but this would only reduce and not eliminate the risk of getting imaginary and/or wrong results. An alternative method is presented later on in [Cor15b].

1.4.1. Comments on reproducibility

The influence of non-controllable-inputs on a measurement instrument is typically estimated trough black-box analysis: The standard deviation of several trials where different non-controllable-inputs have been systematically varied is computed. This standard deviation is denominated reproducibility. As non-controllable-inputs the VIM [VIM08] mentions the influence induced by a different operator, by a different location or by a different apparatus.

Reproducibility is an incomplete description of a measurement system since it depends on the way it is determined. Reproducibility should be used with care to describe the limitation of an experiment, of a laboratory or of a measurement instrument to control or to compensate for influence quantities. Repeatability is estimated similarly as reproducibility, but in this case all controllable-inputs are kept constant. Key concepts and interesting discussion on an adequate definition of the concepts of reproducibility and measurement conditions related to comparisons are are given in [Bar08] and [Pav07].

1.4.2. Validation

Validation can be performed by comparing the measurement results of the same measurand but obtained using different models, different laboratories, or different conditions. For the validation to be successful, the obtained results should be consistent within the uncertainty declarations. The ratio between the distance between two measurement results related to the uncertainty of this distance is called normalized error. In cases where there is more than one result, a reference value is estimated using all

available measurement results. Details on the estimation of reference value and the normalized error are given by [Nie00], [Nie02], [Cox02a], [Cox02b], [Cox07]

For a bilateral comparison, the magnitude of the distance between both results will define if the measurements are consistent or not. For this consistency check the Chi-square test is applied according to the recommendation of [Cox02a]. The paper basically recommends, the use of the inverse-variance-weighted-average as an estimator of the real value if normality can be assumed. This is a result of applying least squares to minimize the uncertainty of the comparison. The observed χ^2 is compared with the theoretical χ^2 for a given confidence requirement, usually 0.05, to accept or to reject consistency.

The condition can be simplified to

$$|d_a - d_b| \leq \sqrt{u_a^2 + u_b^2} \tag{1.3}$$

.

Note that the previous formulations assume the uncertainties reported by the laboratories include the contribution of the transfer standard. Too high transfer standard uncertainty values would not allow any conclusions to be drawn about the laboratories, but only about the transfer standard itself.

1.5. International flow comparisons

International comparisons for high flow rates are rare. The reasons for this are the lack of adequate and robust transfer standards and the large logistic efforts needed to transport safely a transfer standard between the laboratories. The lessons learned during the realization of the flow comparisons during the last decades have been considered during the planning of the actual work and presented partially by [Cor11a] [Cor12]. Details about relevant realized comparisons are given in the following section.

1.5.1. NEL comparison in 1986, 1999 and 2002

Between 1980 and 1986, the National Engineering Laboratory NEL (UK) started and coordinated an international comparison in water flow at ambient temperature [Kin86]. The participants were the Delft Hydraulics Laboratory (Netherlands), the Physikalisch-Technische Bundesanstalt (Germany), The National Research Laboratory for Metrology (now AIST-NMIJ in Japan), Daniel Industries Ltd (USA) and the Hams Hall Calibration Centre (UK). The discharge coefficient of two orifice plates with DN200 and $\beta = 0.5$ were defined as the measurand of the comparison ranging flowrates up to $260\,\mathrm{m^3/h}$ (Reynolds numbers of 0.2, 0.3 and 0.45 E6). Following points were given special attention:

- The influence of the roughness: The spool pieces have been internally painted to avoid changes on roughness
- The flow profile: Up to 15D upstream pipe after a tube bundle have been left to reach good flow conditions
- The drift of the transfer standard: Two flow meters have been measured simultaneously, one before and one after the tube bundle

The data was evaluated graphically using Youden plots. The uncertainty of the laboratories is stated to be around 0.20 %. In order to check for consistency, instead of

analyzing each measured point, a line was fitted trough the results of each laboratory using the relation:

$$C_d = A + B \left(\frac{10^6}{Re_d} \right)^{0.75} \tag{1.4}$$

Considering that the linear term of the Reader Harris-Gallagher equation has the largest weight at larger Reynolds numbers, this simplification seems to be adequate for the aimed uncertainties. The results are reported to be consistent within ±0.25 %; the obtained scattering was attributed to the used orifice plate. This comparison was able to reach the postulated aims; but for the actual uncertainty requirements a better consistency at a lower uncertainty would be necessary.

In 1999 and 2002 the comparison was repeated using orifice plates again and similar characteristics. The participants list changed. The obtained consistency was ±0.2 % and ±0.15 % respectively. Further details are given on [RH99] and [RH02]. Even if the obtained values are closer to the uncertainty declaration of the WZP of 0.04 %, to perform a comparison within ±0.15 % would not justify the validation efforts. If orifice plates are used, excellent flow conditions would have to be reached.

1.5.2. The CCM.FF-K1

In 2003 the fluid flow working group of the CCM started an attempt to proof the equivalence of the water flow rate measurements according to the requirements of the MRA. Two transfer standards were used: a turbine and a coriolis flow meter[4]. The Korean Research Institute of Standards and Science KRISS served as pilot laboratory; the participants were SP from Sweden, the PTB from Germany, National Engeneering Laboratory NEL from the United Kingtdom, the Centro Nacional de Metrologia CENAM from Mexico and the National Metrology institute of Japan.

In contrast to the declaration of the CMCs, the measurement conditions were not clearly defined in terms of flow rate and temperature. Following points were given special attention:

- The influence of mounting and dis-mounting: As part of the measurement program carried out by each flow lab, it was defined to exchange the installation position of the flow meters.
- The flow profile had to be repeatable, however, only 6D upstream pipe were realized downstream of the flow conditioner to produce acceptable flow conditions.
- The drift of the transfer standard: Two flow meters have been measured simultaneously, one before and one after the flow conditioner to detect eventual drifts or malfunctioning.
- The temperature dependence was considered to be implicitly corrected by the flow meter or attributable completely to the Reynolds number.
- The measurement procedure: A very precise step by step guidance of 71 steps was distributed by the pilot laboratory to reduce gross errors during handling.

Instead of fixing the value for flow rate and temperature, the target measurand was defined as the Roshko number. The Roshko number fulfills the relation:

$$Ro = k_r \; Re \; D^3 \tag{1.5}$$

[4] Also an ultrasonic flow meter has been installed at the front of the transfer package, but the obtained data has not been discussed nor made publicly available.

Where k_r is a flow meter constant. The problem of an undefined measurand in terms of flow rate is that if all influence quantities of the transfer standards are not characterized, controlled and considered into the uncertainty analysis, differences in the measurement results, caused by the lack of knowledge of the flow meters would be attributed to the calibration facilities. As a consequence consistency was not reached. Hence, instead of using the weighed average to determine the reference results, a median based approach had to be used. The report for the CCM.FF-K1[Pai07] does not contain information on the exhaustive tests performed, since due to the mis-definition of the measurand, most of the data was of no practical use for the comparison. Engel [Eng09] elucidates briefly the results of the K1 and recommends mainly to use instead of only the Roshko number fixed points for temperature and flow rate.

1.5.3. The CCM.FF-K2

The CCM.FF-K2 [Pat08] was an attempt to proof the equivalence of hydrocarbon flow rate measurements. This comparison benefited from the experiences gained in a previous comparison organized by SP at a European level in 1995 [Lau95]. In both comparisons two flow meters were used: a positive displacement screw meter produced by Kral, and a turbine flow meter. The measurand was defined to be the flow meter Strouhal number:

$$St = f_m \; D^3 \tag{1.6}$$

where f_m is the output of the flow meter proportional to the flow rate. The diameter should be corrected for thermal expansion.

The CCM.FF-K2 has one peculiarity respect to the former comparisons: it uses both approaches: stating the flow rates to be measured but also one Reynolds number. In order to have the results for the desired Reynolds number, five measurements were required in the vicinity of the required Reynolds number; this should allow for interpolation methods to be applied if the exact flow rate and temperature could not be reached. The single Reynolds numbers were used to quantify additional effects of the viscosity into the measurement results of the flow meter. A considerable linear dependency on the viscosity had been detected for both flow meters. By assuming additionally that the effect of viscosity is independent of the Reynolds number, they applied the correction into all flow rate measurements. Only after the introduction of these corrections consistency could be reached. If the assumption could be hold had not been proven.

1.6. Aims and Outline

The first aim is to determine the measurement uncertainty of the higher flow rate range of the WZP.

The second aim is to find general testing strategies to validate the obtained uncertainty estimation by evaluating the consistency of the results prior or even without making an interlaboratory comparison.

The third aim is to perform an interlaboratory comparison to validate the estimated measurement uncertainty.

1.6.1. Research outline

An in depth analysis of the determination of the uncertainty of the WZP is presented in Chapter 2. A special emphasis is given to the diverting system, since it is the most critical component in 3.1 [Cor15b]; a summary of the overall uncertainty budget is given in 3.2 [Cor14b]. 3.2 also introduces the application of the validation methods without involving additional facilities. In section 3.3 the design and characterization of a flow meter for its use as transfer standard is presented as well as the results of a bilateral international comparison. A global analysis of the results and a discussion is presented in Chapter 4.

1.6.2. Central Findings

The findings listed below form the product of this research work:

- In depth uncertainty analysis of gravimetric flow rate facilities for larger flow rates.
- Development of a method to detect biases on gravimetric facilities based on the diverter-error-determination procedure.
- Development of a method to determine the statistical repeatability of a flow rate facility and of the diverter system of this facility.
- Proof that differential pressure flow measurement devices are adequate for high accurate validating of flow calibration results through their direct Reynolds number dependency.
- Determination of the magnitude of the transducer-pocket errors in ultrasonic flow meters.
- Development of a window chamber for simultaneous flow metering and flow profile measurements.
- Validation of the uncertainty declaration of the WZP through a bilateral comparison.

2. Traceability of the flow test facility

Flow rate calibration facilities play an essential role when any process involving flowing media requires traceability. It is not only necessary to have the required technical infrastructure, a very wide variety of tests and vast documentation is required in order to guarantee a flow rate facility is working reliably within the requirements. In the case of National Metrology Institutes (NMI), the overall requirement is the fulfillment of the international recommendation ISO IEC 17025:2005. This recommendation states procedural steps for a laboratory to follow in order to maintain the quality of its calibration services.

Independently of the way a documentation system is kept, the estimation of the uncertainty according to the requirements of the Guide for the expression of the uncertainty in Measurements ([GUM08]) is necessary. As a research laboratory, the fulfillment of the technical requirements of the ISO IEC 17025:2005 constitutes a minimum requirement to use the measurement results for research work.

The uncertainty analysis assumes that no gross errors occur. In order for this assumption to be always correct maintenance and statistical analysis are necessary. The uncertainty budget of the WZP up to a flow rate of $200\,\mathrm{m^3/h}$ has been evaluated in [Mat05]. Mathies showed in detail the different influence factors affecting the accuracy of the flow test rig focusing on the lower flow rate range up to $200\,\mathrm{m^3/h}$. According to Mathies, the most important contribution to the uncertainty factors were the time measurement and the evaporation-related losses. He developed a procedure to detect the timing errors based on the method proposed by the International recommendation ISO 24185:1985 [ISOa]. A more detailed discussion on the methods applied, and substantial improvements on this topic will follow in section 2.4.

Making a transparent and clearly arranged uncertainty analysis is very important. It is straight forward to write a complex equation that includes all contributing factors, only in order to fulfill the requirement of completeness, but if there are too many vaguely organized parameters, it is difficult to understand the relations and focus on relevant components. A trade-off between completeness and clarity has been attempted but without reducing the reliability of the final result.

In the following sections, the analysis of the flow calibration facility will be focused on the high flow rate range up to $1000\,\mathrm{m^3/h}$. The used model is only valid for the WZP, but it can be adapted with reduced effort to other gravimetric flow rate facilities, even for cold water. The most important influence factors that affect the accuracy are statistically analyzed and validated. Historical data acquired for several years form the basis for the analysis for the uncertainty components. For a more detailed description of the hardware please refer to [Mat05].

2.1. The flow meter calibration facility WZP

The flow calibration facility of the PTB has been inaugurated in 2003. It was conceived and built with the main objective of providing legal metrological traceability to the energy measurements based on heat meters, as in district heating for example; but also

with the objective to support the development of new flow meter technologies used in industry and in power plants. Since its creation, it has been subject of constant changes to improve robustness and reliability and to reduce uncertainty. Every introduced change was followed necessarily by an exhaustive phase of characterization in order to ensure the claims of the uncertainty budget and the requirement of 0.04 % expanded uncertainty are being fulfilled.

2.1.1. The working principle

Flow meter calibration facilities have to fulfill two functions at a time. They have not only to be able to measure a flow rate very accurately, but they have also to realize or generate this flow rate within predefined conditions. These conditions may vary depending on the analyzed flow meter, or more specifically, depending on its influence quantities. For most flow measurement principles, the flow profile is the most important influence quantity, but for a gravimetric flow test rig, the influence of the flow profile is irrelevant.

The working principle of a gravimetric flow rate facility is very simple as it can be extracted from Figure 2.1. Basically water is pumped through a flow meter under test (MUT) in a loop until reference conditions have been reached. When the measurement or calibration starts, water is conducted by the diverter almost instantly for a predefined time-period out of the loop into an accumulating weighing tank. The indication of the MUT is logged and totalized. Basically, at the end of this procedure the error of the MUT can be obtained by comparing the total integrated mass and the mass determined by the weighing tank.

The gravimetric principle has the big advantage that it is scalable; the limits are basically set only by the size of the tank and the accuracy of the weighing system, and by the size of the pumping system. There are flow rate facilities measuring down to 1 ml/h based also on this principle as seen in [Dav11], as there are facilities with flow rates above 3000 $\mathrm{m^3/h}$ and a 50 t weighing scale as is the case in the AIST NMIJ described in detail in [Nor09]. Several components can be easily acquired of the shelf, since they are common in industrial processes like closed loop controls for pressure flow rate and temperature. But for the triggering and measurement of time, and for the measurement of mass, unique systems have to be designed and constructed; and as it is the case for every prototype, these have to be continuously improved and optimized. The weighing system and the diverter system are the core components of the WZP for higher flow rates.

The comparison between the two accumulated values can be defined as follows:

$$K = \frac{V_{mut}}{V_s} - 1 \tag{2.1}$$

where V_{mut} is the indication of the meter under test, and V_s the accumulated volume on the tank referred at the conditions of temperature and pressure at the meter under test.

Pulse Triggering

It is usual that more than one meter under test has to be tested at the same time. In this case a one-to-one comparison is not possible. To solve this problem an additional reference meter is introduced. This reference meter is calibrated against the weighing

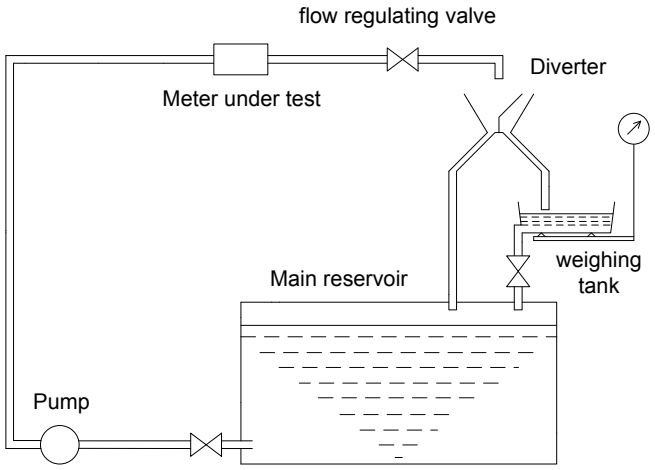

Figure 2.1.: Flow measurement principle and calibration

scale; and as seen in Figure 2.2 the meter under test is calibrated simultaneously against this reference flow meter. The trigger for the calibration of the reference meter is given by the diverter. The diverter is pre-programmed to let a predefined amount of water into the weighing tank and to close the flow into the tank when this amount of water has been accumulated. The trigger for the calibration of the MUT against the reference flow meter, is a pulse of the MUT. A predefined amount of pulses is counted at the MUT. When the amount of pulses is reached, the total count at the reference meter is stored separately. To obtain the highest accuracy, the volume accumulated by the MUT and the water volume in the weighing tank should be the same, but in case a very long calibration is necessary when the MUT has a low resolution it is possible to extend the measurements even after the weighing tank is full. The duration of a measurement should be long enough in order to make random errors due to resolution effects negligible.

In this case equation 2.1 is better changed to:

$$K = \frac{\dot{V}_{mut}}{\dot{V}_s} - 1 \Bigg|_{p,T} \tag{2.2}$$

p and T are usually the pressure and temperature at the meter under test. Depending on the requirements of the application of the flow meter, it might be necessary to extrapolate the actual measurement conditions to some different reference conditions within a small range. Assuming equation 2.2 behaves linearly, in absolute terms, the variances would be related by:

$$\frac{u_{Ka}^2}{K^2} = \frac{u_{\dot{V}muta}^2}{\dot{V}_{mut}^2} + \frac{u_{\dot{V}sa}^2}{\dot{V}_s^2} \tag{2.3}$$

or in relative terms:

$$u_K^2 = u_{\dot{V}mut}^2 + u_{\dot{V}s}^2 \tag{2.4}$$

u_K is the relative uncertainty of the calibration, $u_{\dot{V}s}$ is the uncertainty of the flow rate generated and measured by the flow test rig and $u_{\dot{V}mut}$ is the uncertainty of the

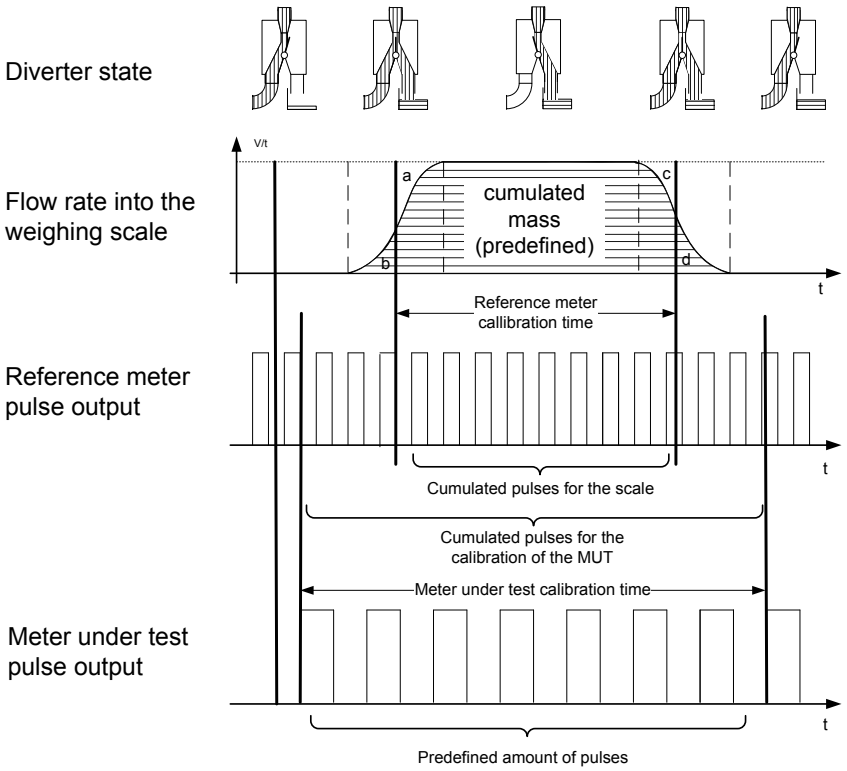

Figure 2.2.: Triggering scheme of the WZP

indication of the meter under test. This last term is normally represented by the flow meters reproducibility (see 1.4.1).

Laboratories have different preferences to express the uncertainty of a calibration. Some laboratories present the uncertainty of the flow test rig and the repeatability of the flow meter separately, and other laboratories present a single calibration uncertainty which contains already both contributions. Given that the focus of interest is the flow calibration facility, only the uncertainty of the flow test rig will be analyzed.

The form of equation 2.4 resulting from equation 2.2 is the most typical form of uncertainty contribution, and will apply to all mass-, density- and time-related contributions. As all sensitivity coefficients are most of the times one or very close to one, uncertainty contributions in relative terms will be preferred.

2.1.2. Functional description of the WZP

The parameters that can be independently set are basically temperature, pressure and the flowrate. Within certain limits it is also possible to vary these quantities dynamically; however, only in a very slow manner, since the installed actuators of the control systems have been optimized to compensate for slow external dynamic influences.

The WZP has been conceived for calibrations at ideal conditions. As ideal conditions we assume a stable temperature within 50 mK, stable pressure within 0.1 bar and a stable flowrate better than 0.5 %. Stable conditions are easily defined and reproducible in different laboratories, in contrast to dynamic conditions that are difficult to reproduce and where the time response behavior of the different components, specially

of the flow meter need to be considered. Most flow meters present a linear behavior under stationary conditions, i.e., error curves run asymptotically towards the zero line. Exposed to dynamic varying conditions, specifications of constant conditions might not be fulfilled.

Another parameter defined as ideal is the flow profile. A fully developed turbulent profile is characterized by its radial symmetry, and by its invariance across the axial direction. As simple as this description might be, the realization is very difficult. The reason are the geometrical characteristics that have to be fulfilled: a diameter straight-length ratio larger than 100, perfectly straight pipes, perfectly round cross section, perfect alignment between sections without any flange missmatch and a constant wall roughness. The experiments made by Mican[Mic99], Eichler [Eic13], [Eic14], Yeh [Yeh94], and Zagarola [Zag98] describe the amount of efforts required to obtain flow reference conditions. Measurement campaigns planned at the WZP to characterize flow meters as seen for example in 3.3 consider the flow profile and the related geometric requirements. However, the uncertainty analysis of the reference value given by the WZP focuses only on the gravimetric traceability.

The main functions

The WZP is a gravimetric flow rate facility with a total capacity of 1000 $\mathrm{m^3/h}$ at up to 90 °C. The main functions are:

To accelerate the fluid against all energy losses due to friction at a constant level. Up to 6 pumps are used to accelerate the fluid from the storage tank through the MUT into the weighing tank, or back to the collection tank. The water between the collection tank and the storage tank is pumped with an additional pump station using up to 6 pumps as seen in Figure 2.3. This allows the regulation of the outlet pressure of the storage tank by introducing an overflow based constant water level system, and additionally by increasing the gas pressure inside the storage tank.

To dissipate all the energy losses in form of heat in order to keep a constant temperature. This is realized through a combination of an external Air-glycol and a glycol-water heat exchanger, assisted if necessary by a compressor based refrigeration unit.

To eliminate all gas bubbles that have been trapped while the water was in air contact. This is realized through a cyclonic gas separator.

To avoid evaporation losses. Evaporation can happen only if a concentration gradient is available, consequently evaporation is reduced by minimizing the surface where a large concentration gradient exists and by minimizing advective and convective flows at these surfaces (2.29).

To reduce flow rate and temperature fluctuations. The flow rate stability can be improved if a constant head tank is used; the WZP realized a constant head tank with a height of 12 m for lower pressure requirements. All water conducting pipes are externally heated, or thermally insulated.

The Figure 2.3 shows the main hardware components of the WZP.

2.1.3. Considerations for uncertainty

Even if flow rate facilities can differ largely in size the following factors define the performance of any gravimetric flow test rig:

- The weighing system
- The density of the fluid

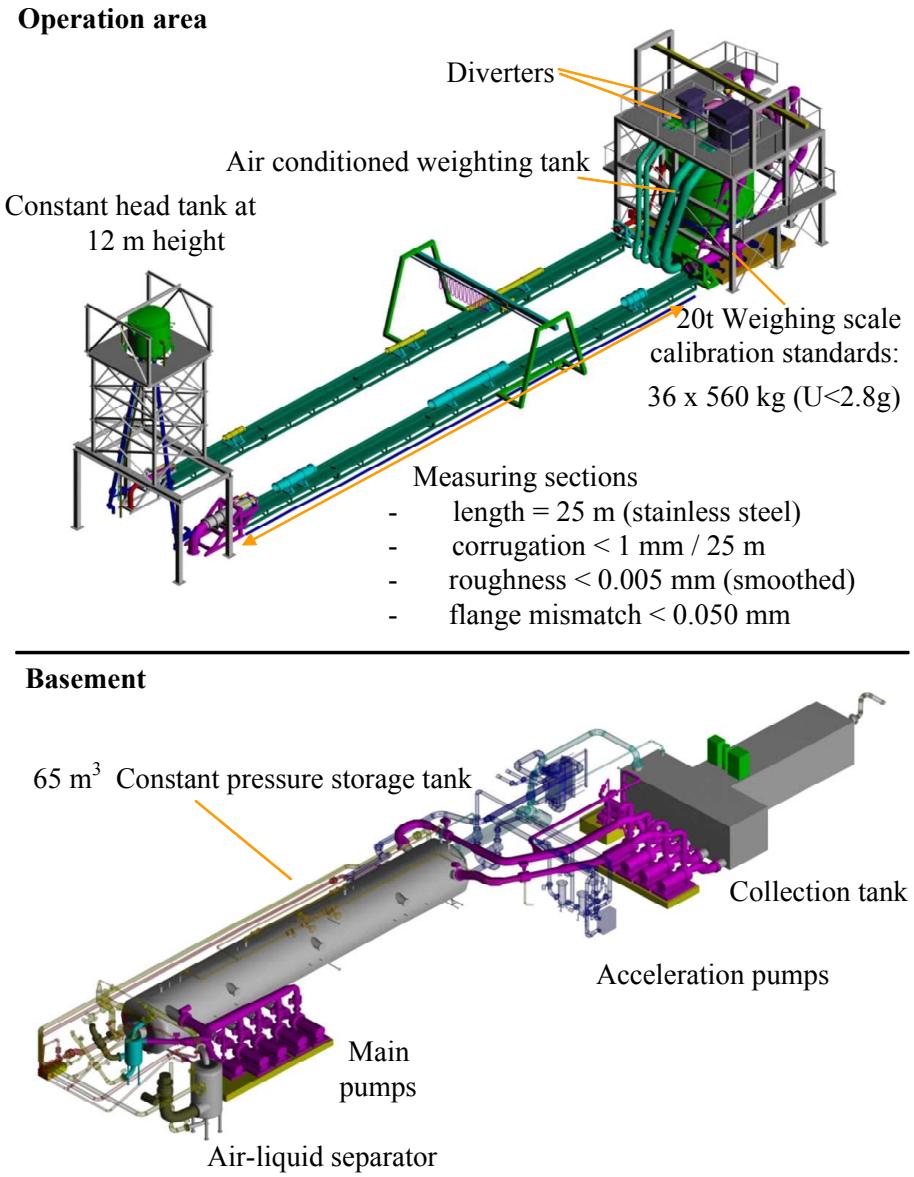

Figure 2.3.: Operational area and Basement of PTB heat meter flow test rig (WZP)

- The time measurement (diverter system)
- Real and apparent loss or gain of water mass

Those influence factors can be collected into the following equation:

$$\dot{V}_s = \frac{W\ k_b\ + \Delta m}{(\rho_w + \Delta\rho_w)\,(t + \Delta t)} \tag{2.5}$$

Where W is the indication of the weighing scale after Tara[1] considering interpolation and calibration correction, k_b is the buoyancy correction, Δm is the compensation for all lost or gained water mass due to evaporation, air entrapment effects, pipe expansion or contraction during the measurement, or changes in buoyancy of the dead weight, due to air density changes. The ideal density ρ is corrected to the actual conditions by $\Delta\rho_w$ and the time t is corrected by Δt to account for a non ideal position of the trigger point in the diverter system.

[1]This assumption will have the consequence, that every measurement starts with an empty tank

Equation 2.5 is well-behaved for the application of the GUM, since the Δ values for mass, density and time will be always significantly smaller than the actual measurand.

Considering equation 2.5 the variance of the flow rate would be given in absolute terms (indicated by the subindex $_a$) by following equation:

$$\frac{u^2_{\dot{V}sa}}{\dot{V}_s^2} = \underbrace{\frac{u^2_{Wa}}{W^2} + \frac{u^2_{k1a}}{k_b^2}}_{Mass} + \underbrace{\frac{u^2_{\rho a}}{\rho^2}}_{Density} + \underbrace{\frac{u^2_{\Delta ta}}{t^2}}_{Time} + \underbrace{\frac{u^2_{\Delta ma}}{\Delta m^2}}_{Process} \tag{2.6}$$

By grouping equation 2.6 and expressing it in terms of relative uncertainties we obtain a very simple form for further analysis:

$$\boxed{u^2_{\dot{V}s} = u^2_m + u^2_\rho + u^2_{\Delta t} + u^2_{\Delta m}} \tag{2.7}$$

Considering there are four main uncertainty contributions making a total of 2×10^{-4}, in order to have an initial rough criteria to discern relevant and irrelevant influences, we can assume a maximum contribution of 1×10^{-4} each.

$$u_i \leq 1 \times 10^{-4} \tag{2.8}$$

Note that due to the simple form of the equation 2.5 all sensitivity coefficients can be assumed to be one as in equation 2.7. This makes it particularly easy to combine different uncertainty contributors. The most frequent type of contributors are distributed following a normal distribution where the standard deviation is the best description. Another also very common type of contribution are randomly distributed within a given interval. In this case the distribution is defined as uniform. The corresponding standard deviation can be estimated with $interval\ width/\sqrt{12}$.

2.1.4. Influence of systematic errors on the measurement results

A very important step during the estimation of uncertainty is the detection of systematic errors. The effects that such errors would have on the measurement results can be observed directly based on equation 2.1 and 2.5. Considering only the main contributor groups we can write

$$K = \frac{\dot{V}_{mut}}{\dfrac{m + \Delta m}{\alpha\rho(t + \Delta t)}} - 1 \tag{2.9}$$

Based on the behavior of a typical flowmeter we can estimate the influence that 10 ms, 1 kg or 0.035 % error in density measurement would have on the shape of the error curve when 4 t and when 20 t total filling mass are used:

In Figure 2.4 we can see that errors made in mass and in time measurement can be easily detected. It is only necessary to determine experimentally the shape of the curve for 4 t and for 20 t. If the obtained curves do not agree, there might be one or several systematic factors affecting the results. If the results are the same for both filling masses no evident systematic errors are present.

In the case of the systematic influence of the type α performing measurements using different filling masses would not influence the shape of the curves, making different strategies necessary as will be shown in section 3.1. This kind of error does not affect only density, but it can accompany mass and time measurements as well.

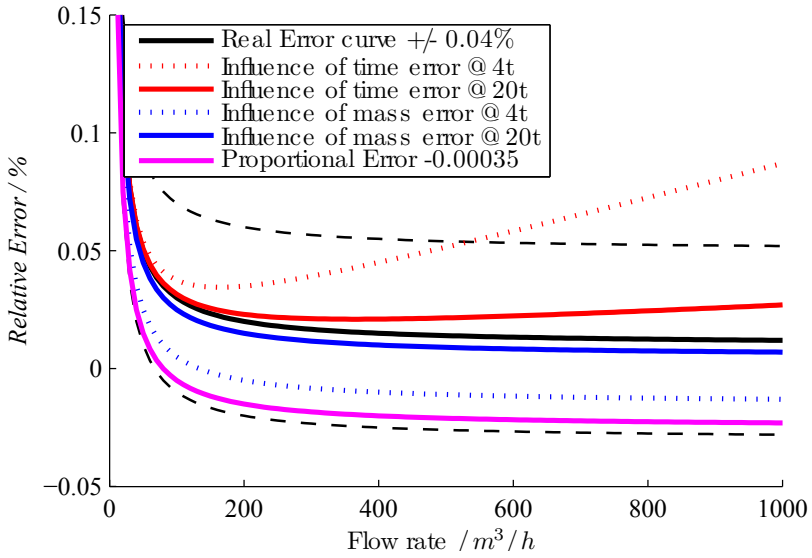

Figure 2.4.: Hypothetical influence of systematic errors on the relative error determination of a flow meter. The effect is shown for 10 ms, 1 kg bias and a proportional error of -0.035%

Uncertainty analysis for gravimetric calibration facilities always consider these three type of influences affecting the end result. Most of them are too small to produce a measurable effect using a regular flow meter consequently a deeper analysis on every uncertainty contributor is necessary.

2.2. The weighing system: Mass determination

The primary weighing system of the WZP is based on four force compensation cells (FCC) with a direct load capacity of 30 kg and more than 1×10^6 scale division[2] each. The upscaling is performed by a mechanical lever system with a ratio of 200. Combined together, they can carry a maximum capacity of 24 t. To obtain the highest accuracy, the weighing system is not used as an independent measurement system, but as a mass comparator: A set of 36 weights with 560 kg mass each are used as a mass standard to make a fully automated scale calibration prior to each measurement if necessary. In order to fulfill the traceability requirements, all weights have been calibrated with an uncertainty of 2.8 g.

It is necessary to maintain the mechanical system under the same temperature conditions during the entire measurement. Not only the surrounding air, but also the weighing system itself has to be in thermal equilibrium. Although the lever system is designed to cancel out temperature effects, uncontrolled temperature gradients may occur and generate variations in the transmission ratio which can influence the actual mass determination. Consequently, it has been decided that additionally to the FCC, a redundant system of 16 strain gauges, four for each FCC are necessary. Although strain gauges have a large temperature dependence and have a lower reproducibility

[2]Scale division is defined in the OIML R76-1 [OIM] as the distance between two consecutive scale marks "d". The term verification interval "e" finds an application only for weighing devices subject to official legal metrology controls

than FCC, the advantage of being independent of the mechanical lever system makes them a good performance indicator as will be shown later on.

Following items define the performance of the weighing system.

- The repeatability and the reproducibility in wet conditions
- The stability of the indication when water is being weighed
- The linearity of the system. Since the weighing scale is calibrated at discrete points but the real measurement points are arbitrary making interpolation necessary.
- The influence of the load distribution on the 4 FCC (eccentricity).
- The buoyancy correction, not directly related to the scale, but to the air conditions during the measurements.
- Temperature influence

2.2.1. Repeatability and reproducibility of the weighing system

The most important performance indicators for a weighing system are its repeatability and reproducibility as defined in the [VIM08]. Repeatability refers to the standard deviation of the measurement results under similar conditions, in contrast to reproducibility which is the standard deviation of measurement results where at least one condition has been varied. Repeatability is relevant when short time intervals between measurement are realizable, for example two consecutive measurements. Reproducibility, takes into account other influences that are not directly quantifiable in a mathematical model, as a different operator, a different temperature, or just a different day. In our particular case, reproducibility is defined as the dispersion of the measurement results, when all known parameters are controlled and compensated for. It is a vague definition of performance, but since not all model parameters can be controlled due to lack of knowledge or due to physical limitations it is the best way to bound the typically occurring influences and estimate the uncertainty of the measurement.

Static load testing

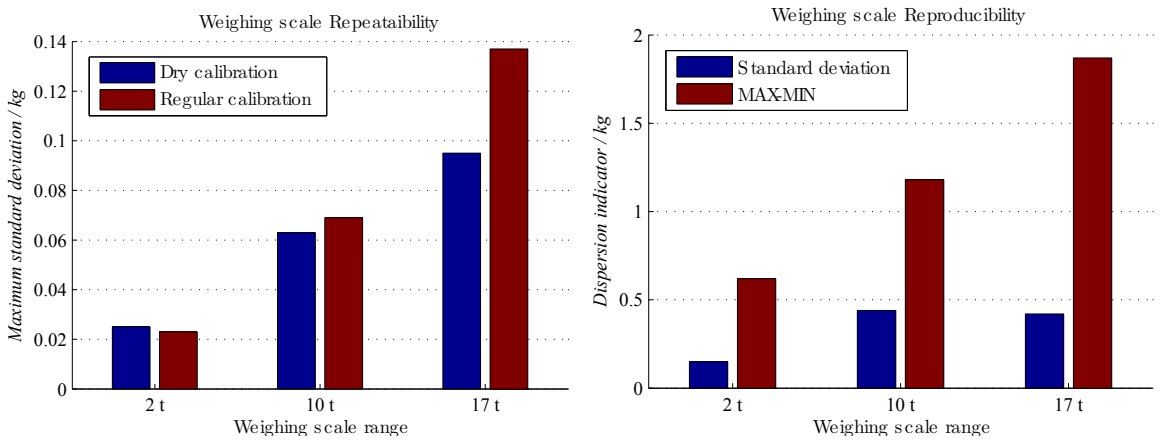

(a) Repeatability of the Weighing system (b) Reproducibility of the Weighing system

Figure 2.5.: Repeatability and reproducibility of the weighing system in wet and dry conditions

Figure 2.5a, shows a comparison between a dry calibration where the weighing tank has been completely dry, and a regular calibration where the tank has been filled and emptied just before the calibration. Only small differences can be found due to eventual water dropping, evaporation or condensation effects. The relevant case to be considered is the wet repeatability, and this only in the cases where a calibration is performed before every single measurement.

Figure 2.5b shows the reproducibility of the weighing system; these measurements have been performed in a time interval of 6 months. All known corrections have been applied, there is no evident correlation with the known influence factors. The difference between the maximum and the minimum indication are also shown. Even if the large difference suggests a strange behavior the normality can not be rejected.

Table 2.1 shows the repeatability and reproducibility of the system for maximum flow rates at large filling volumes. The repeatability is shown only to quantify the influence of evaporation, condensation or eventual dripping. This influence seems to be as high as the dry repeatability itself. Reproducibility is considered only for a loaded system, i.e. from the difference of the initial zero, and the actual measurement result. The zero reproducibility is shown separately and it seems to have no further influence on the overall uncertainty.

Table 2.1.: Repeatability and Reproducibility for high filling volumes

	Parameter	**Uncertainty**	**Total Contribution**
	Repeatability dry[1]	0.095 kg	5.6×10^{-6}
	Repeatability wet[1]	0.135 kg	7.9×10^{-6}
u_{m1}	**Reproducibility[1]**	0.420 kg	2.5×10^{-6}
	Zero reproducibility[1]	0.020 kg	1.2×10^{-6}

[1] Normal distribution

Stability of the system with water loads

During a flow meter calibration, after the weighing tank has been filled, the water inside the tank continues moving causing some oscillations in the weighing scale indications. A special construction has been realized in order to minimize waves and splashing within the tank but not all oscillations can be avoided. Figure 2.6 shows the stabilization times for different filling levels. For this characterization low temperatures below 40 ℃ have been chosen, in order to minimize temperature effects.

Figure 2.6a shows that for filling volumes for the middle and the upper range, the oscillations cease at a time about 150 seconds after flowrate has been stopped. The stability criteria is defined in terms of the standard deviation of the last measurements, when its value is less than 0.050 kg the system stops weighing and stores the indication for further processing. A separated analysis for this standard deviation is not necessary, since it is guaranteed that the threshold has been reached. In case stability is not reached within a predefined time interval, a time-out error is displayed; in this case the measurement result is marked as failed.

For the case of lower filling levels as seen in Figure 2.6b the stabilization takes clearly longer, but the requirement of 0.050 kg is also kept, consequently we can apply for the whole range:

$$\boxed{u_{m2} = 0.050\,\text{kg} \quad (2.9 \times 10^{-6})} \tag{2.10}$$

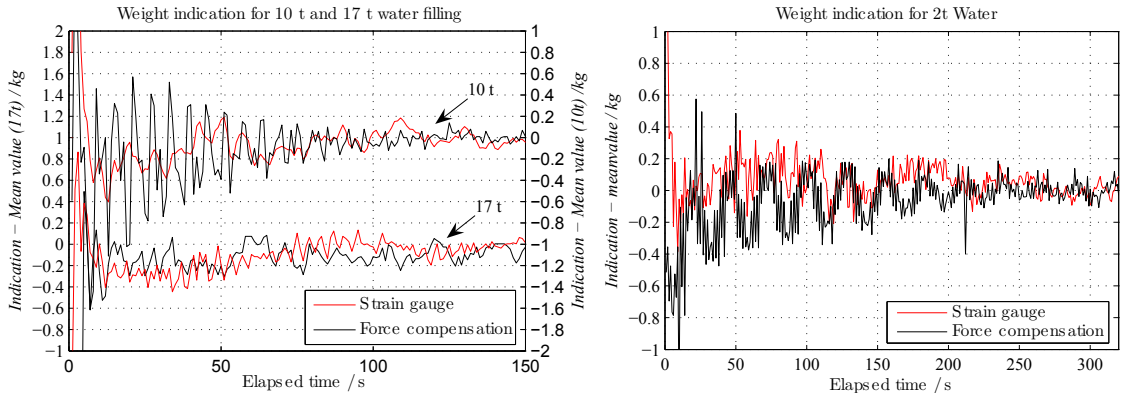

(a) Stabilization of the indication for 10 t and 17 t of water

(b) Stabilization of the indication for 2 t water

Figure 2.6.: Different stabilization times at different water filling volumes

Temperature drift of the force compensation cells FCC

The temperature effect due to buoyancy and the temperature effect on the electronic components of the FCC can not be easily separated. For this reason one FCC has been unmounted and analyzed separately in an climate chamber[3] using a 5 kg weight directly loaded on the cell. The FCC has internal algorithms to compensate for temperature effects when TARA is used, but since the temperature might vary during two TARA procedures, this influence has to be taken into account considering the maximum temperature variation within the weighing scale chamber during one measurement. The effect has been detected to be 0.140 $^{\text{kg}}/_{\text{K}}$ for 1000 kg. Figure 2.7 shows the temperature effects with and without buoyancy correction on the 5 kg weight. According to historical data, the typical maximum temperature variation during one test is 0.12 K. Considering all FCC have been produced in the same conditions, the same temperature influence will be assumed. The total effect can be considered proportional to mass. Considering additionally that the effect would influence the result as an uncorrected bias, the contribution assuming the maximum load would be:

$$\boxed{u_{m3} = 0.336\,\text{kg} \quad (1.98 \times 10^{-5})} \tag{2.11}$$

2.2.2. Linearity interpolation and eccentricity

Full-range linearity

In an ideal case, the weighing scale would deliver a signal directly proportional to the mass, but in reality, there are small deviations to this ideal behavior. These deviations are varying very slowly, and have to be controlled periodically. The result of such a control is shown in the blue curve of Figure 2.8. The effect of reproducibility and repeatability do not affect the linearity tests, since mean-values are used, and not a single result as is the case for a flow meter calibration. Unfortunately, the linearity can be checked only at discrete points. For the points in between, where no calibration

[3]The results of this measurements have been obtained when the WZP was being validated the first time in 2003, a detailed documentation had been prepared. Due to mechanical reasons, it is impossible to repeat this experiment without taking risk of damage of the system

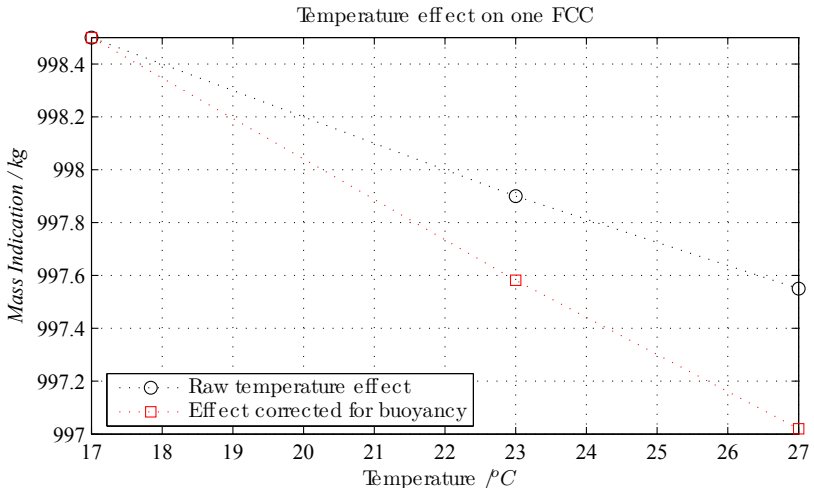

Figure 2.7.: The figure shows the temperature effect on a FCC obtained through artificial temperature variation in a climate chamber. The load has been applied directly to the FCC without a lever system. The drift is compensated for if TARA is applied, but since the FCC is being loaded by a standard weight for this test, buoyancy effects have to be corrected. The red curve is corrected for buoyancy effects

can be performed the correction has to be interpolated. In the case of the WZP, the two calibration points closest to the aimed filling mass are obtained just before the measurements. These points are used to apply a linear interpolation. As shown also by the green curves in Figure 2.8 the error made by considering only two contiguous points resulting in piecewise linear interpolation, is comparable to the quadratic interpolation using all points, which is the best fit for this particular case.

The reason for a quadratic interpolation to deliver the best results is not clear, but since the required accuracy levels are reached by a piecewise interpolation no further analysis is required. There are some cases in which building a model of the weighing system as performed by [Agu12] is necessary, for example in the case of dynamic weighing where the weighing system is used as an instantaneous flow meter, but in the present application, since the influence of reproducibility (see Table 2.1) is much larger than the effect of interpolation, the benefits of a closer analysis would not be perceived.

The Figure 2.8 shows the interpolation error for any amount of weighing standards, if compared with the piecewise interpolation between the two contiguous weights. The size of the mass interval of 1120 kg between points is twice the largest weight difference from a calibration point; therefore, the actual error is expected to be lower than the drawn value. An attempt to make a calibration with steps of 80 kg using 20 kg mass standards is shown in the Figure 2.8. The interpolation and linearity error are considered to be uniformly distributed in the interval $\pm 0.100\,\mathrm{kg}$. Formally, to estimate the uncertainty of interpolation it would be necessary to consider the reproducibility and the resolution, but since the sensitivity of the correction for the magnitude of the reproducibility and resolution is infinitely small, these effects will be neglected.

$$\boxed{u_{m4} = 0.058\,\mathrm{kg} \quad (3.41 \times 10^{-6})} \tag{2.12}$$

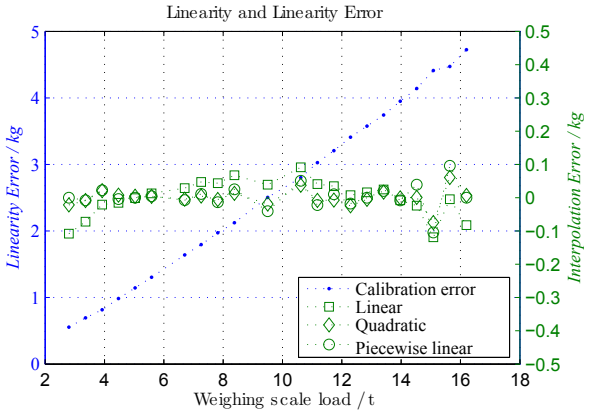

Figure 2.8.: Absolute error in kg at the different calibration points (blue curve). The error given due to three different interpolation algorithms is also shown (green curves)

Short-range linearity

Short-range linearity is also a topic of interest. How can one guarantee the system is well behaving, i.e., linear between two calibration points? In order to validate this, standard weights have been loaded by hand in 80 kg steps on the weighing system[4]20 kg on each corner. The results are shown in the Figure 2.9.

The linearity between two single points can be seen as confirmed, since all 3 lines at 5t, 10t and 15t behave linearly. However, the different angles of these curves, and also of the ideal curve (full line) are irritating. This effect can be considered to be already included as a part of reproducibility. The presence of personal within the weighing area and the unsteady and not repeatable conditions of a loading by hand are causing the weighing system to spread.

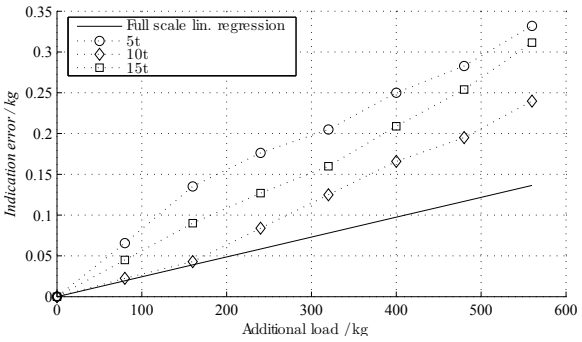

Figure 2.9.: Absolute error in kg at the different points within two calibration points in 80 kg steps. A full scale linear regression is also displayed.

[4]The measurements have been performed during the initial characterization of the weighing system in March 2006.

Eccentricity using static loads

If it would be possible to calibrate each FCC together with the lever system independently, every FCC would have a different behavior[5]. In the best case, the errors would cancel out mutually through averaging. But in case the linearity of at least one FCC is different from the others and a distinct load distribution is present through an asymmetric mass loading, a difference in the indication would be expected when loading the same mass in a symmetrical way.

The comparison of the loads indicated by symmetrical loading using multiples of 560 kg and the loads when using the 20 kg mass standards is shown in the Figure 2.10. The maximum difference is at 15 t and is about 0.04 % or 6 kg.

By doing an eccentricity test using a 20 kg mass standard on each corner, a repeatability of 0.015 kg is found, with an average error of 0.003 kg. This result let us conclude that asymmetric loading is not the cause for the differences obtained in Figure 2.9 since the error is far larger than 0.003 kg. It was not possible to determine what is the reason for the error of 0.2 kg. It can not be attributed to the asymmetric loading. And since this effect can not be attributed to any other component, an additional uncertainty component *bias* will be added. A uniform distribution is considered, since 0.200 kg was the largest difference found. A uniform distributions assumes equal probability for every value up to 0.200 kg.

$$\boxed{u_{m5} = \frac{0.200}{2\sqrt{3}}\,\text{kg} = 0.058\,\text{kg} \qquad (3.41 \times 10^{-6})} \tag{2.13}$$

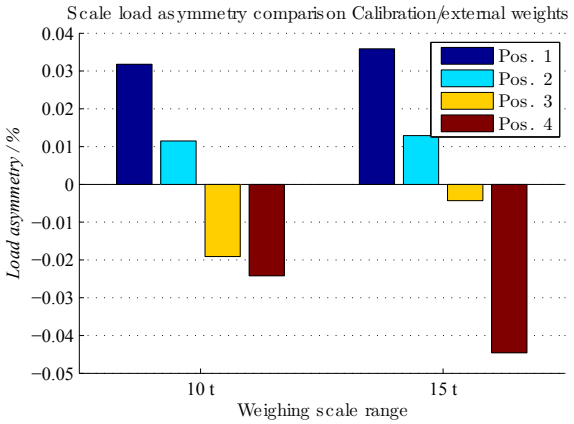

Figure 2.10.: Difference in % of the actual load per single corner that is measurable between the calibrations using the external weights, and calibrations using the internal standards

Eccentricity for water loads

The difference between two different mass standard combinations have been tested and proven to be insignificant. But how large would be the asymmetry when comparing fillings using water and the calibration standards? The Figure 2.11 shows the found differences in percent. Additionally the results for the strain gauges are drawn.

[5]Calibrating each cell without the mechanical lever is not possible, since the FCC is fixed on the lever system

If the results of the strain gauges and the FCC are compared, both, the test for 10 t and the test for 17 t indicate that the mechanical lever system is working properly. The differences on the lower range are caused by a real asymmetric distribution, or due to non-linear behavior of the strain gauges. Since the considered focus is concerning higher flow rates with higher filling volumes, this problem has no further consequences.

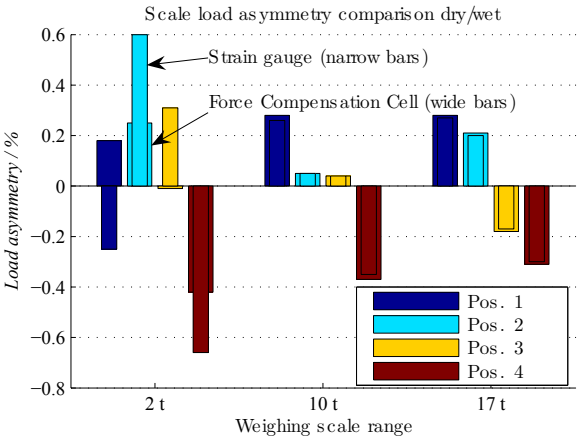

Figure 2.11.: Difference in % of the actual load per single corner that is measurable between the loading using the internal standards, and using water. The differences are shown for the strain gauges and force compensation cells

The load asymmetry is as high as 0.4 % or 68 kg fro 17 t. If for a 20 kg mass there is a bias of 0.003 kg, the corresponding effect on 68 kg would be 0.0102 kg, far less than the overall repeatability or reproducibility. The influence of eccentricity will be neglected.

By comparing the result of the group of 16 strain gauges and four FCC the difference encountered were between 0.15 kg and 0.78 kg this result might encourage to confirm the effect of total effect of eccentricity to be caped by these values, but since the linearity error of the strain gauges is larger than 2 kg no additional information is encountered.

A good way to monitor changes of the weighing system is to display the gravity-center of the load in a 2D-plot as the shown in Figure 2.12. Even if the scale calibration is not showing any strange results, having a look on the gravity-center plot might give direct information on the health of the mechanical lever system. As for example during 2012 where maintenance was required. The error was detected by observing the gravity center moving out from its typical position.

2.2.3. Buoyancy correction

The buoyancy force acting on the weighing tank for maximum filling conditions and an air density of up to1.23 $^{kg}/_{m^3}$ is about 27 kg or 0.16 %; i.e. this effect has to be compensated for. The buoyancy effect can be divided in two parts: the buoyancy acting on to the filled water, and the buoyancy acting on the dead weight of the tank. If the air density during the scale calibration and during flow meter calibration are the same, there is no buoyancy corrections necessary for the dead weight. Buoyancy correction fluctuations due to the dead weight will be considered in section 2.5

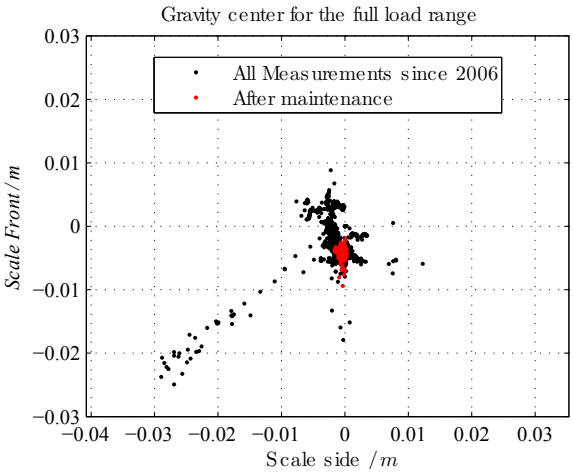

Figure 2.12.: The figure shows the position of the gravity center of the load for the full weighing range before and after maintenance.

The buoyancy correction for the filled water depends basically on the densities of the participating components during calibration and during measurement. The equation has the form:

$$k_b = \frac{1 - \frac{\rho_{as}}{\rho_{ws}}}{1 - \frac{\rho_a}{\rho_f}} \tag{2.14}$$

where ρ_{as} is the air density during the weighing scale calibration, where ρ_{ws} is the weight density during the weighing scale calibration, ρ_a is the air density during measurements, and ρ_f is the air density of water during measurements.

Air density is not measured directly, but indirectly through temperature, absolute air pressure, and air composition. There are two air components that affect air density significantly, those are carbon dioxide and water vapor. Humidity is being measured directly, but for carbon dioxide in our application its enough to make an estimation. The calculations for air density are performed according to the recommendation of the BIPM [Pic08] based on temperature, pressure and humidity measurements.

If instead of measuring all parameters in real time, we assume fixed values together with their typical maximum dispersion, the largest error with a (100% confindence) that would be caused would amount to $12{\times}10^{-5}$ which in the case of the WZP, is an argument to apply real time corrections.

The distribution of the different influence factors is shown in Table 2.2. The influence of the parameters of the same quantity is being grouped. Actual temperature and humidity are very difficult to estimate accurately, since air movement is impossible to avoid completely. Historical data has been used to estimate the maximum variation of temperature, pressure and relative humidity for a typical calibration duration.

The remaining uncertainties in the buoyancy correction in absolute and relative units are summarized in Table 2.2 on a standard level. The last column indicates their relative contribution to u_{m6}.

Table 2.2.: Buoyancy correction uncertainty budget

	Parameter	Uncertainty	rel. Uncertainty	Contribution/%
	Air temperature[2,3]	0.12 °C	5.4×10^{-7}	13.5
	Air pressure[2,3]	0.18 mbar	2.2×10^{-6}	55.8
	Relative humidity[2,3]	5 %	5.3×10^{-7}	13.4
	Water density[1]	0.05 kg/m³	1.5×10^{-7}	3.7
	Standard density[1]	100 kg/m³	5.5×10^{-7}	13.6
u_{m6}	**Buoyancy**	0.048 kg	2.82×10^{-6}	100

[1] Normal distribution
[2] Uniform distribution
[3] The contribution considers the first and the second measurement together

2.2.4. Total uncertainty in mass determination

Table 2.3 presents an overview of all relevant uncertainty contributions with their relative importance. Note that u_{m1} and u_{m3} matter most.

Table 2.3.: Mass uncertainty budget for 17 t

	Parameter	Uncertainty/kg	rel. Uncertainty	Contrib./%
u_{m1}	Reproducibility[1]	0.420	2.47×10^{-5}	58.6
u_{m2}	Water load[1]	0.050	2.94×10^{-6}	0.8
u_{m3}	Temperature effect[1]	0.336	1.98×10^{-5}	37.5
u_{m4}	Interpolation[2]	0.058	3.41×10^{-6}	1.1
u_{m5}	Bias[2]	0.058	3.41×10^{-6}	1.1
u_{m6}	Buoyancy[1]	0.056	2.82×10^{-6}	0.8
u_m	**Mass**	0.548	3.22×10^{-5}	100

[1] Normal distribution
[2] Uniform distribution

2.3. Water density

Water is the fluid which density is best known and studied. Due to its easy availability and due to the low technical resources necessary for purifying it, it is universally used as a density reference material in laboratories worldwide. There are several semi-empirical equations that allow its calculation as a function of temperature with a declared accuracy level up to 1 ppm. The water used as working fluid in the WZP is not ideal water; it is specially filtered and purified but its not pure since it is treated with additives. Additives are necessary, since pure water is not conducting and, therefore, not compatible with the working principle of magmeters. Additionally, for the use of LDV methods, solid tracer particles are added. Tracer particles with a size of up to 12 µm with a density close to water are added in a ratio of less than 1 ppm. In order to determine the influence of such additives in water, probes are periodically controlled in the density laboratory of the PTB.

2.3.1. Water density characterization and stability

Control measurements at the primary laboratory for density of the PTB are yearly made with an uncertainty for k=2 of 0.01 $^{kg}/_{m^3}$ for measurements at 20 °C. The test report contains also an interpolation polynomial for temperatures between 5 °C and 90 °C with a declared uncertainty of 0.05 $^{kg}/_{m^3}$. The obtained results can be also used to monitor the contamination level of the used water. The results can be seen in Figure 2.13. The density of pure water, and the deviation of the WZP water for different years is shown. The difference between ideal water, and water from the WZP is around 0.1 $^{kg}/_{m^3}$. By using the provided polynomial no additional correction is necessary. The correction value remains relatively constant with a maximum variation of about 25 ppm for all temperatures as it can be seen in Figure 2.14.

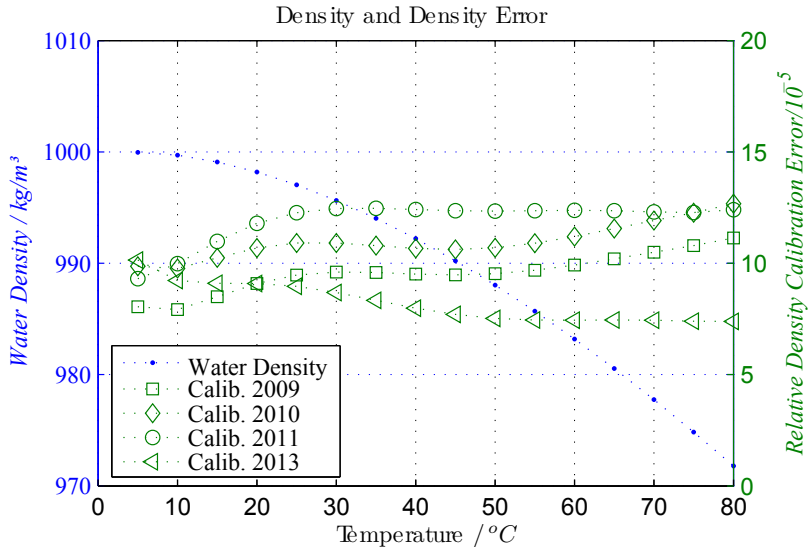

Figure 2.13.: Water density calibration results over 4 years. The blue curve represents the density of pure water as a function of temperature at 101325 Pa absolute pressure; the green curves represent the difference determined from the test report relative to the ideal density for temperatures between 5 °C and 90 °C. The uncertainty of the calibration is 50 ppm for k=2

The uncertainty for the density calibration for the entire temperature range including the influence of contamination for one year can be assumed not to be larger than:

$$\boxed{u_{\rho 1} = 5.0 \times 10^{-5}} \tag{2.15}$$

2.3.2. Influence of temperature

As seen in Figure 2.13, the influence of temperature into water density increases whit temperature. The maximum steepness is given at the maximum temperature of 90 °C and is about 0.67 $^{kg/m^3}/_{K}$. Considering that water temperature measurements at the WZP are realized with an an uncertainty of 15 mK[6] and assuming the temperature

[6] A detailed description of the temperature measurement system is given in [Mat05]

gradient between the temperature sensor and the fluid is neglectable[7] the uncertainty due to temperature errors can be assumed to be maximum 0.01005 $^{kg}/_{m^3}$.

$$\boxed{u_{\rho 2} = 1.01 \times 10^{-5}} \tag{2.16}$$

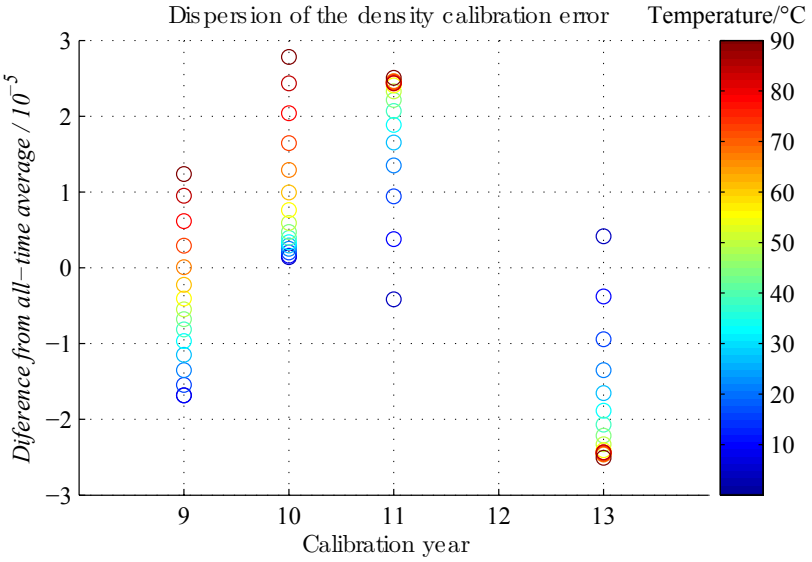

Figure 2.14.: Found deviation of the periodic density measurements from the historic mean value at various temperatures

2.3.3. Pressure dependence of water density: compressibility

The polynomial given by the test report is valid for atmospheric pressure only. But since water is compressed up to 5 bar at the position of the meter under test, the density variations due to pressure have to be considered. The compressibility factor resulting from the recommendation of the IAPWS 97 [IAP07] is shown in Figure 2.15. As it can be seen, the compressibility is also dependent on pressure and temperature. If the mean value of 4.35×10^{-5} is used for simplicity, an additional uncertainty of 0.5×10^{-5} has to be considered.

$$\boxed{u_{\rho 3} = 0.50 \times 10^{-5}} \tag{2.17}$$

2.3.4. Dissolved air

Another condition that varies between the measurements in the laboratory and in the real application in the WZP is the content of dissolved gases. Several authors ignore the relevance of its effects, but considering the measurement results obtained for air-saturated water from the WZP at 20 °C and the same degassed sample of water also at 20 °C where is a clear difference of about 0.007 $^{kg}/_{m^3}$ is found this effect can not be ignored. These measurements were performed almost at the same conditions at the same time, with the same equipment and by the same operator, the uncertainty of the

[7] Temperature measurement points are optimized through adequate depth, geometry and insulation to guarantee the temperature gradient can be ignored for flow rate working interval

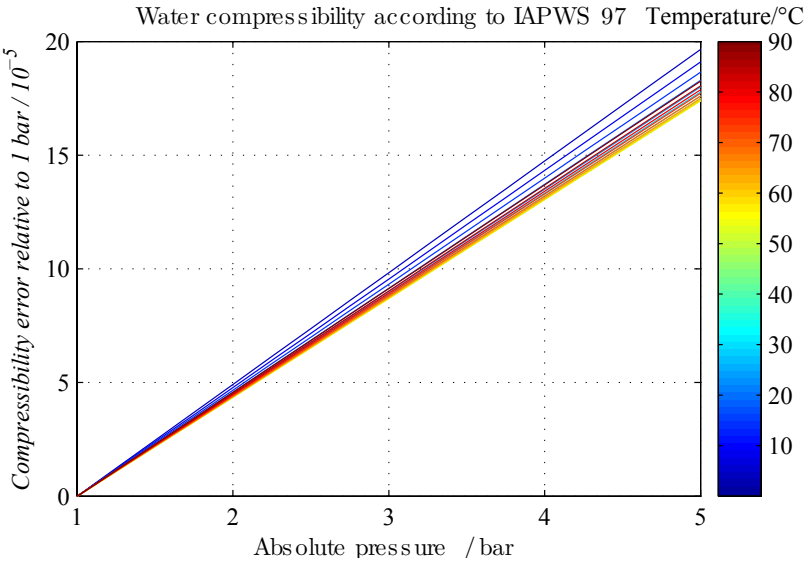

Figure 2.15.: Compressibility of water as a function of pressure

difference is largely correlated and, therefore, the uncertainty is much lower than the declared $0.010\,{}^{\mathrm{kg}}/_{\mathrm{m}^3}$.

We can not assume that the differences encountered in the density laboratory are applicable for all measurements, since the amount of gases dissolved in water is not constant across the process, since temperature and pressure are varied constantly. And given that solubility of air into water increases with pressure, additional analysis will be necessary.

Water is stored in a $65\,\mathrm{m}^3$ tank before its pumped through the test lines; if micro air bubbles are present, due to the increment of pressure in the pumps, these bubbles might dissolve partially, even before they get to the cyclonic-phase-separator installed between the pumps and the test lines. The pressure falls slowly across the pipes and piping accessories until the flow control valve, where the largest pressure drop takes place; at this point the dissolved air becomes to microbubbles since water can not hold any more all dissolved gas.[8].

All water density measurements with high accuracy considering the influence of dissolved air have been made at atmospheric pressure, since there is no practical application to this knowledge. But for studies related to ocean water, the air-water interaction, also depending on temperature and pressure are in the focus of study. Mao [Mao06] proposed a new model to estimate the properties of a Water-NaCl-Nitrogen system under different temperatures, pressures and NaCl concentrations at high accuracy. The proposed model is also capable of predicting water-nitrogen systems. Figure 2.16 presents the induced density variations due to Nitrogen dissolved in water. The effect might be even larger for air, since oxygen is not being considered.

From figure 2.16 the maximum density error due to dissolved nitrogen would be 7.2×10^{-5}, the maximum slope is $1\times10^{-5}/bar$. Engel [Eng12] considers an even lower effect.

[8]If cavitation is happening before the control valve, microbubbles might be created before, which would change the density of water more dramatically than in its dissolved state

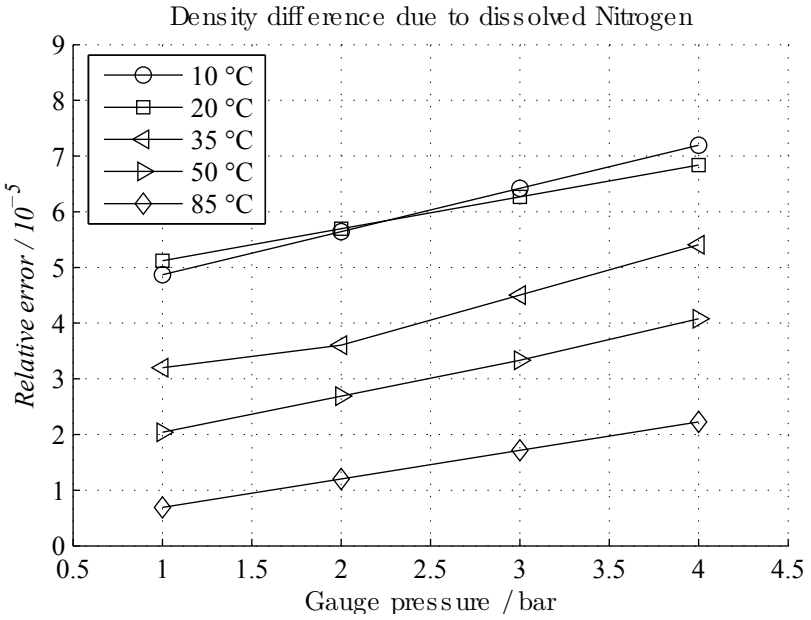

Figure 2.16.: Influence of dissolved nitrogen to water density, when phase equilibrium conditions prevail

2.3.5. Further contributions

An increment of pressure increases water density. The pressure dependency is about $1\times10^{-5}/bar$. How much nitrogen would be necessary to produce the actual offset on water density of the WZP? For the measurements of density at the laboratory at 20 °C and 1 bar absolute pressure, the volume necessary to induce the observed difference would be 15 mL (20 mg). For water at 5 bar and 20 °C the volume of nitrogen necessary would be about 70 mL at 1 bar per kg water or 7 % of the pumped flow rate.

It is not possible that such amount of air would be sucked into the test line, since special care is taken in order to guarantee a constant inlet pressure; even in the form of microbubbles, such a big amount of microbubbles would not remain undetected. Only a specially designed pumping system would allow the introduction of such amount of air.

On-line density measurements at the pressure conditions of a regular calibration would be the best method to validate the fluid density including the influence of dissolved air, but there is no measurement technology available to monitor the density at the required accuracy level and the temperature and pressure conditions. Theoretically, it would be possible to evaluate if pressure differences and consequently density variations would produce at least the same expected slope of $1\times10^{-5}/bar$ but there is no flow meter capable to discern this small variations at the required flow rates. Therefore the worst case will be assumed for a uniform distribution within the limit of 7.2×10^{-5}:

$$\boxed{u_{\rho 4} = 2.07 \times 10^{-5}} \tag{2.18}$$

2.3.6. Gas bubble content

As mentioned in the previous section, when cavitation occurs dissolved air might be extracted and form micro bubbles. These bubbles represent a volume that is being

wrongly measured by volumetric flow meters but not by the weighing scale producing a bias in the error curve.

If the K-factor for a volumetric measurement is given by

$$K = \frac{V_{mut}}{V_{ref}} - 1 \tag{2.19}$$

and the erroneous K'-factor for a volumetric measurement considering the error caused by bubbles is given by

$$K' = \frac{V_{mut} + \Delta V}{V_{ref}} - 1 \tag{2.20}$$

The correct K factor can be written as:

$$K = K' - \frac{\Delta V}{V_{ref}} \tag{2.21}$$

Figure 2.17 shows the results for flow measurements where cavitation occurs at 20 °C 0.8 bar, 2.6 bar and 4.4 bar for flow rates of 390 m^3/h, and also for a measurement at 160 m^3/h at 20 °C and 1.5 bar, 2 bar, 2.5 bar and 3 bar. This early stage of cavitation can be detected through a characteristic noise. Real cavitation would harm the used equipment. The used flow meters are an ultrasonic flow meter (UFM) and three mag-meters. For the measurements at 390 m^3/h at least 20 repetitions were performed, for the points at 160 m^3/h 5 repetitions were performed. Only mean values are shown. All measurements have been repeated once at different days in order to ensure the absence of unknown influence factors. The measurements are performed using two different diverter systems, and using the same weighing load for each flow rate. The flow meters have different error curves, these curves have been shifted to be coincident at a pressure of 3 bar. This is helpful to make a pressure dependence more easily detectable.

Given that cavitation and consequently ΔV increase when pressure decreases, the tendency shown in Figure 2.17 matches the equation 2.21. Figure 2.17 shows also that at a pressure of about 2.5 bar cavitation ceases and error free measurements can be performed. No uncertainty will be considered, since cavitation is easily detectable. But in the studied cases, even if cavitation occurs, the produced errors are small.

2.3.7. Total uncertainty for water density

The total uncertainty would be given by:

Table 2.4.: Density uncertainty budget

N	Parameter	rel. Uncertainty	Contribution/%
$u_{\rho 1}$	Calibration[1]	5.00 $\times 10^{-5}$	81.7
$u_{\rho 2}$	Compressibility[1]	1.01 $\times 10^{-5}$	3.3
$u_{\rho 3}$	Temp. Meas.[2]	0.50 $\times 10^{-5}$	0.8
$u_{\rho 4}$	Dissolved air[2]	2.07 $\times 10^{-5}$	14.1
u_ρ	**Water Density**	5.53 $\times 10^{-5}$	100

[1] Normal distribution
[2] Uniform distribution

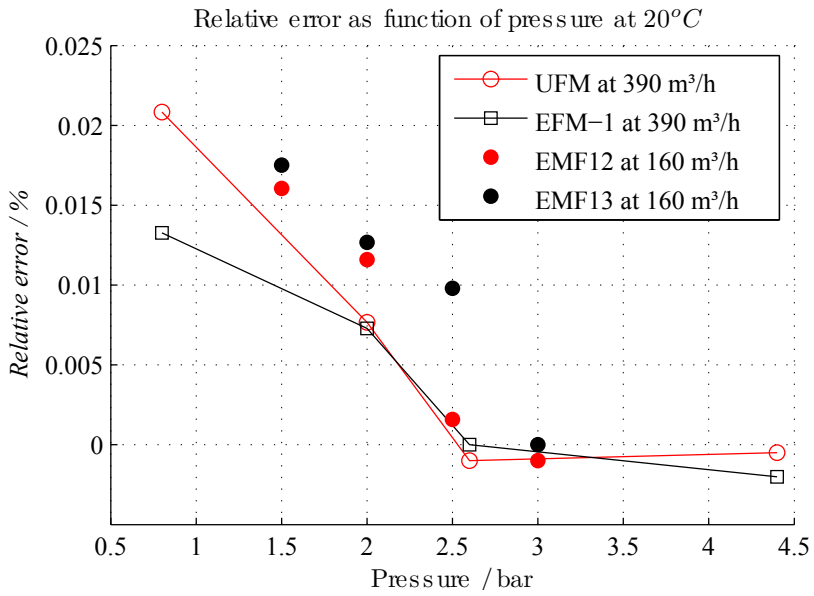

Figure 2.17.: The influence of the gas bubbles with increasing pressure. At higher pressures, the influence of the gas bubbles vanishes

2.4. Time measurement

A diverting system is an open pressure-less two-way-valve. Its most simple representation consists of a blade with one angular degree of freedom within a containment with an entrance at the top, and two outputs at the bottom as represented in Figure 2.18b. The water beam coming from the test lines is directed through a nozzle directly to the rotation center of the blade. Consequently the blade has to withstand fluid forces all the time. In order to reduce splashing, the angles at rest for the end positions of the blade are limited, making larger diverter blades necessary.

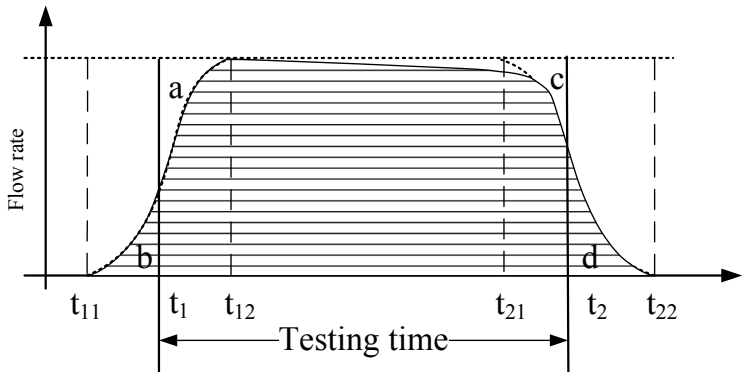

(a) Instantaneous flow rate into the weighing tank

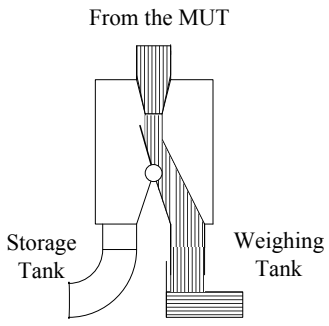

(b) Diverter scheme

Figure 2.18.: The basic function of the diverter can be recognized in figure (a). The accumulated volume under the curve has to fulfill the requirement $a+c = d+e$. Even if the flow rate is not constant. Figure (b) shows a single blade diverter. It can be seen that fluid forces are acting constantly on the blade.

The calibration principle holds for the assumption that the accumulated times for the flow meter, and for the weighing system are known. But since it is impossible to

direct the fluid instantaneously to the weighing tank, a trigger point has to be somehow chosen to measure the time. When this trigger point is not perfectly chosen, a timing error is introduced. Considering Figure 2.18a the error is proportional $(a+c)-(d+e)$.

The diverter system of the WZP

In the case of the WZP basically the same system is used, but instead of using only one diverter system, eight small diverting units are used simultaneously. To reduce the required size of the blades, instead of having the diverting motion actuated by rotation, the motion is performed by the nozzles through translation maintaining the angle between the blade and the flow direction constant, which eliminates the fluid forces acting on the blades. By positioning the nozzles in a radial symmetrical scheme a compact diverter system has been obtained.

Figure 2.19 shows a scheme of the diverter installed on the WZP. Two diverter systems are used, one for the range up to $200\,\mathrm{m^3/h}$ and the other for the flow range up to $1000\,\mathrm{m^3/h}$. The fluid is directed from the bottom to the diverter. The flow is directed there down to the eight nozzles. At each of the nozzles a flow conditioning system with 280 holes is installed. This is necessary in order to obtain a uniform block profile. The trigger point that starts the time measurement and the pulse counting on the MUT is defined geometrically, i.e., for example at 51 % of the total way. It is the same point for both diverting directions. This means that to an early trigger point in the first diverting action corresponds a late triggering point in the final diverting action.

Table 2.5 shows the measurement times, the maximum allowed uncertainty for the given flow rates assuming a maximum relative uncertainty of 1×10^{-4} and the theoretical maximum allowed diverting time, i.e., the time for the diverter to change its position, if no correction would be performed and no knowledge would be available about the dynamics of the diverter motion.

Table 2.5.: Filling time and max allowed uncertainty

Flowrate $\mathbf{m^3/h}$	$\mathbf{L/min}$	**Filling time for 17 t /s**	**Max uncertainty in ms**	**Max. diverting time[1] ms**
100	1667	612,0	61	150
200	3333	306,0	31	75
300	5000	204,0	20	50
400	6667	153,0	15	37
500	8333	122,4	12	30
600	10000	102,0	10	25
700	11667	87,4	9	21
800	13333	76,5	8	19
900	15000	68,0	7	17
1000	16667	61,2	6	15

[1] These values are calculated assuming a triangular distribution and considering no correction is performed.

From Table 2.5 we can see that in order to stay below the established uncertainty limit, it would be necessary to build a diverting system that is able to change its position in less than 15 ms. For small flow rates this is a realizable task, but for larger flow rates, it would be necessary to move massive constructions. This results

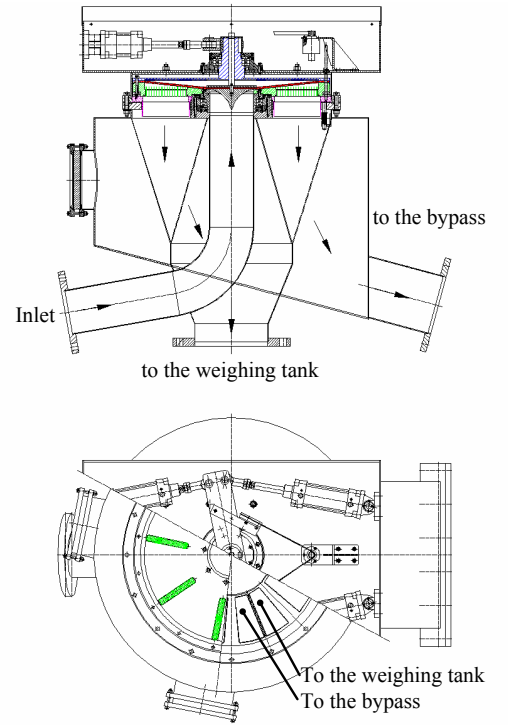

Figure 2.19.: Scheme of the diverter installed in the PTB-Berlin. The working principle is the same as for single blade diverters; the main difference is that instead of using only one blade, several radial positioned blades are used. The fluid is entering the diverting system at the bottom. Water is distributed into the 8 nozzles and directed to the blades. The actuating system consists of four pneumatic cylinders. *Source: Alfons Witt*

in large accelerations forces which require large energy sources and also materials able to dissipate this energy in a short time for a minimum lifetime of some ten thousand times. Consequently, the actual diverting time realizable at the diverting system of the WZP is about 1000 ms compared to the required 15 ms makes clear the importance to apply timing corrections, and to asses the timing error uncertainty contribution.

2.4.1. Previous optimization

In order for the diverter to be error free, following equation:

$$(a + c) - (b + d) = 0 \tag{2.22}$$

has to be valid. There are infinite possible solutions, but the most relevant would be when $a = b$ and $c = d$ (unilateral symmetry) or when $a = d$ and $b = c$ (global symmetry). The curve shown in Figure 2.18a is the instantaneous flow rate directed into the weighing tank. It is influenced by the actual mean flow rate in the flow test rig, but also by the flow profile in the output of the nozzles in close relation to the instantaneous position of the blade (blade dynamics). During an ideal diverter action, the flow rate is constant, the flow profile is eventually unknown but symmetric and constant during both diverting motions, and the blade dynamics is perfectly linear and the same for both diverting motions: a very difficult task.

There are some different approaches presented for example by NIST [Mar06] or by NMIJ [Doi06] where a global symmetry is aimed. This approach is best realized when both diverting actions are always the same: i.e., for example when the first switching action is performed from right to left, and the final switching action also from right to left. By doing so, a symmetric flow profile at the nozzle is not required, and small irregularities in the diverting motion are negligible if they are present during both diverting actions. Details to the construction of such systems can be found in [Mar06], [Doi06] and [Shi03].

A diverting system based in global symmetry is a very smart approach when cold water systems are build, but when the diverter size has to be kept compact to reduce the open water surfaces, its realization is not practicable. Additionally, the main problem this design is aiming to solve, namely the water beam asymmetry, is more easily solved by conditioning the water at the flow nozzles. These reasons support the use of a diverter based on an unilateral symmetry.

Diverter dynamics

Considering equation 2.22, if unilateral symmetry is aimed at, there is a timing error at each diverter motion. At the forward motion Δt_1 and the backwards motion Δt_2. If the mean flow rate during the diverter motion is $\bar{Q}$, the diverter errors can be written as a function of a ,b, c, and d

$$\Delta t_1 = \frac{a-b}{\bar{Q}} \tag{2.23}$$

$$\Delta t_2 = \frac{d-c}{\bar{Q}} \tag{2.24}$$

The instantaneous flow rate Q_i shown in Figure 2.18a can be defined as a function of the velocity profile at the outlet of nozzle:

$$Q_i = \int_0^{x_i} v(x)\ dx \tag{2.25}$$

where $v(x)$ is the actual flow speed at the current blade position. For the following analysis the flow profile will be assumed to be uniform. The influence of non-ideal flow profiles will be analyzed separately. If $x_i = L(t_i)$ is the position of the blade at the instant i a volume under the curve between to instants t_j and t_k would be given by

$$V_{jk} = \int_{t_j}^{t_k} Q_i\ dt \tag{2.26}$$

Assuming again that the flow profile is uniform and constant we can write:

$$V_{jk} = \int_{t_j}^{t_k} \bar{Q}\ L(t)\ dt \tag{2.27}$$

The areas a, b, c and d would be given by:

$$b = \int_{t11}^{t1} \bar{Q}\ L_1\ dt \qquad\qquad a = \int_{t1}^{t12} \bar{Q} - Q\ L_1\ dt \tag{2.28}$$

$$d = \int_{t21}^{t2} \bar{Q}\ L_2\ dt \qquad\qquad c = \int_{t2}^{t22} \bar{Q} - Q\ L_2\ dt \tag{2.29}$$

Since the trigger times t_1 and t_2 are known, assuming the flow rate to be known and constant we can write:

$$\Delta t_1 = (t_{12} - t_1) - \int_{t11}^{t12} \varphi_1 dt \qquad\qquad \Delta t_2 = (t_2 - t_{21}) - \int_{t21}^{t21} \varphi_2 dt \tag{2.30}$$

The total timing error would be given by:

$$\Delta t = \underbrace{(t_{12} - t_{21}) + (t_2 - t_1)}_{Time\quad differences} \underbrace{- \left(\int_{t11}^{t12} \varphi_1 dt + \int_{t21}^{t21} \varphi_2 dt \right)}_{Diverter\quad motion\quad related} \tag{2.31}$$

This implies that we can predict the diverter error only by analyzing the dynamics of the diverting action. In order to be able to measure the dynamics of the diverter, the signal of the installed incremental encoder connected to the main rotation axis has been evaluated. The obtained pulse trail is analyzed with an oscilloscope. About 4000 angular divisions are available to resolve the actual position as a function of time. Figure 2.20 shows the speed and the corresponding position of the diverter in time.

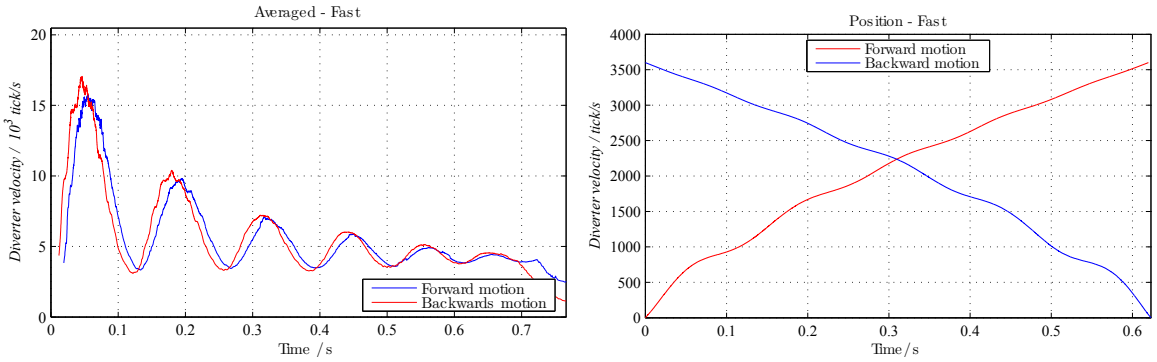

(a) Velocity of the diverting action

(b) Position of the diverter over time

Figure 2.20.: Velocity (a) and position (b) of the diverter of the WZP for a fast diverting action are shown. Note that due to the pneumatic actuator heavy dynamic effects cause the diverter action to oscillate. These effects are not distinguishable with bare eyes.

The diverter is actuated by four pneumatic cylinders. Each cylinder has two chambers. In order for the diverter to act, four chambers have to be evacuated and four have to be pressurized. In order to obtain a smooth and fast movement, it has been necessary to optimize the timing of the valves evacuating and pressuring the cylinders, and to adjust the flowrate of pressurization and evacuation.

As seen in Figure 2.20 the diverter is being actuated fast, but with strong oscillations in the speed. These oscillations are given due to improper balance between pressurization and evacuation, and not due to mechanical friction in the system. The moving action of the diverter has been optimized to obtain a longer diverting time but having a smooth movement. The results of this optimization are shown in Figure 2.21. The Motion is clearly more stable, and consequently, as seen in Figure 2.21b the position of the blade in time seems to change almost linearly.

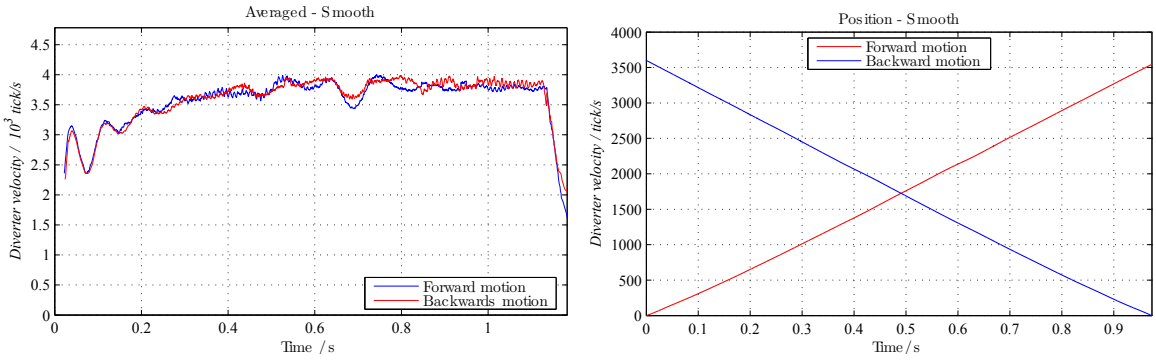

(a) Velocity of the Diverting action (b) Position of the Diverter over time

Figure 2.21.: Velocity (a) and position (b) of the diverter of the WZP for a smooth diverting action are shown. Note that the pneumatic dynamic effects can not be distinguished.

By applying equation 2.30, we can calculate the timing error for given trigger points based on the diverter dynamics. The results can be seen on Figure 2.22. As mentioned before, the best strategy to reduce the timing error is to have an unilateral symmetry by making the areas a and b and the areas c and d to be equal, this occurs when the zero line is crossed.

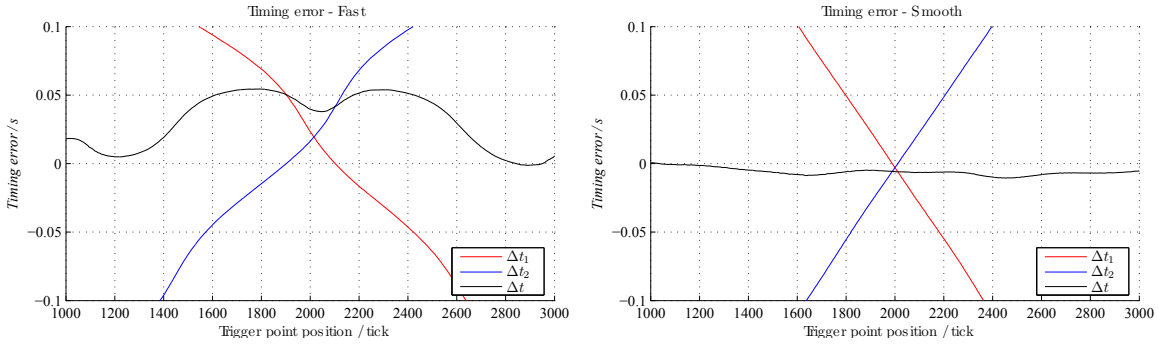

(a) Diverter error for a fast action (b) Diverter error for a smooth action

Figure 2.22.: The timing error based on the assumption of constant flow rate and uniform flow profile at the outlet of the nozzles is shown for a fast, and for a slow velocity diverting action

By taking different trigger points and calculating the corresponding timing error Figure 2.22 is obtained. The horizontal axis represents the position of the assumed trigger point. The blue and the red lines represent Δt_1 and Δt_2 respectively. When each line crosses the zero line, unilateral symmetry is obtained. It can be seen that for Figure 2.22a, the zero crossing points are distant from each other, which means there is a strong dependency on the diverter duration and on the flow rate stability. This is different in Figure 2.22b, where the zero crossing points are much closer. The black lines represent the total timing error.

In Figure 2.22a we can see, that timing error (black line) is not crossing the zero line. It has been common practice to determine the ideal trigger point by assuming the timing error is proportional to the position of the trigger point. If this is the case, it

would be enough to determine the timing error for two different trigger point positions to determine the ideal trigger point. Figure 2.22a shows clearly that given the nonlinear shape of the curve, more than two points would be necessary to find the ideal trigger point, if there is any.

Table 2.6 shows the simulation results of the timing error when a variation of flow rate exists, or when a variation of the duration of the diverter action occurs. The obtained bias is calculated assuming the trigger point is constant considering three different diverter dynamics: One fast action, one smoothed action and one smooth but longer diverting action. Table 2.6 makes clear why an optimization of the diverting action is helpful. Even if variations of flow rates larger than 1 % are not likely to happen, since the actuating system depends largely on the system pressure and on the temperature, variations in the range of 10 % are likely to happen.

Table 2.6.: Influence of variations on flow rate or diverter speeds on the timing error

Diverting action	**Trigger point position**	**Timing error difference[1]/ ms**		
		0 % bias	**2 % bias**	**10 % bias**
Fast (0.7 s)	central	0	1.3	6.8
Smooth (1.1 s)	central	0	0.9	4.8
Long and smooth (1.9 s)	central	0	1.8	9.0

[1] For this table, in order to allow an easier judgment of the influences the timing error was arbitrary assumed to be zero for the trigger point at the central position at tick=2000.

This uncertainty contribution has to be considered. By applying a uniform distribution for the full width 4.8 ms we have:

$$\boxed{u_{t1a} = 1.4\,\text{ms}} \tag{2.32}$$

Variation of the flow profile

To obtain the results in the section above, it has been assumed that the flow profile at the outlet of the nozzle is flat. This assumption is based on the fact that each nozzle has a flow conditioner with a total of 280 holes, making a total of 2240 holes; Each hole will have a particular flow profile, but considering the averaging effect for this large amount of holes, a flat profile would exist. But at the holes at the borders of the nozzle the effect of air friction is acting on the fluid. The distance crossed by the beam before reaching the blade is less than 10 mm but assuming the influence of air makes the flat profile to become slower at the edges, which also may affect the timing error.

A simulation was performed based on data of real blade dynamics considering a linear slope in 10 % and 25 % of the total area at each side (flatness ratio of 0.8 and 0.5 respectively). A calculation for ten different flow profiles for each flatness ratio, by changing the position of the center of the flat area has been performed, starting from its most left position, to its most right position. The results of the simulation for a fast diverter motion, and for a smooth diverter action are shown in Figure 2.23.

The optimized diverter motion is very robust against flow profile variations. Even for different flatness ratios, there is a maximum influence of 5 ms. For the fast diverting action there is clearly a larger influence up to 15 ms.

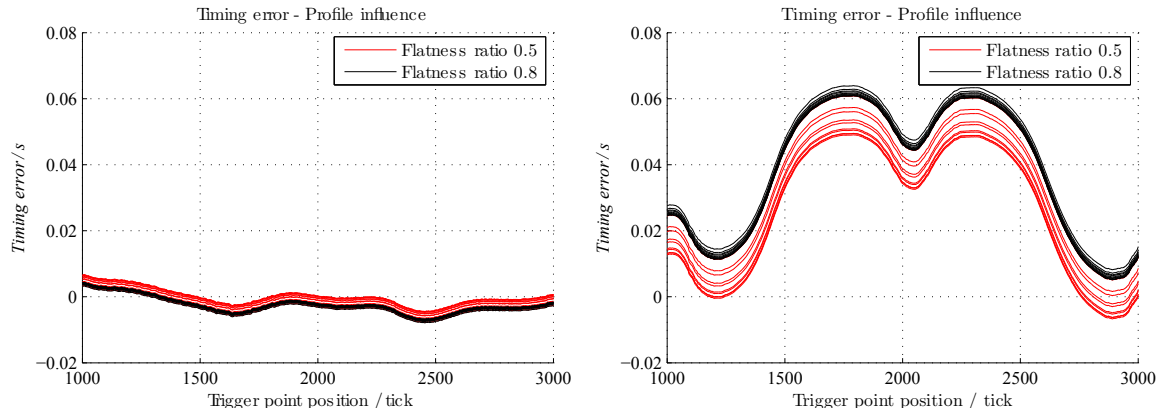

(a) Diverter flow profile influence on the smooth motion

(b) Diverter flow profile influence on the fast motion

Figure 2.23.: The influence of different worst case flow profile scenarios is shown in both figures. The assumed flow profile consists of a non centered flat profile with 50 % and 80 % of the flow surface being flat. Different levels of asymmetry are shown, from its most left position, to its most right. Note the small influence on the smooth profile. The benefits of adjusting the diverter motion can be appreciated by comparing both figures.

The uncertainty due to the unknown velocity profile has to be considered. For the case of the optimized motion, if a uniform probability distribution is assumed, the uncertainty contribution would be:

$$\boxed{u_{t2a} = 1.5\,\text{ms}} \tag{2.33}$$

2.4.2. Statistical analysis of the diverter dynamics

Due to the relevance of the blade dynamics an on-line monitoring system has been developed and installed. Monitoring the blade dynamics allows an on-line diverter error calculation, and makes it possible to discard measurements in case the gross errors appear. A set of 124 measurements, (248 diverter motions) have been analyzed. The above measurements were performed before the diverter system was overhauled and can be considered as a worst case scenario.

The performance of the actuating system is influenced by pneumatic system pressure, by air temperature, and by different friction losses. This causes the total diverting time to vary as it can be observed in Figure 2.24a where the duration of single diverting motions in different conditions are presented. The changes are of random nature. 2.24b shows the same data, but sorted into consecutive diverter motions belonging to the same calibration point.

Since the duration is changing, also the diverter motion dynamics is expected to change. The variation is shown in Figure 2.25. Even if the same shape can be recognized among the diverter motions, the speed variation within one point can be up to 30 %.

By calculating the terms $t_{12} - t_1$ and $t_2 - t_{21}$, and the integrals of equation 2.30 it is possible to observe at which level self cancellation occurs. This is shown in Figure 2.26. Even if different durations, and different dynamics are present, these effects seem to have the same effect but with opposite signs. Figures 2.26 can be used as life monitoring system for the diverter performance.

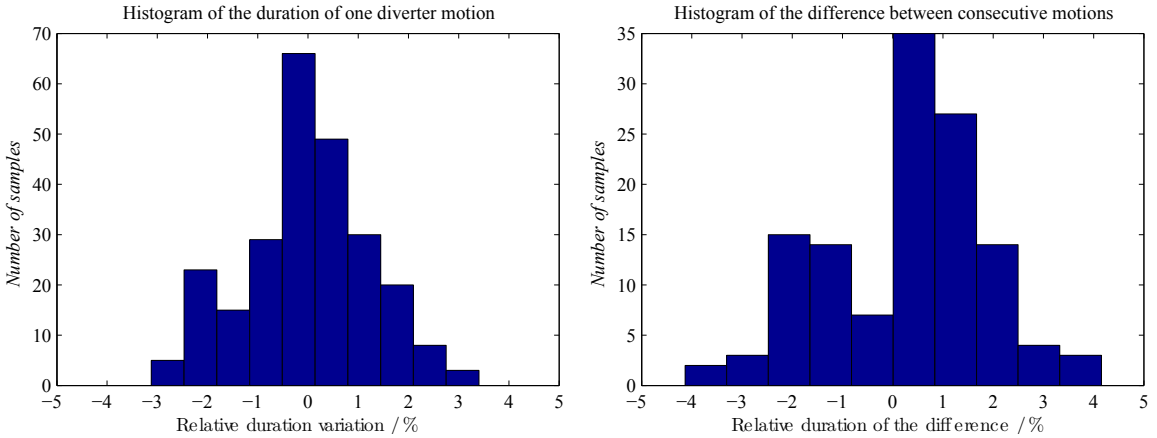

(a) Variation of the diverting time

(b) Variation of the diverting time within one measurement

Figure 2.24.: The total diverting time variation for flowrates up to 750 $\mathrm{m^3/h}$ for individual diverting motions is shown in figure (a), and for the variation within one calibration point in figure (b)

Based on life measurements performed on the diverter dynamics, it is possible to calculate the theoretical diverter error. Note that the assumption of uniform flow profile has to be valid if this timing error will be directly applied. If there is a different flow profile, the real timing error will be different. This can be observed in Figure 2.27 where the ideal timing error is 24 ms and the real timing error determined for the shown measurements is about 25 ms determined by applying the method proposed in [ISOa]. The reason for these small differences can be now attributed to the different flow conditions at the nozzle outputs. The differences however are small, and if the findings regarding the influence on flow profile of Figure 2.23 are applicable, then the consequences about stability and repeatability of the ideal diverter are also valid for the real timing error.

The mean value of the ideal timing error is 24.3 ms, and the mean value of the real timing error is around 25 ms. The difference can be attributed to the flow profile. The standard deviation of the timing error according to Figure 2.27 is 4.3 ms. We assume, therefore, a contribution of the repeatability to be:

$$\boxed{u_{t3a} = 4.3\,\mathrm{ms}} \tag{2.34}$$

In section 3.1 the repeatability of the same diverting system designed for flowrates up to 200 $\mathrm{m^3/h}$ is estimated to be 3.4 ms using a different approach.

2.4.3. Determination of the real timing error

Every time a diverting action is performed and the trigger point is not error free, a constant time error ($-\Delta t$) is added to the time measurement, influencing the calibration result. If measurements with more than one diverting action, i.e., with more than one filling period are performed, the influence on the calibration result would be different. Based on the influence of the number of filling periods during one flow meter calibration it is possible to estimate the constant time error that is being added per diverting action.

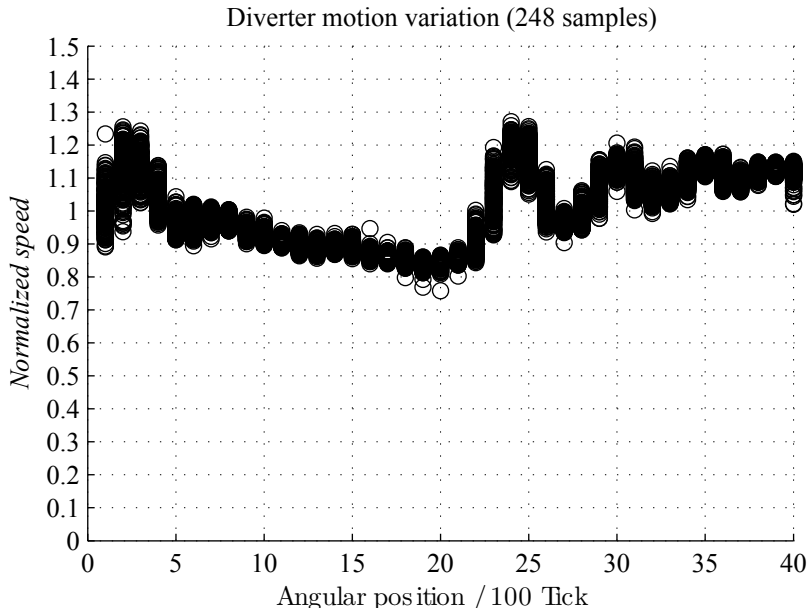

Figure 2.25.: The figure presents 248 diverter motions at diverse flow rates up to $750\,\mathrm{m^3/h}$ acquired during several days. The speed at a single position can vary up to 30 % for different conditions. The single profiles have been acquired using a counting system instead of an oscilloscope. In order to provide a more accurate velocity measurement, 100 angular markings have been taken into account to perform the speed calculation

For this, two measurements are necessary. One with only one filling interval, i.e., a regular calibration, and one with n filling intervals. The time is only measured while the diverter is directing the water into the weighing tank. For further details on the procedure please refer to the ISO 4185[ISOa]. The equation proposed to estimate the diverter error based on these two measurements is:

$$\Delta t = \frac{t'}{(n-1)} \left(\frac{\frac{m_i}{t'_i}}{q_i/q\frac{m}{t'}} - 1 \right) \tag{2.35}$$

Where the symbols t, Δt, q and m, represent the time, the diverter error, the volumetric flow rate and the mass respectively; subindex i refers to interval measurements and superindex "′" refers to apparent magnitudes.

Equation 2.35 has some limitations: the remaining diverter error has to be negligible small $\Delta t << t$, the filling times have to be exactly the same, and density or temperature variations are not considered.

In order to compensate for those phenomena, an additional term k_t for different filling times, and a term k_f for different mass flow rates that include the density variation effect have been introduced. The complete formulation should be:

$$\boxed{\Delta t = \frac{\Delta t + t'}{\left(\frac{n}{k_t} - 1\right)} \left(\frac{\frac{m_i}{t'_i}}{k_f\frac{m}{t'}} - 1 \right)} \tag{2.36}$$

$$k_t = t_i/t \tag{2.37}$$

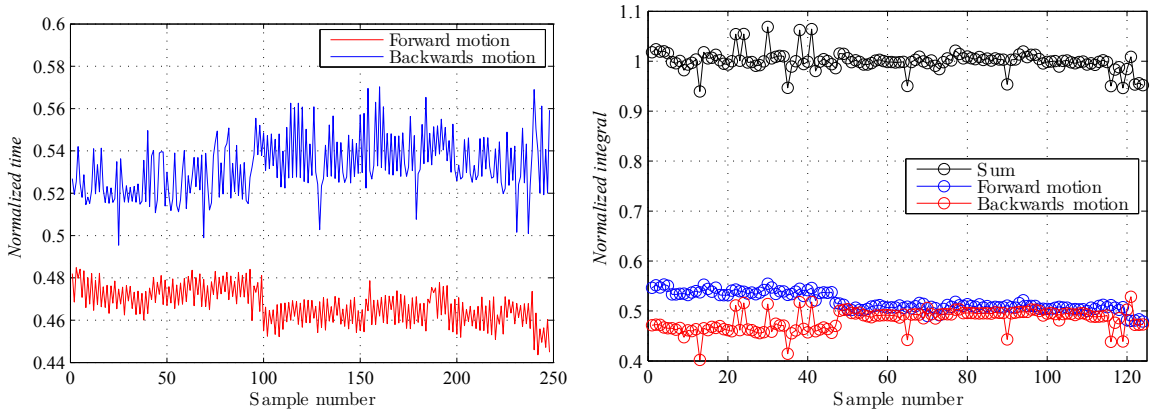

(a) $t_{12} - t_1$ and $t_2 - t_{21}$ (b) Integral of Q_i

Figure 2.26.: Timing error components of Equation 2.31. The time has been normalized to the average duration of a diverter motion, and the integral of the dynamics has also been normalized to its average value.

$$k_f = \dot{m}_i / \dot{m} \tag{2.38}$$

The NIST [Mar06], the NMIJ [Shi03] and Mathies [Mat05] present different timing error equations that if compared with the formulation proposed by the ISO4185 present some differences. However, if equation 2.36[9] is used instead of 2.35 the differences vanish.

For equation 2.36 to be valid, it is necessary that following requirements are fulfilled:

- Regarding the flow rate:
  - the mean flow rate is kept constant
  - the diverter does not influence the flow rate
  - the flow rate during one diverting action is constant
  - the flow measurement device is highly repeatable
  - the flow profile at the diverter inlet does not change
- Regarding the measurement systems:
  - The weighing drift is negligible for the duration of the measurements
  - Nearly the same absolute weighing load is used for both measurements
  - All density, pressure and temperature measurements are functioning properly
- Regarding the diverting system:
  - The duration and the velocity of the diverting action has a normal distribution
  - The position of the trigger point is fixed

Most of these assumptions are applicable also for regular flow meter calibrations. The WZP covers a broad flow rate and temperature range. By applying the corrected equation 2.36 several times at different conditions, a basis for the interpolation of the time error for every condition can be estimated. The obtained mean values and its standard deviations are shown in Figure 2.28. Additionally, a weighted least squares

[9]For a detailed explanation on the derivation of equation 2.36 and of the second method recommended by ISO4185 please refer to 3.1

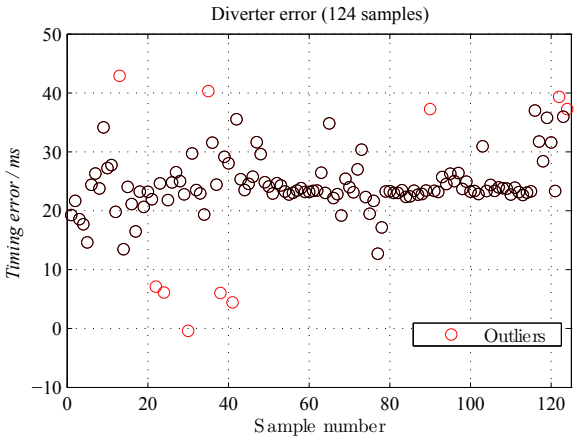

Figure 2.27.: The estimated timing error for 124 flow meter calibrations at diverse flow rates up to 750 $^{m^3}/_{h}$ are shown. In some cases there are gross errors (marked red). The real timing error for these measurements determined using the method proposed by the ISO24185 is around 25 ms

regression using the inverse of the obtained variances at the different temperatures is shown; the results for 20 ℃ and 80 ℃ are in very close agreement, therefore, only one line is shown.

The repeatability of the diverter error can be observed to be much larger for measurements at 80 ℃ than for 20 ℃. At a first sight, this variability would be directly attributed to the diverter system itself, but if a more detailed analysis is performed on equation 2.36, it is found that the largest influence on the repeatability of the diverter error determination is the repeatability of the used flow meters. The error analysis of equation 2.36 will be subject of study in section 3.1.

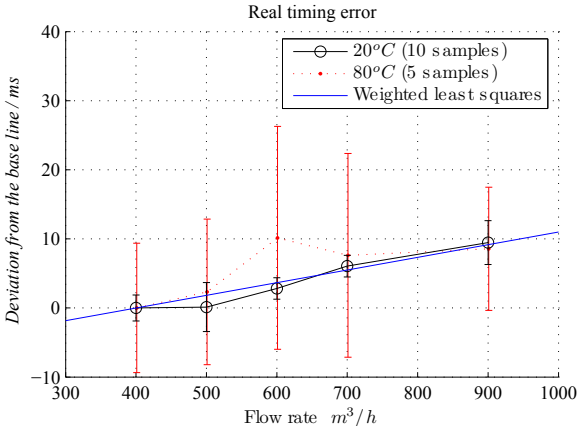

Figure 2.28.: Experimental determination of the timing error at 20 ℃ and 80 ℃. For each point at 20 ℃ 10 repetitions and for 80 ℃ 5 repetitions have been performed. The least squares regression coinncide and are shown in blue

The diverter tests repeatability is the highest for 20 ℃, in this case the contribution due to the reduced size of the sample would be $u_{t4a} = 3.5\,\text{ms}/\sqrt{10} = 1.1\,\text{ms}$. If the linearity assumption for the diverter error can be accepted, which is suggested to be true independently of temperature, the maximum regression error for the mean time would be 2 ms.

But if the repeatability of the diverter test result is analyzed, we can see a very large variation. The reason for that is not the diverter itself, since an unrealistic flow profile variation would be required to obtain those errors. It is furthermore the used flow measurement device that introduced these large variations. Considering that the flow meter performs best at higher flow rates, the maximum difference of 20 ms at 900 $^{m^3}/_{h}$ will be used as an uncertainty contribution. If we assume a uniform probability distribution we obtain both uncertainty contributions for interpolation and diverter repeatability:

$$\boxed{u_{t4a} = 1.1\,\text{ms}} \qquad \boxed{u_{t5a} = 5.8\,\text{ms}} \tag{2.39}$$

2.4.4. Total uncertainty for the time measurement

The overall uncertainty is given in Table 2.7. The contribution for 60 s is considered as a worst case. Filling times may vary up to 360 s.

Table 2.7.: Time measurement uncertainty budget

	Parameter	**Uncertainty**	**Contribution/%**
u_{t1a}	Flow rate stability[2]	1.4 ms	3.4
u_{t2a}	Flow profiles[2]	1.5 ms	3.9
u_{t3a}	Repeatability[1]	4.3 ms	32.1
u_{t4a}	Determination Method[1]	1.1 ms	2.1
u_{t5a}	Linearity[2]	5.8 ms	58.5
u_{ta}	**Timing error**	7.6 ms	100
u_t	**Timing error for 60 s**	1.26×10^{-4}	

[1] Normal distribution
[2] Uniform distribution

2.5. Process uncertainty

2.5.1. Evaporation

When fluid water is in contact with atmospheric air, mass transfer processes take place. Since the density of humid air is lower that density of dry air, natural convection accelerates the mass transfer process. It can be expected that most of the mass transfer happens at the place where the largest surface and the largest gradients are present. In the case of the WZP, the open water surface in the filling tank, and the water beam surface coming from the diverter are the most affected by evaporation and have to be considered carefully.

Assuming that the water content in saturated air at 90 °C is 0.426 $^{kg}/_{m^3}$ and considering that 0.213 $^{kg}/_{m^3}$ of water are contained in 50 % humid air. Humidity variations and gradients within the 32 m^3 of air within the tank may result in a considerable amount of water gain or loss.

In the case of the WZP, the evaporation has been minimized by reducing the open water surface to a minimum, and by maximizing the saturation level of the air around the open water surfaces. When water is filled into the weighing tank during a calibration, the contained air has to be exhausted out. And when after a measurement, water

has to be emptied from the weighing tank into the collecting tank; the air contained in the collecting tank has also to be exhausted. This is taken advantage of by connecting the air volumes of both tanks with air conducts in such a way that saturated air is only moved from one tank into the other when water is being moved, impeding in this way dry air to have contact with the open water surfaces. In order to overcome friction in the air conducts, a bidirectional ventilator is used.

To reduce the surface of the water beam entering the tank, filling is made in two stages by dividing the tank in two levels. The distance from the diverter systems to the top level is small, reducing the falling distance. The bottom of the upper level is provided with 105 perforations with a tube on each that is leading directly to the bottom of the weighing tank. By filling the water through the tubes, the water level rises smoothly.

Since any forces acting on the weighing tank have to be avoided, it is not possible to seal the air within the tank tightly. In order to reduce air movement, small gaps are provided but still, air will transport water vapor out of the weighing tank. The air conducts are thermally insulated, but not actively heated; because of this, air will cool down and water will condense on the walls. The air flowing into the weighing tank will be heated up again and extract more water.

Due to the mentioned hardware limitations, water losses will still take place. An exact determination of the evaporation would require several temperature and humidity sensors to be mounted on the weighing tank, but there is no space available. Therefore, a worst case estimation will be performed based on a single hygrometer installed inside of the weighing tank. Two parameters are measured: the minimum humidity within the weighing tank before the measurement, and the maximum humidity coming out from the weighing tank at the end of the measurement. In a worst case scenario, all water needed to increase the humidity in air has evaporated from the weighing tank instantaneously. During a real measurement, evaporation happens gradually. The water mass evaporated into the exhausted air is given by:

$$m_e = \int_{t_0}^{t_1} Q_{air}\,(f_i - f_0)\;\,dt \tag{2.40}$$

where f_i and f_0 are the absolute water content per cubic meter air, Q_{air} is the air flow rate which is approximately equal to the water flow rate, and t_0 and t_1 are the beginning and the end of a calibration. If Q_{air} is constant, and f_i linear in the form:

$$f_i = f_0 \; + \alpha\; t \tag{2.41}$$

then we can write

$$m_e = Q_{air} \int_{t_0}^{t_1} \alpha\; t\; dt \tag{2.42}$$

$$m_e = Q_{air} \frac{\alpha\; t_1^2}{2} \tag{2.43}$$

for the worst case when f_i is constant and evaporation occurs instantaneously, the evaporated mass of water m_{ew} would be given by:

$$m_{ew} = Q_{air} t_1\,(f_1 - f_0) \tag{2.44}$$

Consequently, since per definition $\alpha\; t_0 = f_1 - f_0$, then we have

$$m_{ew} = 2\; m_e \tag{2.45}$$

Relation 2.45 indicates that the worst case is twice as large as when a linear evaporation rate is considered. The hygrometer used for the measurements is based on the change of capacitance on a thin dielectric layer. In this type of instruments, diffusion governs the reaction time of the measurements; consequently, large time-constants and related errors are expected. A large time constant is an argument for using of m_{ew} as a basis for the uncertainty estimation. The used hygrometer is calibrated with an accuracy of $0.001\,{}^{\mathrm{kg}}/_{\mathrm{m}^3}$ absolute water content per cubic meter, including short term stability. Figure 2.29 shows the maximum humidity content differences between the initial and the final humidity measurements at 50 ℃ 65 ℃ and 80 ℃ for diverse flow rates. Evaporation losses under 50 ℃ are low and can be neglected.

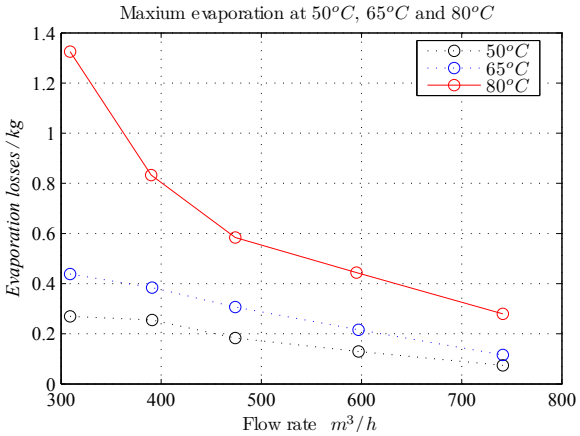

Figure 2.29.: Maximum total evaporation losses for 50 ℃, 65 ℃ and 80 ℃ estimated assuming a total air volume of $32\,\mathrm{m}^3$

Considering the maximum possible variation span after applying the correction corresponds to the values presented in Figure 2.29, the maximum uncertainty contribution of evaporation would be given by:

$$\boxed{u_{p1a} = 0.410\,\mathrm{kg}} \tag{2.46}$$

2.5.2. Buoyancy effects on the dead weight and the air

For clarity reasons buoyancy effects have been divided in two: the buoyancy effects caused by effective load changes, and buoyancy effects caused by dead weights. These last are divided also in two: the buoyancy effect on the solid loads, as the tank, the mechanism for automatic calibration and the insulation, and the buoyancy effect caused by the air inside the weighing tank.

Buoyancy of the weighing tank

The total volume of the solid dead weight is $6.5\,\mathrm{m}^3$ mainly filled by the thermal insulating materials. Air temperature inside the weighing system is feed-back-controlled but air humidity and air pressure are not; as a consequence buoyancy forces vary before and after the measurement. The correction for the buoyancy force difference for the dead weight including the empty weighing tank ΔB_1 would be given by the following equation. The air densities are marked with the subindex a and the index 1 for the initial measurement and the index 2 for the final measurement; the letter s stands for the conditions during the weighing of the mass standards.

$$\Delta B_1 = V_{dw}(\rho_{a1} - \rho_{a2}) \tag{2.47}$$

V_{dw} is the volume of the dead weight. ΔB_1 has to be corrected for and this value can be as high as 4 kg. The uncertainty contribution would be:

$$u_{B1}^2 = V_{dw}^2 \left(u_{\rho a1}^2 + u_{\rho a2}^2\right) \tag{2.48}$$

Equation 2.47 is simplified to improve clarity; the following additional correction term is missing:

$$b_1 \approx V_{dw} \frac{\rho_{as}}{\rho_{fl}} \left(\rho_{a1} - \rho_{as}\right) \tag{2.49}$$

The maximum value for this additional correction term would be in worst case conditions 0.004 kg; introducing this bias directly as an uncertainty contribution[10] the influence would still be very small and can be neglected.

The uncertainty of air density determination based on historical measurements of temperature, humidity and pressure is 0.021 $^{\mathrm{kg}}/_{\mathrm{m}^3}$. Considering the volume of the dead weight of 6.5 m^3 the contribution would be:

$$\boxed{u_{p2a} = 0.193\,\mathrm{kg}} \tag{2.50}$$

Buoyancy on the air inside the weighing tank

The buoyancy force correction acting on the air inside the tank is given by:

$$\Delta B_2 = V_1(\rho_{a1} - \rho_{g1}) - V_2(\rho_{a2} - \rho_{g2}) \tag{2.51}$$

V_1 and V_2 are the empty volumes of the tank. The volume of the empty weighing tank V_1 is 32 m^3, the empty volume after the measurement V_2 is variable and at least 12 m^3. The correction ΔB_2 has to be also applied, since it might get a value of up to 15 kg. The uncertainty contribution would be given by:

$$u_{B2}^2 = V_1^2 \left(u_{\rho a1}^2 + u_{\rho g1}^2\right) + V_2^2 \left(u_{\rho a2}^2 + u_{\rho g2}^2\right) \tag{2.52}$$

Equation 2.51 has been also simplified to improve clarity; the following additional correction term is missing:

$$b_2 \approx \frac{V_1}{\rho_f} \left(\rho_{a1}^2 - \rho_{a1}\rho_{g1}\right) - \frac{V_2}{\rho_f} \left(\rho_{a2}^2 - \rho_{a2}\rho_{g2}\right) \tag{2.53}$$

Its maximum value for worst case conditions is 0.019 kg. Its influence is in this case also neglectable.

Based on temperature, humidity and pressure measurements, the worst case uncertainty of air density determination inside the tank is 0.024 $^{\mathrm{kg}}/_{\mathrm{m}^3}$. The uncertainty contribution for different filling volumes is given by:

$$u_{B2} = \begin{cases} 0.876 & \text{for 5 t filling} \\ 0.771 & \text{for 10 t filling} \\ 0.744 & \text{for 20 t filling} \end{cases} \tag{2.54}$$

[10] There are different ways of including uncorrected biases into the uncertainty analysis, the gum does not treat this point since it is expected from the user to apply always corrections, but in some cases, applying correction might not be wanted; for such cases, Lira and Woeger [Lir98] recommended for example, to include the uncorrected bias directly as an uncertainty component.

For the worst case:

$$\boxed{u_{p3a} = 0.876\,\mathrm{kg}} \tag{2.55}$$

2.5.3. Air accumulation in the pipes

Air bubbles accumulate at the highest points in the piping system. All piping has been designed to avoid such maximum points, but one maximum can not be avoided: the diverter system. Considering Figure 2.19, water enters the diverter in the bottom and leaves the diverter through in the opposite direction. The surface where the fluid changes direction in the diverter is marked in red. The geometry of this surface has been optimized to minimize dead zones at the highest position. However, since the pressure at the diverter system is low, air bubbles expand making dragging of air more difficult.

A bias would be introduced only if the amount of accumulated air would vary within one measurement. Test measurements have been performed by injecting artificially air bubbles into the test line just before a calibration was performed; the air injection has been stopped before the measurement, in order to avoid additional indication errors on the magmeter. No significant differences that can be guaranteed to be caused by this phenomenon have been found between both measurements. Therefore, the uncertainty contribution has to be estimated by other means.

The zone where air would possibly accumulate without being pushed out directly is at most a 3 cm wide gap with a height of 2 cm all around the diverter top. The volume of this gap would be about 2 L. There is no way to estimate if air bubbles are released or accumulated during the measurement, no correction can be applied, instead a uniform probability distribution with ±2 kg would be assumed.

$$\boxed{u_{p4a} = 1.155\,\mathrm{kg}} \tag{2.56}$$

2.5.4. Pipe Expansion

Measurements are performed only after the complete system including the weighing tank has been tempered. The system might cool down between two flow meter calibrations, but since all conducts are filled with tempered water all the time, and are also thermally insulated, the temperature fall should be minimal. A typical calibration point lasts about 15 minutes; 3 minutes for flow stabilization, 3 minutes for the test and 9 minutes for securing the system and to perform data processing; only the test time varies depending on the flow rate. This means that in order for the system not to get tempered in the initial 3 minutes, the heat transfer at the air side should be at least 4 times larger than the heat transport at the fluid side if insulation is ignored. In reality, for the minimum water flow rate assuming a horizontal pipe the heat exchange coefficients would be for the water side in the order of $10^4\,{}^{\mathrm{W}}/_{\mathrm{m^2K}}$ and for the air side in the order of $10\,{}^{\mathrm{W}}/_{\mathrm{m^2K}}$. Consequently, it can be assumed that the pipe temperature will follow the water temperature all times shortly after the flow has been installed.

The maximum temperature variation within one measurement at the highest temperature is according to historical data 40 mK. Given that the differential volumetric expansion coefficient between water and steel is for 50 °C $\Delta\gamma = 4.9\ 10^{-4} 1/\,\mathrm{K}$, the relative volume variation would be 2×10^{-5} of the volume between MUT and diverter.

If DN400 pipes are used, the maximum volume would be $4\,\mathrm{m}^3$. No correction can be applied since heating and cooling may occur indifferently. For this case, the uncertainty contribution considering a uniform distribution for 40 mK[11] would be:

$$\boxed{u_{p5a} = 0.022\,\mathrm{kg}} \tag{2.57}$$

2.5.5. Total uncertainty for the process related contributions

The total uncertainty is given by:

Table 2.8.: Process related uncertainty budget

	Parameter	**Uncertainty / kg**	**Contribution/%**
u_{p1a}	Evaporation[1]	0.410	7.3
u_{p2a}	Tank buoyancy [2]	0.193	1.6
u_{p3a}	Air buoyancy[1]	0.876	33.3
u_{p4a}	Air bubbles[2]	1.155	57.8
u_{p5a}	Pipe expansion[2]	0.022	0.0
u_{pa}	**Process influence**	1.519	100.0
u_p	**Influence for 17 t**	8.935×10^{-5}	

[1] Normal distribution
[2] Uniform distribution

2.6. Uncertainty balance

The shown uncertainty analysis contains the most relevant components assuming in most cases a worst case scenario. Only in cases where contributions are strongly temperature or flow rate dependent a different declaration is made. Following parameters can be seen as a worst case scenario for uncertainty estimation:

- Flow rate:1000 m^3/h
- Temperature range: up to 90 °C
- Filling volume: $17\,\mathrm{m}^3$
- Filling time: 60 s

The uncertainty contributors considering these conditions can be summarized as follows:

[11] 40 mK are considered instead of the standard deviation of 6 mK, since the standard deviation would result in a slightly better result.

Table 2.9.: Uncertainty budget for 17 t, 90 °C and 1000 m^3/h

	Parameter	u in %	Contrib./%
u_m	Mass determination[1]	3.22 $\times 10^{-5}$	3.7
u_ρ	Water density [1]	5.53 $\times 10^{-5}$	10.9
u_t	Time error[1]	12.61 $\times 10^{-5}$	56.8
u_p	Process related[1]	8.93 $\times 10^{-5}$	28.5
u_Q	**u (k=1)**	16.72 $\times 10^{-5}$	100.0
U_Q	**U (k=2)**	3.34 $\times 10^{-4}$	

[1] Normal distribution

The largest influence is given by the diverter system. If we consider a slightly different scenario with a different flow rate of 300 m^3/h uncertainty will be reduced due to the longer filling times as shown in the following table:

Table 2.10.: Uncertainty budget for 17 t, 90 °C and 300 m^3/h

	Parameter	Rel-Uncertainty	Contrib./%
u_m	Mass determination[1]	3.22 $\times 10^{-5}$	7.7
u_ρ	Water density [1]	5.53 $\times 10^{-5}$	22.7
u_t	Time error[1]	3.78 $\times 10^{-5}$	10.6
u_p	Process related[1]	8.93 $\times 10^{-5}$	59.0
u_Q	**Flow rate uncertainty**	11.61 $\times 10^{-5}$	100.0
U_Q	**Expanded uncertainty for k=2**	2.32 $\times 10^{-4}$	

[1] Normal distribution

2.6.1. Full range uncertainty and uncertainty distribution

Tables 2.9 and 2.10 represent the situation in two single calibration conditions. In order to obtain an overview of the performance of the facility Figure 2.30 was generated.

Figure 2.30a shows the main contribution groups. As process and diverter contributions are dependent on filling time and temperature, the total uncertainty will also depend strongly on these parameters. In order to allow for a comparison of the contributors across flow rates it is necessary to define a constant reference. For Figure 2.30a 0.04 % expanded uncertainty has been selected. Independently of the filling time, only those points are shown where the total expanded uncertainty is 0.04 %.

This figure allows for evaluating the weak points of the entire facility depending on the flow rate range. Through such an analysis it is possible for the laboratory administration to make strategic decisions in order to improve the uncertainty of the calibration facility. In this case it is clearly shown that higher flow rates require an improvement of the diverter system, and lower flow rates depend largely on process related contributors as evaporation for example.

Figure 2.30b gives the resulting uncertainties for 50 °C and 80 °C when the filling volume or the flow rate are varied. Differences between 50 °C and 80 °C are greatest for lower flow rates. As seen in section 2.5.1 evaporation losses can only be reduced if the

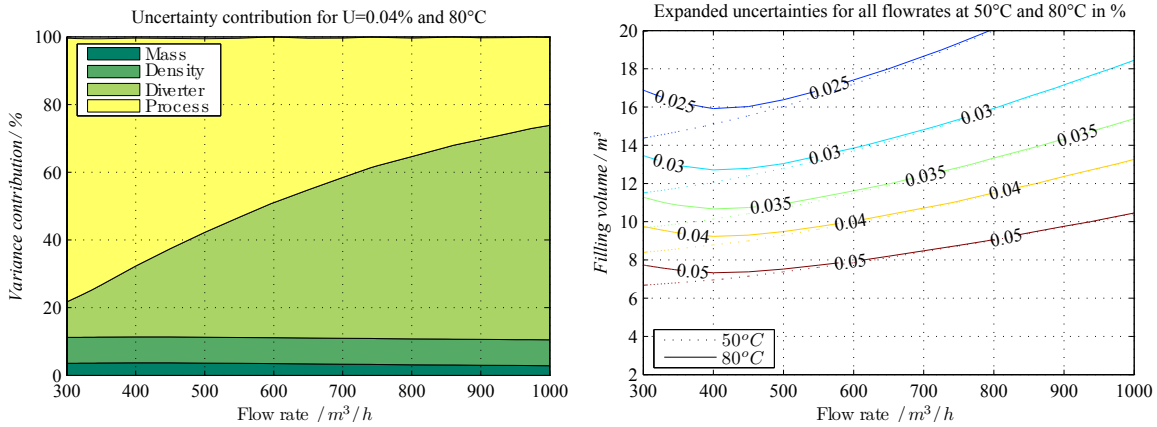

(a) Relative uncertainty contribution for 80 ℃ (b) Expanded uncertainty for 50 ℃ and 80 ℃

Figure 2.30.: Figure (a) shows the different contribution factors for the required expanded uncertainty of 0.04 % in percent. Figure (b) presents the different expanded uncertainty values that can be reached at 50 ℃ or 80 ℃ for different filling volumes.

compensating system is working precisely, i.e., the humidity of the air in the tank before the water is filled in should be controlled, and the flow rate of the outgoing air during the filling procedure should be measured and controlled. The physical limitations of the control systems for humidity and flow rate cause a bias in the lower flow rate range that is not easily controlled, and can not be compensated.

Figure 2.30b provides a realistic estimation of the performance of the WZP. Different uncertainty levels can be aimed at. This figure is particularly useful for planing measurement campaigns with specific uncertainty requirements. For example if only 0.05 % expanded uncertainty are required for 400 m^3/h, only 8 t filling mass would be necessary.

It is also possible to see that only filling masses larger than 14 t allow for the 0.04 % expanded uncertainty to be reached. Please note, that Figure 2.30b does not contain the contribution of the flow meter under test. Depending on the application, if repeatability and/or reproducibility are known, it can be easily included into the representation.

3. Cumulative part

This chapter introduces the publications containing the most important findings of the research work. Every publication can be read independently. As a consequence some contents might be only briefly mentioned while the core topics are treated with more details. For the sake of completeness, the bibliographic references cited only in the publications[1] and not elsewhere are included in the bibliography.

The three articles presented here have been written and conceived by the author of this research work. As valuable co-authors can be mentioned Dr. Thomas Lederer from the PTB and Dr. Noriyuki Furuichi from the NMIJ who contributed through fruitful discussions. Additional information is given for every article.

3.1. [Cor15b] A practical method to assess the performance of gravimetric flow test rigs by using the timing error

This article is based on the analysis of the results obtained by determining the timing error of a gravimetric flow test rig. The introduced methods are effective for evaluating the performance of a gravimetric calibration facility for determining the validity of relevant assumptions. The methods take advantage of the self cancellation of unknown systematic influences that occur implicitly when the timing error is determined. The analysis of the results allows for an extensive evaluation of the performance of the calibration facility and of the installed flow meter. The method is applied to the diverter test results of two different facilities of the PTB, the WZP in Berlin and the HDP (Hydrodynamisches Prüffeld) in Braunschweig. The article is an essential part of the estimation of the uncertainty of the WZP, not only because it validates the diverting systems performance, but because it establishes a methodology to allow the validation of gravimetric calibration systems prior to flow comparisons.

3.1.1. Credits

The article is co-authored by Dr. T. Lederer who participated in the conceptual design of the experiments and contributed to the evaluation of the results. The measurement results of the HDP were kindly provided by Dr. R. Engel of the PTB-Braunschweig

3.1.2. Publication Details

This article has been presented at the tri-anual meeting FLOMEKO 2013 in Paris and was one of the selected articles to be submitted in an extended version at Elseviers Flow Measurement and Instrumentation FLOMEKO Special Edition.

[1] These publications are[Bro13],[Ger05], [Lun00], [Moo00], [Pan90], [Shi10], [Str09], [Taw14], [Vos99], [YBS01], [Yeh97] and [Zhe11]

Flow Measurement and Instrumentation 44 (2015) 61–70

Contents lists available at ScienceDirect

Flow Measurement and Instrumentation

journal homepage: www.elsevier.com/locate/flowmeasinst

A practical method to assess the performance of gravimetric flow test rigs by using the timing error

L. Cordova *, T. Lederer

Heat and Vacuum Laboratory of the Physikalisch-Technische Bundesanstalt, Germany

ARTICLE INFO

Available online 25 December 2014

Keywords:
Gravimetric flowmeter calibration facility
Diverter system repeatability
Diverter test
Flow test rig performance

ABSTRACT

This paper proposes an improved method to assess the performance of a gravimetric flow test rig. It addresses the study of two of the most important measurement systems: the weighing scale and all mass-related corrections, and the time measurement system. By performing a regular diverter test according to ISO 4185:1980 several times and under different conditions, it was possible to determine not only the statistical variances of the diverter system, but also the variances of the meter under test and of the flow test facility separately. The proposed method allows also under special conditions the determination of systematic errors in the mass determination. The method has been successfully applied at the large water flow calibration facilities of PTB in Braunschweig and Berlin and is recommended as a routine to test the performance of gravimetric flow test facilities.

1. Introduction and motivation

For any flow laboratory the uncertainty estimation of its flow test rig used for research or traceability purposes and its validation is of central importance. The uncertainty estimation methods are universally accepted and the main components like the weighing system, the water density determination, the flow conditions and the repeatability of the meter under test (MUT) are well known and have been the subject of several studies and publications. Nevertheless, there are no standardized methods for the validation of the obtained uncertainty.

The most recognized way of validating declared uncertainties is through inter-laboratory comparisons. It is expected that the degree of equivalence, i.e. the difference between a laboratory's result and the comparison reference value, is to be smaller than the declared best measurement capability. In order for the reported data of each laboratory to be comparable and consistent, all participants have to measure exactly the same measurand, i.e. all relevant measurement conditions have to be identical at every laboratory. It is hard to achieve those preconditions. Since inter-laboratory comparisons often are the only way to detect biases, it is most likely that participants will have undetected sources of uncertainty, which makes it difficult, or even impossible to explain the encountered differences.

One way of avoiding this problem is by taking advantage of an external reference. This could be achieved by performing more than one round in a comparison; the first round should then allow an initial view into the participant's performance giving them the possibility to roughly recognize their flaws and to correct them if possible. Subsequently, a second comparison round can be performed. The efforts needed to perform a double comparison round are huge, therefore a different option would be preferred. An ideal option should allow participants to check their systems qualitatively in order to detect major problems before the comparison is started.

In the following a method is presented to qualitatively detect if important components of the flow test rig are working properly. It is an extended version of the timing error detection test proposed by ISO 4185 [1]. It performs, from a metrological point of view, the quality control of the flow test rig performance. Additionally it suggests a way to quantify the repeatability of the test flow measurement device, and consequently of the test bench alone.

2. Model of the diverter error

The time (Δt_d) the diverter takes to change from one end position to the other may vary from a few milliseconds up to 1 s. During this time, the flow directed into the weighing tank increases from zero to the actual flow rate. The form of the incrementing flow rate within Δt_d is not known. The magnitude of the ratio $\Delta t_d/t$ defines whether analysis is necessary.

There are two ways of estimating the timing error: through modeling and characterizing the blade dynamics and the water jet, or by modeling the effects that are caused indirectly by the diverter. The first method delivers more information on the system like the repeatability of the diverting phenomena itself. However, large modeling and measuring efforts are necessary to assess the flow profile measurements at the outlet of the nozzle, and to characterize the motion dynamics of the blades. This analysis was

* Corresponding author.
E-mail address: cordova.leopoldo@gmail.com (L. Cordova).

http://dx.doi.org/10.1016/j.flowmeasinst.2014.11.010

performed by Engel and Baade. [3]. The second method is empirical and was introduced by the international standard ISO 4185. The advantage of this method is its universal applicability, since no additional measurement systems are required.

Considering Fig. 1, to obtain an error-free measurement, the area defined by the testing time limits and the flow rate must be equal to the dashed area and the following must apply:

$$a+c=b+d \tag{1}$$

If the flow rate during both diverting motions is different, in the case that the diverting time Δt_d is large, it is advisable to additionally apply the following symmetry conditions:

$$a=b, \quad c=d \tag{2}$$

If only the first condition was used to adjust the trigger point, the measurement would be error-free only if the flow rate is exactly the same for both diverting actions. Even symmetric diverters like the uni-diverter from NIST [2] or the double wing diverter from AIST [5] have to ensure very stable flow rates at the beginning and at the end of the measurement. But if also condition (2) were fulfilled, the diverter would cancel its error automatically even if the flow rate differences are large. Adjusting the trigger point to fulfill condition (2) for every flow rate might, however, not always be possible.

2.1. The ISO 4185 diverter equation

Every time a diverting action is performed during a flow meter calibration, a constant time error ($-\Delta t$) is added to the time measurement. If a regular flow meter calibration is repeated including several diverting actions or "interruptions", it is possible to calculate the constant time error introduced by the diverting system.

For this, two measurements are necessary. The first measurement consists of only one filling interval, i.e. a regular calibration, and the second measurement is performed with n interruptions. The time and pulses are only counted while the diverter is directing the water into the weighing tank. For further details on the procedure refer to ISO 4185. The equation proposed by ISO 4185 to estimate the diverter error based on these two measurements is

$$\Delta t_{iso}=\frac{t'_c}{(n-1)}\left(\frac{\frac{m_i}{t'_i}}{q_i/q\frac{m_c}{t'_c}}-1\right) \tag{3}$$

The symbols t, Δt, q and m, represent the time, the timing error of the diverter, the volumetric flow rate and the collected mass respectively; subindexes i and c refer to interrupted or continuous interval

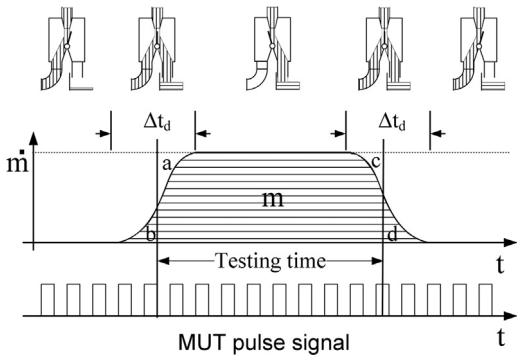

Fig. 1. Diagram of the timing error concept. The curve shows the mass flow rate entering into the weighing tank. The dotted line represents the mass flow rate. The time the diverter takes to change its position is marked with Δt_d. The ideal testing time is defined as the time in which the dashed area becomes equal to the area defined by the testing time limits and the dotted line. The pulse trail shown below schematically represents the uninterrupted flow rate perceived by the meter under test.

measurements respectively, and superindex $'$ refers to apparent magnitudes that are directly measured.

Eq. (3) contains simplifications that in some cases might introduce systematic errors. The unbiased formulation requires the introduction of two additional factors: k_t to correct for different filling times, and k_f to correct for different mass flow rates instead of volume flow rates. If no simplifications are introduced in the deduction, the resulting equation, rearranged to have the same form of the equation proposed by the ISO is given by

$$\Delta t=\frac{\Delta t+t'_c}{\left(\frac{n}{k_t}-1\right)}\left(\frac{\frac{m_i}{t'_i}}{k_f\frac{m_c}{t'_c}}-1\right) \tag{4}$$

$$k_t=t'_i/t'_c \tag{5}$$

$$k_f=\dot{m}_i/\dot{m}_c \tag{6}$$

Considering

$$k_m=\frac{m_i}{m_c} \tag{7}$$

it can be easily shown that the systematic error introduced by Eq. (3) is defined by

$$\frac{\Delta t}{\Delta t_{iso}}=\frac{n-1}{n-\frac{k_m}{k_f}}k_t \tag{8}$$

Note. For a detailed derivation of the timing error equations proposed by the ISO 4185:1980, refer to Appendixes A and B.

If Eq. (3) is used iteratively to either calculate the real flow rates or to adjust the trigger point to eliminate the time measurement error to zero, then the bias has no considerable influences.

If the flow test rig calculates the flow meter correcting factor automatically, it might be more practical to use the following equivalent form (see Appendix C):

$$\frac{\Delta t}{t_c}=\frac{k'_i-k'_c}{\frac{n}{k_t}k'_i-k'_c} \tag{9}$$

where k'_c and k'_i are the apparent flow meter correction factors defined as

$$k'=\frac{Indication\ of\ the\ MUT}{Indication\ of\ the\ reference} \tag{10}$$

In order to determine the sensitivity to systematic errors, we would use Eq. (3) due to its simplicity. If we introduce the dimensionless variables including the time

$$\epsilon=\frac{\Delta t}{t_c} \tag{11}$$

we obtain

$$\epsilon=\frac{1}{n-k_t}\left(\frac{k_m}{k_f}-k_t\right) \tag{12}$$

The time measurement is typically measured with an uncertainty below 10^{-6}. For this reason, the term k_t will be neglected for the following analysis:

$$\epsilon=\frac{1}{n-1}\left(\frac{k_m}{k_f}-1\right) \tag{13}$$

Eq. (13) shows the robustness of this method. The measured variables are involved through measurement ratios. The use of ratios has the advantage of reducing statistical variability, and minimizing the effects of biases.

2.1.1. Assumptions

The aim of comparing flow rate facilities is to ensure that the calibration results of any given flow meter are independent of the laboratory used within the reproducibility of the flow meter. How to determine the reproducibility of the flow meter is a complicated and demanding metrological problem that has to be customized each time to the flow meter used. However, the most important parameters to check for in a gravimetric facility are always the measured mass including all corrections, and the measured time.

The diverter test mentioned in the section above has the potential to serve as a method not only to determine the timing error, but also to validate the flow test rig results. This is possible, since the requirements for the test to deliver consistent results overlap with the requirements of a gravimetric flow test rig. The assumptions to be fulfilled for a diverter test are the following:

Regarding the weighing systems:

- The weighing drift is negligible for the duration of the measurements.
- There is no time-dependent water loss or gain due to leaks, condensation or evaporation.
- The linearity error of the weighing scale in the working range is negligible.

Regarding the flow rate:

- The distribution of the error of the flow measurement device at the flow rate used is normally distributed.
- The flow measurement device error can be linearized in the flow rate region used.
- The flow rates during the initial and the final diverter motion are the same.
- The diverter motion does not influence the flow rate.

Regarding the actuator of the diverting system:

- The duration of the diverter motion has a normal distribution.
- The velocity of the diverter motion as a function of time, is nearly constant and normally distributed.

To make this concept clear, let us consider two sets of 10 timing-error determination tests. Each set is performed at the same temperature and flow rate, but using a different filling mass and/or a different number of filling interruptions. If any of the assumptions above happened not to be fulfilled, this would be detected through a bias in the timing error determination between the two sets as explained in the section below.

2.2. Systematic influences

For a diverting system to work properly, it is required that the introduced timing error is normally distributed. Any correlation of the timing error to any quantity different than flow or temperature would be an indication of undetected systematic errors. By undertaking a sensitivity analysis on Eq. (12) we can estimate the magnitude of the introduced biases.

2.2.1. Mass sensitivity

Let us assume that there is a bias in the mass determination. The reason for this could be an error in the buoyancy correction, a non-linearity effect between two mass calibration points or mass variations due to evaporation, condensation or leaks. If this bias is for example 1 kg for a filling mass of 15 000 kg and if we attempted to detected the bias through a flow meter calibration, in order to be able to detect its influence, it would be necessary for the repeatability of the flow meter to be better than 7×10^{-6} which is not possible. But by using this method, random variability is reduced through the use of measurement ratios making it possible to detect small biases.

One precondition has to be given: biases are only detected if they are dependent on time or on the total accumulated mass. If this is not the case, they will remain undetected. A bias on both mass measurements on the same direction would be canceled out and remain undetected. This is the advantage of the method: if all conditions are kept constant, biases are canceled out, and the timing error can be calculated accurately. However if slightly different conditions are used, small biases can be detected.

Based on Eq. (13), we can write:

$$\frac{\Delta t}{t} \approx \frac{1}{n-1}\left(\frac{1}{k_f}\frac{m_i}{m_c} - 1\right) \tag{14}$$

Since we assume that $k_t \approx 1$, we can write

$$\Delta t \approx \frac{1}{n-1}\left(\frac{1}{k_f}\frac{m_i}{\dot{m}_c} - t\right) \tag{15}$$

and the sensitivity would finally be given by

$$\frac{\partial \Delta t}{\partial m} \approx \frac{1}{\dot{m}(n-1)} \tag{16}$$

We can see that the sensitivity of Δt to a mass variation is independent of the filling times and filling masses. Based on this equation, Fig. 2 can be drawn. The influence that 1 kg total bias on mass would have on the determination of the timing error is shown. For example, if a diverter test is performed at a flow rate of 200 m^3/h with 10 filling intervals, if a mass bias of 1 kg exists, a systematic error of 2 ms would affect the value of Δt.

2.2.2. Sensitivity to the flow measurement

For this case, the same condition applies: the bias has to be different on both performed measurements. Otherwise it would remain undetected. One thinkable phenomenon causing an asymmetrical bias on the flow rate measurement would be when the diverter action causes dynamic changes to the flow rate. This is the case where closed coupled valves are used. Depending on the nature of the flow rate variations and on the flow meter working principle the volume integrated by the flow meter will be more or less biased. The introduced bias has a reduced importance for a regular calibration, but it is important for the timing error determination. Note also that the flow measurement result and the fluid density measurement always appear together. Due to this, their effects cannot be separated.

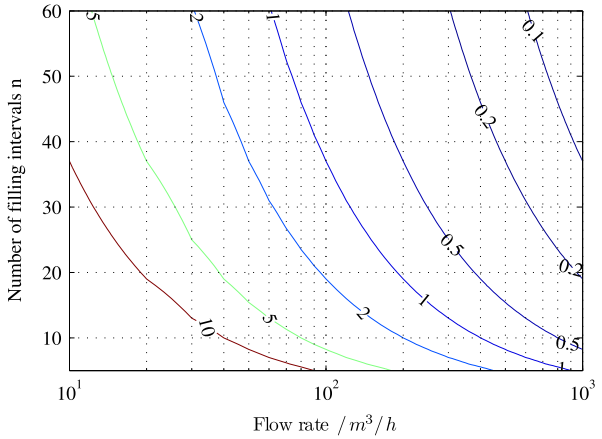

Fig. 2. Sensitivity of the timing error to a systematic mass error of 1 kg, given in milliseconds.

Based again on Eq. (13) and assuming k_m to be approximately 1, we can write

$$\frac{\Delta t}{t} \approx \frac{1}{n-1}\left(\frac{\dot{m}_c}{\dot{m}_i} - 1\right) \tag{17}$$

$$\frac{\partial \Delta t}{\partial \dot{m}_i} \approx \frac{t}{(n-1)} \frac{-\dot{m}_c}{\dot{m}_i^2} \tag{18}$$

assuming the flow rate bias is small we can finally write

$$\frac{\partial \Delta t}{\partial \dot{m}} \approx \frac{-t}{(n-1)\dot{m}} \tag{19}$$

Based on Eq. (19) we can draw Fig. 3.

From the deductions above, it can be concluded that if the diverter test is performed with slightly different filling times or masses, it is a sensitive test to determine the influence of biases that would remain undetected otherwise.

2.3. Variance of the method

It is necessary to estimate the variance of the method to include it into the uncertainty budget. For this the experimental sample variance would suffice. From Eq. (13) we can see that the variance of the flow measurement, the variance of the mass measurement and the variance of the diverter itself have to be related.

Since time measurements are performed normally at an accuracy better than 10^{-6} s, we can assume $\sigma_{kt} \approx 0$, justifying the use of *Eq.* (13). The associated variance of the method would be given by

$$\sigma_e^2 = \left(\frac{1}{n-1}\right)^2 \frac{1}{k_f^2}\sigma_{km}^2 + \left(\frac{1}{n-1}\right)^2 \frac{k_m^2}{k_f^4}\sigma_{kf}^2 \tag{20}$$

As a first conclusion we can say intuitively, if the number of interruptions increases, the variance should decrease rapidly.

Analyzing Eq. (20), we can see that the variance of the diverter system itself σ_δ^2 does not apparently play a role. This assumption would be physically incorrect. The contribution of σ_δ includes the effects of σ_{km}, since every variation of the blade dynamics, or of the nozzle flow profile would be detected by the weighing system.

Note. The variance $\sigma_{\Delta t}$ describes the spread of the timing error determination method. The diverter variance σ_δ depends on different parameters; it represents an additional contribution to $\sigma_{\Delta t}$.

Given that $k_f = \dot{m}_i/\dot{m}_c$, and that the variance of the flow meter remains constant

$$\sigma_{\dot{m}i} = \sigma_{\dot{m}c} = \sigma_{\dot{m}} \tag{21}$$

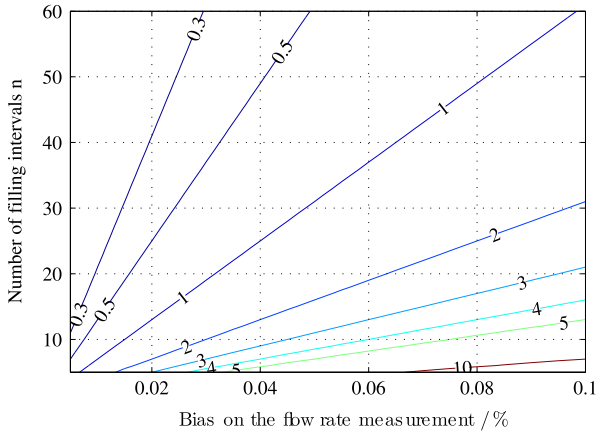

Fig. 3. Sensitivity of the timing error to a systematic error in one flow rate measurement, calculated for 1 min filling time, given in milliseconds. A bias on one density measurement would produce the same influences.

the value of σ_{kf} depends on the level of correlation r of $\sigma_{\dot{m}}$:

$$\sigma_{kf} = \sigma_{\dot{m}}\sqrt{2-2r} \tag{22}$$

The results of an ideal measurement instrument are not autocorrelated ($r = 0$). This means that all relevant systematic effects are known and have been compensated, and that all remaining influences are of random nature. But in reality there is a small correlation remaining since not all influence quantities can be compensated. The level of correlation between $\dot{m}_i$ and $\dot{m}_c$ can be determined empirically. But in order to be able to estimate autocorrelation, it is necessary for the flow rate indications to be normalized to the same reference. Consequently, the correlation analysis cannot be performed based directly on the flow rate indications, but has to be based on the correction factors of the flow meters. Therefore, since the same reference is used, an additional correlation source is introduced. Nevertheless, it is considered that for low correlation factors, the estimation of the correlation factor through the correction factors is sufficiently accurate.

For k_m special treatment is necessary. As stated before, if the mass ratio measurement is unbiased, and the measurements have been performed under repeatability conditions,[1] the variations of k_m can be attributed only to the randomness of the diverter motion σ_δ. By rewriting k_m as a function of flow rate and time, we can include the effects of the randomness of the diverter motion:

$$k_m = \frac{\dot{m}_i\left(t_i' + \sum_{j=1}^{n} \Delta t_j\right)}{\dot{m}_c(t' + \Delta t)}$$

The mass flow rates are per definition of the true flow rates and can be assumed to be constant, if additionally $\dot{m}_i \approx \dot{m}_c$, we obtain

$$k_m = \frac{\left(t_i' + \sum_{j=1}^{n} \Delta t_j\right)}{(t' + \Delta t)} \tag{23}$$

Note that $\lim_{n\to\infty} \sum_{j=1}^{n} \Delta t_j = n\Delta t$ but $\Delta t \neq \Delta t_j$. Considering that due to the averaging effect we have

$$\sigma_{\sum \Delta t_j} = \frac{\sigma_\delta}{\sqrt{n}} \tag{24}$$

and given that it can be easily proven that $\sum_{j=1}^{n} \Delta t_j$ and Δt can be treated in this application as independent random numbers, the variance of σ_{km} can be approximated by

$$\sigma_{km}^2 = \frac{(t_i' + n\Delta t)^2}{(t' + \Delta t)^4}\sigma_\delta^2 + \frac{n^2}{(t' + \Delta t)^2}\sigma_\delta^2 \frac{1}{n} \tag{25}$$

Assuming also that the filling times are the same, and that the timing error is small

$$\frac{(t_i' + n\Delta t)}{(t' + \Delta t)} \approx k_t \approx 1 \quad \text{and} \quad k_f \approx 1 \tag{26}$$

the variance of consecutive mass measurements caused by the diverter variations would be given by

$$\sigma_{km}^2 = \frac{1+n}{t_c^2}\sigma_\delta^2 \tag{27}$$

By introducing Eq. (27) and applying the conditions of (26) into Eq. (20), we obtain

$$\sigma_e^2 = \left(\frac{1}{n-1}\right)^2 \frac{1+n}{t_c^2}\sigma_\delta^2 + \left(\frac{1}{n-1}\right)^2 \sigma_{kf}^2 \tag{28}$$

[1] Repeatability conditions include in this case the environmental and fluid temperature, as well as a short time between measurements.

Reintroducing $\sigma_{\Delta t}$ and rearranging the terms gives

$$\sigma_{\Delta t}^2 = \frac{n+1}{(n-1)^2}\sigma_\delta^2 + \frac{t_c^2}{(n-1)^2}\sigma_{kf}^2 \tag{29}$$

As we can see the resulting value of $\sigma_{\Delta t}$ depends on the duration of the tests and on σ_{kf}. By observing Eq. (29) it becomes clear that it is possible to extract the values of σ_{kf} and σ_δ.

3. Experimental results

Exhaustive diverter tests have been performed at the heat meter testing laboratory of the PTB-Berlin (PTB-1) and at the flow test facility of the PTB-Braunschweig (PTB-2). Some of these results are published by Mathies and Lederer in [4] or by Engel and Baade [3]. The configuration of the diverter installed at the PTB-Berlin has some different characteristics compared to typical diverters for cold water. The reason is that water temperatures up to 90 °C are used to test heat flow meters. Due to the high evaporation rates expected at temperatures above 40 °C open water surfaces have to be avoided.

The most simple representation of a diverter consists of a blade with one angular degree of freedom within a containment with an entrance at the top, and two outputs at the bottom. The water beam coming from the test lines is directed through a nozzle directly to the rotation center of the blade. This type of diverter is used by PTB-2.

In the case of PTB-1 basically the same system is used, but instead of using only one diverter system, eight small diverting units are used simultaneously. To reduce the required blade size, instead of having the diverting motion actuated by rotation, the motion is performed by the nozzles through translation maintaining the angle between the blade and the flow direction constant. This eliminates the fluid forces acting on the blades. The eight diverter systems are coupled and positioned in a radial symmetry to reduce the required space as seen in Fig. 4.

Fig. 4 shows a diagram of the diverter installed at PTB in Berlin (PTB-1). Two diverter systems are used, one for the range up to 200 m^3/h and the other for the flow range up to 1000 m^3/h. The fluid is directed from the bottom into the diverter. There the flow is directed down to the eight nozzles. At each of the nozzles a flow conditioning system with 280 holes is installed. This is necessary in order to obtain a uniform block profile. The trigger point that starts the time measurement and the pulse counting on the MUT is defined geometrically, i.e. for example at 51% of the total way. It is the same point for both diverting directions. This means that an early trigger point in the first diverting action corresponds to a late triggering point in the final diverting action. In spite of being almost completely encapsulated, the diverter still works without influencing the flow. The actuators are pneumatic ensuring fast dynamics; the position is monitored using a radial incremental encoder.

The test conditions are summarized in Table 1. The flow meters used are of the electromagnetic type in both cases. For the PTB-1 100 pulses per liter were configured, and for the PTB-2 about 13 pulses per liter. In order to guarantee normality, rough errors have been filtered out using standardized methods prior to their inclusion in the analysis.

As we can see in Fig. 5, the determination of the diverter error can be as accurate as 1 ms for $n > 50$.

Considering Fig. 6, PTB-2 does not present any anomaly. For PTB-1 a dependence of the timing error on the amount of interruptions seems to exist. This is physically not possible. The reason for this deviation can be explained through a systematic influence of the weighing system. Considering Section 2.2 as seen in Fig. 2 a bias of 1 kg would be necessary to produce a bias of about 2 ms at

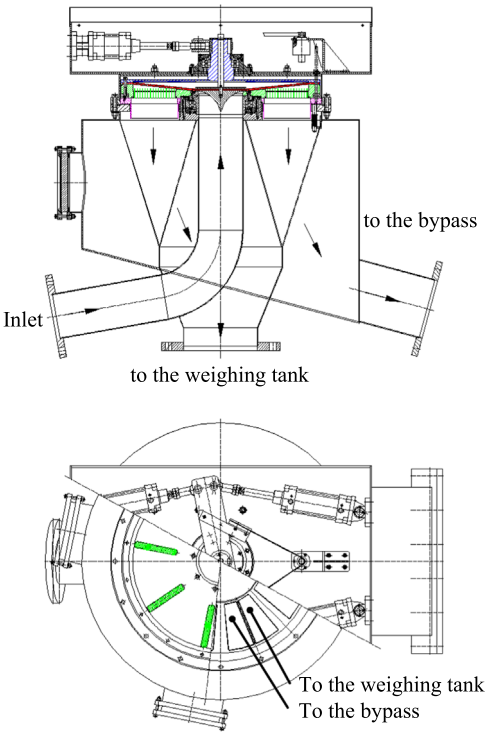

Fig. 4. Diagram of the diverter installed at PTB-Berlin (PTB-1). The working principle is the same as for single blade diverters; the main difference is that instead of using only one blade, several radial-positioned blades are used. The fluid enters the diverting system at the bottom. Water is distributed into the 8 nozzles and directed to the blades. The actuating system consists of four pneumatic cylinders. Source: Alfons Witt.

Table 1
Diverter test conditions.

Parameter	PTB-2	PTB-1
Temperature (°C)	20	50
Flowrate (m^3/h)	90	199
Interruptions	7, 14, 26, 51	8, 17, 33, 54
Duration (s)	100	260
Mass (kg)	2500	14 000[a]
Repetitions	15	15–20
Timing error (ms)	4.6	8.6
Corre. r for k_m	0.076	0.170
Flow repeat.[b] (%)	0.008	0.016

[a] Some measurements have been performed at 19 900 kg.
[b] Refers to the repeatability of the k-factor of the reference flow meter.

200 m^3/h and $n=9$ in the timing error, the actual bias is of about 1 ms, which would correspond to a bias on the mass measurement of about 0.5 kg. The weighing scale of PTB-1 is calibrated on a daily basis, and if required, before every measurement. The loads used for calibration are increased at 560 kg steps. The loads in between are validated, but not calibrated periodically using external weights. The tolerable mass bias (linearity error), due to this lack of calibration between points, is as large as 0.2 kg between two calibration steps. The diverter tests for $n=9$ and $n=14$ have been performed with masses $m_i \approx 13\,700$ kg and $m_c \approx 14\,300$ kg. The results strongly suggest that there has been a bias of different signs on both mass measurements. The loads used m_i and m_c are just between two calibrated points. A bias cannot be rejected.

Given the nature of the sensitivity of the timing error to a mass bias, the measurements with large n provide a good estimation despite the small mass measurement errors. A mass bias of this

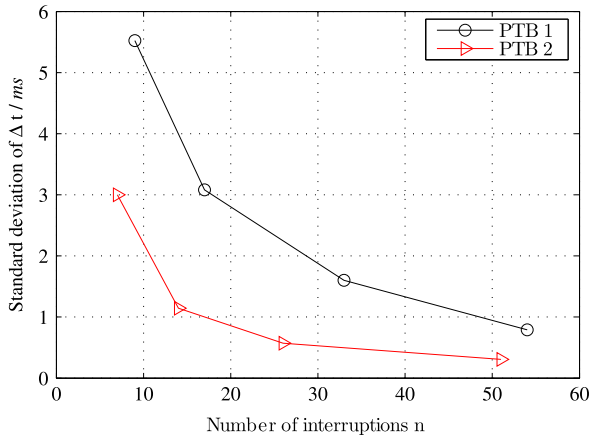

Fig. 5. Standard deviation of the timing error for different amounts of filling interruptions during the tests in the PTB-Braunschweig (2) and PTB-Berlin (1). The standard deviation values are based on 15 repetitions, only the last point of PTB-1 is based on 20 repetitions.

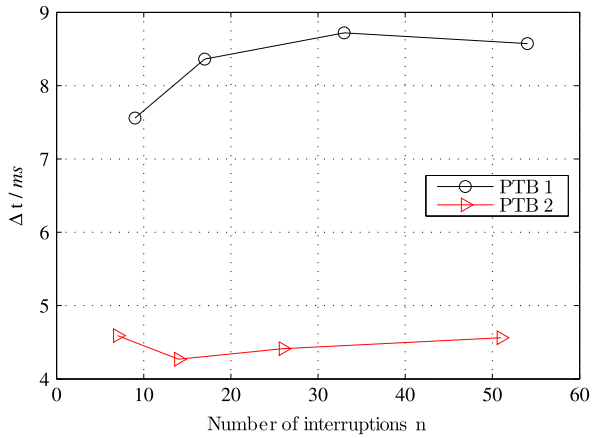

Fig. 6. Timing error at both laboratories.

magnitude is being considered already in the uncertainty budget of the calibration facility.[2]

3.1. Estimation of the parameters

The parameters of Eq. (29) can be estimated through a weighted least square linear regression. For this purpose, the equation will be rearranged introducing the independent parameter λ and the dependent parameter ϕ:

$$\phi = \sigma_{\Delta t}^2 \frac{(n-1)^2}{(n+1)} \tag{30}$$

$$\lambda = \frac{1}{(n+1)} \tag{31}$$

By doing so we obtain

$$\phi = t^2 \sigma_{kf}^2 \lambda + \sigma_\delta^2 \tag{32}$$

Now it is easier to fit the values of σ_δ and σ_{kf} in Eq. (32) based on the experimental data. Considering that for a normal distribution the variance of the sample variance is given by

$$\sigma_{\sigma\Delta t}^2 = \sigma_{\Delta t}^2 \sqrt{2/N} \tag{33}$$

as weights for the weighted least squares we will use the inverse variances of the sample variances.

The results of the regression are the slope S and the 0-crossing ϕ_0. Given these two parameters and considering Eq. (22) we can write

$$S = t^2 \sigma_{kf}^2 = 2\ t^2 \sigma_m^2 (1-r) \tag{34}$$

$$\phi_0 = \sigma_\delta^2 \tag{35}$$

In Figs. 7 and 8 we can see the obtained sample variances, the 0.95 confidence intervals of the sample variances, the weighted least square regression line, and the 2-sigma region for the zero-crossing (ϕ_0). Fig. 9 shows the fitting results back in the domain of n and $\sigma_{\Delta t}$. Table 2 resumes the regression results shown in Figs. 7 and 8.

Considering Eqs. (34) and (35), it is clear that the slope S of the regression line, and the 0-crossing point ϕ_0 have to be positive to produce real results. However, the weighted least squares result in very small negative values for ϕ_0. This can be attributed to the uncertainty of the experiment itself. But considering for example the 0.95 confidence intervals of the sample variances for both experiments at PTB-1 and PTB-2, we can see on Figures 7 and 8 that for these experiments, a family of possible solutions that fit between both 0.95 limits, and that fulfill the condition of $\phi_0 > 0$ does exist.

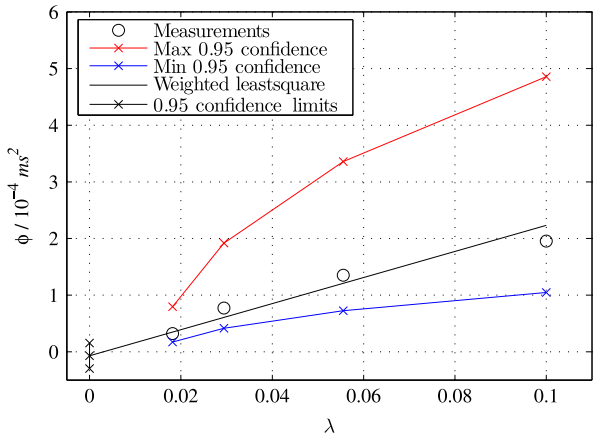

Fig. 7. Linear fit function of the parameters ϕ and λ for the tests carried out at the PTB-Berlin.

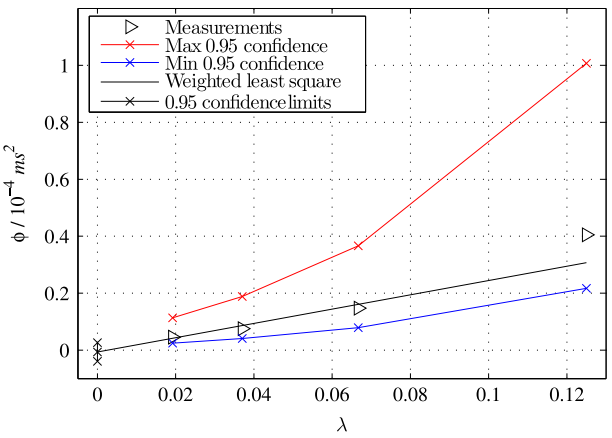

Fig. 8. Linear fit function of the parameters ϕ and λ for the tests carried out at the PTB-Braunschweig.

[2] Due to the small mass measurement bias detected, a redundant weighting system based on strain gauges has been installed in PTB-1. This measure improved the robustness against linearity errors between calibration points. The results of these improvements are the subject of a different study.

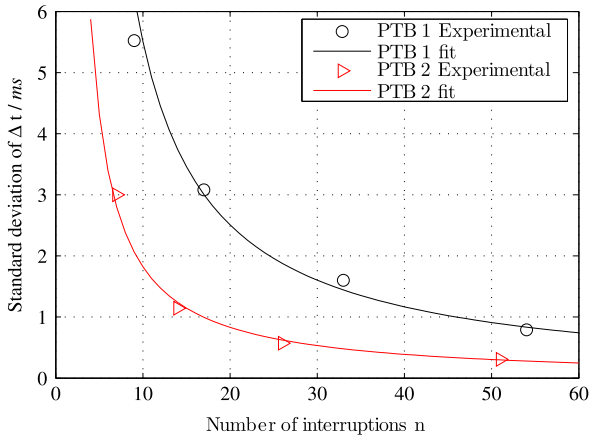

Fig. 9. Measured and fitted standard deviation of the timing error for different amounts of filling interruptions during the tests in the PTB-Braunschweig (2) and PTB-Berlin (1).

Table 2
Weighted least squares results with its corresponding standard errors.

Parameter	PTB-1	PTB-2
S	23.03E−04	2.511E−04
σ_S	4.17E−04	0.52E−04
ϕ_0	−7.07E−06	−0.67E−06
$\sigma_{\phi 0}$	11.31E−06	1.64E−06
$\sigma_{\dot{m}}$	1.43E−04	1.16E−04
$\sigma_{\sigma\dot{m}}$	0.61E−04	0.53E−04

By applying a weighted least squares regression instead of regular least squares, the obtained results are not just single points, but rather result ranges defined by an upper and a lower limit. The real value is between those limits. These limits are defined by the uncertainty associated to the regression results. A simple strategy for obtaining a robust worst case estimation of the wanted parameter is to use those limits that result in the largest uncertainty. Please consider the following interesting numerical example extracted from [6] for selecting the appropriate limits. Considering the characteristics of the variance of the sample variance $\sigma_{\sigma sv}$, if normality is given, the 0.95 confidence region would be defined by

$$P\left\{\left|\sigma_{\sigma sv}^2-\sigma^2\right| \le 1.96\sigma^2\sqrt{2/N}\right\}=0.95 \tag{36}$$

if we state a requirement of a maximum error of 10%, then we would obtain

$$\frac{\left|\sigma_{\sigma sv}^2-\sigma^2\right|}{\sigma^2}=0.10 \tag{37}$$

$$\frac{1.96\sigma^2\sqrt{2/N}}{\sigma^2}=0.10 \tag{38}$$

consequently, the required sample size would be

$N_{0.95} \approx 750$

By reducing the confidence down to 0.68, would require

$N_{0.68} \approx 200$

This lets us conclude that even the requirement of a confidence level of 0.68 for any regular measurements where the sample variance is directly estimated is hard to fulfill. Therefore, in the following analysis a confidence level of 0.68 will be considered to be sufficiently rigorous. Consequently, the expansion factor for the variance of the sample variance would be 1.

For the timing error, the worst case scenario would be given by

$$\max(\sigma_\delta)={\phi_0}^{0.5}+{\sigma_{\phi 0}}^{0.5} \tag{39}$$

In this case, the value of ϕ_0 is negative, therefore we assume ${\phi_0}^{0.5}$ approx 0. The extreme values for the repeatability of the flow meter are defined by

$$\max(\sigma_{\dot{m}})=\sigma_{\dot{m}}+\sigma_{\sigma\dot{m}} \tag{40}$$

$$\min(\sigma_{\dot{m}})=\sigma_{\dot{m}}-\sigma_{\sigma\dot{m}} \tag{41}$$

As seen in Table 3 the standard deviation of the diverting systems of the PTB-Braunschweig is 1.2 ms and for the PTB-Berlin 3.3 ms. Engel and Baade [3] have proven, using the modeling approach, that the uncertainty contribution of the timing error at the PTB-Braunschweig is not greater than 4 ms. This result can be considered compatible with the results found in this paper. In the case of the PTB-Berlin it is not possible to establish a full model of the diverting phenomena. The reason for this is that the flow at the entrance of the diverter will always be unknown since there is no possibility of measuring the velocity profiles. For this reason, the obtained value of 3.3 ms will be included in the uncertainty budget.

3.2. Repeatability of the test bench

The repeatability of the test bench alone σ_{ref} can be expressed based on the repeatability of the calibration factor σ_{cal} of the flow meter, and on the repeatability of the flow meter alone $\sigma_{\dot{m}}$. By considering this we have

$$\sigma_{ref}=\sqrt{\sigma_{cal}^2-\sigma_{\dot{m}}^2} \tag{42}$$

If we considered the upper limits for the repeatability of the flow meter $\sigma_{\dot{m}}$, we would underestimate the repeatability of the test bench; therefore, the lower limit should be used in order to have a worst case estimation. The following results were obtained (Table 4).

The repeatability of the flow rate facilities, including all systems taking part in the measurement have been estimated to be at the most 0.64×10^{-4} and 0.87×10^{-4} for both facilities. This is the only method that provides a well-founded result to estimate the repeatability of the test bench alone.

4. Discussion

In order to obtain the presented results about 120 flow meter calibrations were required for each facility. About 3000 diverting actions per diverter were performed. Considering the large effort required and the material fatigue induced on the diverter

Table 3
Repeatability of the flow meter and of the diverter.

Parameter	PTB-1	PTB-2
$\max(\sigma_{\dot{m}})$	2.04E−04	1.69E−04
$\sigma_{\dot{m}}$	1.43E−04	1.17E−04
$\min(\sigma_{\dot{m}})$	0.82E−04	0.64E−04
$\max(\sigma_\delta)$	0.0034 s	0.0013 s

Table 4
Fitting results for σ_{ref}.

Laboratory	$\sigma_{\dot{m}}$	σ_{cal}	σ_{ref}
PTB-1	0.82E−04	1.20E−04	0.87E−04
PTB-2	0.64E−04	0.90E−04	0.64E−04

components, if the goal was only to determine the diverter induced timing error and its uncertainty, it is questionable whether the invested resources would always justify the results. Even more so if we consider that only one flow rate at one fluid temperature has been analyzed. Performing tests for several flow rates and temperatures should be analyzed well, since aging might cause a drift of the diverter characteristics, and the conclusions drawn might not be valid.

However, if the aim of the test is to obtain an estimation of the repeatability of the test bench, or the repeatability of one or of several flow meters installed during the tests, then the efforts might be seen as reasonable. One might consider avoiding measurements with a lower number of filling intervals since they do not weigh much during the least squares regression. But if we consider that systematic errors on the mass determination are detectable only using low n, these measurements are important as those with large n.Given that the method aims to obtain a worst case estimation, the fact that the regression analysis delivers a very small negative value does not invalidate the results, but underlines instead the importance of estimating also the variance of the regression results by using the weighted least squares analysis.

The estimation of systematic errors in the mass measurement through the diverter tests can give well-founded evidence of the presence of errors. The evidence of a small mass bias on the results of the PTB-1 confirm the sensitivity of the method. Nevertheless, it cannot be used as a general calibration replacement, since the reasons for a bias may be diverse, and require a more detailed study to be isolated and eliminated.

Only by using the weighted least squares method is it possible to estimate adequately the standard error of the regression, and consequently to establish boundaries on the obtained variances. The present approach is considered a good option to determine the repeatability of the flow test rig. Other methods based on correlation and variance subtraction as proposed by Hayward [7] and Poeschel [8] are considered difficult in practice given the fact that the variance of the sample variance requires hundreds of measurements to deliver accurate results.

5. Conclusions

It can be concluded that the proposed method is applicable to test the overall performance of a flow test rig, providing a tool to detect whether the mass determination is working properly. Additionally, it allows the estimation of the variances of the diverter system, and of the flow meter and the flow test rig independently.

It has been shown that small statistically relevant differences in the determined timing errors indicate if a bias has occurred. Furthermore, it can also be inferred that the weighted least squares regression would deliver plausible results only if all measurements have been performed under repeatability conditions.

The regression results give further insight into the diverter characteristics, into the flow meter used, and into the flow test rig itself. If this method is used periodically as part of a validating procedure, relevant biases that could affect the results, of interlaboratory comparisons for example, could be detected early and eliminated.

Considering that the diverting systems, like every mechanical system, are prone to aging, it is recommended to keep the amount of tests to a minimum.

Acknowledgments

The measurement results used to undertake the analysis of the flow rate facility at PTB-Braunschweig were kindly shared by Dr. Rainer Engel from the Flow Laboratory of the PTB-Braunschweig. We acknowledge his cooperation gratefully.

Appendix A. ISO 4185 method 2

Consider Figs. 10 and 11. The timing error shown in the horizontal axis can also be interpreted as an apparent flow rate error. The dashed area is the mass error that would originate through timing error Δt.

For a continuous test run:

$$\Delta m_c = \Delta \dot{m}_c \cdot t'_c \tag{43}$$

$$\Delta m_c = \Delta t \cdot \dot{m}_c \tag{44}$$

For a discontinuous test run:

$$\Delta m_i = n \cdot \Delta t \cdot \dot{m}_i \tag{45}$$

$$\Delta m_i = t'_i \cdot \Delta \dot{m}_i \tag{46}$$

eliminating Δm_c and Δm_i from Eqs. (43)–(46), we obtain the apparent flow rate variation:

$$\Delta \dot{m}_c = \frac{\Delta t}{t'_c}\dot{m}$$

$$\Delta \dot{m}_i = \frac{n \cdot \Delta t}{t'_i}\dot{m}_i$$

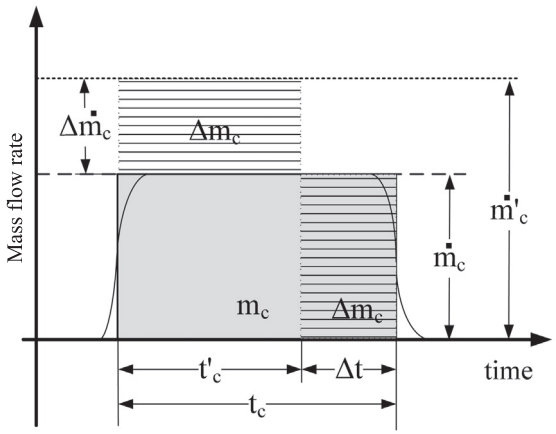

Fig. 10. The figure shows that the diverter error in the time measurement shown in the horizontal axis can also be seen as an error on the vertical axis as a flow rate error.

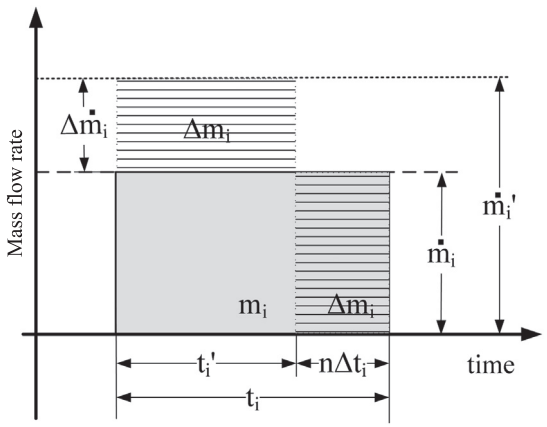

Fig. 11. The figure shows that also for an interval filling measurement the diverter error can also be seen as an error on the vertical axis as a flow rate error. The diagram is simplified. Off-times, where water flows to the bypass, are not shown.

Considering a continuous test run we obtain the following relations:

$$\dot{m}'_c = \frac{m}{t'}$$
$$\dot{m}_c = \dot{m}'_c - \Delta\dot{m}_c$$
$$\dot{m}_c = \frac{m_c}{t'_c} - \frac{\Delta t}{t'_c}\dot{m}_c \tag{47}$$

solving for $\dot{m}$

$$\dot{m}_c = \frac{m_c}{t_c}\frac{1}{1+\frac{\Delta t}{t_c}} \tag{48}$$

Analogously, considering an interrupted test run we obtain

$$\dot{m}_i = \frac{m_i}{t'_i} - \frac{n\cdot\Delta t}{t'_i}\dot{m}_i \tag{49}$$

$$\dot{m}_i = \frac{m_i}{t_i}\frac{1}{1+\frac{n\Delta t}{t_i}} \tag{50}$$

Ideally, the continuous test run, and the one with interval filling periods should be performed under the same conditions, i.e. exactly the same flow rates should be installed and the same filling times should be aimed at. When this is however not possible or not wanted, a correcting factor k_q can take into account the small flow rate variations. Similarly we apply k_t to compensate for different filling times:

$$k_t = t'_i/t'_c$$
$$k_f = \dot{m}_i/\dot{m}_c \tag{4}$$

By inserting Eqs. (48) and (50) into k_f and applying k_m and k_t

$$k_f = \frac{k_m}{k_t}\frac{1+\frac{\Delta t}{t'_c}}{1+\frac{n\Delta t}{t'_i}} \tag{51}$$

rearranging the equation gives

$$\frac{k_m}{k_t k_f} = \frac{t'_c + \frac{n\Delta t}{t'_i}t'_c}{t'_c+\Delta t} \tag{52}$$

subtracting 1 yields

$$\frac{k_m}{k_t k_f} - 1 = \frac{t'_c + \frac{n\Delta t}{t'_i}t'_c - t'_c - \Delta t}{t'_c+\Delta t} \tag{53}$$

Factorizing Δt on the numerator

$$\frac{k_m}{k_t k_f} - 1 = \frac{\Delta t\left(\frac{n}{k_t}-1\right)}{t'_c+\Delta t} \tag{54}$$

and solving for Δt on the numerator we finally obtain

$$\Delta t = \frac{\Delta t + t'_c}{\left(\frac{n}{k_t}-1\right)}\left(\frac{\frac{m_i}{t'_i}}{k\frac{m}{t'_c}} - 1\right) \tag{4}$$

The simplifications made in the equation proposed by ISO 4185 might be adequate for most of the cases, but under certain circumstances they may introduce a considerable bias on the diverter error as seen. Eq. (4) is completely equivalent to the equations used for example in [2,4].

Appendix B. ISO 4185 method 1

The second approach introduced by ISO 4185 has not been treated in this paper. However it was considered relevant to provide the way it works in order to allow a better judgment of the methods used to test the diverter system. This approach is also based on the comparison of two calibrations, but instead of varying the number of diverting actions, only the duration of the test is changed. Since the diverter error does not change, the effect on the resulting apparent flow rate allows the determination of the diverting error.

By rewriting Eq. (48) in terms of the apparent flow rate for two measurements in different conditions $\dot{m}'_1$ and $\dot{m}'_2$:

$$\dot{m}'_1 = \left(\frac{\Delta t}{t_1}\dot{m}_1 + \dot{m}_1\right)$$

$$\dot{m}'_2 = \left(\frac{\Delta t}{t_2}\dot{m}_2 + \dot{m}_2\right)$$

Subtracting term by term and reordering we obtain

$$\Delta t\left(\frac{\dot{m}_1}{t'_1} - \frac{\dot{m}_2}{t'_2}\right) = (\dot{m}'_1 - \dot{m}'_2) - (\dot{m}_1 - \dot{m}_2) \tag{55}$$

and dividing by $\dot{m}'_2$ we obtain a similar equation presented by ISO 4185.

$$\frac{\Delta t}{\dot{m}'_2}\left(\frac{\dot{m}_1}{t'_1} - \frac{\dot{m}_2}{t'_2}\right) = \frac{(\dot{m}'_1 - \dot{m}'_2) - (\dot{m}_1 - \dot{m}_2)}{\dot{m}'_2}$$

As seen in Eq. (55), this method is strongly dependent on the accuracy of the flow meters used. In order to reduce this random error, several measurements have to be made. Considering that Δt is the slope of the equation of a line drawn by Eq. (55), the international recommendations suggest estimating its value by means of a linear regression. This method has the advantage that no additional special measurements have to be performed. It is basically possible to include every measurement made by the test rig to confirm or to monitor the diverter error, provided that the reference flow meters used are stable and repeatable.

Appendix C. K-factor formulation

The apparent relative error of a flow meter for the continuous and the interrupted measurements are defined as

$$k'_c = \frac{\dot{m}'_c}{\frac{m_c}{t'_c}} \tag{56}$$

$$k'_i = \frac{\dot{m}'_i}{\frac{m_i}{t'_i}} \tag{57}$$

The real relative error would be given by

$$k_{cr} = \frac{\dot{m}'_c}{\frac{m_c}{t'_c+n\Delta t}} \tag{58}$$

$$k_{ir} = \frac{\dot{m}'_i}{\frac{m_i}{t'_i+\Delta t}} \tag{59}$$

By expressing Eqs. (58) and (59) as a function of k'_c and k'_i we can write

$$k_{cr} = k'_c + \frac{\Delta t}{\frac{m_c}{\dot{m}'_c}} \tag{60}$$

$$k_{ir} = k'_i + n\frac{\Delta t}{\frac{m_i}{\dot{m}'_i}} \tag{61}$$

Assuming that the relative error of the flow meter for the region near the working point is constant, then we can write

$$k_{cr} = k_{ir} \tag{62}$$

Finally, solving for Δt gives

$$\frac{\Delta t}{t_c} = \frac{k_i' - k_c'}{\frac{n}{k_t} k_i' - k_c'} \tag{63}$$

References

[1] International Standard ISO 4185. Measurement of liquid flow in closed conduits —weighing method, first ed. ISO; Beuth Verlag, Berlin, 1980.
[2] Marfenko Iryna V, Yeh Tsyh T, Wright John D. Diverter uncertainty less than 0.01 percent for water flow calibrations. In: International symposium for fluid flow measurement conference proceedings. Queretaro; 2006.
[3] Engel Rainer, Baade Hans. Model-based flow diverter analysis for an improved uncertainty determination in liquid flow calibration facilities. Meas Sci Technol 2010;21(2).
[4] Mathies N, Lederer T. Neue Methode zur Bestimmung des Zeitfehlers für Umschalteinrichtungen von gravimetrischen Messanlagen [New way of estimating the diverter timing error for gravimetric flow calibration systems] tm - Technisches Messen, vol. 74(6); June 2007.
[5] Shimada T, Oda S, Terao Y, Takamoto M. Development of a new diverter system for liquid flow calibration facilities. Flow Meas Instrum 2003;14(June (3)).
[6] Yaakov-Bar-Shalom, Rong Li X, Kirubarajan Thiagalingam. Estimation with applications to tracking and navigation: theory algorithms and software. Weinheim, Germany: John Wiley & Sons. Inc.; 2001. p. 107.
[7] Hayward ATJ. Measuring the repeatability of flow meters. NEL Report no. 636. National Engineering Laboratory; May 1977.
[8] Poeschel W. Internal and external comparison measurements for ensuring accuracy and traceability in flowmeter calibration. In: International symposium on fluid flow measurement. Denver, USA; 1999.

3.2. [Cor14b] Application of a novel method for validating the uncertainty estimation of a flow test facility

This article presents in the first part an overview of the methodology established to determine the uncertainty of the WZP. Special attention is given to the characterization of the weighing and the diverting system. A novel method is presented to characterize the contribution of the diverting system based on the analysis of the diverter motion by logging its position in time. In the second part, this article introduces a method to validate the calibration results that, in contrast to 3.1, only require regular calibration results. The smooth Reynolds dependency of the discharge coefficient of an orifice plate made it possible to compare high accurate measurements at different conditions but at the same reynolds number. Due to the high reproducibility of the installation conditions it was possible to establish a reference curve that depends only on the reynolds number. If the measurement results lay on the curve the measurement point can be considered to be consistent. If the results are within the declared uncertainties, it can be rejected that unknown relevant systematic errors are present. In order to confirm the method, results of a bilateral comparison with the flow laboratory of the NMIJ are briefly presented.

3.2.1. Credits

The article is co-authored by Dr. N. Furuichi and Dr. T. Lederer. Dr. N. Furuichi performed the measurements for the bilateral comparison at the NMIJ and provided the technical equipment and technical assistance during the orifice plate measurements. Dr. T. Lederer has contributed to the planning of the measurement campaigns for the uncertainty determination of the WZP.

3.2.2. Pulication details

A central part of this article is the uncertainty determination of the WZP, the Heat meter test facility of the National institute of Metrology of Germany. The article has been submitted to and published by - tm - Technisches Messen.

Beiträge

Moritz Leopoldo Cordova Murillo*, Noriyuki Furuichi, and Thomas Lederer

Application of a novel method for validating the uncertainty estimation of a flow test facility

Anwendung eines neuen Verfahrens für die Validierung von Durchflusskalibrieranlagen

Abstract: After a large heat meter flow test rig was overhauled, making a thorough characterization and revalidation of the associated uncertainty is necessary. Validating the uncertainty through interlaboratory comparisons takes years and is not always successful. Therefore, a method is proposed to validate the uncertainty estimation based on a flow meter Reynolds number similarity in between comparisons. The newly estimated uncertainty of an overhauled facility is schematized and the proposed method is applied. The obtained results are confirmed through a conventional international interlaboratory comparison.

Keywords: Uncertainty validation, flow calibration facility, orifice plate, Reynolds dependency.

Zusammenfassung: Immer wenn eine Durchflusskalibrieranlage verändert wird, ist die Messunsicherheit dieser Anlage neu zu bestimmen. Die Validierung der Messunsicherheit mittels Ringversuchen erfordert jedoch öfters Jahre und die resultierenden Ergebnisse sind nicht immer aussagekräftig. Aus diesem Grund wird ein neues Verfahren vorgestellt, welches basierend auf der Reynolds-Ähnlichkeit eines Durchflusssensors erlaubt, die langen Zeiten zwischen Ringversuchen zu decken. Nach der Skizzierung der Messunsicherheitsbestimmung einer Messanlage wird die Anwendung des Vefahrens vorgestellt. Die Ergebnisse werden schließlich durch einen konventionellen internationalen Ringvergleich überprüft.

Schlüsselwörter: Messunsicherheitsvalidierung, Durchflusskalibrieranlage, Messblende, Reynolds-Abhängigkeit.

DOI 10.1515/teme-2014-1039
Received June 24, 2014; accepted July 15, 2014

1 Introduction

Flow rate calibration facilities play an essential role when any process involving flowing media requires traceability. Their performance does not rely only on the technical infrastructure, but also on the methodology that is followed to guarantee the performance specifications are being met. This is accomplished through the maintenance of a quality management system which necessarily includes the estimation of the uncertainty according to the requirements of the Guide to the expression of uncertainty in measurement [2]. The uncertainty analysis takes as granted that no gross errors occur. In order for this assumption to be always true, a systematic maintenance of the hardware and a routine statistical analysis are unavoidable.

The most accepted way of validating that the uncertainty estimation is free of relevant undetected systematic errors and has been modeled adequately are interlaboratorial comparisons. The challenges to finish a comparison with success are of technical and of logistical nature. Depending on uncertainty levels of laboratories participating in the comparison, the efforts required to characterize the comparison flow-meter-set may take several months. For uncertainty requirements below 0.1 %, undetected influence quantities may overlap the measurements to such extent that drawing conclusions about the uncertainties of the participating laboratories would be impossible. Considering that a comparison may take several years to get completed, at the moment the results are available, the conditions at the laboratories might have changed; as a consequence participants with undetected systematic ef-

***Corresponding author: Moritz Leopoldo Cordova Murillo,** Physikalisch-Technische Bundesanstalt (PTB), Abbestraße 2–12, 10587 Berlin, Germany, e-mail: leopoldo.cordova@ptb.de
Thomas Lederer: Physikalisch-Technische Bundesanstalt (PTB), Abbestraße 2–12, 10587 Berlin, Germany
Noriyuki Furuichi: National Institute of Advanced Industrial Science and Technology (AIST), Tsukuba Central 3, Umezono 1-1-1, 305-8563 Ibaraki, Japan

fects would disseminate their errors to their customers for years without knowing it.

This is a condition that should be avoided. The DIN EN ISO/IEC 17025:2005 suggests under 5.9 among other, to *replicate calibrations using the same or different methods*, and to *apply correlation of results for different characteristics of an item*. A direct application of those suggestions is only applicable if the reproducibility and the long-term stability of the flow meter are sufficiently high. An adaptation of the suggestions of the standard to flow calibration facilities will be described in this paper. By applying the proposed approach, systematic errors might be quickly detected and wrong measurements can be minimized.

On 2013 the heat meter calibration facility of the PTB (Wärmezählerprüfstrecke WZP) has been subject to general overhaul. Several essential systems have been changed making a new characterization of most uncertainty components necessary. Since a validation of the obtained estimation is also necessary, both an internal and an external validation have been performed. The present paper will illustrate the validation methods applied to the WZP.

The content of this paper is structured as follows: In the first part the WZP and the uncertainty estimation of the most relevant overhauled components will be outlined. The second part will show details on the internal validation, and the third part will present the results of the external validation with the NMIJ.

2 Uncertainty estimation of a heat meter testing facility

The Wärmezählerprüfstrecke (WZP) is a hot water gravimetric flow test facility[1] and, as every flow meter calibration facility, it has to fulfill two functions at a time. It has to be able to measure a flow rate very accurately, and it has to realize or generate this flow rate within predefined conditions. These conditions may vary depending on the analyzed flow meter, or more specifically, depending on the influence quantities,[2] as pressure and temperature. For most flow measurement principles the flow profile is the most important influence quantity, but for a gravimetric flow test rig, this influence is irrelevant.

The gravimetric principle has the big advantage that it is scalable; the limits are basically set only by the size of the tank, by the accuracy of the weighing system, and by the size of the pumping system. There are flow rate facilities measuring down to 1 ml/h based also on this principle, as seen on [9], as there are facilities with flow rates above 3000 m^3/h and a 50 t weighing scale, as is the case in the AIST NMIJ described in detail in [10].

The most important characteristics of the WZP are given in Table 1. For a detailed description, please refer to [5].

The hardware components of the WZP were finished in 2002 and the first validation of its performance was performed by Mathies [5] in 2003. During 2013, after more than 30 000 single measurements, the most important components of the WZP have been subject of extensive maintenance: the diverter systems were renewed; the force isolating and force transmitting components of the weighing scale had been adjusted; a redundant strain gauge system had been installed; the humidity determination systems were improved; the pumping systems were partially replaced and other proactive maintenance measures were taken. Given these considerable hardware changes, a comprehensive characterization was required to ensure not only that every system was working properly, but also that the required uncertainty levels were maintained.

The uncertainty estimation of the WZP has been divided into four groups: the mass determination, the time determination, the density determination and the determination of the process-related corrections. This last group includes all additional mass correction due to thermal expansion, air entrapment, buoyancy variations and evaporation losses.

Figure 1b shows the influence of temperature and filling volume on uncertainty. It can also be seen that higher

Table 1: WZP specifications.

Property	Value	Std. deviation
Max. flow rate	1000 m^3/h	0.1 %
Temperatures	4 °C to 90 °C	50 mK
Scale capacity	20 t	0.140 kg
Pipe diameter	DN50–DN400	50 µm[1]
Test line	25 m	
Max Pressure	0.5 MPa	
Pipe roughness[2]	0.09 µm	

[1] Maximum flange mismatch
[2] Available for DN100, DN200 and DN400

1 The general working principle of a gravimetric flow test facility is given, e. g., in [1].

2 The term influence quantity is defined in the International Vocabulary of Metrology. It refers to quantities that might influence the measurement result, but do not change the actual quantity being measured.

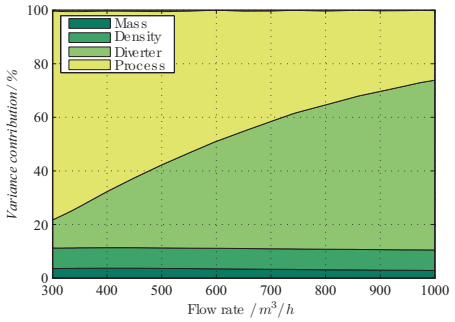

(a) Uncertainty contribution factors for the required expanded uncertainty of 0.04 % in percent for 80 °C

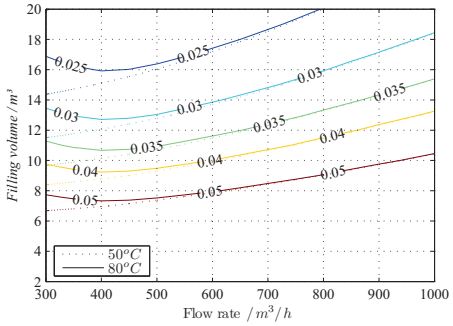

(b) Different expanded uncertainty values that can be reached at 50 °C or 80 °C for different filling volumes.

Figure 1: Uncertainty analysis of the WZP.

temperatures play only a role for lower flow rates. And, as expected, it can be also seen that depending on the required uncertainty, a minimum filling volume is necessary. Figure 1 does not consider the contribution of the meter under test.

Figure 1a shows graphically how the uncertainty components interact when an expanded uncertainty of 0.04 % is required. It can be seen that if larger flow rates are required, the major component is the timing error; for lower flow rates the process-related corrections have the largest contribution. If working properly, the mass and the density determination systems have a very low contribution to the overall uncertainty.

The type of diagrams used in Figure 1b and 1a give a good impression of the uncertainties that can be reached by the WZP. But it would be wrong to believe that this potential is automatically reached every time. The efforts required to make this potential available are not part of any uncertainty budget. They can only become visible through the implementation of a quality system.

2.1 Mass determination

The uncertainty estimation of mass determination is based on the same indicators used for regular weighing systems as linearity, repeatability, eccentricity and reproducibility to thermal influences and to short and midterm drifts. But in contrast to regular weighing systems used for static solid loads, we have to consider for the weighing systems of flow calibration facilities additionally the influences caused by water dripping, by water waves, and by possible tangential forces due to mechanical contact to static subsystems as the diverter or the signal and power cables.

The reproducibility of the weighing scale gets affected, if the tank surface is wet. This can be observed in Figure 2. The results have been obtained through automatic calibration using standard weights. The dry measurements have been performed after a several days long drying period to guarantee all surfaces are water free. The regular calibration results have been obtained between regular flow meter calibrations, i. e., the inner surfaces of the weighing tank were wet and the absence of dripping could not be guaranteed. There seems to be a slightly larger influence of the wet surfaces on reproducibility when larger volumes are filled. In all cases, the influence of wet water surfaces and dripping can be neglected.

Figure 3 shows the influence of waves and water movement on the indication of the force compensation based weighing system (FC), and of the strain gauge based weighing system (SG). Both weighing systems are installed in series. The FC requires a mechanical lever system to reduce the force to the range of the force transducers; in the case of the SG, the forces are transmitted directly to 16 single force

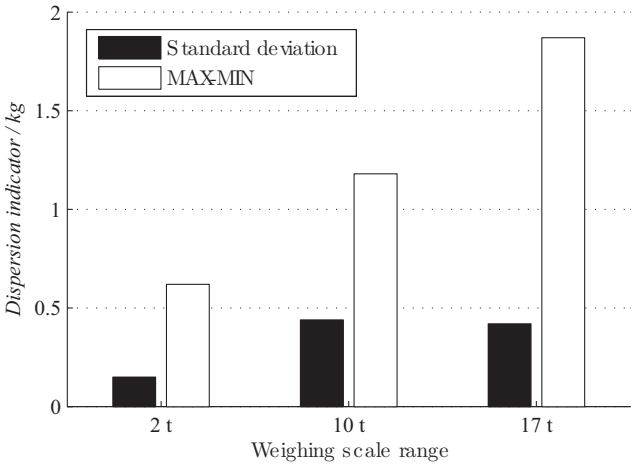

Figure 2: Reproducibility of the weighing system for dry and wet conditions.

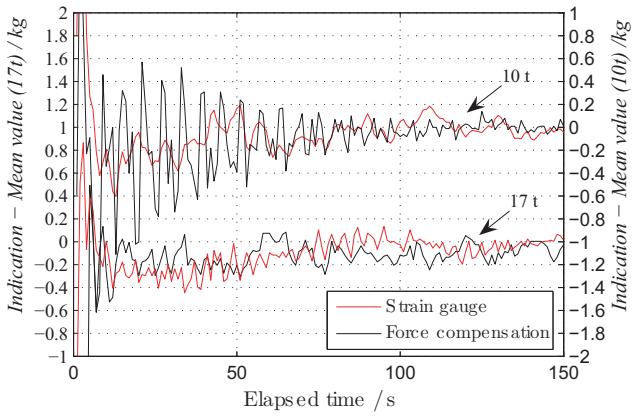

Figure 3: Influence of waves on the stabilization time.

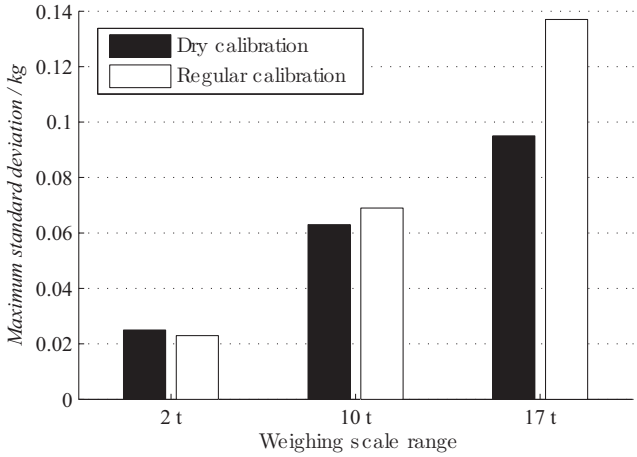

Figure 4: Repeatability of the weighing system for dry and regular conditions.

transducers. Since the forces due to water waves are the same for both systems, the oscillations seen on the indication of the FC system are caused by the FC system itself. For larger filling volumes, the indications of the FC system and the SG system get closer. This means that the signal becomes independent of the used system. Consequently, we can conclude that the force transmission and lever system are working properly.

The overall reproducibility of the weighing system in a period of several months can be seen in Figure 4. A first impression reveals a large difference between the maximum and minimum indications; the difference is about 1.9 kg for the high range. But even in this case, this max-min difference is within the 99 % limits established by the standard deviation, which given the large amount of measurements involved is a plausible result.

The center of gravity of the filled weighing tank for a given water volume should be constant; this allows a great repeatability and reproducibility to be reached, since the mechanical structure of the weighing scale is always loaded in the same way. In the case of the WZP, the weighing scale is calibrated automatically; this leads also to a very high repeatability, since the weights are positioned every time in the same way. Figure 5 shows the difference measured between a calibration using weights, and by filling the weighing tank with about the same mass. In order to avoid the influence of bias, relative values have been used. The maximum difference occurs at the lowest range and is about 0.6 %. The differences for higher loads are not larger than 0.4 %. Within this small band it is expected that eccentricity errors caused by different linearity responses of each corner are negligible.

A good indication for the system's overall status is the trajectory of the center of gravity. Figure 6 shows the position of the center of gravity after and before maintenance as calculated from the indication of the single FC cells. As it can be seen, apparently the center of gravity is moving

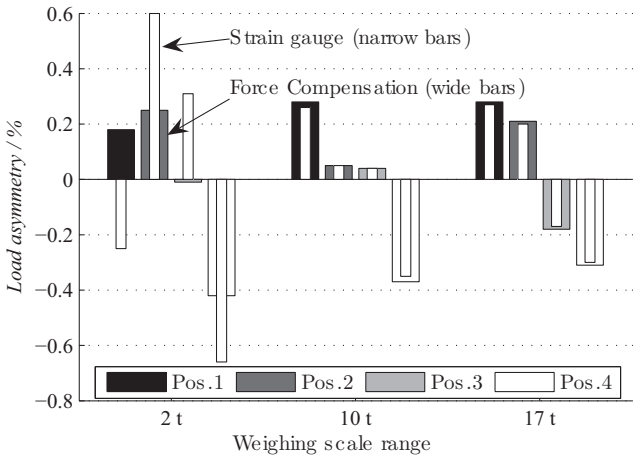

Figure 5: Eccentricity of the weighing system.

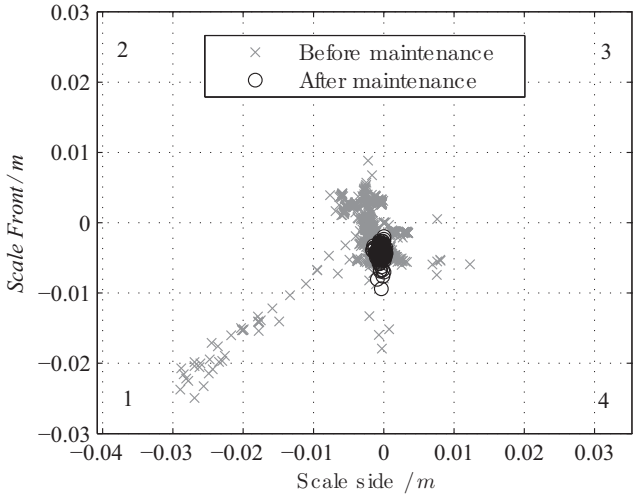

Figure 6: Center of gravity monitoring scheme.

towards corner "1" up to 3 cm. A lateral displacement of this magnitude is physically impossible; therefore, it was assumed that the force transmission on FC cell 1 was defect. The maintenance confirmed the assumption: a mechanical adjustment of the tangential force compensation bearings was necessary.

The aim of the new SG system is to detect anomalies in the force transmission system. It is expected that any anomalous oscillations or eccentricity effect will be immediately detected.

2.2 The time determination

Every time a back and forth diverter motion is performed during a flow meter calibration, a constant time error is added to the time measurement, this distorts the obtained K-factor. By changing the amount of diverting actions or interruptions "n" in one calibration, it is possible to calculate the constant time error introduced by the diverting system.

Considering that k' is given as a function of the relative error k through $k' = k + 1$, the timing error can be determined using:

$$\frac{\Delta t}{t_c} = \frac{k'_c - k'_i}{\frac{n}{k_t}k'_c - k'_i} \tag{1}$$

where the subscripts c and i correspond to a regular calibration and to a calibration with interruptions, Δt is the timing error, t is the filling time of a regular calibration, and $k_t = t_i/t_c$.

The deduction of Equation (1) is given in the Appendix. Further details on the diverter error determination can be found, e. g., in [1, 3, 8] or [4].

The diverter system of the WZP has to open in the sense that it does not influence the flow rate on the test line; but it has to be closed in order to avoid the hot water to evaporate out of the weighing tank. The solution involves the use of tight sealed plastic joints and an air labyrinth seal. The deformation of the used plastic sealing at higher temperatures in the presence of water can be slowed down, but not impeded completely. As a consequence, periodic maintenance is necessary.

As seen in Figure 1, the contribution of the timing error is very important for larger flow rates. Therefore, beyond the single determination of the timing error, it is necessary to monitor the performance of the diverter permanently. Only a few milliseconds would suffice to make the uncertainty estimation of the time measurement invalid.

If we assume that the diverter error is only dependent on the dynamics of the diverter motion, by assuming for example that the flow profile entering the diverter is uniform, and knowing the position of the trigger point for the time measurement, it is possible to estimate the timing error based on the integration of the diverter speed only. The assumption of a uniform flow profile is not correct, but for the purpose of determining the diverter motion influence it is acceptable.

The diverter is actuated by four pneumatic cylinders. Each cylinder has two chambers, and in order for the diverter to act, four chambers have to be evacuated and four have to be pressurized. In order to obtain a smooth but fast movement, it is necessary to optimize the timing of the valves evacuating and pressuring the cylinders, and to adjust the air flow rate of pressurization and evacuation.

Figure 7 shows the diverter motion before the adjustment of the pneumatic system, and Figure 8 shows the diverter dynamics after the adjustment. The motion has been logged using an oscilloscope on the incremental encoder mounted on the diverter main axis. One diverter motion

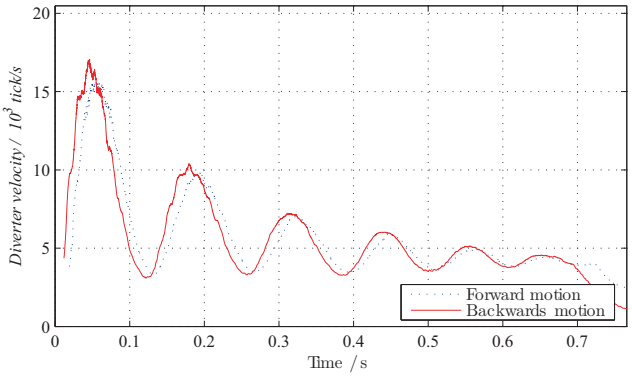

Figure 7: Diverter motion before adjustment. Back and forth motions are displayed.

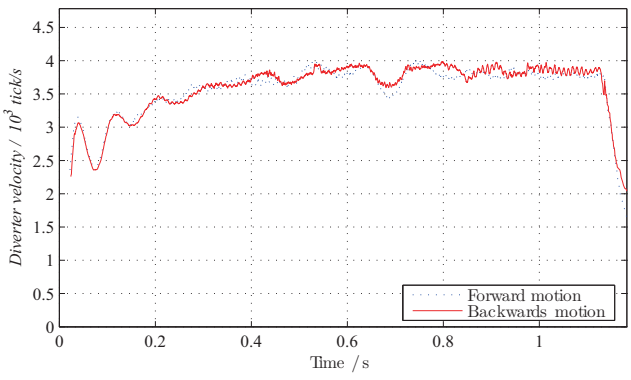

Figure 8: Diverter motion after adjustment. Back and forth motions are displayed.

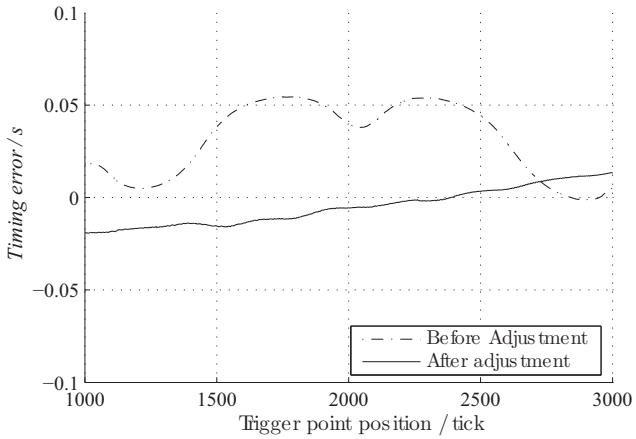

Figure 9: Timing error for different trigger point positions.

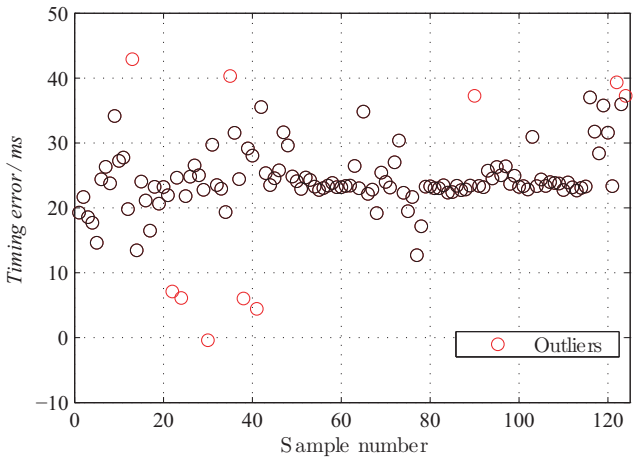

Figure 10: Theoretical timing error based only on the diverter dynamics. The flow profile at the entrance of the diverter has been assumed to be constant.

is equivalent to about 4000 markings or ticks of the incremental encoder. The velocity has been averaged with a moving average of 10 values.

A great improvement has been obtained in the diverter motion; in contrast to the measurements before the adjustment, the velocity is almost constant for the entire interval. The consequence of the improvement can be seen in Figure 9. The figure shows the theoretical timing error that would exist as a function of the position of the trigger point. It can be seen that the curve corresponding to Figure 7 does not cross the zero-error line. This means that there is no trigger point where the timing error can be fully compensated.

Figure 10 shows the theoretical timing error estimated from 124 measurements. It can be seen that most timing errors are within a narrow band. However, there are some measurements outside the 95 % confidence interval. This method allows the detection of outliers even before the K-factor of the flow meter to be calibrated is calculated.

2.3 The density determination

The density of pure water is a function of temperature and pressure; the empirical equations proposed by the IAPWS97 can be used for example for its determination outside the calibration ranges of the density determination laboratory. It is common practice to assume that small amounts of contaminants introduce a bias independent of temperature and pressure; thus it would be sufficient to determine the bias introduced by contaminants of the working fluid at laboratory conditions, and to apply this correction to the fluid at working conditions. But this procedure cannot be applied directly if the contaminants are dissolved gases. Dissolved gases are introduced mainly when water surfaces are open to the environment and splashing occurs. The solubility of air varies as a function of pressure and temperature; when the vapor pressure of the fluid gets close to environmental pressure, the dissolved gasses tend to get released becoming bubbles and changing the equivalent fluid density. When the temperature is low and the pressure is high, small air bubbles dissolve completely. When no bubbles are present the introduced bias can be treated as it would be a solid or liquid contaminant. When the pressure is not high enough, there might be still small bubbles present in the fluid, affecting the equivalent density of the fluid.

No changes on the density determination systems of the WZP were necessary. Figure 11 shows the effect of pressure on the calibration result of diverse flow meters before

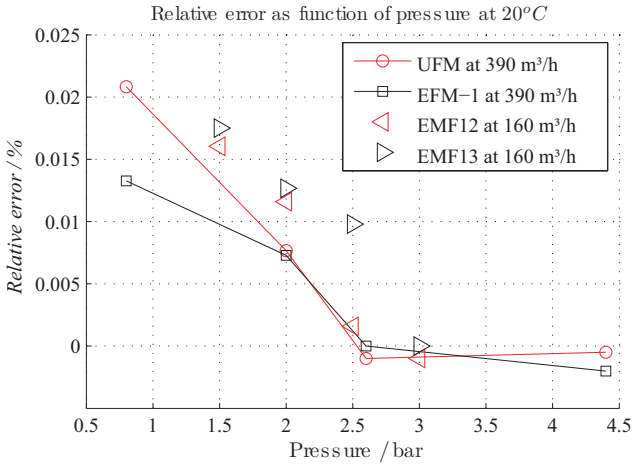

Figure 11: Flow meter K-factor as a function of pressure showing the influence of density variations due to air bubbles.

the maintenance. It is expected that conclusions can also be applied to the actual system. Three electromagnetic flow meters (EMF) and one ultrasonic flow meter (UFM) have been calibrated at 20 °C. According to the specifications of the flow meter, the influence of pressure on the used flow meter for changes under 1 MPa should remain imperceptible; hence the pressure dependency can be fully attributed to the density variations.

As a consequence, depending on the required uncertainty it might be necessary to determine up to which extent it is necessary to proof that the fluid density is independent of the pressure under the current conditions.

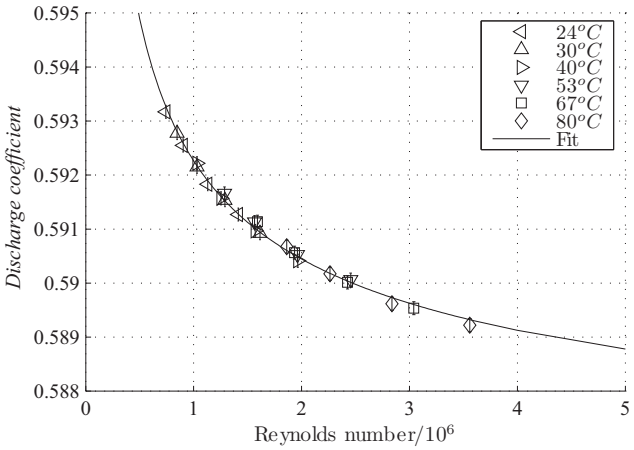

Figure 12: Reynolds dependence of the discharge coefficient of an orifice plate.

2.4 The uncertainty of process-related contributions

All additional uncertainty contributions can be regarded as mass corrections: evaporation at higher temperatures, condensation at lower fluid temperatures, pipe expansion or contractions, air entrapment and air release, buoyancy variations; if occurring during the flow meter calibration, all of these contributions produce a direct influence on the scale indication. The assessment of each of these contributions is based in most cases on plausible estimations, consequently the introduced uncertainty contributions may be over- or underestimated. This is the most important reason to perform a validation of the uncertainty budget: to determine if all model simplifications and assumptions are correct.

3 Internal validation

Every uncertainty contribution varies as a function of different parameters. The timing error for example is a function of test duration and flow rate. The buoyancy corrections and the evaporation are functions of the air and fluid temperature. The weighing error is a function of filling volume. None of the contributions is a function of the Reynolds number. This can be taken advantage of. Considering a flow meter that is strongly dependent on the Reynolds number as an orifice plate, if we determine its discharge coefficient as a function of the Reynolds number by varying the temperature, the flow rate, the duration of the test and the filling volume, we will be able to detect any systematic influence introduced by the flow calibration facility through jumps or discrepancies relative to the discharge coefficient curve.

If we consider for example only the temperature dependence or the flow rate dependence of the discharge coefficient separately, as shown in Figure 13 and 14, it is not possible to separate the contributions of the flow meter and the contributions of the flow calibration facility itself. The flow rate dependence of the orifice plate overlaps with the time and flow rate dependence of the diverter, the temperature dependence may be given by the facility or by the flow meter. Only when the Reynolds number's dependency is analyzed it is possible to separate the contributions of the facility and of the flow meter.

The change of the discharge coefficient as a function of the Reynolds number can be observed in Figure 12. In order to allow a better interpretation, a regression line based on form of the Rearder-Harris-Gallager equation as presented in ISO 5167 [6] and 0.02 % error bars have been added. The maximum difference is about 0.02 % at $Re = 1.6 \times 10^6$.

Considering, for example, the influence of temperature: the maximum vapor pressure gradient is given be-

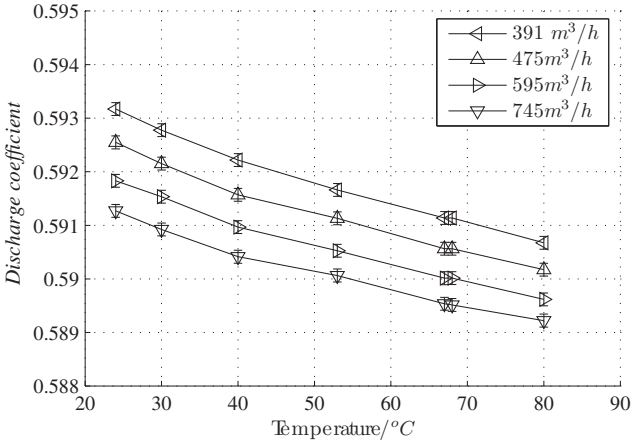

Figure 13: Temperature dependence of the discharge coefficient of an orifice plate.

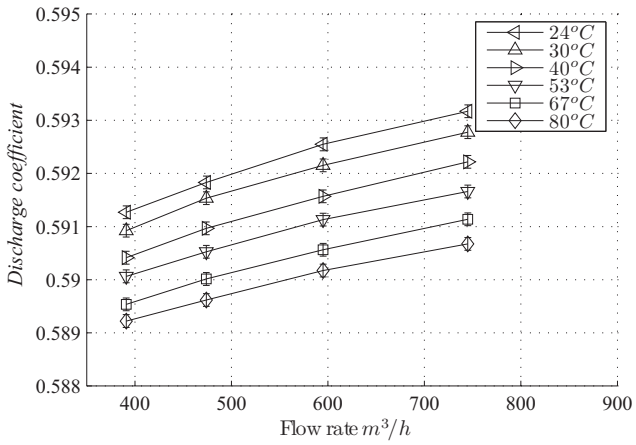

Figure 14: Flow rate dependence of the discharge coefficient of an orifice plate.

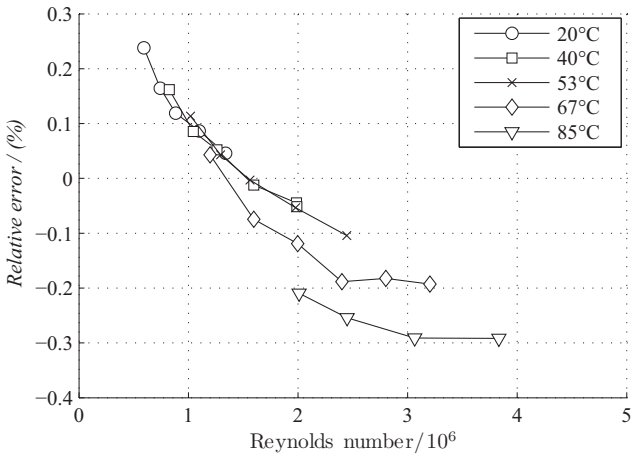

Figure 15: Reynolds dependence of an electromagnetic flow meter after with a disturbed flow profile. .

tween 67 °C and 80 °C; the discharge coefficient curves at these temperatures are closer than 0.01 %, consequently we can confirm that any remaining temperature-dependent contribution as evaporation or buoyancy can be considered to be even in the worst case lower than 0.01 %.

Considering that filling times of coincident Reynolds numbers at different temperatures differ at least with 20 s, and considering also that differences on the discharge coefficient are smaller than 0.01 % and of random nature, a remaining timing error would have to be considerably lower than 0.002 s in order to introduce the observed differences. As a consequence, the performance of the diverter at different temperatures and flow rates is better than 0.002 s.

There is no argument to reject the model nor the assumptions made. It can be considered that the internal validation based on the Reynolds number dependency of the orifice plate has been successful.

To be able to apply this method, stable and repeatable flow conditions had to be guaranteed. In this sense, the orifice plate was installed with an upstream pipe of 90D, the stability of the flow rate during the measurements

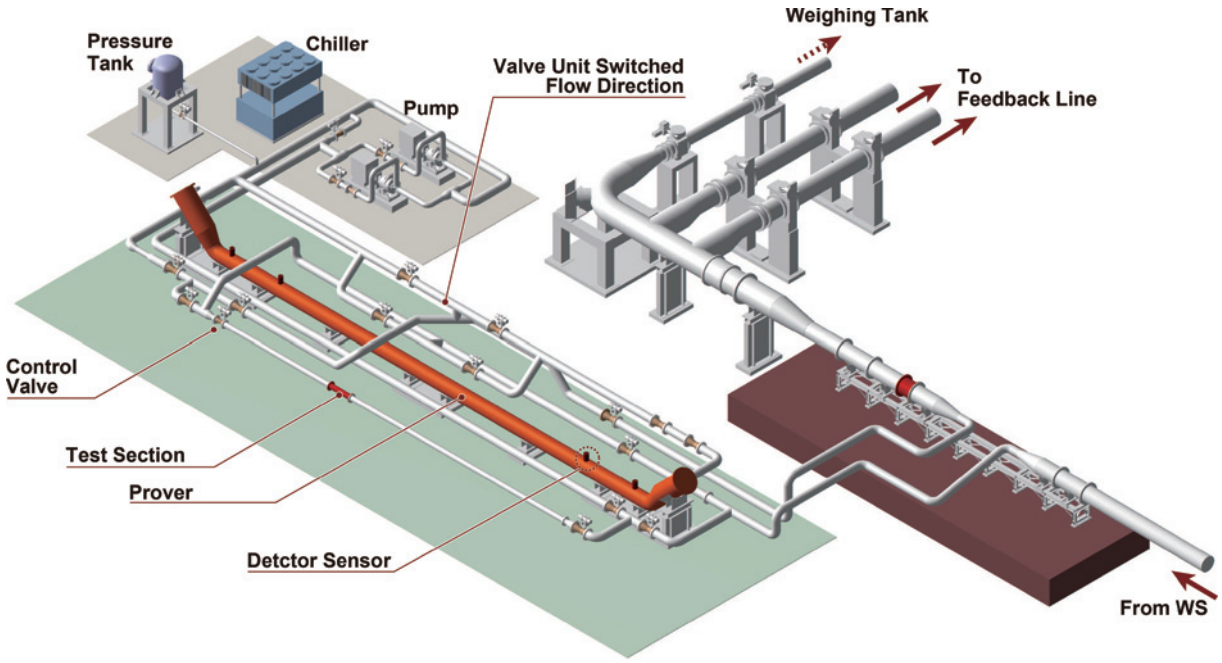

Figure 16: Scheme of the ball prover system of the NMIJ.

was better than 0.1 % and the maximum filling volume has been always chosen as suggested by Figure 1.

A similar test has been performed with the reference EMF flow meter. Since the flow meter is installed with not more than 15D upstream-pipe, and after several pipe accessories, the flow profile conditions are unstable, making the results unusable, as can be seen in Figure 15.

4 External validation

Finally, as the last step of the validation, a bilateral comparison with the flow rate facility of the National Institute of Advanced Industrial Science and Technology AIST NMIJ has been performed. For this purpose a DN200 time-of-flight parallel path ultrasonic flow meter has been selected. The characterization of the flow meter and the design of the comparison are explained in detail in [7]. The configuration can be extracted from Figure 17.

4.1 The flow rate facility of the NMIJ

The flow rate facility of the NMIJ has been described in detail by N. Furuichi in [10]. It is rather a flow calibration complex composed by several gravimetric and volumetric facilities. The calibration range spans up to 12000 m^3/h and 70 °C. All weighing systems are working at ambient temperature. Direct gravimetric traceability at higher temperatures is not possible; therefore, in order to make the higher temperatures traceable, it is required to transfer the accuracy obtained by the gravimetric systems to a tempered volumetric system.

The facility used in this comparison is the prover system shown in Figure 16. This facility is capable of generating flow rates between 200 m^3/h up to 800 m^3/h at temperatures between 20 °C and 80 °C ± 0.5 °C. The highest pressure of the test line is 0.7 MPa. The nominal pipe diameter of the test line is DN200 and the length of test line is approximately 12 m. The maximum Reynolds number in the test section is approximately 3.7×10^6. The reference flow rate is given by the volumetric method. Inside of the pipe, a sphere ball which has 102 % diameter of the pipe is installed. This ball activates detection sensors positioned at the ends of the cylinder when moving from one side to the other. The flow rate is given as the standard volume between two detection sensors divided by the elapsed time. The standard volume between the two sensors is calibrated by the transfer flow meters which are calibrated by the gravimetric systems.

The uncertainty sources of the prover system are the standard volume of the prover, correction of the standard volume for the temperature and pressure, and the measurement of the elapsed time. As mentioned, the standard volume is calibrated using the gravimetric system and the transfer meter and it is the dominant uncertainty source of the prover system. The expanded uncertainty ($k = 2$) of the facility is 0.068 %. The minimum elapsed time is 15 seconds. The measurement is repeated normally 20 times.

4.2 Measurement results

As reported in [7], the purpose of the comparison was to measure the full temperature range. But due to the lack of reproducibility caused by thermal expansion on the installation above 50 °C as explained in [7], only the results at 20 °C and 40 °C are valid. The results are presented on Figure 18. The declared uncertainties of the PTB and the NMIJ are also shown in the figure.

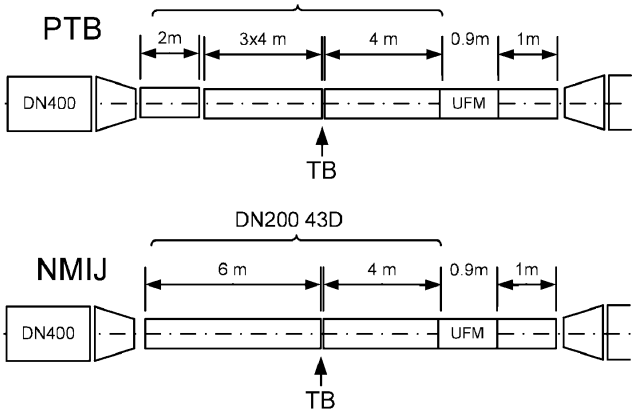

Figure 17: Installation conditions at the NMIJ and at the PTB.

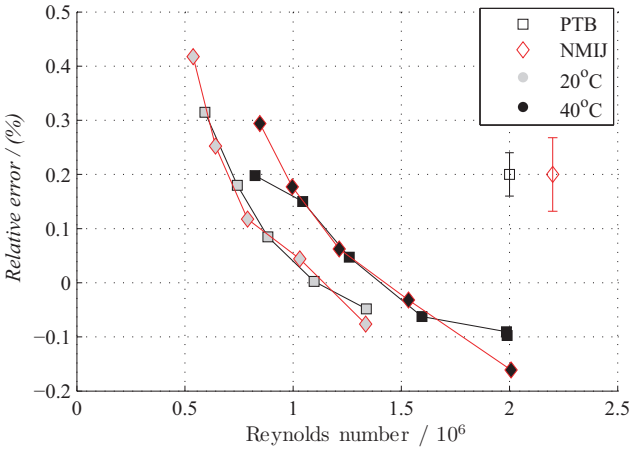

Figure 18: Results of the comparison between the NMIJ and the PTB.

5 Discussion and conclusions

It has been shown that in order to guarantee the proper function of the WZP it is necessary to monitor all contributing subsystems. The load distribution on the different corners of the weighing systems gives insights into the health of the FC system and its force transmission lever system. The addition of a redundant SG system independent of the force transmission lever system allows to infer on the status of the mechanical transmission. The proper functioning of the diverter can be monitored by observing the dynamics of the diverter motion. The influence of gas bubbles can be detected through a flow meter calibration. Only the remaining process-related contributions are difficult to isolate and consequently to validate.

The proposed internal validation procedure based on the orifice plate delivers enough information to reject any doubt on the uncertainty determination of the WZP. The maximum discrepancy is 0.02 % and is not of systematic nature. However, as seen in Figure 15, not every flow meter and not every installation condition is apt for applying this procedure.

The bilateral comparison between the NMIJ and the PTB has proven their mutual consistency for flow rates between 391 m^3/h and 745 m^3/h at 20 °C and at 40 °C. Combining the results of the internal and the external validation, we can consider that the uncertainty budget of the WZP cannot be rejected.

Appendix

If the mass flow rate measured directly by a flow meter is given by $\dot{m}'$ and the mass flow rate given by the calibration facility is given by the ratio of the corrected mass and the effective time as in $\dot{m} = m/t$, we can write for relative errors k_c and k_i:

$$k_c + 1 = k_c' = \frac{\dot{m}_c'}{\frac{m_c}{t_c'}},$$
$$k_i + 1 = k_i' = \frac{\dot{m}_i'}{\frac{m_i}{t_i'}}. \quad (2)$$

The real relative error would be given by:

$$k_{cr} = \frac{\dot{m}_c'}{\frac{m_c}{t_c' + n\Delta t}}, \quad (3)$$

$$k_{ir} = \frac{\dot{m}_i'}{\frac{m_i}{t_i' + \Delta t}}. \quad (4)$$

By expressing Equations (3) and (4) as a function of k_c' and k_i', we can write:

$$k_{cr} = k_c' + \frac{\Delta t}{\frac{m_c}{\dot{m}_c'}}, \quad (5)$$

$$k_{ir} = k_i' + n\frac{\Delta t}{\frac{m_i}{\dot{m}_i'}}. \quad (6)$$

Assuming that the relative error of the flow meter for the region near the working point is constant, then we can write

$$k_{cr} = k_{ir}. \quad (7)$$

Finally, solving for Δt gives:

$$\boxed{\frac{\Delta t}{t} = \frac{k_c' - k_i'}{\frac{n}{k_t}k_c' - k_i'}} \quad (8)$$

The advantage of using Equation (8) is its simple application. The timing error can be calculated directly without any intermediate variables, since the k-factors should be directly available at the flow calibration facilities. Another important advantage is that the flow rate measurement during the calibrations with interruptions is measured indirectly only when water is flowing into the weighing tank. This is only relevant if the diverter system introduces pressure fluctuations into the test line, as is the case when coupled-valve-based diverter systems are used.

Acknowledgement: The active cooperation of Konstantin Richter during the characterization and the comparison measurements in Berlin is greatly appreciated.

References

1. International Standard ISO 4185, Measurement of liquid flow in closed conduits – Weighing method, first edition, ISO (1980).
2. International Recommendation, Guide to the expression of uncertainty in measurement, (ISO 2005).
3. R. Engel, H. Baade, Model-based flow diverter analysis for an improved uncertainty determination in liquid flow calibration facilities, Measurement Science and Technology, Volume 21, Issue 2, 2010.
4. T. Shimada, S. Oda, Y. Terao, M. Takamoto, Development of a new diverter system for liquid flow calibration facilities, Flow Measurement and Instrumentation, Volume 14, Issue 3, June 2003.

5. N. Mathies, Messunsicherheit einer gravimetrischen Kalt- und Warmwasser-Normalmessanlage für große Volumenströme, Dissertation, Technische Universität Berlin, Mensch & Buch Verlag, Berlin, 2005.
6. ISO 5167-2:2003 Measurement of fluid flow by means of pressure differential devices inserted in circular cross-section conduits running full – Part 2: Orifice plates 2003.
7. L. Cordova, N. Furuichi, T. Lederer, Qualification of an ultrasonic flow meter as a transfer standard for measurements at Reynolds numbers up to 4×10^6 between the NMIJ and the PTB, Submitted to Flow Measurement and Instrumentation.
8. L. Cordova, T. Lederer, A practical method to assess the performance of gravimetric flow test rigs by using the timing error, Submitted to Flow measurement and Instrumentation for the Flomeko 2013 Edition.
9. C. David, Novel water flow facility in France – Range extension to low flow rates (10 000 ml/h down to 1 ml/h), Proceedings of the Flomeko 2010, Taiwan, 2010.
10. N. Furuichi, Y. Terao, M. Takamoto, A new calibration facility of flow rate for high Reynolds number, Flow Measurement and Instrumentation, 20-1, pp. 38–47, 2009.

Moritz Leopoldo Cordova Murillo
Physikalisch-Technische Bundesanstalt (PTB), Abbestraße 2–12, 10587 Berlin, Germany, Tel.: +49-30-34817385, Fax: +49-30-34817386
leopoldo.cordova@ptb.de

M. Leopoldo Cordova M. is a research associate at the Department "Heat and Vacuum" of the PTB

Noriyuki Furuichi
National Institute of Advanced Industrial Science and Technology (AIST), Tsukuba Central 3, Umezono 1-1-1, 305-8563 Ibaraki Japan, Tel.: +81-29-861-2293, Fax: +81-29-861-4242
furuichi.noriyuki@aist.go.jp

Noriyuki Furuichi is Chief Researcher at the Flow Division of the AIST.

Thomas Lederer
Physikalisch-Technische Bundesanstalt (PTB), Abbestraße 2–12, 10587 Berlin, Germany, Tel.: +49-30-34817230, Fax: +49-30-34817386
thomas.lederer@ptb.de

Thomas Lederer is Head of the Department "Heat and Vacuum" of the PTB, Institute Berlin.

3.3. [Cor15a] Qualification of an ultrasonic flow meter as a transfer standard for measurements at Reynolds numbers up to 4×10^6 between NMIJ and PTB

This article has a central role for the validation of the calibration results of the WZP. It describes the procedure used to characterize the transfer standard: a parallel path ultrasonic time of flight flow meter. Based on experimental flow meter characterization, it defines the procedure to perform the bilateral comparison between the PTB and the NMIJ. The results are presented and analyzed. Additionally, the flow profile of the WZP is characterized for the ideal conditions at DN200 and relevant findings about the used ultrasonic flow metering technology are presented.

3.3.1. Credits

The article is co-authored by N. Furuichi and T. Lederer. N. Furuichi performed the measurements for the bilateral comparison at the NMIJ and provided a critical analysis of the comparison results. T. Lederer has contributed to the planning and design of the characterization of the Transfer standard, and contributed also to the analysis of the comparison results.

3.3.2. Publication details

This article was submitted to and published by Elseviers Flow Measurement and Instrumentation.

Flow Measurement and Instrumentation 45 (2015) 28–42

Contents lists available at ScienceDirect

Flow Measurement and Instrumentation

journal homepage: www.elsevier.com/locate/flowmeasinst

Qualification of an ultrasonic flow meter as a transfer standard for measurements at Reynolds numbers up to 4×10^6 between NMIJ and PTB

L. Cordova [a,*], N. Furuichi [b], T. Lederer [a]

[a] Physikalisch-Technische Bundesanstalt, Germany
[b] National Institute of Advanced Industrial Science and Technology, Japan

ARTICLE INFO

Article history:
Received 19 June 2014
Received in revised form
7 April 2015
Accepted 19 April 2015
Available online 24 April 2015

Keywords:
Interlaboratory comparison
Ultrasonic flow meter
Reynolds number dependence
Flow traceability
Transducer cavity

ABSTRACT

The quality of any laboratory intercomparison depends to a large extent on the performance of the used flow meter. To find a flow meter that is capable of reaching a reproducibility better than 0.05% requires bounding all involved influence quantities down to the required level. The present paper describes the efforts performed while qualifying a time-of-flight ultrasonic flow meter as a transfer standard. It was determined that the most relevant influence quantity besides the flow profile within the bulk flow is the effect caused by the transducer pockets in the meter body. By taking advantage of a specially designed window chamber, it was possible to determine the magnitude of the errors introduced by the transducer pockets and to define, based on the findings, a procedure to perform a bilateral comparison between the hot water calibration facilities of the Physikalisch-Technische Bundesanstalt and the National Institute of Advanced Industrial Science and Technology. The results of the bilateral comparison are presented.

1. Introduction and motivation

Water is used as an energy transporting medium in every type of power plant involving turbines; also industrial and district heating depend on accurate measurements of flow rate. In most cases, the actual measurement uncertainty is in the order of 1%. Consequently, every improvement of the measurement uncertainties has direct consequences for the safety and efficiency of the involved systems.

Flow rate measurements in the field are performed ideally by instruments that have been tested at National Metrology Institutes (NMI) or at a calibration laboratory that has been accredited and/or is participating in proficiency tests organized by the corresponding NMI as can be seen in Fig. 1. Any bias introduced by a calibration laboratory would have a direct impact on the price, on the quality or on the competitiveness offered by its clients. In order for measurements to be globally consistent, it is required that NMIs prove their mutual consistency periodically through international comparisons. The Mutual Recognition Arrangement of the International Committee for Weights and Measures (CIPM-MRA) has established mechanisms in order to allow the NMIs to prove their mutual consistency transparently and based on the same rules and principles. Actually there are more than 53 states and 152 institutes, designated by the signatory bodies, participating in the CIPM-MRA.

The traceability of a flow rate calibration facility is normally assessed on a quantity-based calibration, i.e. mass, volume, time, density and temperature standards are calibrated separately. Only in cases where there is a flow meter capable of delivering reproducibilities much lower than the required calibration uncertainties it is possible to provide a direct flow-rate traceability. This is possible in low-flow hydrocarbon measurements as reported by Shimada. Highly reproducible measurement instruments are available as seen, for example, at the Calibration Intercomparison on Flow Meters for Kerosene carried out on 1995 [10] and the CIPM-MRA international key comparison of liquid hydrocarbon flow facilities CCM-FF-K2 [11]. Without direct flow-rate traceability, systematic errors in any system of the calibration rig might remain undetected.

There are several relevant flow rate measurements in the field performed without a calibration as depicted in Fig. 1. This situation is given mostly in cases where the measurement conditions cannot be reproduced in a laboratory. Under these circumstances the only alternative is to apply flow measurement technology that has a predictable working principle that allows the use of similarity principles to infer the calibration result and uncertainty of measurements under conditions different from those present during calibration.

The relevant ranges for energy transport through hot water vary mainly between 50 °C and 250 °C. Flow rates larger than 3500 m^3/h have been reported and Reynolds numbers up to 30×10^6. According

* Corresponding author.
E-mail address: cordova.leopoldo@gmail.com (L. Cordova).

http://dx.doi.org/10.1016/j.flowmeasinst.2015.04.006

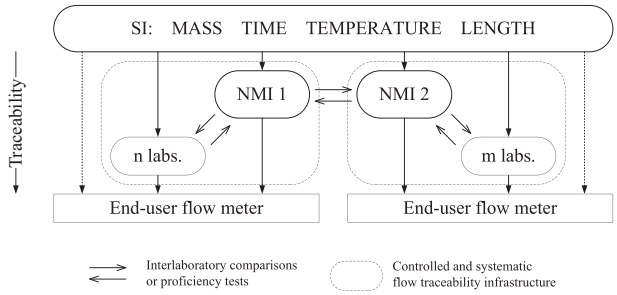

Fig. 1. Traceability concept for hot water flow rate measurements. Representation used by Shimada [1] to show traceability on hydrocarbon measurements in Japan.

to the CMC tables[1] there is only one facility that comes close to these requirements: the AIST, NMIJ (hereafter, NMIJ). With temperatures of up to 70 °C and flow rates up to 12 000 m^3/h, it is able to reach Reynolds numbers up to 20×10^6; the declared expanded uncertainty varies depending on the flow-rate range between 0.04% and 0.08%. The next flow rate facility that can be considered for hot water flow traceability studies is the heat meter testing facility of PTB. For a declared 0.04% expanded uncertainty it is able to measure between 4 °C and 90 °C and a flow rate up to 1000 m^3/h. Section 2 will give more details on both facilities.

In this sense, the flow measurement laboratories for hot water of PTB and NMIJ cooperate in order to validate flow measurement principles that allow similarity conditions to be applied. And given that the required uncertainties to determine the influence quantities acting on the flow measurement techniques are in the order of magnitude of the uncertainties declared by the NMIs themselves, PTB and NMIJ need to prove their mutual consistency before reliable experiments involving both laboratories are possible. Steps towards this first goal are described in this paper.

Firstly, an overview on the used flow measurement technology and on the calibration facilities of PTB and NMIJ is given. In the second part, the results of the characterization of an ultrasonic flow meter made at PTB are shown in two steps: through conventional linearity, repeatability and reproducibility tests using an established industrial flow meter, and through the simultaneous measurements of the flow profile and the flow meter indication at a very carefully constructed DN200 90D long test line using a specially designed window chamber. By using the characterization results, a strategy is defined to apply a robust industrial flow meter as a transfer standard in less advantageous conditions. The transfer standard is provided with a tube bundle to increase robustness against geometry differences in the inlet pipe layouts and internal pipe diameters. The final part of this paper presents the comparison results and provides first conclusions on the application of ultrasonic flow meters under conditions outside the calibration ranges.

1.1. Traceability of flow meters outside calibration ranges

An established flow metering technology based on the similarity laws concerns orifice plate flow meters. They allow a best possible uncertainty, in the ideal case not smaller than 0.7% as extracted from ISO5167 [6], in any condition where calibration is not possible. The basis for the ISO5167 is decades of enormous research efforts and ten thousands of internationally coordinated experiments.

In the past few years, ultrasonic flow meter manufacturers have been introducing their products for applications where no calibration is possible. Based on calibrations performed under laboratory conditions, they propose to extrapolate the uncertainty to levels below 0.7% and replace differential pressure meters. Important steps towards global standardization of ultrasonic flow meter technology have been undertaken in the GERG project on ultrasonic gas flow meters [2].

1.2. Ultrasonic flow meters

The type of ultrasonic flow meter used most is the parallel path time-of-flight flow meter (hereinafter UFM). Its simplicity makes it a good candidate for the defined purpose.

1.2.1. Ideal case integration

In the ideal case, any path of a UFM installed at any position r/R when exposed to a fully developed flow profile shows a curve similar to the one depicted in Fig. 2(a). The area under the curve represents the flow rate; when the bulk speed is defined to be one, the area under the curve is equal to the volume of a cylinder with unity radius and unity height (π). Flow measurement through the UFM can be regarded as the problem of integrating the area under this curve.

If the flow is fully developed, any path can be used as a flow meter as can be seen in Fig. 2(b). 10 single normalized paths, referred to their own indication for $Re = 10^6$, are shown as a function of the Reynolds number. For every path position there is a monotonic relation between the indication and the real flow rate.

The following equation describes the use of multiple paths P_i and weights w_i:

$$Q = k \sum_{i=1}^{n} w_i P_i \tag{1}$$

The factor k of Eq. (1) is a correction factor of a semi-empirical nature introduced to compensate for temperature and pressure variations and to add empirical linearizing as seen, for example, in [12]. The introduction of a k-factor is comparable to the determination of the discharge coefficient at orifice plates. It would be desirable to find a valid formulation for the UFM as is the case for orifice plates as proposed by Reader-Harris et al. (as presented in [6]).

1.2.2. Real case traceability limits

It is easily concluded that the bias produced by the sum of any combination of parallel paths becomes asymptotic. In the ideal case, if the amount of paths n increases, the accuracy gets improved. If the position of the nodes is selected based on an interpolating integration technique, as the different forms of the Gauss quadrature for example, more degrees of freedom are obtained making the method capable of compensating, to some extent, for small deformations on the projected flow profile caused by flow asymmetries. Several studies exist on this topic; see, for example, [7–9].

Considering the bulk flow within the flow meter, the ideal-flow-meter assumption requires that only axial velocity components are present. The existence of secondary components, radial or tangential, has a strong influence and can produce errors in the order of several percent. In the common case, where secondary components can be considered to be constant while moving through the flow meter, if every path has a counter part downstream with the opposite angle and at the same level, the introduced error is cancelled out automatically. This condition has been taken advantage of by different flow meter producers.

Considering the transducer pockets, they disturb the flow and introduce secondary velocity components within and outside of them. Zheng et al. [13] determined numerically that the influence originated within the pockets is responsible for up to 4% of the total signal. This effect gets reduced at higher diameters where the

[1] Accessed on 02 June 2014 on http://kcdb.bipm.org/appendixc/

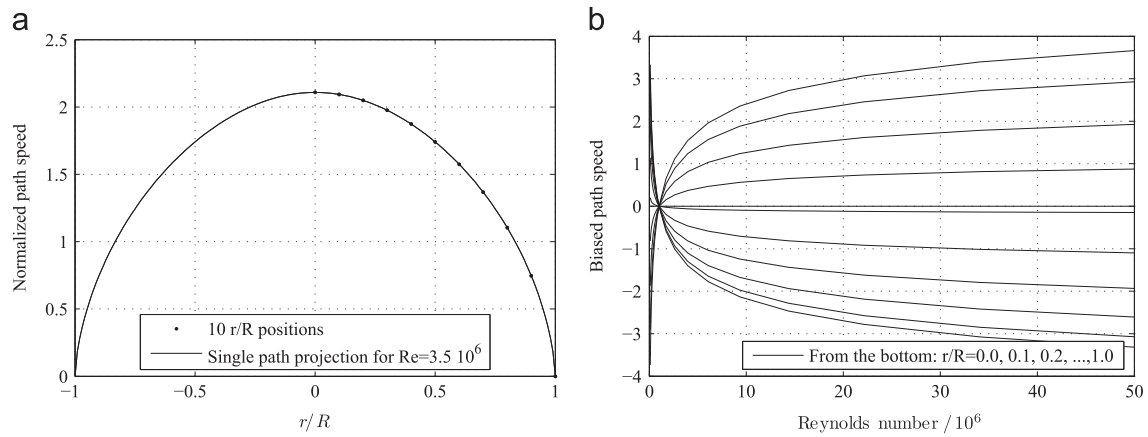

Fig. 2. Theoretical path indication as a function of the Reynolds number. The flow profile projection was normalized to the bulk speed based on the semi-empirical model proposed by Gersten. A biased representation allows for better comparison. (a) Flow profile projection as seen by ultrasonic flow meter for $Re = 2 \times 10^6$. (b) Projection of single paths for different Reynolds numbers referred or biased to $Re = 1 \times 10^6$.

transducers are negligible, compared to the total diameter: as stated in the recommendation of the PTC-18:2011 [3] for hydraulic turbines, the error introduced by protruding transducers for diameter of 1 m is in the order of 0.35%, for diameter of 5 m of 0.05%.

The ISO 12242:2012 [4] and the AGA Report 9 [5] recommend assessing the reproducibility of an ultrasonic flow meter in reference to the calibration base line by testing the flow meter under very adverse flow conditions. Measurements at different pipe configurations known to produce strong secondary components and asymmetries are considered. It is expected that the represented pipe layouts reflect the worst conditions existing in a real application bounding the maximum errors that the instruments would produce. As shown by Drenthen et al. [21] or by Caldon [22], the introduced linearity errors are in the range of 0.2%. This result provides a solid basis for interpolation, but if extrapolation is required, more solid arguments are necessary.

For the application of UFM in hot water measurements, it can be assumed that given the low Mach numbers in the order of 0.01 the path can be considered to be straight [14]. Time delays introduced, provided they remain constant, can also be neglected.

2. The flow test rigs

In the following section, both the PTB and the NMIJ facilities are presented. Special attention will be given to the calibration facility of PTB that was used for the characterization of the ultrasonic flow meters.

2.1. Flow rate facility NMIJ

The flow test facility of NMIJ has been described in detail in the previous publications [15]. The flow test facility of NMIJ is based on several weighing systems working at ambient temperature. In order to make the higher temperatures traceable, it is required to transfer the accuracy obtained by the gravimetric systems, to a tempered volumetric system. The facility used for the measurements presented in this paper is the prover system shown in Fig. 3. This facility generates flow rates from 200 m^3/h up to 800 m^3/h at 20 °C up to 80 °C ±0.5 °C. The prover system is a core component to provide traceability to the large Reynolds number facility. The highest pressure of the test line is 0.7 MPa. The nominal pipe diameter of the test line is DN200 and the length of the test line is approximately 12 m. The maximum Reynolds number in the test section is approximately 3.7×10^6. The reference flow rate is given by the volumetric method of the prover. Inside of the pipe, there is a spherical ball with a diameter about 2% larger than the pipe diameter to avoid leakage. The ball activates the start and stop detection sensors when moving from one side to the other. The flow rate is given as the standard volume between two detection sensors divided by the elapsed time. The standard volume between the two sensors is calibrated by the gravimetric system through the transfer flow meters. The uncertainty sources of the prover system are the standard volume of the prover, correction of the standard volume for the temperature and pressure, and the measurement of the elapsed time. As mentioned, the standard volume is calibrated using the gravimetric system and the transfer meter, and it is the dominant uncertainty source of the prover system. The expanded uncertainty ($k = 2$) of the facility is 0.068%. The minimum elapsed time is 15 s. The measurement is normally repeated 20 times.

2.2. Flow rate facility PTB

The heat meter testing facility of PTB (Waermezaehlerpruefstrecke WZP) is a gravimetric flow test rig for temperatures up to 90 °C. A more detailed description is available at [16]. A schematic of the facility is shown in Fig. 4. It is divided basically into two levels: the basement level with the flow rate generation systems, and the upper level with the test lines and the measurement systems. The flow rate is generated with two sets of pump cascades, with an overflow constant pressure tank in between to ensure highest flow rate stability. Since the measurements are performed on a flying start/stop basis, a diverter system has to be used. Evaporation at higher water temperatures is controlled by reducing the vapor concentration gradient in the air near all free water surfaces. This is accomplished by encapsulating the diverting system and by introducing saturated tempered humid air into the empty tank before the measurements. Evaporation cannot be completely avoided: thus by performing a water vapor mass balance based on humidity measurements on the air evacuated by the water, the amount of water loss can be estimated. A weighing scale calibrated on a daily basis is the reference system. The heat meter testing facility of PTB is designed, maintained and used to deliver an expanded flow rate realization uncertainty not larger than 0.04% and a very high repeatability for temperatures between 4 °C and 90 °C and flow rates up to 1000 m^3/h. The length of the test lines is 25 m.

During 2013, the most important components of the flow calibration facility were overhauled. After more than 100 000 diverter motions, the diverter systems were renewed. The force isolating and force transmitting components of the weighing scale were adjusted and a redundant strain gauge system was also installed. The humidity determination system was improved. Given

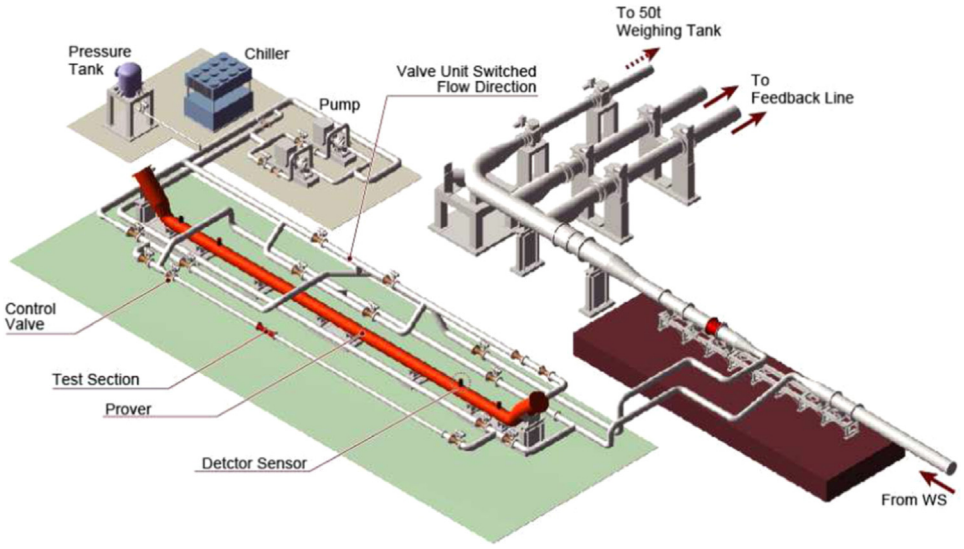

Fig. 3. Test facility with prover system of the NMIJ.

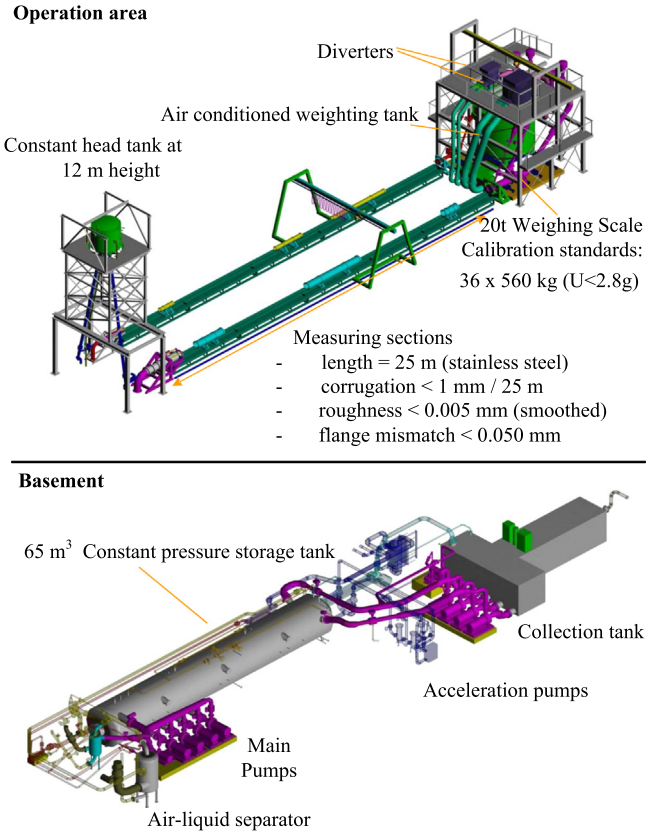

Fig. 4. Operational area and basement of PTB heat meter flow test rig (WZP).

these important hardware changes, a comprehensive characterization was required. A more detailed publication of the results is the subject of a different paper. Here, only an overview will be given.

The uncertainty of the flow rate facility is assessed, divided into four groups: the mass measurement, the density measurement, the timing error, and the process-related components. The last group includes all additional mass correction due to thermal expansion, air entrapment, buoyancy variations and evaporation.

Fig. 5(a) shows graphically how the uncertainty components interact, in this case when an expanded uncertainty of 0.04% is required. We can see that if larger flow rates are required, the major component is the timing error; for lower flow rates the process-related corrections have the largest contribution.

Fig. 5(b) shows the influence of temperature and filling volume on uncertainty for different filling volumes. The resulting uncertainties from 0.025% up to 0.05% are shown. It can also be seen that higher temperatures play only a role for lower flow rates. The largest problem at higher temperatures is evaporation. There are several measures applied in order to compensate for or to avoid evaporation. It has been determined empirically that these measures are less effective at lower flow rates. The uncertainties shown in Fig. 5(b) do not include the contribution of the flow meter under test.

2.3. Internal consistency test for the flow calibration facility

The only component of a gravimetric flow rate facility that depends on the Reynolds number is the diverter; the reason is the flow profile at its entrance. Depending on the flow rate and on the temperature, the flow profile will change. This effect is systematic and is overlapped with the temperature dependence of the pneumatic actuator system. Consequently, the timing error is determined periodically at different temperatures and flow rates. If the corrections are applied correctly, there is no residual Reynolds number dependency left on the measurement results of the WZP. By taking this into account, when calibrating an orifice plate that has a strong Reynolds number dependency at different temperatures and flow rates, it should be possible to determine if the different components of the gravimetric flow rate facility are working properly. This was done with a highly repeatable DN200 orifice plate with $\beta = 0.75$. The results are shown in Fig. 6.

Fig. 6 shows six different temperatures where the flow rates 390 m^3/h, 475 m^3/h, 595 m^3/h and 745 m^3/h have been measured repeatedly. The results are presented as a function of the Reynolds number $Re = v\,D/\nu(T)$, where v is the bulk velocity, D the pipe diameter and ν the kinematic viscosity that is a function of the temperature. Given that a single discharge coefficient can be realized at different conditions, the results of measurements of the discharge coefficient at different temperatures overlap as seen in Fig. 6, i.e. the first point at 745 m^3/h corresponds to 390 m^3/h at a different temperature. For these two flow rates different filling times were used (156 s and 82 s). If there is any time dependent

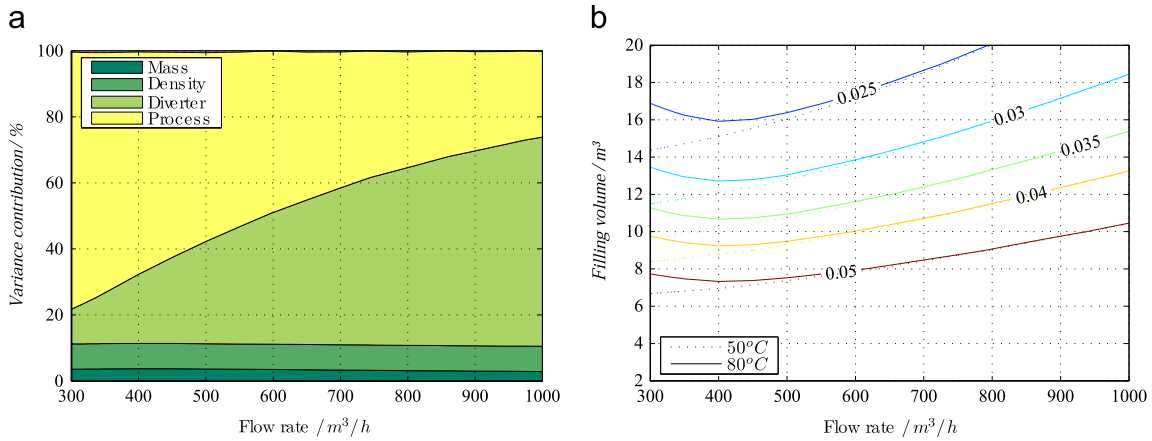

Fig. 5. (a) Uncertainty contribution factors for the required expanded uncertainty of 0.04% in percent for 80 °C. (b) Different expanded uncertainty values that can be reached at 50 °C or 80 °C for different filling volumes.

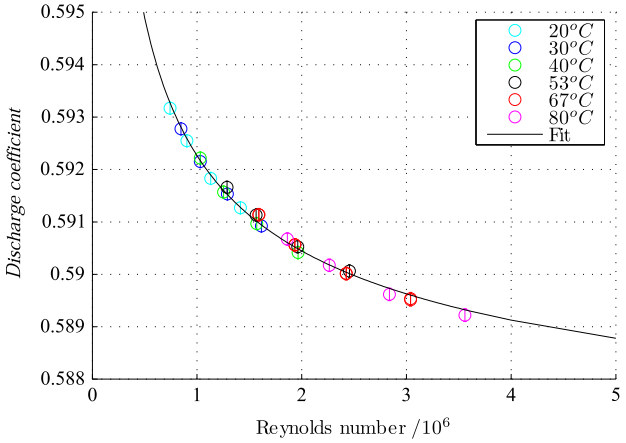

Fig. 6. Discharge coefficient as a function of the Reynolds number for an orifice plate at PTB for a $\beta = 0.75$ DN200. The error bars correspond to 0.01% of the discharge coefficient.

error, it should be visible at these points, but no differences were detected.

The error bars shown correspond to 0.01% of the discharge coefficient; the black curve is the result of a regression based on the Reader–Harris–Gallagher equation as presented in [6]. As can be seen, there is extraordinary agreement across all flow rates and temperatures. The pure Reynolds number dependency of the orifice plate is observed. Therefore, we can confirm that all systems are working properly and that all corrections are being applied correctly. Additionally, the observed results also confirm that the flow profile at the WZP is the same for coincident Reynolds numbers at different temperatures and flow rates, since orifice plates are very sensitive to flow profile changes.

3. Methods

Two flow meters are used for the experiments. An industrial flow meter as a transfer standard and a specially designed flow meter with an optical access or window to the body to perform profile measurements. Initially, preliminary measurements are performed in order to define the performance of the transfer standard and to define the best conditions to perform the comparison. The next stage is to characterize the flow profile within the flow meter at the calibration facility in order to be able to define in a next step the ideal working conditions and the main influence quantities for using an UFM, but applying both time-of-flight and also flow profile measurements.

3.1. Preliminary measurements

The industrial five-path flow meter (I-UFM) used is a part of a meter run package composed of a 4 m long upstream pipe and a 1 m downstream pipe. To guarantee repeatable measurement conditions and robustness against differences in the upstream flow profiles an ISO5167 tube bundle flow straightener (TB) was installed. This is necessary because even if the involved facilities have long upstream pipes the internal diameter sizes do not match exactly. In addition, the upstream section flanges are pinned to guarantee repeatable mounting. For the analysis only raw data delivered by the I-UFM were used. All correction and compensation factors provided by the manufacturer were deactivated, because during characterization of the different influence quantities, any overlapping correction would disturb the analysis.

As a first assessment, linearity, repeatability and reproducibility tests were performed. All results were in a band of $\pm 0.1\%$ for a given configuration, but no clear Reynolds dependency could be observed, as explained in Section 1.2.2. Repeatability reached values in the range of 0.02% and 0.04% for all temperatures, flow rates and configurations. Regarding reproducibility, measurements with and without TB differed by about 0.4%. A surprising result was obtained by changing the exact position of the TB. Different rotation positions produced differences of about 0.15%. These results are shown in Fig. 7.

To test robustness against flange mismatch, the upstream section was mounted with a 0.5 mm off-axis on its upstream side. The produced differences were systematically in the range of 0.05%.

The preliminary tests in summary:

- Independent of the measurement conditions the I-UFM delivers a highly repeatable result.
- If measurements with a reproducibility better than 0.1% are required, UFMs should be mounted with great care in terms of alignment and configuration
- The TB, in spite of fulfilling the requirements of ISO5167, introduces repeatable asymmetries that prevail after the 4 m upstream pipe and depend on its rotation angle.

Since the geometry and location of the transducer pockets vary, the unknown systematic effects causing the errors might be different for each single path. If besides the axial velocity related path velocities P_i each measurement path is influenced by the

error e_i, the following equation would apply:

$$Q = k\sum_{i=1}^{n} w_i P_i + \sum_{i=1}^{n} w_i e_i \quad (2)$$

The errors introduced by each path are unknown; in order to minimize the total error, it might be necessary for the weighing factors w_i of Eq. (2) to acquire also negative values. If an additional summation term Q_k is added instead, as in $Q = k\sum_{i=0}^{n} w_i P_i + Q_k$, the problem of using negative weighing factors can be avoided. However, the determination of both types of corrections is at the current state of the art only possible through empirical treatment. By determining the calibration factors at the same laboratories where the UFM is tested, unpredictable correlations would be introduced leading to a biased estimation of consistency.

Even if all w_i and k of Eq. (2) are assumed to be known for an ideal case, since the distribution of e_i cannot be guaranteed to be random, there will be systematic influences that are not eliminated through averaging that invalidate the obtained results.

Therefore we decided to use, instead of the weighed summation of all single paths, each path independently, free of any empirically determined constants. Due to its symmetry and to the maximum length, the central path is predestined to serve as a reference.

Only by knowing the flow profile within the UFM will it be possible to determine the performance of the flow meter. To make this possible, a hybrid flow meter with an optical access has been specially built. The design goal was to enable velocity profile measurements within the UFM by means of Laser Doppler Velocimetry (LDV) and Ultrasonic Velocity Profiling (UVP) but without introducing additional disturbances. UVP offers the advantage of measuring secondary components if they are mounted on the same plane as LDV. Refer to [26] for further details.

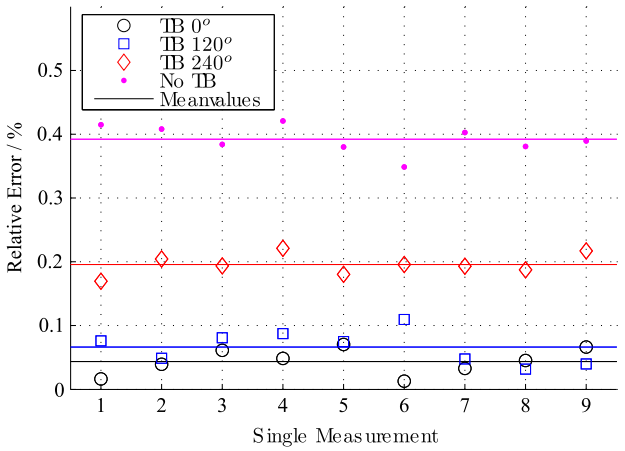

Fig. 7. Measurements without TB and with the TB mounted in 3 different rotation positions. The conditions were 20 °C and 390 m^3/h. The single measurement points are shown to give an impression of the repeatability.

3.2. Velocity profile measurement

3.2.1. The window chamber

The designed window chamber (WCH) is based on a 5-path UFM (UFM-WCH). The outer paths *P*1 and *P*5 are on the same vertical plane mounted at 45° from the flow axis; the three central paths P2, P3 and P4 are on a plane at −45° space from the flow axis, perpendicular to the outer path plane. Normally, P3 is mounted on the same plane as P1 and P5, but by changing its position as seen in Fig. 8(b), there is enough space left for positioning an LDV and UVP access in between the paths. Fig. 8 (b) shows the glass insert mounted on the UFM-WCH and the transducer pockets of paths P2, P3 and P4. There are four inserts mounted in total every 90°. The glass insert was thermally hardened and polished afterward to minimize any gaps or disturbances on the wall. Hardening had a negative influence on the optical quality, but it was unavoidable in order to guarantee operation safety. Due to the large surface of the insert exposed to the internal pressure, forces of several thousand Newton are applied. These forces could cause small changes to the thickness of the sealings, which would have negative consequences on the beam positioning. Therefore, an elaborate sealing system has been designed to avoid displacement of the glass due to geometrical variation of the seals, but without compromising safety. For making the UVP measurements the inserts have been finished using polyoxymethylene.

The setup for the LDV measurements can be seen in Fig. 10. A regular *XY* traversing system for the LDV probe would only provide small optical access into the flow. Therefore, a combination of a circular shaped traverse and a linear table has been designed. By positioning the center of the circular shaped traverse near the insert, a much larger view of the flow is possible as seen in Fig. 9. The figure shows the typical standard deviation of the mean axial speed obtained, estimated from the empirical measured turbulence and the amount of valid bursts detected. As can be seen, the amount of burst varied greatly, such that $\sigma_{\overline{uz}}$ shows values up to 2.5%, the reason for this was the numerous reflections coming from the stainless-steel body, and the poor optical quality of thermally strengthened glass.

The uncertainty of the LDV measurements was determined to be under 1% for a single point. This has been accomplished through the characterization of the traversing system at a coordinate measuring table and by means of a rotating disc calibration for the LDV probe. More details on LDV calibration uncertainty of the equipment used can be found in Ref. [17].

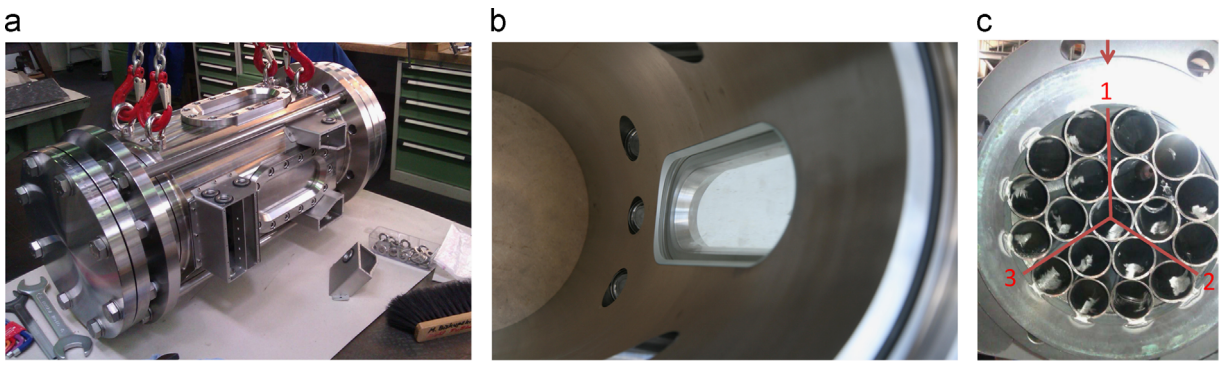

Fig. 8. Window chamber details and a tube bundle frontal view. (a) DN200 window chamber. (b) Inner view of the window chamber. (c) Tube bundle.

3.2.2. The flow profile

The main purposes of LDV were to determine the reason for the large differences present under the different installation conditions

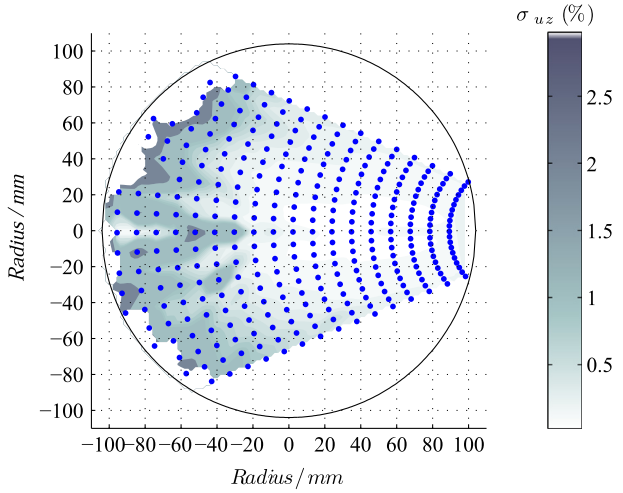

Fig. 9. LDV measurement grid and standard deviation of the mean axial speed $\overline{u_z}$.

Fig. 10. Typical set-up for an LDV measurement using the UFM-WCH.

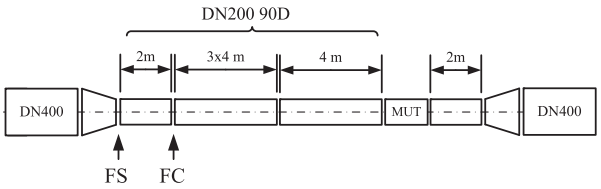

Fig. 11. Installation conditions for the measurements of the flow profile. FS is the flow straightener and FC is the flow conditioner.

and to confirm that a fully developed profile exists. The resulting profile is shown in Fig. 12(a).

The window chamber was positioned with an upstream length of 90D. The configuration is shown in Fig. 11. A honeycomb-type flow straightener with square cells (FS) and a perforated plate flow conditioner (FC) were installed.

The task force for Laseroptical Flow Diagnostics (TFLD) based on the work of Yeh and Mattingly [18] recommended the use of four performance indicators for flow calibration facilities for heat meters. Three of them will be used here: indicators for the flow profile peakedness, for the flow profile asymmetry and for the turbulence intensity. The flow profile peakedness and the flow profile asymmetry are defined for diametral (2D) slices of the flow profile. The turbulence degree is defined for the central core of the flow. The "Guidelines for the fluid mechanical validation of calibration test-benches in the framework of EN-1434" [20] give a full description on its calculation and establishes limits for a nearly fully developed flow profile.

The flow profile peakedness and asymmetry indicators are defined for the axial component of the velocity, and are calculated according to the recommendation of Yeh.[2] To enable the comparison of indicators across different flow rates and pipe sizes, Yeh normalized the results to a fully developed flow profile. The FTLD recommended to assume as a fully developed flow profile the semi-analytical formulation proposed by Gersten [19] for smooth pipes. See [20,18,19] for further details.

Since the view of the flow profile is limited, the performance indicators will be calculated for $r/R \leq \pm 0.65$, which is the largest coaxial circle that can be fully measured. Consequently, given the fact that the indicators for peakedness and asymmetry are defined for 2D slices with limits $r/R = \pm 1$, the estimations for $r/R \leq \pm 0.65$ will be biased. In case of the profile factor, flow profile changes in the central part of a flow profile are overrated if seen only in a 2D slice, since only the length is used as a "weight" instead of the area, as in the real case. But in order to allow comparisons and rating according to the recommendation of the TFLD, 2D slices will still be used for the calculations. The relevant performance indicators are summarized in Table 1.

Fig. 12(b) shows measurements at 600 m^3/h using LDV and UVP. Both systems deliver the same results and are very close to the theoretical profile. The differences encountered are within their declared uncertainties. The LDV and UVP measurements were performed with the parameters shown in Table 2.

As can be seen, the flow profile at the position of the UFM-WCH can be considered to be fully developed. The LDV measurements were performed from both sides. This was achieved on different days and also after taking out and remounting the UFM-WCH. The results are consistent and confirm the reproducibility of the configuration.

3.2.3. Measurements of the TB profile

The following measurements were obtained with the TB installed 20D from the UFM-WCH.

At the 120° position shown in Fig. 13(b) some measurement points delivered less than 100 bursts for the established time. For this reason it was not possible to calculate some of the performance indicators reliably.

It was assumed initially that the flow profile should rotate together with the TB, but as can be seen in Fig. 13 the profile does not rotate, it changes every time. It seems that small asymmetries on the flanges and on the TB cause the configuration to be a little different for each position of the TB.

The maximum speed on the TB flow profile is about 4% higher than on the flow profile measurement without TB. This is clearly seen in the profile factor values; the undisturbed flow has a profile factor of 0.94, while the measurements with TB about 1.2. If the flow rate were measured only on one diametral path, it would be expected that the flow rate is overestimated due to the peak in the central region. But the opposite case is observed: an underestimation of about 0.4% was measured. This is an indication that the peak is not the only reason for the differences. Either the influence of the TB on the transducer pockets, or undetected secondary components, or both, are causing the bias.

The position 0° is apparently the best choice to install the TB. The error is small and the profile has the most symmetric shape considering the maximum K_a, if only the central diametral K_a' is considered. The 240° position seems to be symmetrical, but it can be seen that the peak position and the gravity center have a larger displacement from the axis.

[2] Yeh introduced different performance indicators to evaluate the influence of a reducer installed in front of an orifice plate using LDV. Among the family of indicators he proposed in [18], P_5 and S_{10} are the basis for the work of the TFLD.

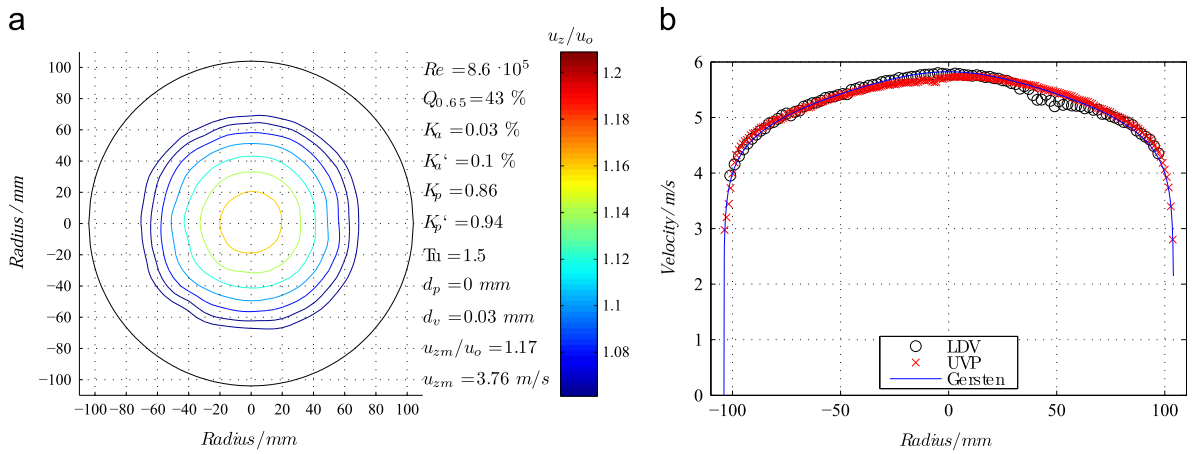

Fig. 12. DN200 LDV and UVP measurements after 90D upstream pipe. (a) Fully developed flow showing performance indicators with LDV measurements from both sides. (b) LDV and UVP velocity measurements at DN200 and 600 m^3/h.

Table 1
Symbols used in the performance evaluation figures.

Symbol	Limits[a]	Units	Description
D		mm	Pipe diameter 208 mm
Re			Pipe Reynolds number
$Q_{0.65}$		% of Q	Flow rate within $r/R \leq \pm 0.65$
K_a		% of D	The asymmetry factor for $r/R \leq \pm 0.65$
K_a'	< 1	% of D	The asymmetry factor for the horizontal path for $r/R \leq \pm 1$
K_p			The maximum profile factor for $r/R \leq \pm 0.65$
K_p'	0.8 to 1.3		The profile factor for the horizontal path for $r/R \leq \pm 1$
Tu	< 2		Turbulence factor
d_p		mm	Distance from the peak to the pipe axis
d_v		mm	Distance from the gravity center of the flow to the pipe axis
u_{mz}/u_o			Maximum relative axial fluid velocity
u_{mz}		m/s	Maximum axial fluid velocity

[a] Extracted from [20].

Table 2
LDV and UVP main specifications.

Property	LDV[a]	UVP[b]
Velocity resolution	–	0.005 m/s
Average meas. Volume width	1 mm	25 mm
Average length	5 mm	3 mm
Average height	1 mm	25 mm
Number of points	100	224
Time per path	60 min	< 1 min
Tracer particles	10 μm	100 μm

[a] 75 mW Nd:YAG 532 nm and 45 mm beam distance and 250 mm focal length.
[b] MET-flow UVP-DUO and 1 MHz transducer at 7°. The parameters vary depending on the requirements. The data serves only as a reference and corresponds to the results shown in Fig. 12(b).

3.2.4. Radial components on the central path

The central path is insensitive to swirl, provided that the swirl is coaxial with the pipe axis. Recalling that the UFM-WCH is installed behind a flow straightener installed 90D upstream of the measurement position, we can assume that the secondary components within the pipe diameter are negligible. But in the region near the transducer, the pocket might introduce an additional bias. UVP has been used to determine the magnitude of these effects. Fig. 14(a) shows the measurements using a 1 MHz UVP with a 13 mm effective diameter. The pulse repetition frequency was 1805 Hz and the resolution 0.005 m/s.

To interpret the results of Fig. 14(a), Fig. 14(b) has to be considered first. This figure shows the shape of the UVP measurement volume within the pipe and inside of the transducer pocket. In contrast to LDV which provides a good spatial resolution, the UVP measurement volume considers the speed of a much larger area and is affected by reflections. For the bulk flow within the pipe, the spatial resolution is small enough, but for small scaled measurements as is the case with the transducer pocket, only a very rough idea of the flow profile can be given.

In addition, when the UVP measurement volume is truncated by the pipe wall, reflections occur deforming its space. Special care has to be taken if these effects are expected. Signals originated from reflections can be filtered out by limiting the receiving time window. In some cases, reflected doppler signals are weak compared to the signals coming from the main flow and can be neglected, but since the size of the volume left outside of the wall is reduced a displacement of the effective center has to be considered. In our case, in order to be able to receive signals from inside of the cavity, the time window has not been reduced. Reflections cannot be neglected and the shape of the measurement volume is affected.

The shapes of the measurement volume for different depths influenced by reflections are shown in Fig. 14(b). The shapes have been simplified assuming that the pocket is squared. In the real case, only the front face of the transducer is flat, as in the squared case producing a stronger signal than the pocket wall. The section E–E of Fig. 14(c) is depicted in Fig. 14(b) (the transducer face is located on the upper side).

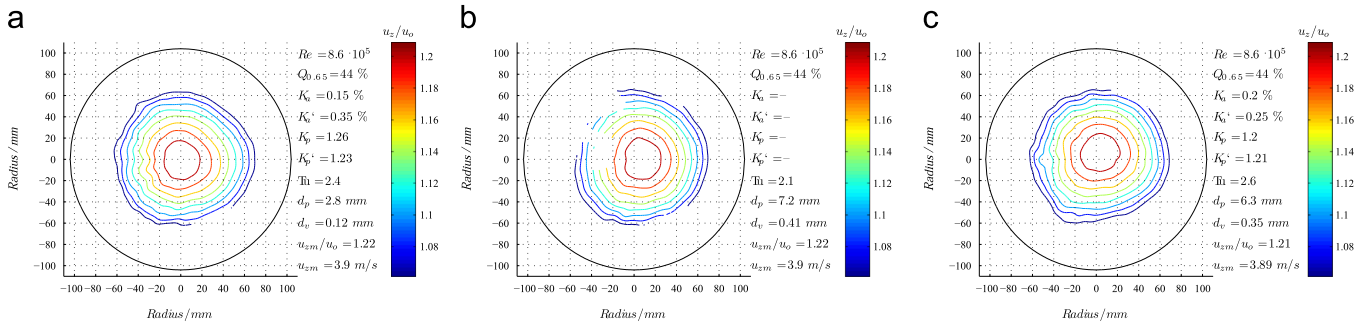

Fig. 13. Tube bundle flow profile at 3 different positions for 390 m^3/h and 30 °C. (a) Position 0°, (b) position 120°, and (c) position 240°.

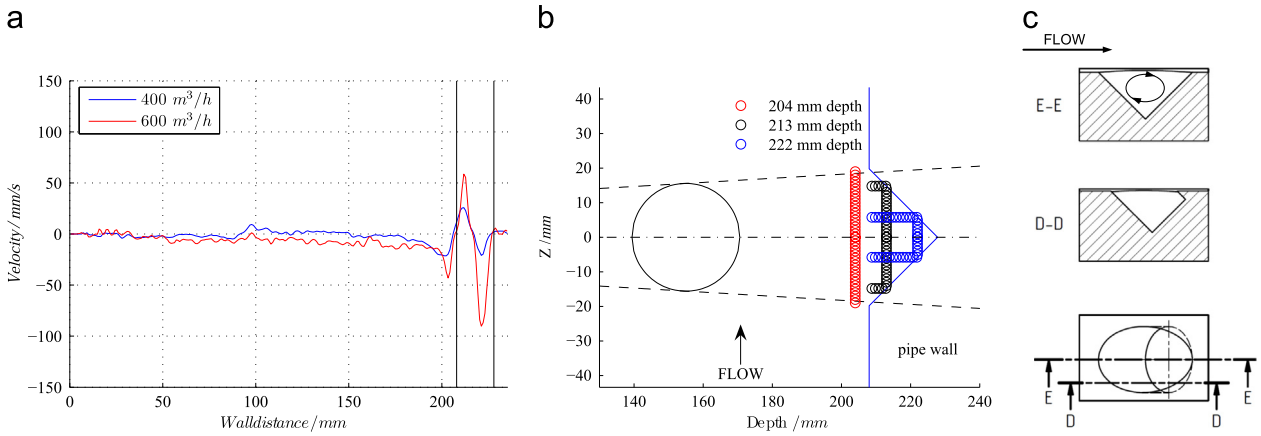

Fig. 14. UVP central path transducer pocket measurement. (a) UVP velocity measurements on the UFM-WCH for the central pocket. (b) Divergence of the 1 MHz ultrasonic beam and shape of the measurement volume at different depths. (c) Pocket shape and vortex scheme.

Fig. 15. Qualitative indication of the eddies existing within the pockets with 30 °C and 400 m^3/h for $r/R = 0.8$ on the left and $r/R = 0.5$ on the right. The flow direction is from left to right.

Due to the deformation of the measurement volume we can assume that measurements without interaction of the wall are correct, i.e. up to a depth of 208 mm. In the near wall region, the radial component seems to be dependent on the flow rate. For the region within the pocket, the rough spatial resolution does not allow drawing final conclusions on the flow profile within the pocket. The U-shaped measurement volumes might be simultaneously perceiving radial and axial components. This could explain the two peaks found in Fig. 14(a) at 213 mm and 222 mm. If the peaks were only caused by radial components, the peak at 222 mm would indicate a flow rate leaving the bottom of the cavity, which cannot be true. Therefore we can assume that the peak is caused by the axial components of a vortex in the cavity.

We can conclude from this experiment that even for the simply shaped central transducer pocket, the influences on the main flow cannot be ignored. Even if a fully developed flow free of secondary components is given, the transducer pockets interact with the bulk flow causing radial components to occur.

The study of the flow within UFM cavities is a complex problem. For a qualitative impression see the eddies which formed in two non-diametral pockets in Fig. 15 at 390 m^3/h. Air bubbles were introduced to make the eddies visible with the simple eye. Microbubbles used for UVP are not visible. The center of rotation of the vortex coincides with the axis of the ultrasonic path. This is relevant for UFM since most components remain unperceived, but up to what extent the eddy influences the flow outside the pocket is an actual topic of research.

PTB is actually using the capabilities of the window chamber to characterize the flow within ultrasonic in-line flow meters. For this purpose, differently shaped cavities will be installed and characterized by means of LDV and UVP. The cavity characterization project is in its initial stage.

3.3. Single path measurements

The next step is to test the performance of the UFM-WCH under fully developed flow conditions. For this purpose measurements were performed at temperatures 20 °C, 30 °C, 40 °C and 50 °C and at the flow rates 390 m^3/h, 475 m^3/h, 595 m^3/h and 745 m^3/h. Since all corrections have been turned off, the temperature correction was compensated subsequently according to $k_T = (1+\alpha\Delta t)^3 \approx 1+3\alpha\Delta t$.

The result of each normalized path at each temperature and flow rate condition is depicted in Fig. 16. It is difficult to recognize deviations on the flow profile based on this figure alone. For a more detailed view, the relative deviation of each path relative to the ideal, fully developed flow profile at the respective Reynolds number is shown in Fig. 16(b).

For a fully developed flow all points should be around the 0-line. But in this case, the maximum difference to ideal conditions is about 4.4%. The required geometrical displacement to produce such a large error is about 2 mm. Manufacturing tolerances can be guaranteed to be far below 0.1 mm. Therefore this deviation can be attributed to the actual existing flow profile. It is also remarkable that the results of symmetrically mounted paths are not symmetrical. On a large scale, the asymmetry is independent of the temperature, of the flow rate and of the Reynolds number since the rough position of the path errors remains constant. To determine if there is some dependency on a smaller scale, every single path curve will have to be observed independently.

Fig. 17 shows the results of the measurement campaigns. Fig. 17 (a)–(e) shows the relative error of each path at different temperatures and flow rates as a function of the Reynolds number. Each path has been considered as an independent flow meter scaled to fit between −0.4% and +0.6% using a different proportional factor for each of them. The error that these different factors would have on a fully developed flow profile is shown in Fig. 17(g). The weighted sum of the single paths is shown in Fig. 17(f).

A first look reveals immediately that the Reynolds number dependency is given only for path 3. Apparently paths 1 and 5 have no Reynolds number dependency, but rather a flow rate dependency since independent of temperature, the maximum flow rates behave similarly. Measurements on path 5 were invalid for 40 °C and 50 °C. But even only for 20 °C and 30 °C it can be observed that the dependency is given rather for the flow rate.

Paths 2 and 4 are distributed in a narrower band. The shapes of the curves are also rather independent of the Reynolds number, but a clear dependency on the flow rate can be disregarded due to the results for 50 °C.

Path 3 delivers a strong dependence on the Reynolds number as expected with a range of about 0.7%. But as can be extracted from Fig. 17(g) the theoretical curve has a different slope and the considered range has a slope of 1.2. Given that LDV measurements have measured the central path completely and proved a nearly fully developed flow condition, and considering also that UVP has proven that no considerable disturbances are present on the wall to wall measurements, the large differences in the steepness and in the position of the curves for the central path can be clearly attributed to the influence of the pockets.

The integration capability for removing disturbances is remarkable. This can be seen in Fig. 17(f). Considering the deviations encountered on each path, the final result is very flat and within a narrow band. The absence of signals on path 5 for 40 °C and 50 °C has been compensated automatically with the internal algorithms of the ultrasonic systems installed.

For the purpose of a bilateral comparison and for the validation of the flow measurement principle, it is not enough to consider the results of Fig. 17(f), since the reasons for the deviations on each path are not understood. Nevertheless, the results given by path 3 confirm the potential of this technology to be capable of serving as high quality transfer standard and of providing a solid basis for extrapolation.

3.4. Design of the comparison

Each path will be used as an independent flow meter. But only the central path will be used as a reference. The indication of the outer paths will serve as an indication that the flow conditions at both laboratories are the same and constant. The weighted sum of the flow rate will be considered only as an initial indication.

In order to be able to detect possible flow rate and temperature dependencies, the measurement points will be chosen in such a way that constant temperatures, constant flow rates, but also constant Reynolds numbers will be aimed at whenever possible.

The industrial flow meter used has an internal diameter of 202.7 mm; the upstream and downstream pipes have a diameter of 206 mm. In order to avoid a step on the wall, the I-UFM has a small conical reduction. Given this change in the geometry, a fully developed flow will never be given. If we consider also that the

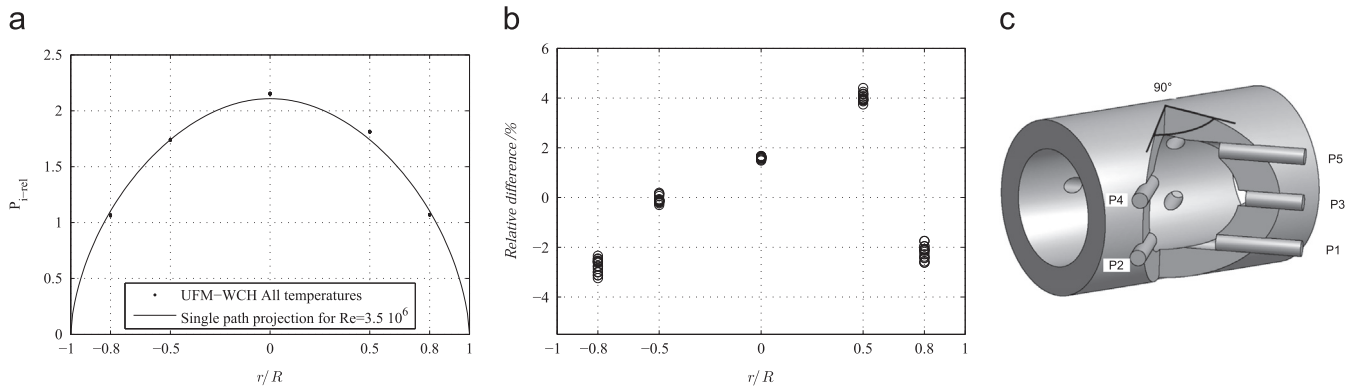

Fig. 16. Normalized path speeds on a flow profile projection of the UFM-WCH and its relative path errors referred to a fully developed flow profile. (a) Flow profile projection for a normalized bulk speed of 1 and single path results for 4 flow rates and 4 temperatures. (b) Single path speed normalized to fully developed flow conditions. Mean values for 4 flow rates and 4 temperatures are shown at each position. (c) UFM path configuration scheme. For the UFM-WCH, P3 is parallel to P2 and P4; for the IUFM it is parallel to P1 and P5.

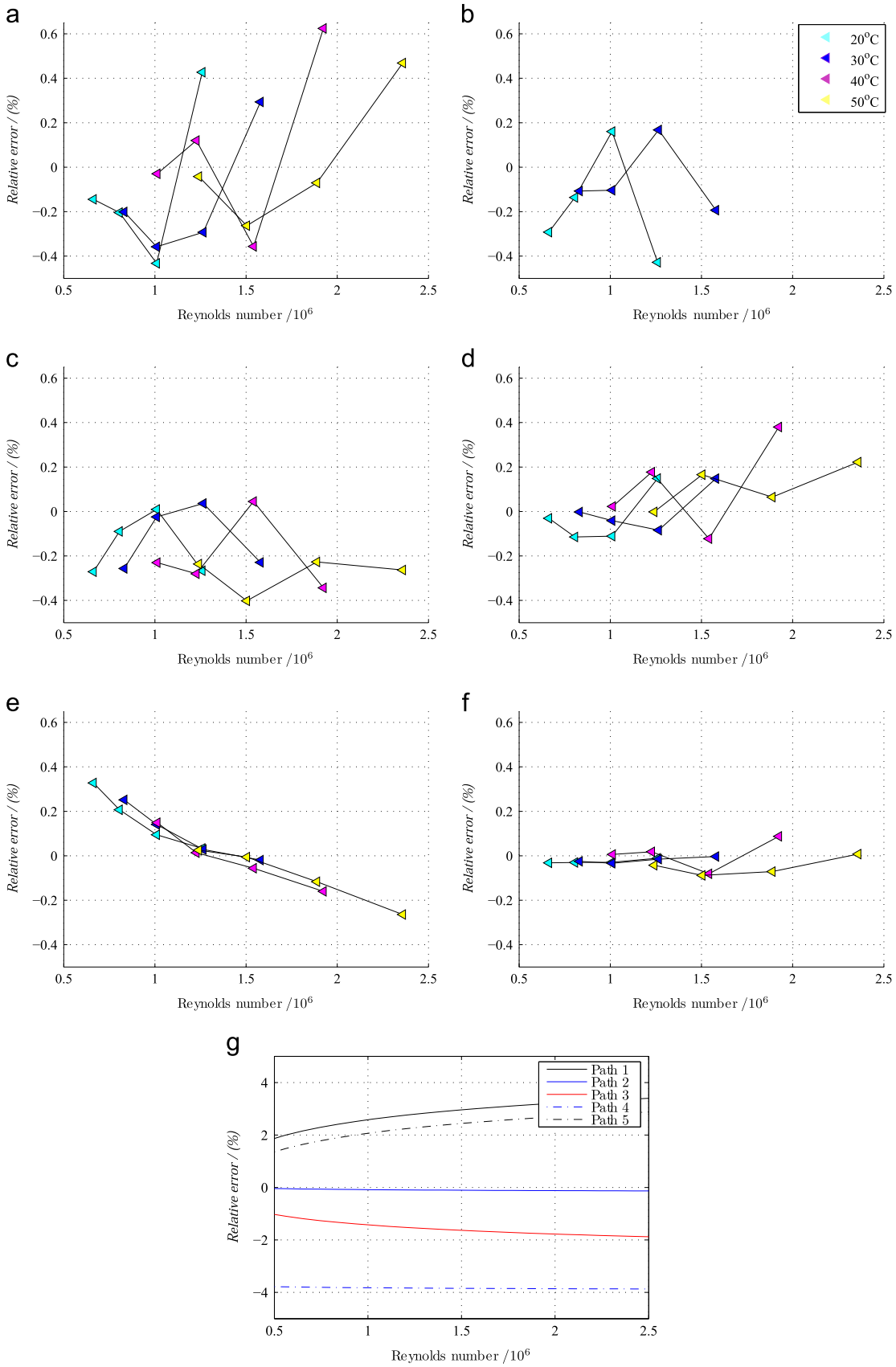

Fig. 17. Measurement results for the UFM-WCH at PTB. (a) Path 1, (b) path 5, (c) path 2, (d) path 4, (e) path 3, (f) sum, and (g) expected errors.

pipe diameters upstream of the meter run package in both laboratories are different, no defined conditions would be possible. For this reason, as mentioned in Section 3.1, in order to be more independent of the installation conditions, it has been decided to perform the measurements using the TB. The rotation position at the 0° was fixed for the measurements, since it gives repeatable and the most symmetrical results. As seen in Fig. 18(b), the TB is always installed 20D in front of the flow meter.

4. Results

The results are presented in two parts: the single path results presented as a flow profile indicator and the path by path relative flow rate error results.

4.1. Measurement conditions

The measurement results have been obtained within 2012 and 2013. The chosen measurement points shown in Fig. 18(a) enable measurements at constant flow rates, constant temperatures and nearly constant Reynolds numbers. The Reynolds numbers are not exactly the same, but they are close enough to allow a Reynolds dependency analysis. Each point was repeated at least 5 times at PTB and 20 times at NMIJ.

The pressure was held at both laboratories at 3 bar. The piping configuration is shown in Fig. 18(b). Fig. 16(c) schematizes the ultrasonic path configuration of the used I-UFM.

4.2. Path projection results

The obtained relative path errors are shown in Fig. 19. The single errors are connected with lines to improve readability. As in the case of the UFM-WCH, the single path errors are as much as 5% distant to the 0-line.

The dispersion of the different points is the highest for the outer paths P1 and P5 (at $r/R = \pm 0.8$) and is reduced for P2 and P4 (at $r/R = \pm 0.5$). The dispersion of P3 is in most cases the lowest. In the case of PTB, the measurements at 67 °C and 80 °C have a stronger dispersion for P3.

Apparently, the flow conditions at NMIJ vary depending on the temperature. If closer attention is paid to P4 and P2 we can see that while P4 increases with rising temperature, P2 is reduced. The same can be observed at paths P1 and P5 but to a lesser extent.

The only reason for this kind of disturbance is swirl. But how can swirl be generated at NMIJ and not at PTB if the same configuration were being used? A TB is introduced to eliminate swirl coming from the flow test rig. Therefore, it can be assumed that if swirl is the cause for the path asymmetry, it was generated by the tube bundle itself, but only in the configuration at NMIJ, since the measurements at PTB have been proven to be swirl-free. Similar experiences with TB have been made by Brown et al. [24].

Considering the measurements at 20 °C and at 80 °C of P4, the asymmetry has doubled from about 1% to 2%. If the TB generates swirl 20D upstream of the I-UFM, a decay as a function of the distance and of the Reynolds number should exist. Referring to the experimental results of Mattingly et al. [23] for the maximum swirl angle, the decay 20D downstream of the TB should vary very little between 61% and 64% for the considered Reynolds number range. This would suggest an apparent independence of swirl to the Reynolds number. But when the temperature and, consequently, the Reynolds number changes, the swirl effects change remarkably, which is in contradiction to the findings of Mattingly. The last possible reason for swirl would be a temperature dependent change in the pipe and flange geometry due to thermal expansion of the solid components affecting the tube bundle itself, or the supporting system of the pipe setup.

In any case, the path error asymmetry is caused by the disturbances in the pockets, by swirl or by an interaction of both. Fortunately, P3 is not affected by the observed effect.

4.3. Path by path comparison results

Fig. 20 shows all the results of the measurements at NMIJ and PTB. Fig. 20(a)–(e) shows the relative error of each path considered as an independent flow meter. In order to make the results comparable, a different proportional factor was used with each path. The effect on the relative error that these used factors would have on a fully developed flow profile is shown in Fig. 20(g). The weighted sum of the single paths is shown in Fig. 20(f).

The differences in the outer paths between both laboratories become evident. P1 shows differences of up to 1% for the 67 °C and 80 °C measurements. The lower temperature seems to be in better agreement. The results of NMIJ are widespread in contrast to the results of PTB which show a more consistent behavior in terms of the Reynolds number. A direct flow rate dependency seems to affect the results of NMIJ. The error increases for the lowest flow rates and decreases for the higher flow rates. P5 shows a clear Reynolds dependency for both laboratories; however, the differences are between 0.2% and 0.4%.

P2 and P4 show for PTB a consistent Reynolds dependency. For NMIJ the paths P4 and P2 but to a lesser extent show the temperature dependent error. As in the case of P1 and P5, the errors are always in opposite direction.

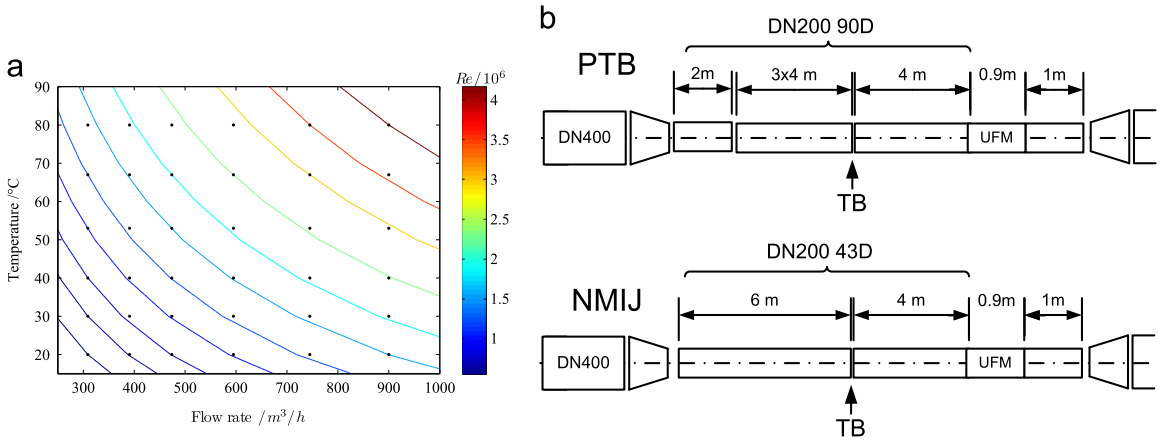

Fig. 18. Measurement conditions for the measurements at NMIJ and PTB using the I-UFM. (a) Preferred measurement points. (b) Installation configuration at PTB and at NMIJ. The TB is installed in both cases about 20D in front of the flow meter.

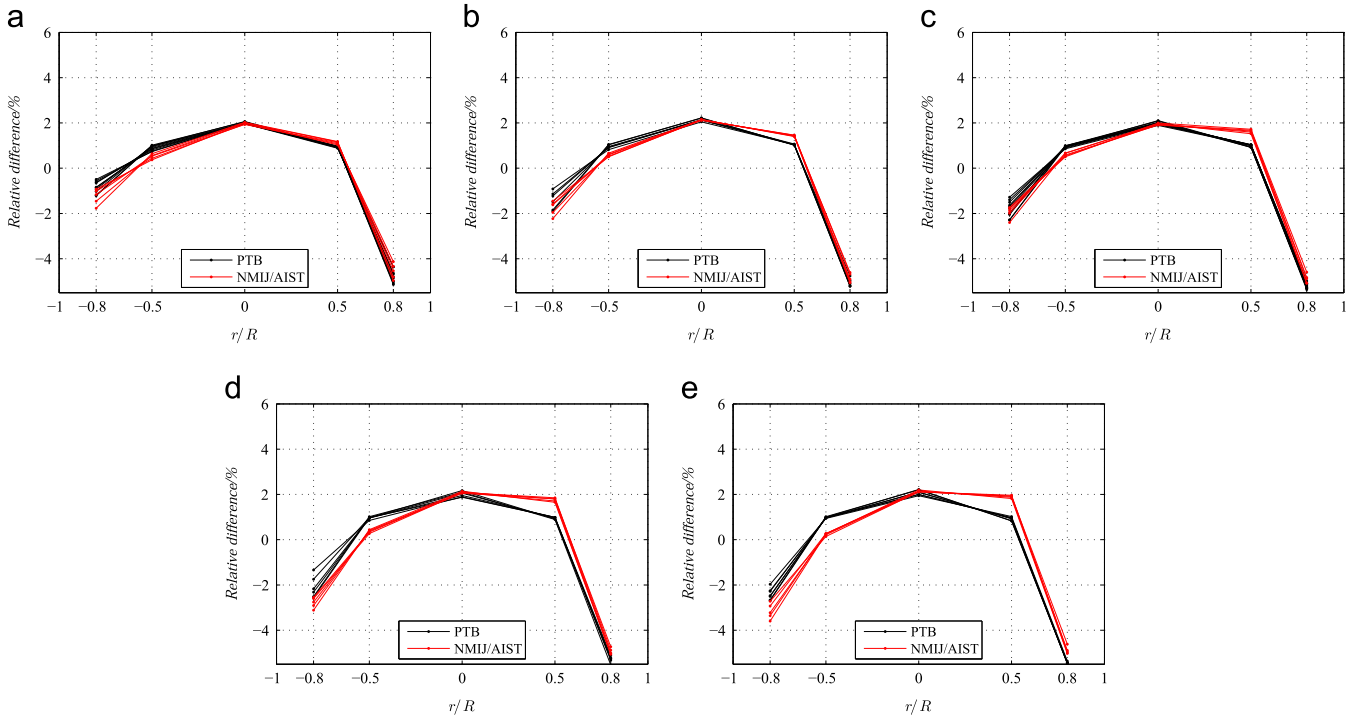

Fig. 19. Profile projection for the measurements using the I-UFM at PTB and NMIJ. P1 and P5 correspond to $r/R = \pm 0.8$, P2 and P4 correspond to $r/R = \pm 0.5$ and P3 corresponds to r/R=0. (a) 20 °C, (b) 40 °C, (c) 53 °C, (d) 67 °C, and (e) 80 °C.

As expected, we can see that the error curve of P3 is consistent for both laboratories. A clear Reynolds dependency is observed but some additional temperature effects are observed; a difference of up to 0.3% exists at $Re = 2 \times 10^6$. By taking a closer look at the data of P3, we can observe that the lines for 20 °C and 40 °C are in full agreement, while for 50 °C, 67 °C and 80 °C the differences rise up to 0.15%.

The fact that the errors occur in different directions for each couple of symmetrical paths has taken advantage of when the weighted sum is used as a flow rate indication. But in contrast to P3, the measurements at 20 °C show a larger difference.

Fig. 20(g) summarizes the results of all other curves. Each point represents the root mean square differences of each temperature across all flow rates. The figure offers an overview of the performance of each path. The differences are smallest for P3 and for the weighted average, the latter always below 0.1%. For all other results 0.2% and more can be expected.

5. Discussion

The preliminary measurements using the WCH at the carefully constructed 90D step-free and gap-free honed upstream pipe have proven that even if nearly fully developed conditions exist, every single path introduces an additional error. The magnitude of the error is up to 5%. If measurements are performed with and without flow conditioner, differences of about 0.4% can be observed if the weighted sum indication is used. These differences cannot be attributed to the peakedness of the flow profile introduced by the tube bundle, since peakedness would produce deviations in the opposite directions; the cause of the differences is probably the transducer pockets.

The velocity field within the transducer pockets has been assessed qualitatively with the WCH. The pockets with $r/R = 0.5$ and $r/R = 0.8$ have eddies that are coaxial with the transducer; the central pocket has an eddy whose axis is perpendicular to the transducer axis. The influence of the central pocket has been estimated via UVP as seen in Fig. 14(a); if the flow rate is incremented, the influence is also increased. P3 is the only path that shows a clear Reynolds dependency and, due to its position, it is insensitive to symmetrical swirl. Because of this, it is assumed that the introduced error of the central pocket is also dependent on the Reynolds number. The same condition cannot be applied to the outer paths. There is not enough knowledge to explain the shape of the error curves. Therefore, actually only the central path is capable of serving as a transfer standard.

Weighted summation is a robust method to deal with disturbances, if used adequately the UFM will deliver results within 0.15% . But the weighted summation does not only have positive aspects. If the measurement results with P3 at 20 °C from Fig. 20 (e) are considered it would be expected that the weighted summation also delivers a good result, but an error in the range of 0.09% is introduced.

In order to prove mutual consistency between the two laboratories, a transfer standard with a reproducibility at least in the order of their declared uncertainties should be used. UFMs have repeatabilities in the range of 0.02%. Their reproducibility depends in theory mostly on the ability to establish the same flow profile. Consequently, the measurements can be considered valid if the same flow profile is present. In the case of Fig. 20(e), we can observe that measurements at 20 °C and 40 °C follow exactly the same pattern.

The only cause of overlapping results in spite of having a different flow profile would be the existence of the same bias at both flow test rigs. But since PTB is using a gravimetric system with a filling volume of 17 m^3, and NMIJ is using a completely different measurement principle with a volume of 3.5 m^3, the probability that a possible error introduced by the flow profile and a hypothetical bias of the flow test rigs is fully compensated for two temperatures and five flow rates is negligible.

Consequently, we consider as confirmed that PTB and NMIJ are consistent for 20 °C and 40 °C and flow rates up to 740 m^3/h. In the case of PTB, the measurements with the orifice plate shown in Fig. 6 show that there is no reason to believe that only

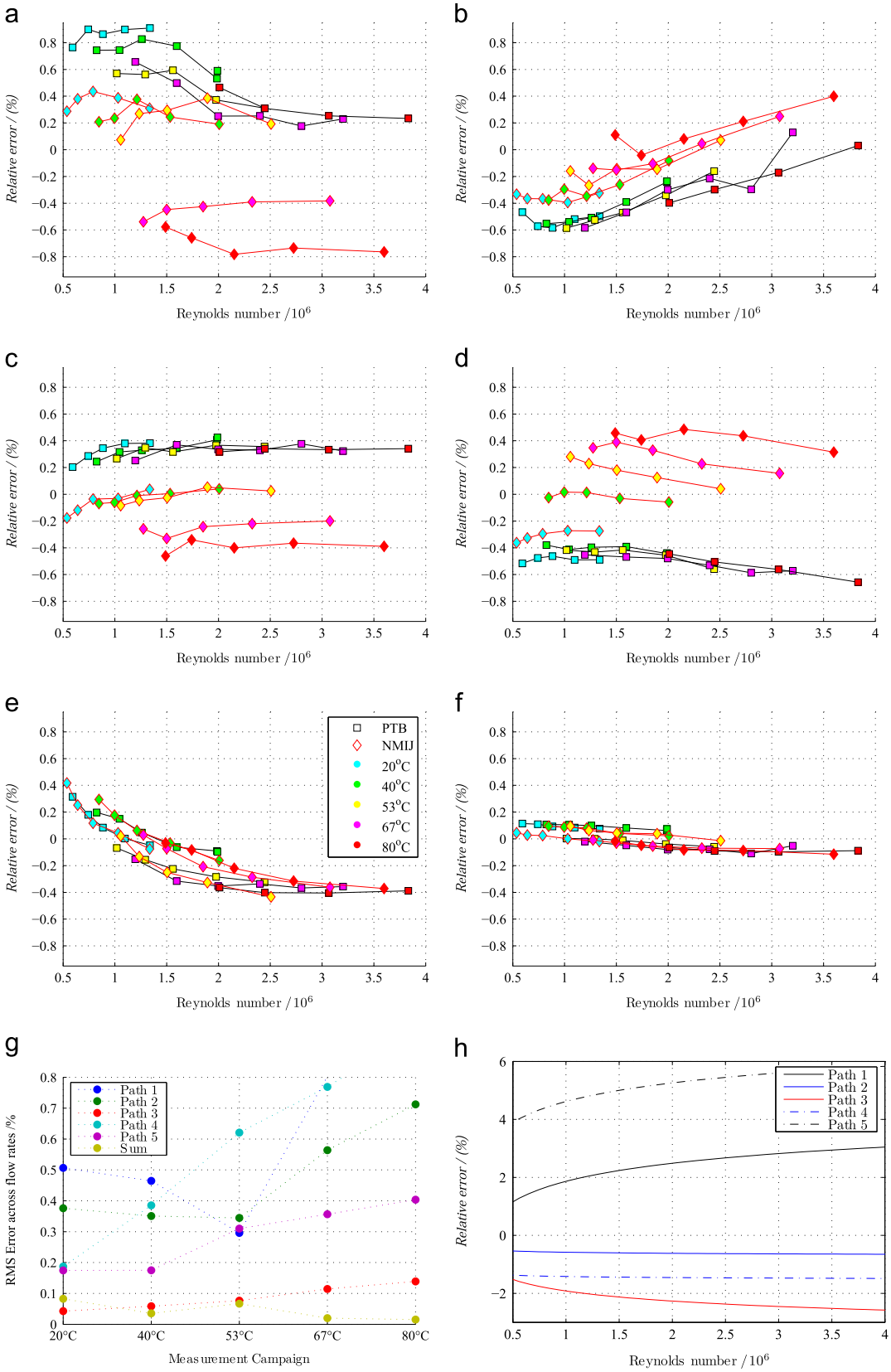

Fig. 20. Measurement results for the I-UFM at PTB and NMIJ. (a) Path 1, (b) path 5, (c) path 2, (d) path 4, (e) path 3, (f) sum, (g) RMS difference between PTB and NMIJ across flow rates, and (h) path expected errors.

measurements at 20 °C and 40 °C are correct. Therefore, we consider PTB's measurements for the full temperature and flow rate range to be valid.

In the case of NMIJ, similar arguments can be presented by the measurement of a flow nozzle as shown in the Ref. [25]. The discharge coefficients measured are on the same curve as a

function of the Reynolds number not only for 20 °C and 40 °C but also for higher temperatures. Consequently, the measurements in NMIJ for the full temperature and flow rate ranges are also valid.

Given the fact that the degree of complexity of the geometry of a diametral path is lower than the complexity of the geometry of an orifice plate and its corresponding taping systems, it is believed that the UFM will be capable of improving the uncertainty provided by orifice plates.

Based on the actual experiences, it should be taken into consideration that a UFM based flow measurement device that could be used to extrapolate the result to conditions outside the calibration ranges should be based on one or more central paths, provided that predictable flow profiles exist, as for example after a long inlet pipe, or after a diameter reduction.

6. Conclusions

The central path of the UFM has fulfilled the conditions to serve as a transfer standard. It has a good repeatability, and provided the same flow profile is given, also has a good reproducibility. The error introduced by path 3 is dependent on the Reynolds number. This is the basis for any similarity based extrapolation.

The weighted sum used in the UFM is a robust method to compensate for asymmetries and for errors introduced by the different paths. Since non-Reynolds-dependent errors are mutually cancelled, the result of a weighted summation appears to be, to some extent, only Reynolds dependent. This technique is the best choice if nearly fully developed flow conditions cannot be reached and a reproducibility of about 0.15% is sufficient.

Analyzing the performance of flow meters it is of great value if it can be guaranteed, for example via UVP or LDV, that fully developed flow conditions exist.

7. Further work

There are several open questions about the errors introduced by the pockets. It has been confirmed that the error of the central path is Reynolds dependent, but its exact description has not been performed. Using the WCH, a measurement campaign will be started to characterize the behavior of the error of the central path with aid of UVP and LDV. The experiences on path 3 will be the basis for a later characterization of the outer paths.

Acknowledgments

The generous cooperation of the KROHNE Company which provided, installed and configured the ultrasonic systems in the window chamber is greatly appreciated, as well as the active collaboration of Konstantin Richter during the measurement campaigns in Berlin.

References

[1] Shimada T, Doihara R, Terao Y, Takamoto M. Development of primary standard for hydrocarbon flow and traceability system of measurement in Japan. Synthesiology 65/110—English edition 2010;3(1).
[2] Lunde P, Frysa KE, Vestrheim M. GERG project on ultrasonic gas flow meters, phase II technical report. Groupe Europeen de recherches gazieres; 2000.
[3] Hydraulic turbines and pump-turbines. PTC 18-2011. ASME, New York; 2011.
[4] ISO 12242:2012. Measurement of fluid flow in closed conduits—ultrasonic transit-time meters for liquid; 2012.
[5] AGA Report 9. Measurement of gas by multipath ultrasonic meters; 1998.
[6] ISO 5167-2:2003. Measurement of fluid flow by means of pressure differential devices inserted in circular cross-section conduits running full—Part 2: Orifice plates; 2003.
[7] Moore PI, Brown GJ, Stimpson BP. Ultrasonic transit-time flowmeters modelled with theoretical velocity profiles: methodology. Meas Sci Technol 2000;11:1802.
[8] Voser Alexandre. Analyse und Fehleroptimierung der mehrpfadigen akustischen Durchflussmesung in Wasserkraftanlagen. Dissertation ETH No. 13102, Zurich 1999.
[9] Pannell CN, Evans WAB, Jackson DA. A new integration technique for flowmeters with chordal paths. Flow Meas Instrum 1990;216(1):224.
[10] Lau Peter, Stolt Krister. Calibration intercomparison on flow meter for kerosene synthesis report. Swedish National Testing and Research Institute SP Report; 1995. p. 77. ISBN 91-7848-606-8.
[11] Paton Richard. Final report on international key comparison of liquid hydrocarbon flow facilities. CCM-FF-K2 2008 Metrologia 45, 07019.
[12] Tawackolian K, Büker O, Hogendoorn J, Lederer T. Investigation of a ten-path ultrasonic flow meter for accurate feedwater measurements. Meas Sci Technol 2014;25:075304.
[13] Zheng D, Zhang P, Xu T. Study of acoustic transducer protrusion and recess effects on ultrasonic flowmeter measurement by numerical simulation. Flow Meas Instrum 2011;22:488–93.
[14] Yeh TT, Mattingly GE. Computer simulation of ultrasonic flow meter performance in ideal and non-ideal pipeflows. In: Proceedings of ASME FEDSM'97; 1997.
[15] Furuichi N, Terao Y, Takamoto M. A new calibration facility of flow rate for high Reynolds number. Flow Meas Instrum 2009;20(1):38–47.
[16] Mathies N. Messunsicherheit einer gravimetrischen Kalt- und Warmwasser-Normalmessanlage für große Volumenströme [Dissertation]. Technische Universität Berlin. Berlin: Mensch & Buch Verlag; 2005.
[17] Thorns J. Analytische und experimentelle Untersuchung der Messunsicherheit eines Geschwindigkeitsnormals zur Kalibrierung von LDV-systemen [Master's thesis]. Technical University of Berlin; 2010.
[18] Yeh TT, Mattingly GE. Pipeflow downstream of a reducer and its effects on flow meters. Flow Meas Instrum 1994;5:S181–7.
[19] Gersten K. Fully developed pipe flow. In: Merzkirch W, editor. Fluid mechanics of flow metering. Berlin, Heidelberg: Springer-Verlag; 2005.
[20] Richtlinie zur strömungstechnischen Validierung von Kalibrier-Prüfständen im Rahmen der EN 1434; October 2009.
[21] Drenthen J, Kurzt M, van Klooster J, Vermeulen M. Reducing installation effects on ultrasonic flow meters. In: The seventh international symposium on fluid flow measurement; 2009 .
[22] Cousins T, Estrada H, Augenstein D. Installation effects and diagnostic interpretation using the Caldon ultrasonic meter. In: North sea flow measurement workshop, St Andrews, Scotland; October 2004.
[23] Mattingly GE, Yeh TT. Flow meter Installation Effects due to several elbow configurations. In: Proceeding of the second international symposium on fluid flow measurement, Galgary, Alberta, Canada; 1990. p. 271–83.
[24] Brown GJ, Griffith BW. A New flow conditioner for 4-path ultrasonic flow meters. In: Proceedings of the FLOMEKO 2013, Paris; 2013.
[25] Furuichi N, Cheong KH, Terao Y, Nakao S, Fujita K, Shibuya K. Experimental results of flow nozzle based on PTC 6 for high Reynolds number. In: Proceedings of the ASME 2014 power conference, POWER2014-32116, July 28–31, 2014, Baltimore, Maryland, USA.
[26] Takeda Y. Ultrasonic doppler velocity profiler for fluid flow. 1st ed.. Tokyo: Springer-Verlag; 2012.

4. Overall review

The gravimetric flow calibration rig for heat metering of the PTB, the WZP, is used in applications where the uncertainty of the realized average flow rate is actually expected to be below 0.04% for a 95% confidence interval for temperatures up to 90 °C and flow rates up to 1000 m^3/h. The uncertainty requirement results from two different reasons, on one side from the constant technical advances of industry where measurement uncertainty is inversely related to efficiency and quality, and on the other side from legal requirements that are defined by regulatory instances.

Since consumer and producer protection is part of the tasks of national metrology institutes, they are committed to test the performance of measurement devices involved in commercial transactions, or devices that may affect health, safety or the environment. In this case an objective pass-or-fail criterion has to be established. Based on the measurement results, a decision has to be made if the product, activity or service involving the tested measurement device can be offered to the general public or not. In order for the decision to be independent of the testing laboratory or equipment, it is legally established for the testing equipment to have an uncertainty not larger than a predefined fraction of the the maximum tolerable error of the tested measurement device.

The uncertainty of measurement can be estimated using two different approaches. The first approach is based on the effects uncertainty causes on the measurement results. In this case the distribution of measurement results of known references at different conditions is characterized statistically; the observed standard deviation is reported as the uncertainty. This approach is typically applied in biological or complex chemical systems where establishing a complete mathematical description that includes all corrections is not possible.

In the second approach the uncertainty of the final result is estimated based on previous knowledge about the measurement system such as the measurement model and information about the influence quantities. After the influence quantities have been identified and characterized, the sensitivity of the final result to the influence quantities is determined, either experimentally or based on a previous established model. When these two steps are fulfilled the probability distribution of the result can be estimated analytically or numerically using the Monte Carlo method.

An important intrinsic drawback of the model based approach and simultaneously an advantage of the experimental approach regards the ability to detect errors in the measurement model. In the case of the model based approach, if not all influence quantities have been found, or if the interaction between influence quantities has not been adequately considered, the resulting uncertainty-estimation will be most of the times underestimated and wrong. The most reliable results are obtained when both, experimental and analytical methods are combined. Firstly determining the uncertainty of the measurement system using the model based approach, and secondly by evaluating experimentally if the observed results are consistent with the expectations.

The task of characterizing and validating the WZP has been divided into three steps. The first step was determining the uncertainty of the WZP by conventional methods.

In order to start with the uncertainty analysis it was necessary to understand the most important influence quantities first, as a result [Cor15b] is dedicated entirely to the determination of the uncertainty contribution of the time measurement. With all influence quantities having been characterized, [Cor14b] is partially dedicated to the uncertainty determination of the WZP presenting the most relevant results of the contents of Chapter 2.

The second step was to validate the uncertainty estimation by methods applicable without an external reference or additional laboratories. In [Cor15b] a method is proposed to detect certain types of systematic errors that may occur during the determination of the timing error. The presence of these kind of discrepancies would invalidate the timing error and consequently also the overall uncertainty.

Other validation methods are proposed in [Cor14b] and Chapter 2. They rely on repeated calibrations of the same flow meter using different filling times and different temperatures. Depending on the working principle and on the repeatability of the flow meter, it is possible to detect or to reject the existence of different types of systematic errors.

The third step is described in [Cor15a]. It consists on a comparison with an external reference. A bilateral comparison using an ultrasonic flow meter with a laboratory with similar characteristics was organized. In contrast to the validation methods using flow meter proposed in the previous paragraph, not only high repeatability but also high reproducibility were required. Given that actual of-the-shelf flow meter were not known to fulfill the requirements, it was necessary to characterize the best available flow meter, to find its most favorable working conditions, and to define the optimal evaluation method. The following sections will extract the most important findings of the three articles presented including also relevant figures. These findings will be analyzed and discussed in the context of the goal of the overall research work. For further details the full articles will be referred. Given that the contents of the articles are strongly interlaced, the treatise will be performed mostly on a topic base instead of on an article base.

4.1. Understanding the timing-error

A measurement result of the WZP is defined as the average water flow rate that passed through a flow meter installed on the test line during a determined period of time at a predefined temperature. Given that all parameters are directly or indirectly proportional to the flow rate, the uncertainty can be estimated through the summation of the relative uncertainties of mass, density, time and mass-corrections:

$$u_{\dot{V}s}^2 = u_m^2 + u_\rho^2 + u_{\Delta t}^2 + u_{\Delta m}^2 \tag{2.7}$$

Considering that the time needed to direct the water from the bypass to the weighing tank takes about 1 second, and considering that the measurement duration might be less than 100 second, it becomes clear that the measurement of time plays a central role when gravimetric calibration facilities are analyzed. Before any detailed uncertainty analysis was performed on the WZP, it was necessary to understand the way time determination worked, that in contrast to the weighing system was not thoroughly analyzed. [Cor15b] was the first step towards understanding the behavior of the diverting system, and the working principle of the timing error determination methods.

The time measurement is started and stopped when a trigger is activated. This trigger is located somewhere on the way passed by the diverter by switching from one position to the other. The measurement of time itself is easily performed with conventional tools; it is the location of the trigger points that is challenging. Ideal trigger points exist when the interval between start- and end-trigger point during a measurement is equal to the time that would have been required to obtain the exact amount of accumulated water as in the dashed area of Figure 2.18(a) at the same flow rate. It is not always possible to move the trigger point physically with the required accuracy, in those cases, instead of determining the ideal position of the trigger point applying a correction to the testing time called the timing-error or diverter-error is usually done.

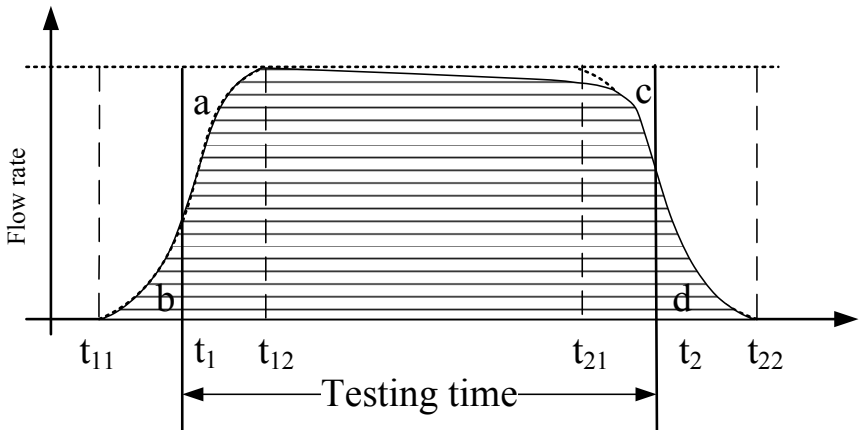

(a) Instantaneous flow rate into the weighing tank

Figure 2.18a.: The basic function of the diverter can be recognized in figure (a). The accumulated volume under the curve has to fulfill the requirement a+c = d + e. Even if the flow rate is not constant (initially shown in page 37)

The testing time will be always shorter than the time between the first and the last drop have fallen into the weighing tank (t_{11} to t_{22}) but longer than the time where the full flow rate is available at the weighing tank (t_{12} to t_{21}). If the difference between these two durations is negligible in relation to the expected uncertainty, the contribution of the diverter can be ignored; otherwise a deeper analysis is necessary.

The timing-error is determined by taking advantage of its independence on the total time, and its dependence on the amount of filling periods used. The timing-error will have a different influence on the result if shorter or longer filling times are used, and similarly it will produce different results if measurements are performed with a varying amount of filling periods. The ISO-4185 proposed two methods that take advantage of these parameters independently.

The proposed methods produce timing-error corrections that are more or less repeatable. Some authors attribute these variations entirely to the diverter systems. Mathies [Mat09] went a step further and considered the repeatability of a series of timing-error determination trials as the uncertainty of the diverter system itself, what was proven to be wrong in [Cor15b]. [Cor15b] analyzed the timing-error determination method and deduced a direct relation between the observed distribution of the results and the uncertainty of the diverter motion. This method was applied to historical data of two

facilities. The obtained results were compared with those estimated by Engel [Eng10] who determined the uncertainty of one of the analyzed diverter system analytically.

Given to mechanical limitations of the diverting system used between 200 m^3/h and 1000 m^3/h, it is not possible to perform enough repeated measurements without harming the system. However, deeper understanding on the timing-error and on its determination method enabled the determination of the most suitable method to determine the uncertainty contribution of the timing error.

4.1.1. Uncertainty contribution of the timing error

For estimating the uncertainty of the diverter system, the dynamics of diverting action itself and the flow profile at the entrance of the diverter have been considered. Both characteristics determine the instant flow rate into the weighing tank during the diverting action. The trigger points are defined at the WZP by an absolute angular position of the diverting motion. There are about 4000 unique markers or ticks on the diverter motion. Each of these can be set as the trigger point. Depending on the chosen trigger point, on the dynamics of the diverter blade and on the flow profile, the resulting testing time was calculated. This is shown in Figure 4.2.

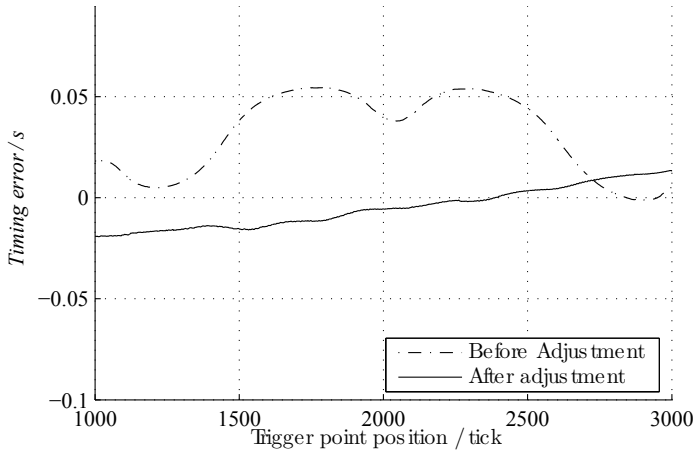

Figure 4.2.: Timing error for different trigger points before and after adjustment of the diverter motion speed (initially shown as Figure 9 in [Cor14b])

Figure 4.2 shows additionally the effect that oscillating speed of the diverter motion, as before the adjustment, may have on the timing-error. If the speed of the diverter is not approximately constant as after the adjustments, the timing error might never be canceled. Furthermore, if empirical trial-and-error methods are used to find the trigger point, when non-steady speed is present, finding the ideal trigger point assuming linearity might become impossible.

The timing-error uncertainty and timing-error correction of the WZP have been characterized experimentally. It can be seen on Figure 2.28 that the timing-error correction is independent of temperature; however, the repeatability of its determination is strongly dependent on temperature. The results for 80 °C showed a much larger repeatability as the results for 20 °C. As the least square regression gives the same result for both temperatures, it was concluded that there are no systematic effects, but random effects that cancel out if enough measurements are made. Note that the dispersion seen in Figure 2.28 is not the dispersion of the timing error, but shows the limitations of the timing-error determination method.

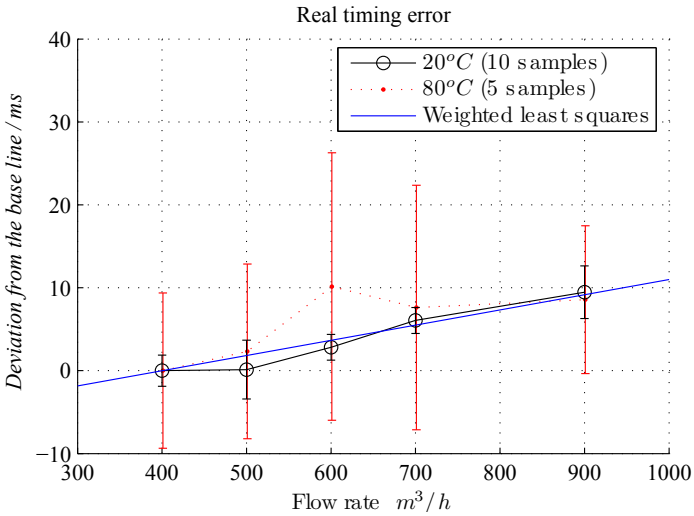

Figure 2.28.: The timing error for 20 ℃ and for 80 ℃ has been determined experimentally. For each point at 20 ℃ 10 repetitions and for 80 ℃ 5 repetitions have been performed. The least squares regression of both temperatures coincides and is shown in blue. (initially shown in page 48)

4.2. The uncertainty estimation of the WZP

Considering that the uncertainty has to be defined not only for a single working point but for the entire flow rate and temperature range it is helpful to represent the result of the uncertainty analysis as in Figure 2.30. Details on how the Figures were drawn are given in Chapter 2.

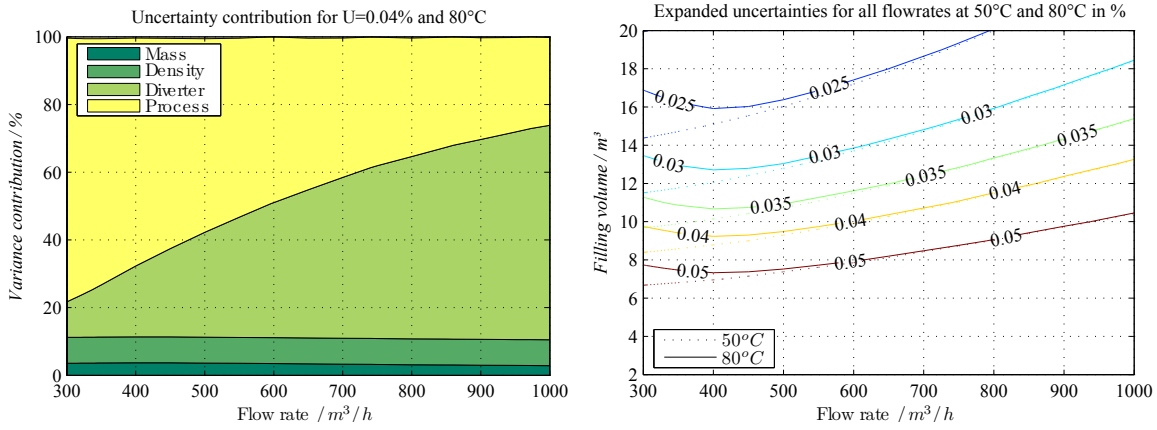

(a) Relative uncertainty contribution for 80 ℃ (b) Expanded uncertainty for 50 ℃ and 80 ℃

Figure 2.30.: Figure (a) shows the different contribution factors for the required expanded uncertainty of 0.04 % in percent. Figure (b) presents the different expanded uncertainty values that can be reached at 50 ℃ or 80 ℃ for different filling volumes. (initially shown in page 56)

As underlined in [Cor14b] Figure 2.30b allows for evaluating the weak points of the entire facility depending on the flow rate range. In this case it is clearly shown that higher flow rates require an improvement of the diverter system, and lower flow rates depend largely on process related contributors as evaporation for example. Figure

2.30b provides an estimation of the performance of the WZP at different working points. This figure is particularly useful for planning measurement campaigns with specific uncertainty requirements. The uncertainty estimation has been performed according to the BIPM - Guide to the Expression of Uncertainty in Measurement; however having an uncertainty budget is no guarantee of delivering correct results, unknown systematic errors might be still present. An experimental approach that uses the final measurement result of the facility is still necessary.

4.3. Uncertainty validation methods - Tests within the laboratory

A very useful tool to check for systematic errors on the timing-error is provided in [Cor15b]. When performing a diverter test according to the ISO 4185, there are two parameters that can be varied: the filling times and the amount of filling periods. When one or both of these parameters are changed without changing the temperature or the flowrate substantially, the same results should be obtained. It has been observed that when repeated diverter tests are performed with varying parameters, different results might be obtained if systematic errors occur. If the determined results are consistently different by a few milliseconds, the reason could be a bias in the mass measurement, or a bias in the flow rate measurement. The effects caused by both type of biases can be observed in Figure 4.5.

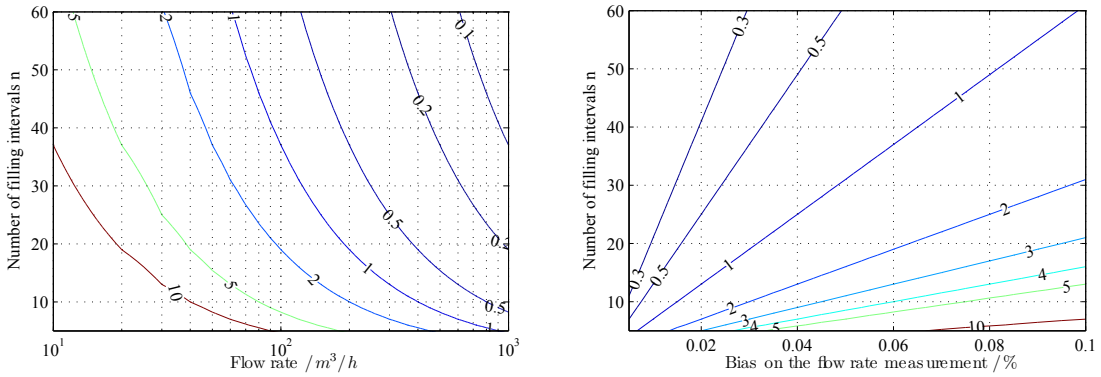

(a) Sensitivity of the timing error to a systematic mass error of 1 kg, given in milliseconds

(b) Sensitivity of the timing error to a systematic error on one flow rate measurement, calculated for one minute filling time, given in milliseconds

Figure 4.5.: Sensitivity to systematic errors when determining the timing error (initially shown as Figures 2 and 3 of [Cor14b])

Consequently, only if the results for different durations and different filling times are the same it is possible to assume that the systems are working properly and that the assumptions are valid. Analogously, if a flow meter is calibrated several times using different filling volumes at the same flow rate is considered, if the resulting error is not constant is an indication that there are uncorrected systematic effects. If the experiment is performed only at one flow rate, it would be difficult to find the cause of the bias. But if the experiment is repeated at several flow rates, based on the differences observed across flow rates it would be possible to determine the nature of the error.

The resulting errors are shown in an example in Figure 2.4. An error on mass would be independent of flow rate, an error in time would rise by constant filling times with increasing flow rate.

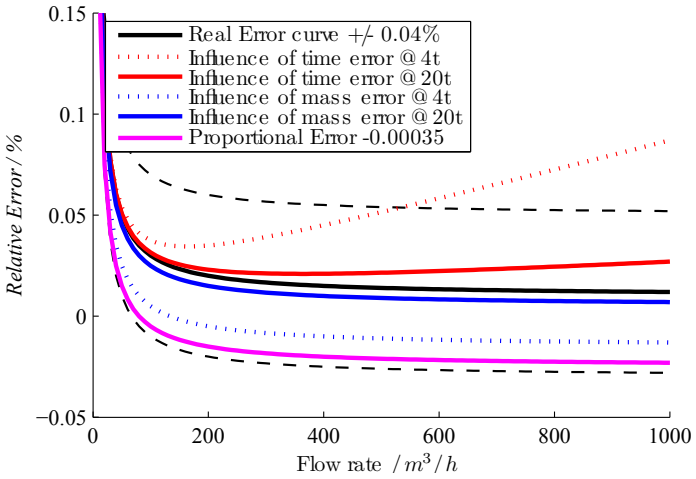

Figure 2.4.: Hypothetical influence of systematic errors on the relative error determination of a flow meter. The effect is shown for 10 ms, 1 kg bias and a proportional error of -0.035 % (initially shown in page 22)

For the correct application of the former method it is necessary for the used flow meter to behave consistently under repeatability conditions. Most flow meters fulfill this requirement if the installation conditions are not changed. But for example when the fluid temperature is changed the measurement results vary no longer only due to systematic effects on the facility alone, but due to systematic effects on the flow meter as well. Under these circumstances it is not possible to verify if there are still systematic effects originated by temperature. In [Cor14b] a method is proposed to overcome this limitation using Orifice plates.

Orifice plates are not regarded as highly accurate and precise flow meter. Their main advantages are stated to be their robustness and their simplicity. Considering that for a given orifice plate, the influence quantities are limited only to the flow conditions, if the flow profile coming to an orifice plate can be guaranteed to be stable and repeatable, it should be possible at least to obtain very repeatable results. Furthermore, it is known that an orifice plate is strongly dependent of the Reynolds number. This is a very advantageous condition since it makes it possible to compare obtained results at a given temperature and flow rate with several other temperature-flow rate couples that result in the same Reynolds number. The use of the measurement points shown in Figure 18a of [Cor15a] allowed for planning effective measurement campaigns.

Also electromagnetic flow meter are dependent on the Reynolds number, the disadvantage of those is a considerable temperature dependence that overlaps to the smooth Reynolds effects. Figure 4.8 shows the result of the flow meter used as master flow meter in the WZP. As it can be seen, the Reynolds dependency is overlapped with temperature effects on the flow meter.

There are temperature dependent effects that are being compensated in the WZP: as the evaporation effects in the weighing tank and thermal expansion of the weighing lever systems. According to the dependency of the discharge coefficient of an orifice plate at several temperatures and flowrates shown in Figure 4.8, we can conclude that all

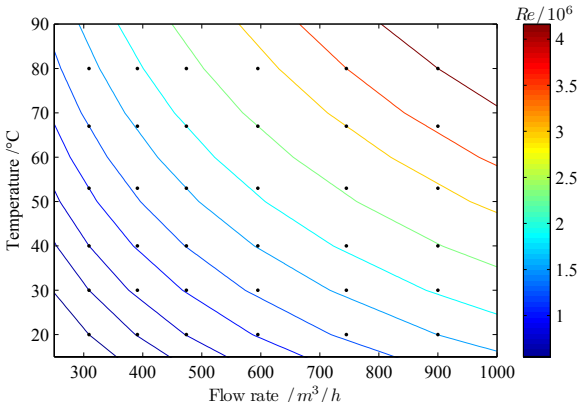

Figure 4.7.: Preferred measurement points with constant temperature, constant flowrate and nearly constant Reynolds number (initially shown as Figure 18.a in [Cor15a])

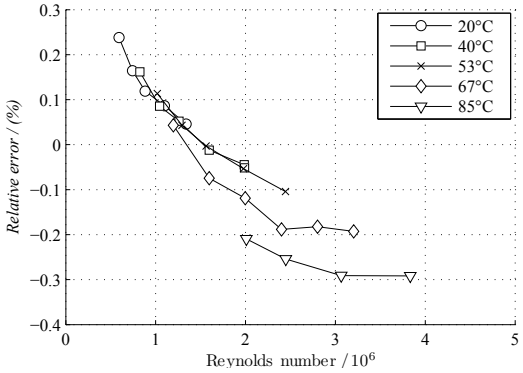

(a) Reynolds number dependence of an electromagnetic flow meter. The installation conditions were not ideal (initially shown as Figure 15 in [Cor14b])

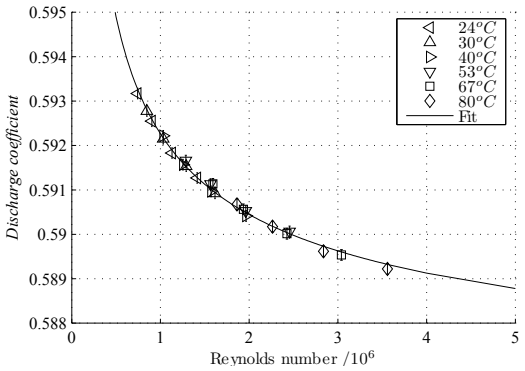

(b) Experimentally determined Reynolds dependence of the discharge coefficient of an orifice plate (initially shown as Figure 12 in [Cor14b])

Figure 4.8.: Reynolds dependence of an orifice plate and an electromagnetic flow meter

corrections are working as expected since no bias is observed. This simple procedure introduced in [Cor14b] is a very robust argument for proving the correctness of the temperature related compensations.

4.4. Validation of uncertainty - Bilateral comparison with the NMIJ

Even after the characterization of the relevant influence quantities, and after applying experimental validation methods the results of the WZP might still be biased. There is still one type of error that could not be proven to be absent. Errors proportional to any of the influence quantities but independent of temperature, flow rate, filling volume, filling time or even Reynolds number would remain undetected. Plausible scenarios are errors on the calculation software or when wrong calibration constants or biased references are used. Unknown systematic errors are a common phenomenon

as observed in past comparisons of flow calibration facilities for heat meter reported in [Cor14c] and [Cor12].

In order to discard this last type of errors, a bilateral comparison with the National institute of metrology of Japan NMIJ was organized. The reason for selecting the NMIJ is the similarity on temperature and flow rate working ranges, the equivalent declared uncertainty and the fact that the working principle is volumetric. During a bilateral comparison, both laboratories see each other as a reference; using different working principles reduces the risk of correlation errors when both laboratories have the same bias or model error. Details on the comparison and on the methods used to qualify the used transfer standard are elucidated in [Cor15a].

Performing only one comparison trial at a reduced flow rate range and with only two participating laboratories cannot comprise all working scenarios; however, the kind of undetected systematic errors that we are looking for affect the entire range. In the case of the WZP and the laboratory of the NMIJ, the uncertainty levels are similar. The measurement comparison can be defined to be successful if the differences found between both laboratories can be explained by considering only the uncertainties of the laboratories and of the reproducibility of the transfer standard. Considering that the maximum uncertainty of the WZP is 0.04 % and for the NMIJ 0.068 %, the maximum accepted difference between both laboratories considering the recommendations of the BIPM in [Cox02a] would be 0.079 %.

Ultrasonic flow meter are the only alternative left for applications with wide temperature ranges. However, the actual state-of-the-art accuracies are about 0.2 % as found by Drenthen in [Dre09]. Considering that the upstream pipe would be at least 43D long, and that the installation would be carefully made, it was expected for the technology to deliver results better than 0.1 %. Preliminary tests were performed using two different ultrasonic flow meters. A five path ultrasonic flow meter with a robust configuration used typically in industrial environment (I-UFM), and a five path ultrasonic flow meter with optical windows, to allow for flow profile measurements to be made using LDV or UVP (WCH-UFM).

The I-UFM preliminary test showed that the installation still has to be performed with care if highly reproducible results are necessary. The I-UFM did not show a clear Reynolds number dependency and furthermore there was a strong influence of the installation angle of the flow straightener with differences up to 0.2 %.

The WCH-UFM was used to proof that the flow profile after 90D straight upstream pipe was fully developed using LDV. The WCH-UFM was also used to determine the most favorable installation angle of the flow straightener using LDV. Furthermore, the WCH-UFM allowed measuring the secondary components available at the central path of an ultrasonic flow meter by means of UVP. These results, as explained in [Cor15a], confirmed the existence of transducer-cavity-born errors that are inherently present in every measurement using ultrasonic flow meter.

Based on the results of the WCH-UFM it has been determined that the signal coming from each path has a different Reynolds number dependency which is overlapped with additional effects. These additional effects resulted to be smaller for the central path than for the outer paths which can be seen in the asymptotic conversion of the error with increasing Reynolds number of the black lined squares in Figure 20e or Figure 17e of [Cor15a] (on page 91). Consequently, it was decided to use only the central path for the evaluation. It is remarkable that mirrored paths produced for both flow meter

very different errors. These differences can be attributed to geometric tolerances below 0.1 mm. since no other differences could be observed.

In Figure19 of [Cor15a] (on page 93) we can see clearly that the curves corresponding to the NMIJ have strong asymmetrical temperature dependence. The paths located at +0.5 and -0.5 are changing in positive and in negative direction. Such a behavior, based on the findings of Mattingly [Mat90], can be only explained by changes on the geometry generated by thermal expansion. Variations caused only by viscosity changes would result in smaller differences. In contrast to the lateral paths, the central path behaved regularly as expected.

Finally, only measurements at 20 °C of the central path showed consistent results as it can be seen in Figure 4.9. The results are excellent considering that the magnitude of the blue bar of 0.079 % is the maximum tolerable distance between the curves for the results to be considered consistent. If the best case uncertainty of the WZP is taken instead of the worst case the maximum tolerated difference reduces to 0.074 %, which is still clearly fulfilled. The lack of robustness of the existing transfer standards made the validation of the full range of the involved flow calibration facilities through a bilateral comparison not possible. This does not mean that the results cannot be seen as valid. Both, the PTB and also the NMIJ delivered independently consistent results for a validation based on Reynolds dependent flow meters at different temperatures. The efforts of characterizing and optimizing the WZP, making an uncertainty estimation, applying several validation strategies and performing a bilateral comparison with the NMIJ were necessary steps to be able to confirm the validity of the results of the WZP.

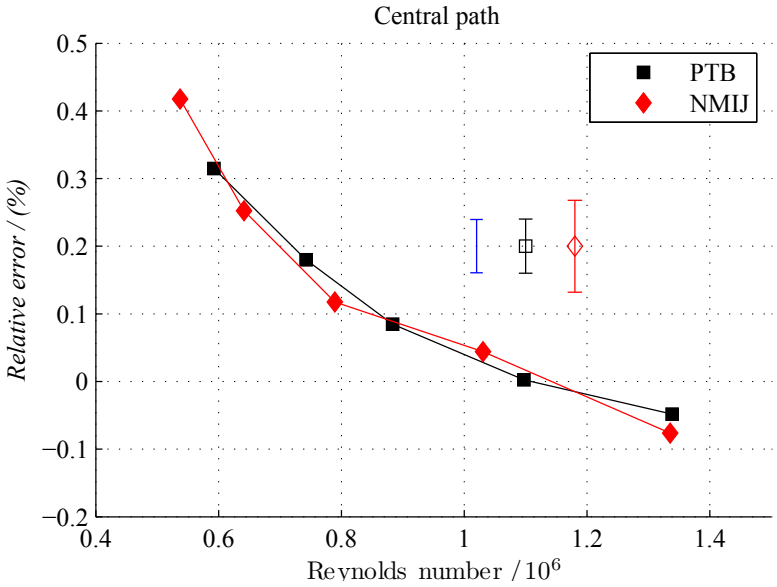

Figure 4.9.: Only 20 °C results for the central path are shown. The error bars denote the expanded uncertainty of 0.04 % and 0.068 % for the PTB and NMIJ respectively. The blue bar represents the maximum tolerable distance of 0.078 % between curves for the measurements to be considered consistent according to [Cox02a]. The overlapping of the curves is far below the required 0.078 %

4.5. Recommendations and Outlook

For guaranteeing the quality of the results of such a complex system as a gravimetric hot water calibration rig, it is unavoidable to implement a metrological assurance program. Periodical tests have to be part of the daily work. If such a work is not reasonable it should be considered introducing automated periodical tests to guarantee the correct functioning of relevant components.

Regardless of the temperature, flow rate range and of the working principle of the calibration facility, an interlaboratory comparison does not have to cover the entire working range if the used transfer standards are not proven to be robust enough to fulfill the requirements. And even if they do, it has to be pondered if the efforts are really necessary, since internal validation methods offer a deeper insight into the uncertainty models and require fewer efforts to be realized. For the particular case of hot water calibration facilities, performing a comparison at different temperatures is not necessary if a validation using a Reynolds dependent flow meter as an orifice plate can be performed. The condition for that test is to provide a fully developed flow profile and to be able to perform the measurements without dismounting the differential pressure flow meter ensuring repeatability conditions.

Orifice plates have proven to be powerful flow meters. Their unambiguous dependency on the Reynolds number is a convincing argument for making validations. Furthermore, their application as transfer standard for high accurate comparisons should be considered. After the completion of the presented research work, an additional intercomparison trial was performed. For this the same orifice plate used in the WZP was measured at the NMIJ. The first attempt gave inconsistencies of about 0.2 % due to small variations on the flow profile. It was suspected that the different flow conditioners used in the WZP and the NMIJ produced slightly different flow profiles. A second attempt however, using the same flow conditioning plates in both laboratories resulted in a maximum discharge coefficient difference below 0.03 % between the PTB and the NMIJ. See [Fur15]. This confirms the fact that it is possible to obtain outstanding results if sufficient efforts are made to guaranty the flow conditions.

The performance of the transfer standard using the weighed summation over all paths resulted in an excellent performance within 0.1 % as shown in Figure 4.10b, which is remarkable considering that ideal conditions have not been reached. If the influences on each path can be assumed as randomly generated, the averaging effect would considerable. An optimization of the summation techniques can make ultrasonic flow meter robust against certain type of disturbances. But since disturbances may eliminate the necessary monotonic relation between the obtained result and the real flow rate, using the summation as flow rate indication cannot be considered unconditionally as metrologically traceable, even if excellent results as shown in [Cor13] are obtained.

In contrast to the outer paths, the central paths are less sensitive to disturbances. Consequently, it is presumed that if symmetric and swirl free flows are present, the installation of more than one central path in a flow meter should deliver a high accurate flow meter if favorable flow profiles are present. Furthermore, if it is possible to ensure that a flow is fully developed and if the influence of the transducer pockets into the ultrasonic signal can be described in terms of its geometry, it is a valuable topic of research to establish an extrapolation method based on the Reynolds number for ultrasonic flow meter used in extreme conditions, similar to the Reader Harris-Gallagher equation for orifice plates. A challenging question would be to explain why the results

of the central path of the WCH-UFM are fully Reynolds dependent and those of the I-UFM not.

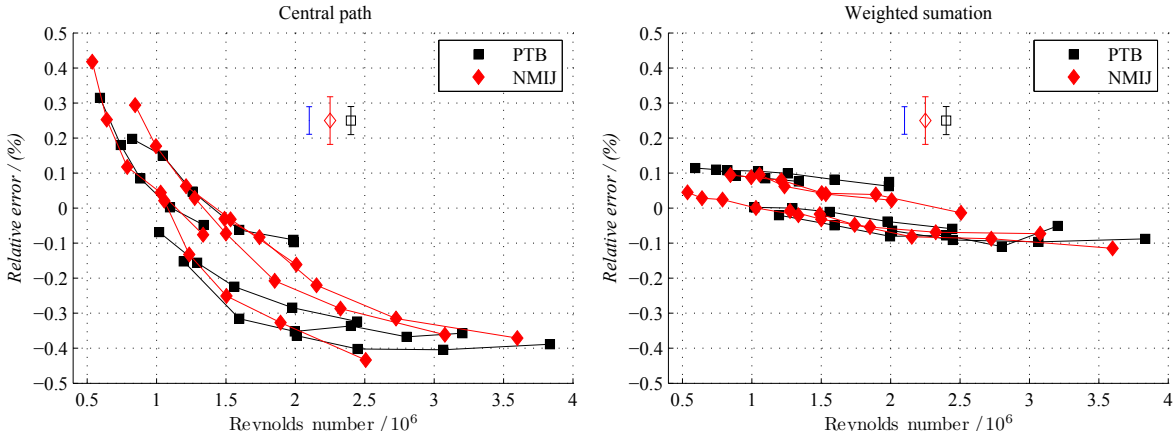

(a) All results for the central path

(b) All results for the weighted summation

Figure 4.10.: All results of the comparison between the PTB and the NMIJ are shown. The single error bars denote the expanded uncertainty of 0.04 % and 0.068 % for the PTB and NMIJ respectively. The blue bar represents the maximum tolerable distance between curves for the measurements to be considered consistent according to[Cox02a]

Bibliography

[AGA03] AGA Report 3 Part 4: Orifice Metering of natural gas and other related hydrocarbon RepPart. Published by the American Gas Association and American Petroleum Institute, 2003.

[Agu12] J. Aguilera. *Dynamic weighing calibration method for liquid flowmeters - A new approach*. Ph.D. thesis, Technische Universität Ilmenau - Fakultät für Maschinenbau, 2012.

[Bar08] A. C. Baratto. Measurand: a cornerstone concept in metrology. In *Metrologia*, 45:299–307, 2008.

[Ben15] M. Benkova, S. Makovnik and B. Mickan. Final Report: Comparison of the primary (national) standards of low-pressure gas flow. In *Metrologia*, 52(1A), 2015.

[Bro13] G. Brown and B. Friffith. A new flow conditioner for 4-path ultrasonic flow meters. In J.-P. Vallet, ed., *Proceedings of the 16th FLOMEKO Conference*. Paris, France, 2013.

[Bue10] O. Bueker. *Untersuchungen zur Darstellung und Weitergabe der Skala Volumen von Wasser mithilfe laseroptischer und konventioneller Messverfahren*. Ph.D. thesis, Fakultät III der Technischen Universität Berlin, Berlin, Germany, 2010.

[CIP99] CIPM. Mutual recongnition of national measurement standards and of calibration and measurement certificates issued by national metrology institutes. online-access, 1999.

[Cor11a] L. Cordova. Berücksichtigung der Messunsicherheit vei Vergleichsmessungen am Beispiel von Wärmezählern. In *260. Seminar, Berechnung der Messunsicherheit -Empfehlungen für die Praxis*. Physikalisch- Technische Bundesanstalt, Berlin, 2011.

[Cor11b] L. Cordova. Traceability and Data Reconciliation. In *Proceedings of the Thermal Power and Feed water FLow Measurement Workshop and Seminar*. SP, Paris, 2011.

[Cor12] L. Cordova and F. Espig. Ergebnisse des AGFW Ringvergleichs. In *8. Internationale EMATEM-Sommerschule*. European Metrology Association for Thermal Energy Measurement, 2012.

[Cor14a] L. Cordova. Ultraschall Doppler Messtechnik. In *10. Internationale EMATEM-Sommerschule*. European Metrology Association for Thermal Energy Measurement, 2014.

[Cor14b] L. Cordova and T. Lederer. Application of a novel method for validating the uncertainty estimation of a flow test facility. In *tm - Technisches Messen*, 81(9):431 – 441, 2014.

[Cor15a] L. Cordova, N. Furuichi and T. Lederer. Qualification of an ultrasonic flow meter as a transfer standard for measurements at Reynolds numbers up to 4 E6 between NMIJ and PTB. In *Flow Measurement and Instrumentation*, 45:28 – 42, 2015. doi:http://dx.doi.org/10.1016/j.flowmeasinst.2015.04.006.

[Cor15b] L. Cordova and T. Lederer. A practical method to assess the performance of gravimetric flow test rigs by using the timing error. In *Flow Measurement and Instrumentation*, 44:61 – 70, 2015. doi:http://dx.doi.org/10.1016/j.flowmeasinst.2014.11.010. Flomeko 2013 Special Edition - Selected Extended Papers.

[Cou04] T. Cousins, H. Estrada and A. D. Installation effects and diagnostic interpretation using the Caldon ultrasonic meter. In *Proceedings of the North sea flow measurement workshop*. St Andrews, Scotland, 2004.

[Cox02a] M. G. Cox. The evaluation of key comparison data. In *metrologia*, 39:589–595, 2002.

[Cox02b] M. G. Cox. The evaluation of key comparison data: An introduction. In *metrologia*, 39:587–588, 2002.

[Cox07] M. G. Cox. The evaluation of key comparison data: determining the largest consistent subset. In *metrologia*, 44:187–200, 2007. doi:doi:10.1088/0026-1394/44/3/005.

[Dav11] C. David and P. Claudel. Novel water flow facility in france range extension to low flow rates (10 000 ml/h down to 1 ml/h). In *MAPAN*, 26(3):203–209, 2011. doi:10.1007/s12647-011-0019-0.

[Doi06] R. Doihara, T. Shimada, Y. Terao and M. Takamoto. Development of weighing tank system employing rotating double wing diverter. In *Flow Measurement and Instrumentation*, 17(3):141 – 152, 2006. doi:http://dx.doi.org/10.1016/j.flowmeasinst.2006.01.002. Calibration FacilitiesCalibration Facilities.

[Dre09] J. Drenthen, M. Kurth, J. van Klooster and M. Vermeulen. Reducing installation effects on ultrasonic flow meters. In *The seventh international symposium on fluid flow measurement*. 2009.

[Eic13] Eichler. *Comparison of "Stereo Particle Image Velocimetry" (SPIV) with traced-back methods and investigation of defined disturbed conditions in pipes*. Ph.D. thesis, Technische Universität Berlin, Fakultät III - Prozesswissenschaften, 2013. doi:http://dx.doi.org/10.14279/depositonce-3501.

[Eic14] T. Eichler. Entwicklung des Strömungszustandes an einer gravimetrischen Kalt- und Warmwasser- Normalmessanlage für große Volumenströme. In *tm - Technisches Messen*, 81(6):343 – 351, 2014. doi:10.1515/teme-2014-0309.

[Eng09] R. Engel and B. Mickan. Aspects of traceabillity and comparisons in flow measurement. In *Proceedings of the 7th International Symposium on Fluid Flow Measurement*. 2009.

[Eng10] R. Engel and H.-J. Baade. Model-based flow diverter analysis for an improved uncertainty determination in liquid flow calibration facilities. In *Measurement Science and Technology*, 21(2):025401, 2010.

[Eng12] R. Engel and H.-J. Baade. Water density determination in high-accuracy flowmeter calibration - Measurement uncertainties and practical aspects. In *Flow Measurement and Instrumentation*, 25:40 – 53, 2012. doi:http://dx.doi.org/10.1016/j.flowmeasinst.2011.05.002. Advances in Flow Measurement, Selected Papers from the 15th FLOMEKO Conference.

[Fox81] T. F. Fox. A theoretical and experimental investigation of a range-gated ultrasonic Doppler flow detector. In *Journal of Physics E: Scientific Instruments*, 14(3):330, 1981.

[Ger05] K. Gertsen. *Fluid Mechanics of Flow Metering*, chapter Fully developed pipe flow, pages 1–22. Springer-Verlag Berlin Heidelberg, 2005.

[GUM08] Evaluation of measurement data - Guide to the expression of uncertainty in measurement (GUM 1995 with minor corrections). published by Joint Committee for Guides in Metrology, 2008.

[Hay77] A. Hayward. Measuring the repeatability of flow meters, NEL Report no. 636. Technical report, National Engineering Laboratory, 1977.

[Hog11] J. Hogendoorn, H. Hofstede, P. van Brakel and A. Boer. How accurate are ultrasonic flowmeters in practical conditions; beyond calibration. In *Proceedings of the 29th International north sea flow measurement workshop*. Tonsberg, Norway, 2011.

[IAP07] Revised Release on the IAPWS Industrial Formulation 1997 for the Thermodynamic Properties of Water and Steam, 2007.

[ISOa] Durchflußmessung von Flüssigkeiten in geschlossenen Leitungen - Wägeverfahren ISO 4185:1980.

[ISOb] Measurement of fluid flow by means of pressure differential devices inserted in circular corss-section conduits running full - Part 2: Orifice Plates ISO 5167-2:2003.

[Jul14] M. Juling and J. Steinbock. Entwicklung eines hochpräzisen Positioniersystems für ein LDA-Volumenstrommessnormal. In *Fachtagung Lasermethoden in der Strömungsmesstechnik*. Deutsche Gesellschaft für Laser-Anemometrie GALA e.V, 2014.

[Jul15] M. Juling and J. Steinbock. Laser-Doppler-Volumenstromnormal. In *EMATEM European Metrology Association for Thermal Energy Measurement*. 2015.

[Kin86] F. Kinghorn, D. J. M. Simth and A. McKay. A Six-Laboratory intercomparison of water flow measurement facilities. Technical report, National Engineering Laboratory, Glasgow, UK, 1986.

[Lau95] P. Lau and K. Stolt. Calibration Intercomparison on Flowmeters for Kerosene Synthesis Report. Synthesis Report 3476/1/0/203/92/9-BCR-S(30), Swedisch National TEsting and REsearch Institute, 1995.

[Lir98] I. H. Lira and W. Woeger. The evaluation of the uncertainty in knowing a directly measured quantity. In *Measurement Science and Technology*, 9(8):1167, 1998.

[Lun00] P. Lunde, K. Frysa and M. Vestrheim. GERG Project on ultrasonic gas flow meters phase II. Technical report, Group Europeen de recherches gazieres, 2000.

[Mao06] S. Mao and Z. Duan. A thermodynamic model for calculating nitrogen solubility, gas phase composition and density of the N2 H2O NaCl system. In *Fluid Phase Equilibria*, 248(2):103 – 114, 2006. doi:http://dx.doi.org/10.1016/j.fluid.2006.07.020.

[Mar06] I. Marfenko, T. Yeh and J. Wright. Diverter Uncertainty Less Than 0.01 percent for Water Flow Calibrations. In *International Symposium for Fluid Flow Measurement Conference Proceedings*. 2006.

[Mat05] N. Mathies. *Messunsicherheit einer gravimetrischen Kalt- und Warmwasser-Normalmessanlage für große Volumenström*. Ph.D. thesis, Technische Universität Berlin, 2005.

[Mat09] N. Mathies and T. Lederer. New Way for Estimating the Diverter Timing Error for Gravimetric Flow Calibration Systems. In *tm - Technisches Messen*, 74(6):333 – 341, 2009.

[Mf] Met-flow. Ultrasonic Velocity Profiling - A short introduction. Power point presentation.

[Mf11] Met-flow. *Ultrasonic Velocity Profiler - Users Guide*. Lausanne, Switzerland, 5.1 edition, 2011.

[Mic99] B. Mickan. *Systematische Analyse von Installationseffekten sowie der Effizienz von Strömungsgleichrichtern in der Großgasmengenmessung*. Ph.D. thesis, Fachbereichs MAschinentechnik der Universität GH Essen, 1999.

[Moo00] P. I. Moore, G. J. Brown and B. P. Stimpson. Ultrasonic transit-time flowmeters modelled with theoretical velocity profiles: methodology. In *Measurement Science and Technology*, 11(12):1802, 2000.

[Nie00] L. Nielsen. Evaluation of measurement intercomparisons by the method of least squares. Technical report, Danish Institute of Fundamental Metrology, 2000.

[Nie02] L. Nielsen. Identification and handling of discrepant measurements in key comparisons. Technical report, Danish Institute of Fundamental Metrology, 2002.

[Nor09] NoriyukiFuruichi, H. Sato, Y. Terao and M. Takamoto. A new calibration facility for water flowrate at high Reynolds number. In *Flow Measurement and Instrumentation*, 20(1):38 – 47, 2009. doi:http://dx.doi.org/10.1016/j.flowmeasinst.2008.11.001.

[OIM] OIML R-76.1 Non-automatic weighing instruments. Part 1: Metrological and technical requirements - Tests. published by the International Organization of Legal Metrology.

[Pai07] J. S. Paik, K.-B. Lee, P. Lau, R. Engel, A. Loza, Y. Terao and M. Reader-Harris. Final report on CCM.FF-K1 for water. In *Metrologia*, 44(1A):07005, 2007.

[Pan90] C. Pannell, W. Evans and D. Jackson. A new integration technique for flowmeters with chordal paths. In *Flow Measurement and Instrumentation*, 1(4):216 – 224, 1990. doi:http://dx.doi.org/10.1016/0955-5986(90)90016-Z.

[Pat08] R. Paton. Final report on international key comparison of liquid hydrocarbon flow facilities, CCM-FF-K2. In *Metrologia*, 45(1A):07019, 2008.

[Pav07] F. Pavese. The definition of the measurand in key comparisons: lessons learnt with thermal standards. In *Metrologia*, 44:327–339, 2007. doi:10.1088/0026-1394/44/5/009.

[Pic08] A. Picard, R. S. Davis, M. Gläser and K. Fujii. Revised formula for the density of moist air (CIPM-2007). In *Metrologia*, 45(2):149, 2008.

[Poe99] W. Poeschel. Internal and external comparison measurements for ensuring accuracy and traceability in flowmeter calibration. In *Proceedings of the International Symposium on fluid flow measurement*. Denver, USA, 1999.

[PTC11] *Hydraulic Turbines and Pump-Turbines: ASME PTC 18-2011: Performance Test Codes*. American Society of Mechanical Engineers, 2011.

[RH99] M. J. Reader-Harris. An Intercomparison Between NEL, NRLM, Delft HHydraulic, Alden Research Laboratories, CENAM and NIST using a 200 mm twin orifice plate Package in Water. Technical report, National Measurement System Directorate, Department of Trade & Industry, London, UK, 1999.

[RH02] M. J. Reader-Harris, R. Rusworth and I. G. Nicholson. An Intercomparison between NEL, CMS/ITRI, SIPAI, KRISS, IPT and CENAM using a 200mm Twin Orifice Palte Package in Water. Technical report, National Measurement System Directorate, Department of Trade & Industry, London, UK, 2002.

[Shi03] T. Shimada, S. Oda, Y. Terao and M. Takamoto. Development of a new diverter system for liquid flow calibration facilities. In *Flow Measurement and Instrumentation*, 14(3):89 – 96, 2003. doi:http://dx.doi.org/10.1016/S0955-5986(03)00016-5.

[Shi10] T. Shimada, R. HDoihara, Y. Terao and M. Takamoto. Development of primary standard for hydrocarbon flow and traceability system of measurement in Japan. In *Synthesiology English edition*, 61/110, 2010.

[Sto78] J. Stolz. A universal equation for the calculation of discharge coefficient of orifice plates. In H. Dijstielbergen and E. Spencer, eds., *Proceedings of the FLOMEKO Conference*, pages 519–534. North-Holland Publishing Co, Amsterdam, 1978.

[Str09] A. L. Stroemungsdiagnostik. Richtlinie zur strömungstechnischen Validierung von Kalibrier-Prüfständen im Rahmen der EN1434. Guideline, 2009.

[Tak85] Y. Takeda. Velocity profile measurement by ultrasound Doppler shift method. In *Fluid Control and MEasurement*, page 851. 1985.

[Tak12] Y. Takeda, ed. *Ultrasonic Doppler Velocity Profiler for Fluid Flow*. Springer Japan, 2012.

[Taw14] K. Tawackolian, O. Bueker, J. Hogendoorn and T. Lederer. Investigation of a ten-path ultrasonic flow meter for accurate feedwater measurements. In *Measurement Science and Technology*, 25(7):075304, 2014.

[Tho10] J. Thorns. *Analytische und experimentelle Untersuchung der Messunsicherheit eines Geschwindigkeitsnormals zur Kalibrierung von LDV-Systemen*. Master's thesis, Technische Universität Berlin, 2010.

[Tho14] C. Thomas. Presentation to The BIPM key comparison datadata KCDB. online-access, 2014.

[VDI00] Messunsicherheit bei Abnahmemessungen an energie- und kraftwerktechnischen Anlagen Grundlagen VDI-2048, 2000.

[VDI03] Messunsicherheit bei Abnahmemessungen an energie- und kraftwerktechnischen Anlagen - Beispiele, insbesondere Retrofitmaßnahmen VDI-2048, 2003.

[VIM08] International vocabulary of metrology - Basic and general concepts and associated terms (VIM). published by Joint Committee for Guides in Metrology, 2008.

[Vos99] A. Voser. *Analyse und Fehleroptimierung der mehrpfadigen akustischen Durchflussmesung in Wasserkraftanlagen*. Ph.D. thesis, ETH, 1999. ETH Nr. 13102.

[YBS01] Yaakov-Bar-Shalom, L. Rong and K. Thiangalingam. *Estimation with aapplication to tracking and navigation: Theory algorithms and software*, page 107. John Wiley & Sons Inc, 2001.

[Yeh94] T. Yeh and G. Mattingly. Pipeflow downstream of a reducer and its effects on flowmeters. In *Flow Measurement and Instrumentation*, 5(3):181 – 187, 1994. doi:http://dx.doi.org/10.1016/0955-5986(94)90017-5.

[Yeh97] T. Yeh and G. Attingly. Computer simulation of ultrasonic flow meter performance in ideal and non-ideal pipeflows. In *Proceedings of ASME FEDSM 97*. 1997.

[Zag98] M. V. Zagarola and A. J. Smits. Mean-flow scaling of turbulent pipe flow. In *Journal of Fluid Mechanics*, 373:33–79, 1998. doi:10.1017/S0022112098002419.

[Zhe11] D. Zheng, P. Zhang and T. Xu. Study of acoustic transducer protrusion and recess effects on ultrasonic flowmeter measurement by numerical simulation. In *Flow Measurement and Instrumentation*, 22(5):488 – 493, 2011. doi:http://dx.doi.org/10.1016/j.flowmeasinst.2011.08.003.

[Zim99] H. Zimmermann. Examination of disturbed pipe flow and its effects on flow measurement using orifice plates. In *Flow Measurement and Instrumentation*, 10(4):223 – 240, 1999. doi:http://dx.doi.org/10.1016/S0955-5986(99)00015-1.

A. Methods

A.1. Ultrasonic Doppler Velocity Profiler

The basic working principle of the ultrasonic doppler velocity measurement method for industrial applications was first detailed described by FOX in 1981 [Fox81]. Nevertheless, Its first usage has been in medical applications by measuring blood flow in 1955 by Shigeo Satomura. Only in 1985 Y. Takeda [Tak85] presented a systematic research that allowed the application of this method for fluid flow. The system used for the present studies was presented at [Cor14a] By applying a short ultrasonic pulse trail to a moving fluid, if this fluid contains some particles, the ultrasonic waves will be scattered by these particles, and due to the fluid movement a doppler frequency shift will be observed, the shifted frequency is directly proportional to the particle speed. By additionally measuring the time of flight between emission and detection of the pulse trail and by knowing the velocity of sound on the media, the position of the measured particles can be calculated. Since one sent pulse trail is scattered by all particles on its way forward, it is possible to measure almost instantaneously the velocity of the fluid on the axis of the transducer. Nowadays ultrasonic Doppler velocity profiling successfully applied for velocity profile measurements of opaque fluids as metals or food products, or fluids with large amounts of sediments like rivers. The basic principle is easy to understand, but due to some physical limitations its application requires special care as described in the following sections.

A.1.1. Resolution

Due to the properties of ultrasound the beam generated by the transducer is not cylindrical; Its shape can be simplified to a cone. The half-angle of the described cone is determined by the following equation:

$$\gamma_0 = sin^{-1}\left(0.514\frac{\lambda}{D_0}\right) \tag{A.1}$$

where λ is the wavelength and D_0 is the effective diameter of the resonator. Since diameter and wavelength are having antagonistic effects on the size of the volume, the effective diameter of the resonator and the frequency are important selection parameters defining the spatial resolution of the measurements.

The pressure field generated by a transducer can be divided in two parts, the near field where there are interference zones with several maxima and minima and the far-field characterized by a central pressure lobe. The measurement volume within the near field does not weight the velocity of the particles uniformly since it has several maxima and minima, but is still usable for measurements if the additional averaging uncertainty is considered.

Figure A.1.: Raman photograph of US beam. Source: Met-Flow [Mf]

A.1.2. Frequency detection

The detection of the frequency shift is a difficult task, it is technically not possible to determine the frequency shift of a short pulse trail using one echo only. In order to be able to detect the variation, it is necessary to take several echos instead. Several pulse trails are sent with a frequency denominated the pulse repetition frequency f_{prf}. Assuming that the measurement volume is acting as one representative reflector, every echo will be detected with a different phase; The phase shift would be caused by the displacement of the reflector Δz since its is changing the time of flight minimally $c = 2\Delta z/\Delta t$ twice since the sound has to travel this additional displacement back and forth. The different echos received from a group of pulse trails can be used to determine the shift frequency. This detected frequency, according to Takeda [Tak12] is given by

$$\frac{d\phi_{us}}{d\ t} = \frac{2v\ f_t}{c} = f_D \tag{A.2}$$

Due to this technological limitation there are additional constrains imposed to the method. Since the shift frequency is measured by sampling, the maximum detectable velocity is limited by the sampling frequency f_{prf}. Applying the nyquist criteria we have:

$$v_{max} = \frac{c\ f_{prf}}{4 f_t} \tag{A.3}$$

Where v_{max} is the maximum speed, f_t is the transducer frequency. In a group of pulse trails, consecutive pulse trails are only send when the prior pulse trail has returned already from the most distant measurement depth. This relates the maximum depth to the pulse repetition frequency:

$$P_{max} = \frac{c}{2 f_{prf}} \tag{A.4}$$

There is a trade of relation established by the f_{prf} to define maximum measuring depth and maximum detectable velocity.

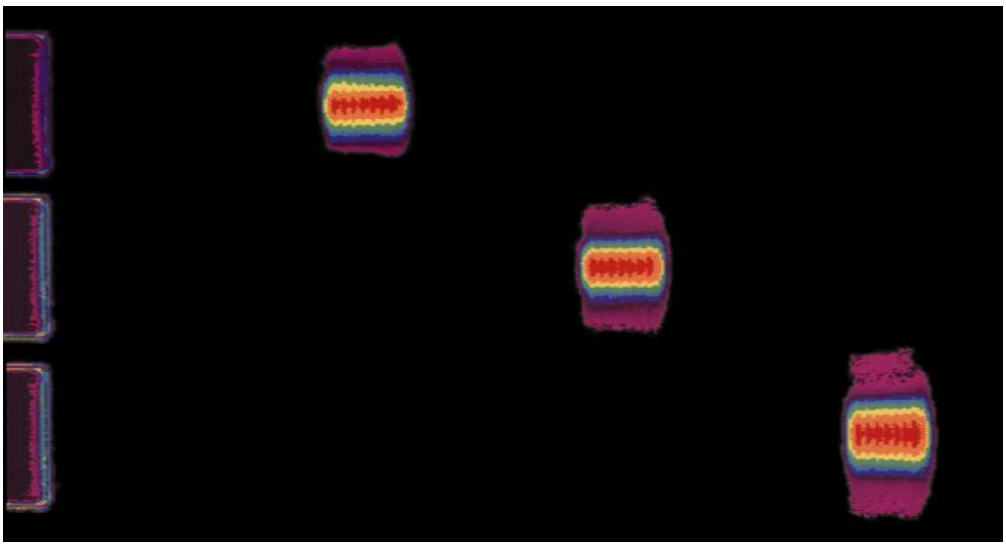

Figure A.2.: Raman photograph of US pulses leaving the transducer - three photographs are merged. Source: Met-Flow [Mf]

A.1.3. Reflectors

In order to detect the position of the echo, back scattered signals are necessary. Without reflectors only forward frequency shifting would be possible. This technique, if used with a couple of facing emitter and receiver transducers, allows the determination of the average speed within the traced path, but without giving any near information about the velocity profile. Reflectors need to fulfill several conditions.

The Size Too large reflectors increase the chances to get multiple reflections causing a disturbance and even a biasing of the detected frequencies; They also might not follow the flow properly. To small reflectors produce a very weak echo that is eventually covered by noise. According to practical experiences the ideal reflector size starts at about one quarter wave length [Mf11].

Concentration In order to detect the frequency shift at the measurement line it has been assumed that one particle is detected while passing through each measurement volume by a group of pulse trails. This means that there have to be enough reflectors, at least one per measurement volume, but to many reflectors might change the properties and the velocity profile to be measured.

Density and Impedance Reflectors have to produce a large scattering. Large scattering is produced by spherical particles with an acoustic impedance very different from the acoustic impedance of the fluid. On the other hand, if the Density is to distant from fluid density, buoyancy effects might modify the analyzed flow. In several applications, the fluid contains already reflectors, as in the case of blood cells, or sand particles in rivers. Where contamination is not a problem, there is a wide variety of solid seeding that can be used. But if there is no possibility to add solid seeding, micro-air-bubbles are a good choice.

A.1.4. Assumptions made

The conditions for adequate results to be produced are framed by a small group of assumptions and requirements.

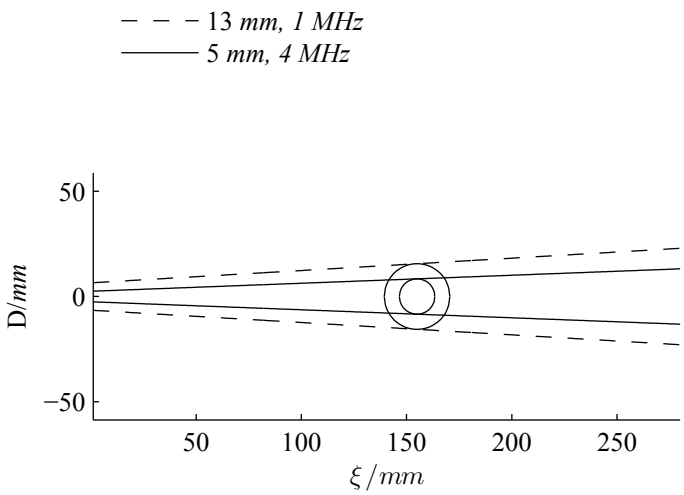

Figure A.3.: Divergence for two different transducer sizes and frequencies

- The frequencies to be detected are within the maximum detection frequency determined by the f_{prf}
- The maximum depth is set as the maximum distance to avoid additional echoes
- There is no echoes coming from different sources or walls
- The reflector size is larger than $\lambda_{us}/4$.
- There is only one reflector per measurement volume, or in case there are several reflectors, the conglomerate of reflectors acts in the sum as only one reflecting particle
- The reflector is following the flow

A.1.5. Practical limitations

UVP has some practical limitations. The fact that the ultrasonic beam diverges generates a large measurement volume compared with LDV. See for example Figure A.3 where the beam divergence for two different transducer sizes and frequencies is shown. This reduces its ability to detect local structures. Additionally, even if the structures are large, the averaging nature of the measurement volume produces a bias of the measurement result. This can be observed in Figure A.4 where the required correction is depicted for 1 MHz transducer with different measurement angles.

The maximum detectable speed is limited by the nyquist sampling Theorem. Speeds going beyond the established limit are rolled over the scale, even if there is no overlapped signs on the calculated velocities, there is no way to guarantee the recorded flow profile is not actually one ore several full scales biased.

A.1.6. The window chamber

Ultrasonic velocity profile measurements have been made at the window chamber and ultrasonic flow meter WCH-UFM. UVP Measurements have been made by replacing the glas insert used for LDV by a POM insert. Details on the tested inserts are shown in Figure A.5.

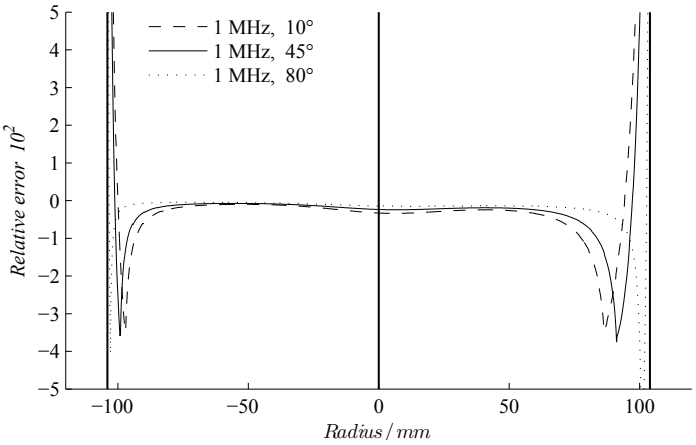

Figure A.4.: The curves show a theoretical correction for a fully developed flow given to the measurement volume size

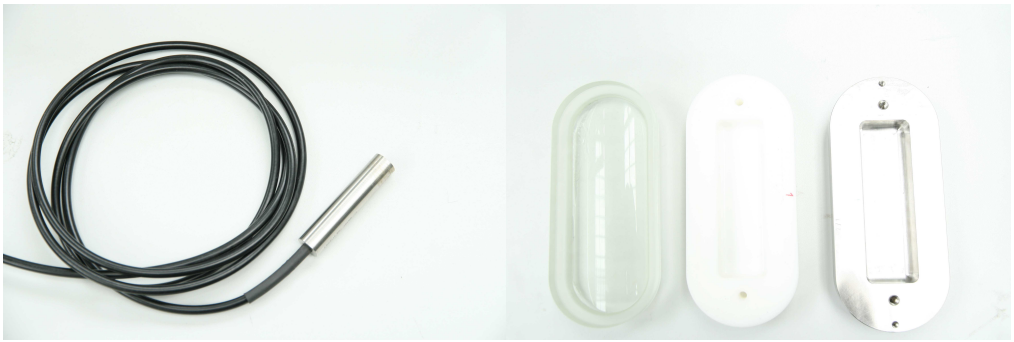

(a) 1 MHz Transducer

(b) Glass, POM and steel inserts

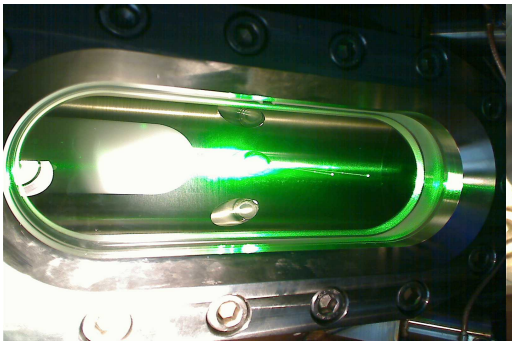

(c) WCH-UFM POM and Glass window

(d) WCH-UFM glass windows

Figure A.5.: UVP required elements and details on the window chamber. a. shows the used transducer. b. shows the different inserts used for the UVP and LDV measurements. c. shows an LDV measurement on the front, and the POM insert for the UVP measurement in the back. d. shows a front and a back glas window for LDV measurements

A.2. Laser Doppler Velocimetry - LDV

The LDV equipment was an ILA-Fp50 LDV System with 75 mW Nd:YAG 532 nm, 45 mm beam distance, 250 mm focal length. The same as used by Bueker [Bue10], Eichler [Eic13] and Thorns [Tho10]. The traversing system was designed by the author to allow a larger area to be scanned by applying a circumferential traverse. Two degrees of freedom, the angle α and the distance to the center of the arc-traverse d allowed the two-dimensional axial LDV measurements as shown in Figure A.6b.

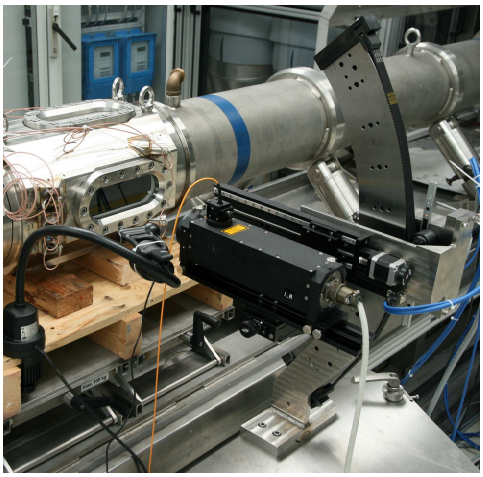

(a) Traversing System and window chamber

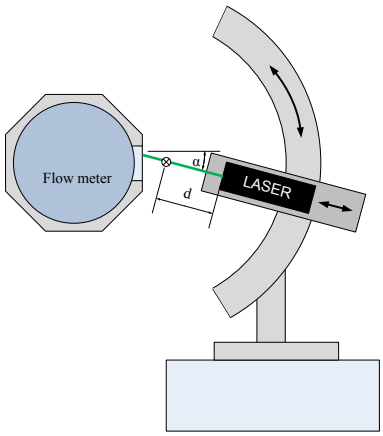

(b) Traversing variables α and d

Figure A.6.: The left picture shows the traversing system and the DN200 window-chamber mounted on the WZP. The picture on the right schematizes the two degrees of freedom given and the position of the arc center which remains constant during the measurements

A.3. Used software

Following software programs have been used for the realization and the presentation of the present research work.

- For modeling and calculations: MATLAB and Optimization Toolbox Release 2010, The MathWorks, Inc.
- For data processing: Origin (OriginLab, Northampton, MA)
- For typesetting pdfLaTeX, B ibLaTeX and TeXnicCenter
- For data acquisition Systemdesignsoftware LabVIEW, National Instruments tm. and proprietary hardware related software UVP-DUO from Met-Flow and also ILA GmbH.